



THE UNIVERSITY *of* EDINBURGH

This thesis has been submitted in fulfilment of the requirements for a postgraduate degree (e.g. PhD, MPhil, DClinPsychol) at the University of Edinburgh. Please note the following terms and conditions of use:

This work is protected by copyright and other intellectual property rights, which are retained by the thesis author, unless otherwise stated.

A copy can be downloaded for personal non-commercial research or study, without prior permission or charge.

This thesis cannot be reproduced or quoted extensively from without first obtaining permission in writing from the author.

The content must not be changed in any way or sold commercially in any format or medium without the formal permission of the author.

When referring to this work, full bibliographic details including the author, title, awarding institution and date of the thesis must be given.

Multiparton Webs in Non-abelian Gauge Theories at Three Loops and Beyond



Mark Stuart Harley

Doctor of Philosophy
University of Edinburgh
October 2015

For Kayleigh

Lay Summary

Quantum Field Theory (QFT) is the theoretical framework through which we understand the interactions between fundamental particles. QFT's primary output are scattering amplitudes which can be thought of, roughly speaking, as the square root of the probability for a certain state containing some number of particles carrying particular momenta to have originated from the scattering of a particular state of incoming particles and associated momenta.

For QFTs in which the strength of interactions between particles is small, we compute said scattering amplitudes through a perturbative expansion. This means that, since we are unable to fully determine the scattering amplitudes of the QFTs commonly found in nature, we approximate by considering increasingly small corrections to the amplitude which at some point are small enough that they will not be relevant for present practical purposes and so can be disregarded. We call the corrections which are of the same size an 'order' in the series, with the actual, as opposed to approximated, amplitude being equal to the sum over all orders of corrections. This allows us to produce predictions for scattering experiments, such as the Large Hadron Collider (LHC), that would otherwise be impossible to obtain.

However, it does however have a drawback. The contributions which we must compute in the perturbative expansion of scattering amplitudes are often infinite when particles carry vanishingly small energy. This phenomenon is known as an infrared (IR) singularity. These infinities, when carefully treated and combined, cancel when all of the contributions at each individual order in the series are summed to produce a meaningful physical prediction. This treatment is non-trivial and has been an area of active research since the conception of phenomenological QFTs.

The IR singularities of Quantum Chromodynamics (QCD), the QFT which

describes the interactions between the quarks and gluons which constitute protons and neutrons, have been computed only up to two orders in the perturbative series and so in this thesis we take steps towards computing the IR singularities for any QCD amplitude at the third order in the expansion. We do so through a modern theoretical tool, known as a web, which allow the computation of the singularities' coefficients without having to compute the full third order correction.

Abstract

Amplitudes in theories with a massless gauge boson suffer from so-called infrared divergences where off-shell states become asymptotically close to the mass-shell in loop or phase-space momentum integrals. These singularities have been shown to cancel intricately order-by-order in the perturbative expansion. However, in order to obtain meaningful and precise predictions for physical observables, we must understand and compute such divergences to high orders.

This can be accomplished by calculating webs: weighted sets of Feynman diagrams which, when exponentiated give the complete infrared singular component of the amplitude, known as the soft function. This quantity is formally equivalent to a vacuum expectation value of a product of Wilson lines. In this thesis we shall study webs correlating multiple Wilson lines, which differs from the two line case due to the possibility of non-trivial colour flows. This renders the soft function matrix valued in the space of colour flows, thus making its calculation and renormalisation non-trivial. At present, the infrared singularities of non-abelian, multiparton scattering amplitudes are known only to two loops in general kinematics, and to three loops in a simplifying kinematic limit. This thesis will thus form part of a program of work aimed at calculating and understanding the three-loop singularities in general kinematics and in doing so we aim to gain all-order insights into the perturbative structure of non-abelian gauge theories.

We first specialise to a subset of webs which we have called Multiple Gluon Exchange Webs (MGEWs), which contain only those diagrams with direct exchanges of soft gauge bosons directly between Wilson lines with no intervening three- or four- boson vertices. Studying their properties allows us to construct a basis of functions which describes all examples of such webs, and we conjecture will continue to do so at any order. Furthermore, we find that the basis functions can be described by a simple, one-dimensional integral over only logarithms. We

go on to compute several examples providing evidence for the validity of our basis and demonstrate the utility of the framework we have built by computing a four-loop web and providing some all-order results for particular classes of MGEW.

We then consider a step beyond MGEWs, that is, webs which contain a single three-gluon vertex sub-diagram. In particular we study the simplest web in this class correlating four lines at three loops and attempt to calculate it through the numerical fitting of a physically motivated ansatz. We show that this web cannot carry kinematic dependence through conformal invariant cross ratios, which arise when connected subdiagrams correlate at least four lines. Hence, it is subject to the same constraints as MGEWs with regards to their symbol alphabet, from the physical considerations in their lightlike limit and spacelike/timelike analytic continuation. Like all other known webs satisfying such constraints, we therefore argue that it can be written in terms of sums of products of MGEW basis functions. Symmetries inherent to our parameterisation of the cusp angles, Bose symmetry and transcendental weight further constrain this ansatz, resulting in forty parameters for which we present preliminary results of a numerical fit.

Declaration

Except where otherwise stated, the research undertaken in this thesis was the unaided work of the author. Where the work was done in collaboration with others, a significant contribution was made by the author.

In particular the results of chapters 3 and 4 were produced in collaboration, and appear (or are planned to appear) in the following publications,

- **Chapter 3** – [1] G. Falcioni, E. Gardi, M. Harley, L. Magnea, C.D. White, *Multiple Gluon Exchange Webs*, JHEP **1410** (2014) 10, [arxiv:1407.3477]
- **Chapter 4** – [2] G. Falcioni, E. Gardi, M. Harley, L. Magnea, C.D. White, *Webs containing a single three-gluon-vertex*, to appear



M.S. Harley
October 2015

Acknowledgements

First and foremost, I would like to thank Einan Gardi, my supervisor, for his guidance, dedication, and infectious enthusiasm for physics. I will always be grateful to him for introducing me to the subject which has become my passion. Also, I would like to thank my collaborators: Giulio Falcioni, Lorenzo Magnea and Chris White for our many fascinating discussions and for the hard work we've shared. I look forward to continuing our work together in the near future.

Many thanks go to Samuel Abreu, Øyvind Almelid, Simon Badger, Claude Duhr, Gustav Mogull, Donal O'Connell, Alexander Ochirov, Jenni Smillie, Andries Waelkens and Stephanie Yeomans for many interesting discussions. Moreover, thanks to all of the PPT group for the coffee break discussions, Friday whiskies, etc. I wish to express special gratitude to Sam and Jack for their conversation, the climbing and generally for their friendship.

I would like to extend my sincerest thanks to Lorenzo for his hospitality during my time in Turin. I am indebted to him for the opportunity to experience such a wonderful place. I must also thank friends who made my time in Italy so special. To name a few: Giulio, Stefania, and their families; our 'openspace' friends; Vale, Wee Vale, Salvo, Alice, Sefora and the rest at Lungo Dora. I would also like to thank and Ruth Britto for her hospitality during the last weeks of thesis writing. I look forward to working together over the coming years.

I am unable to fit on this page the words of gratitude I owe to my parents who have provided me with the love and support that have made it possible for me to reach where I am. Many thanks also to my family for their support and friendship.

This thesis is dedicated to Kayleigh, my wife, without whom this work would not have been possible. Thank you, Kayleigh, for getting me through the rough times, for being there to share, and amplify, the good times and for letting me be there to share yours.

Contents

Lay Summary	i
Abstract	iii
Declaration	v
Acknowledgements	vi
Contents	vii
List of figures	viii
List of tables	xi
1 Introduction	1
2 Review: Infrared Singularities	7
2.1 Introduction	7
2.2 Factorization	13
2.3 Exponentiation and Webs	18
2.4 Renormalization of multiparton webs	21
2.4.1 Aside: correlators of lightlike Wilson lines	26
2.5 Computing web kinematics	27
2.6 Webs and polylogarithms	38
2.7 Outlook	41
3 Multiple Gluon Exchange Webs	45
3.1 Introduction	45
3.2 The colour structure of webs and collinear reduction	47
3.3 General structure of MGEW integrals	51
3.3.1 Feynman integral for a MGE diagram	52
3.3.2 Feynman integral for a MGE web	55
3.3.3 Feynman integral for a MGE subtracted web	57
3.4 A basis of functions for MGEWs	60

3.4.1	Constructing a basis	60
3.4.2	Testing the basis: a three-loop, two-line web	67
3.5	Results for three-loop, three-line webs	74
3.5.1	The (2,2,2) web	75
3.5.2	The (1,2,3) web	80
3.6	A four-loop, five-line web	84
3.7	The Escher Staircase and (2, 2, . . . , 2) webs	88
3.8	Conclusion	94
4	Webs Containing Three-Gluon Vertices	99
4.1	Studying the (1,1,1,2) subtracted web	102
4.2	Fitting the two-loop web	112
4.3	Fitting the three-loop (1,1,1,2) integral	117
4.4	Conclusions	124
5	Conclusions and Outlook	127
A	Multiple Gluon Exchange Webs	131
A.1	Basis Functions	131
A.2	Calculation of the (2,2,2) web	135
A.2.1	Unsubtracted web	135
A.2.2	Subtracted web	136
A.3	Calculation of the (1,2,3) web	139
A.3.1	Unsubtracted web	139
A.3.2	Subtracted web	141
A.4	Calculation of the (1,2,2,2,1) web	142
A.4.1	Unsubtracted web	142
A.4.2	Subtracted web	145
B	Triangle Integrals	147
C	t_0 fitting details	152
D	t_1 fitting details	156
	Bibliography	164

List of Figures

1.1	A soft photon emission from a hard external parton in a general amplitude. This will generate a propagator with singular limits in the momentum k , $D(p+k)$, as shown in Eq. (1.1).	2
2.1	The one-loop correction to QED form factor	8
2.2	The n -loop ‘ladder’ diagram	9
2.3	Diagrammatic exponentiation of the soft function in an abelian theory. Only ‘connected’ diagrams contribute.	18
2.4	Diagrammatic exponentiation of the soft function in a non-abelian theory. Note the appearance of diagrams such as the second which would be ‘disconnected’ in an abelian theory.	19
2.5	(1,2,2,1) web and associated exponentiated colour factor represented by the rightmost diagram.	20
2.6	The one-loop web, $w^{(1)}$, found in the familiar cusp anomalous dimension (see e.g. Ref. [3])	30
2.7	Diagrams contributing to the (1,2,1) web through the combination given in Eq. (2.74)	34
3.1	An illustration of collinear reduction from an n -line to an $(n-1)$ -line web by identifying the lines labeled i and j . The encircled gluon–Wilson-line vertices with subscript $+$ indicates that after replacing $j \rightarrow i$ in the web colour factors, the anticommutator of the attachments is to be taken: $T_i^{\{a,b\}} = T_i^a T_i^b + T_i^b T_i^a$. The corresponding kinematic factors are determined by replacing $\beta_j \rightarrow \beta_i$ and multiplying by the appropriate symmetry factors.	51
3.2	An example of a multiple gluon exchange diagram connecting five Wilson lines at five loops; it is part of the (1,2,3,3,1) web. The lines meet at a local effective vertex representing the hard interaction. For this diagram $\Theta_D[\{s_k, t_k\}] = \theta(t_1 > s_2) \theta(s_3 > t_2 > s_4) \theta(t_4 > s_5 > t_3)$	53
3.3	The two-loop crossed graph connecting two Wilson lines, and the corresponding effective vertex graph containing a double emission vertex V_2 on each of the two lines.	62

3.4	The (1,2,2,1) web, connecting four Wilson lines at three loops. . .	64
3.5	The (1,2,2,1) web in the effective vertex formalism.	65
3.6	Effective vertex diagram for the (1,1,1,3) web.	66
3.7	The two diagrams contributing to the (3,3) web at the three loop order. Diagram (a) has a twin under the symmetry swapping the two Wilson lines; its kinematic integral yields the same function as (a).	69
3.8	The elements of the (3,3) web in the effective vertex formalism. The diagram on the left hand side, where each Wilson line features a (symmetrized) pair of V_2 and V_1 vertices, can be obtained from the (1,2,2,1) web of Fig. 3.5 upon taking collinear limits, as explained in the text.	70
3.9	The (2,2,2) web connecting three Wilson lines at three-loop order.	74
3.10	Effective vertex diagrams for the (2,2,2) web. The first three cases, a , b and c , can be obtained via collinear reduction from the (1,2,2,1) web of figure 3.5 and its permutations.	78
3.11	The (1,2,3) web connecting three Wilson lines at three-loop order.	80
3.12	The three components of the (1,2,3) web using the effective vertex formalism. The components described by the two upper diagrams can be obtained via collinear reduction of: (a) the (1,1,3,1) web; (b) the (1,2,2,1) web. Diagram (c) shows the connected colour factor that features one vertex on each line and cannot be determined by collinear reduction.	84
3.13	The (1,2,2,2,1) web connecting five Wilson lines at four loops. . .	86
3.14	Example of an Escher staircase with six external legs. There are two staircases at arbitrary order, related by reflection.	89
4.1	Two-loop diagram which gives the web $w_{3g}^{(2)}$, three-gluon vertex between three Wilson lines.	100
4.2	Diagrams contributing to the (1,1,1,2) web through the combination given in Eq. (4.5)	101
4.3	Scalar triangle with three external masses	105
4.4	Parameter fits for the t_0 ansatz. Horizontal axis indicates size of dataset in units of (number of points)/5. Vertical axis indicates fit value for corresponding parameter. The value of MaxErrorIncreases (MEI) used in integrating the data is indicated.	115
4.5	Example of t_1 parameter fits. Horizontal axis indicates size of dataset. Vertical axis indicates fit value for corresponding parameter. The value of MaxErrorIncreases (MEI) used in integrating the data is indicated.	121
B.1	Scalar triangle with three external masses, massless propagators propagators to power of $1 - \epsilon$	147

C.1 Parameter fits for the t_0 ansatz. Horizontal axis indicates size of dataset in units of (number of points)/5. Vertical axis indicates fit value for corresponding parameter. The value of **MaxErrorIncreases** (MEI) used in integrating the data to fit is indicated. 155

D.1 Parameter fits for the t_0 ansatz. Horizontal axis indicates size of dataset in units of (number of points)/5. Vertical axis indicates fit value for corresponding parameter. The value of **MaxErrorIncreases** (MEI) used in integrating the data to fit is indicated. 163

List of Tables

2.1	Interpretation of the notation T^a in Yang-Mills theory. t^a are the fundamental representation generators and f_{cab} the $SU(N)$ structure constants.	15
3.1	Symbols of all the linearly independent functions of the MGEW basis of Eq. (3.35) up to weight five. We use the shorthand notation $\eta = \alpha/(1 - \alpha^2)$	68
3.2	Kinematic integral associated with each colour factor in the (2,2,2) web of Fig. 3.9, where $A \equiv \mathcal{F}(A)$ and similarly for B, C , etc. . . .	76
3.3	Kinematic Feynman integrals accompanying each connected colour factor for the (1,2,3) web of Fig. 3.11, where $A \equiv \mathcal{F}(A)$, etc. . . .	81
4.1	Building ansatz terms for t_0 . All products of basis functions at weight three with factors of $r(\alpha)$ necessary to ensure $\alpha \rightarrow 1/\alpha$ symmetry. A ‘●’ indicates no contribution from functions of additional angles.	114
4.2	Fit parameters from ansatz, Eq. (4.44), for t_0 , Eq. (4.4), obtained using a least-squares fit with 200 points of numerical data obtained with <code>MaxErrorIncreases</code> set at 12000. Gives a chi-squared per degree of freedom of 0.2. Actual values obtained from direct calculation, Eq. (4.4).	116
4.3	Weight four terms for t_1 ansatz. A ‘●’ indicates no contribution from functions of additional angles.	117
4.4	t_1 ansatz terms with no rational factor $r(\alpha_{ij})$. A ‘●’ indicates no contribution from functions of additional angles.	118
4.5	t_1 ansatz terms with two and three rational factors $r(\alpha_{ij})$. A ‘●’ indicates no contribution from functions of additional angles. . . .	118
4.6	t_1 ansatz terms with one rational factor $r(\alpha_{ij})$. A ‘●’ indicates no contribution from functions of additional angles.	119
4.7	Fit parameters from ansatz, Eq. (D.1), for t_1 , Eq. (4.41), obtained using a least-squares fit with 350 points of numerical data obtained with <code>MaxErrorIncreases</code> set at 12000. Gives a very high chi-squared per degree of freedom of 9.67×10^7	122

4.8 Fit parameters from ansatz, Eq. (D.1) with $\lambda_{39} \rightarrow 0$. This is obtained using a least-squares fit with 350 points of numerical data obtained with `MaxErrorIncreases` set at 12000. Gives a very high chi-squared per degree of freedom of 1.44×10^8 . Note that the values differ substantially from Tab. 4.7 indicating instability of the fit. 123

Chapter 1

Introduction

Beyond the leading order of the perturbative expansion of gauge theory scattering amplitudes, off-shell degrees of freedom with undetermined momenta (loops) result in amplitudes which are expressed in terms of divergent Feynman integrals. Different regions in the loop momenta phase-space produce these divergences, requiring different techniques to resolve meaningful physical observables from the theory's amplitudes.

The most famously studied of these divergences arise from infinitely large momentum transfer in loops and so are named ultraviolet (UV). This issue, first encountered in QED in the 1930s, was not resolved until the 1940s by Dyson, Feynman, Schwinger, Tomonaga, et. al. through the process of renormalization. This procedure makes use of an infinite shift of the 'bare' parameters, themselves infinite, of the lagrangian to absorb the divergences of the scattering amplitudes, leading to finite observables. This makes some intuitive sense given that infinitely high energy particles are probing infinitely short distances and so are treated as corrections to the interaction vertices of Feynman graphs. Renormalized quantum field theories have had tremendous success in recent years, in particular the Standard Model of particle physics which has proven incredibly accurate in comparison with collider data.

In theories with massless propagating particles, scattering amplitudes suffer from so-called infrared (IR) and collinear divergences where the components of loop momenta vanish resulting in propagators coming asymptotically close to the mass shell. To illustrate this, consider the emission of an off-shell gauge boson with momentum k from a massless particle with fixed momentum p as depicted

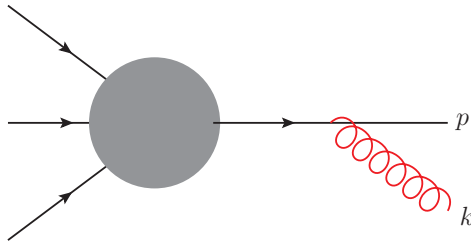


Figure 1.1: A soft photon emission from a hard external parton in a general amplitude. This will generate a propagator with singular limits in the momentum k , $D(p+k)$, as shown in Eq. (1.1).

in Fig. 1.1. We will find that the amplitude contains a propagator, which in the limit where the emitted gauge becomes soft¹, i.e. $k^\mu \ll p^\mu$,

$$D(p+k) = \frac{1}{(p-k)^2} \xrightarrow{k^\mu \rightarrow 0} -\frac{1}{2p \cdot k} = -\frac{1}{2E_p E_k (1 - \cos \theta)}. \quad (1.1)$$

Here, E_p and E_k are the energies carried by the particles with momenta p and k respectively, and θ is the angle between their respective three-momenta. In the integration over the momentum k , IR singularities will arise where $E_k \rightarrow 0$ and collinear singularities where $\theta \rightarrow 0$. Note also these singular regions can overlap where E_k and θ vanish simultaneously resulting in higher order poles of the amplitude. However, if the emitting particle is instead massive then no such collinear singularities arise, and naturally no overlapping region exists².

Where the high energies of UV momenta probe short distances, the IR region corresponds to long distance scales. Thus, the problem invites different solutions than the local treatment of renormalization. Fortunately, no further modification of the mathematical framework of the theory is necessary. The IR singularities arising from virtual (loop) diagrams cancel with those arising from real emission diagrams order-by-order in the perturbative series (the famous KLN theorem [9, 10]) for so-called *infrared safe* observables [9–11], which are insensitive to

¹Often in the literature ‘soft’ and ‘IR’ are used interchangeably. Similarly the high energy particles of the amplitude are referred to as ‘hard’.

²A more rigorous treatment than this requires the use of Landau equations [4] which give the necessary conditions for which to find divergences in general Feynman integrals; the Coleman-Norton physical picture [5] for associating the solutions of the Landau equations to singularities of the amplitude; and power counting techniques [6, 7]. While these topics will not be covered in this thesis, there are now a number of excellent reviews covering the classification of these singular regions, e.g. [8], which lead to the factorization theorem we shall discuss in Sec. 2.2.

long-distance physics. We can interpret this by considering the definition of the S-matrix in such theories, which requires a Fock space of free asymptotic states³. This is inconsistent with the existence of long-distance interactions which result in degenerate final states with arbitrary numbers of soft bosons, which are indistinguishable. The KLN theorem states that observables constructed from sums over all such degenerate states are IR finite to all orders in perturbation theory, and manifests in Feynman diagrams as precisely this cancellation between real and virtual soft and collinear singularities. KLN applies in non-abelian theories and is a generalization of the Bloch-Nordsieck cancellation in abelian theories [15].

Though IR singularities cancel, it is vital that they are computed and thoroughly understood for several reasons. For the purposes of phenomenology, problems arise when attempting to integrate over the phase-spaces of final state particles. For instance, if we consider again Fig. 1.1 and Eq. (1.1) above but with the momentum k carrying particle now on-shell, the phase-space integration over k and p will generate the same singular regions at the level of the cross-section. In order to achieve meaningful results from such integrals numerically, one must somehow implement the cancellation of the IR poles encountered in this phase-space integral with the IR divergences coming from virtual corrections at each order in the perturbative series. Such *subtraction algorithms*, are difficult to produce for arbitrary processes. In fact, at present an algorithm for generic processes is only known at Next-to-Leading-Order (NLO) [16–18].

Furthermore, the cancellation between real and virtual IR singularities is incomplete in that it leaves residual large logarithmic corrections to infrared safe observables. Schematically this takes the form

$$\underbrace{\frac{1}{\epsilon}}_{\text{virtual}} + \underbrace{(Q^2)^\epsilon \int_0^{m^2} \frac{d(k^2)}{(k^2)^{1+\epsilon}}}_{\text{real}} + \mathcal{O}(\epsilon^0) = \log\left(\frac{Q^2}{m^2}\right) + \mathcal{O}(\epsilon^0), \quad (1.2)$$

where Q^2 represents some hard energy scale, such as one of the Mandelstam invariants; m is some process dependent phase-space limit, for example a jet mass, and $\epsilon = (4 - d)/2$ is the dimensional regularization parameter, where d is

³The physical asymptotic states in such theories are actually *coherent states* with an indeterminate number of constituent particles [12, 13]. Theories of coherent states have S-matrices free from IR divergences [14].

the number of space-time dimensions. Therefore, in kinematic limits where there is a strong hierarchy between these scales (e.g. $Q^2 \gg m^2$) such logarithms provide a dominant contribution to the observable. This also threatens the convergence of the perturbative series where corrections involving powers of $\alpha_s \log(Q^2/m^2) \sim \mathcal{O}(1)$ and where there are overlapping soft and collinear singularities there are even powers of $\alpha_s \log^2(Q^2/m^2)$ which ruin convergence for $\log(Q^2/m^2) \sim 1/\sqrt{\alpha_s}$. By studying the structure of IR singularities in the amplitude it is possible to resum these large logarithms, restoring convergence and providing increased precision for certain collider observable predictions. The effect of this technique is to collect the large logarithms into an exponential pre-factor multiplying the fixed order perturbative terms. Given that the exponential function has an infinite radius of convergence and we are working in the perturbative regime of the gauge theory, both of these factors are now well behaved allowing correct predictions of physical observables. The computation of IR and collinear singularities is therefore vital given that the coefficients of these logarithms is dictated by the coefficient of the virtual pole in Eq. (1.2), and is made possible through the IR factorisation and exponentiation theorems we shall review in chapter 2. This technique has found many phenomenological applications, for example in the study of jet physics [19, 20], top-quark pair production [21] and event shapes [22–24]. It not only provides increased precision for collider observables, but can in some cases be the only way to recover the correct functional form of certain observables from a fixed order calculation. A typical example of this is the thrust differential cross-section for quark-antiquark production, which is covered along with a review of the subject in Ref. [25]. For further review see Refs. [8, 26].

From a theoretical perspective, IR singularities are of interest as the Feynman integrals involved in their computation are simpler than those encountered in complete amplitudes, though they retain non-trivial dynamical and charge information. They also exhibit useful and interesting properties such as universality (Sec. 2.2), factorization (Sec. 2.2), and exponentiation (Sec. 2.3). Moreover, it is now well known (and will be discussed in Ch. 2) that the IR and collinear singularities of amplitudes can be mapped to the UV divergences of correlators of Wilson line operators [3, 27–32] which are of interest in both gauge and gravity theories [3, 27, 31–41]. In maximally supersymmetric ($\mathcal{N} = 4$) Yang-Mills it has been found that the iterative structure found in IR singularities

persists in the finite parts of planar amplitudes [42, 43] and the study of the IR is also providing insights into the structure of its non-planar amplitudes (see, for example, Refs. [44–46]). Furthermore, the IR singularities of $\mathcal{N} = 4$ super-Yang-Mills provide a link between the weak and strong coupling regime [47–55].

In non-abelian theories, such as QCD, there is a fundamental difference between the case where the amplitude contains only two hard, colour-charged partons (for example $e^+e^- \rightarrow q\bar{q}$) and the case of *multiparton* scattering in which three or more hard colour charged partons are present. In the latter, scattering amplitudes involve non-trivial colour flows leading to a far richer structure [1, 56–61]. Multiparton scattering amplitudes are therefore vectors in the space of possible colour configurations which is acted upon by its factorized soft component as a matrix in this space (see Sec. 2.2 for more details).

In QCD processes involving only two hard partons, the IR divergences have been calculated up to two-loop order [3] (see also [62]), and very recently to three loops in Refs. [63, 64] with some partial results at four loops [50, 52]. In $\mathcal{N} = 4$ super-Yang-Mills theory it is known to three loops [49, 51], and partial results have been recently obtained at four loops [50, 52]. For multiparton amplitudes, the soft anomalous dimension has been calculated up to two-loop order for both massless [65, 66] and massive [67–70] Wilson lines (see also [60, 71–76]).

Where we consider only massless hard partons, the two-loop result [65, 66] turns out to have the same colour-dipole structure as found in the one-loop correction, motivating an ansatz for the all-order structure of infrared singularities in massless gauge theories, the *dipole formula* [77–79]. This structure can be violated starting at three loops through highly constrained corrections [46, 77–88], and very recently, results have been presented for the multiparton three-loop singularities in the limit where the parton masses are taken asymptotically small [89], confirming the breakdown of the dipole structure. Further evidence of a discrepancy with the dipole formula has been found at four loops [88].

With massive hard partons, much of this simple structure is lost, as ‘colour tripole’ corrections are present beginning at two loops [67–69]. The asymptotic massless limit, where the tripole correction vanishes, involves a subtle cancellation between different diagrammatic contributions, which have different analytic behaviour in the massive case. At present however, the IR singularities at three loops for multiparton amplitudes have yet to be computed in general kinematics

(i.e. away from the asymptotic lightlike limit [89]).

As mentioned above, and as will be discussed in the chapter to follow, IR singularities in both abelian and non-abelian gauge theories exponentiate. This exponent is given a diagrammatic interpretation through *webs* [90–92]: sets of Feynman diagrams related by exchanging the order of emission along the hard partons⁴; weighted by combinatorial factors [56]; and accompanying a so-called exponentiated colour factor (ECF) corresponding to fully connected colour graphs [61, 91, 92]. When phrased in this way, the problem of computing singularities is simplified as the number of diagrams is greatly reduced. Moreover, a number of physical constraints can be placed on webs [56, 58], providing many useful checks, and revealing a rich structure of their own. Recent advances have been made in the calculation of multiparton webs [56, 58, 60, 61], web combinatorics [56, 59, 61, 93] and their analytic structure [60]. Our goal then in this thesis is to build upon these results towards a calculation of the three loop multiparton exponent in general kinematics.

The outline of the thesis is as follows. In Ch. 2 we review the methods we shall use to study IR singularities and introduce the notation and concepts which shall appear in the bulk of the thesis. In Ch. 3 we specialize to a particular class of webs in which the gluons are exchanged directly between hard partons with no intervening three- or four-gluon-vertices, named *multiple gluon exchange webs* (MGEWs) in [60]. We study their all-order properties and conjecture an all-order basis of functions describing these webs. We go on to compute several examples providing evidence for the validity of our basis and demonstrate the utility of the framework we have built by computing a four-loop web and providing some all-order results for particular classes of MGEW. Following this, in Ch. 4 we consider the next class of webs in the determination of the three-loop exponent, those containing a single three-gluon-vertex convoluted with multiple gluon exchanges. In particular we focus on the simplest of this class, which correlates four hard partons, and explore means by which it can be computed. We present preliminary results for a numerical fit of an ansatz, based on MGEW basis functions, which we argue will describe this web. Throughout we work in dimensional regularization with $d = 4 - 2\epsilon$, and will calculate in the Feynman gauge unless otherwise explicitly stated.

⁴This definition is specific to the multiparton case, though the technicalities shall be reviewed in Ch. 2.

Chapter 2

Review: Infrared Singularities

2.1 Introduction

Given the above motivation, we are now prepared in this chapter to review the study of IR singularities. This will provide the background and framework for the discussions to follow. To illustrate the relevant concepts, let us consider a one-loop contribution to the e^+e^- QED form factor, see Fig. 2.1,

$$F^{(1),\mu}(Q, m^2) = \int \frac{d^d k}{(2\pi)^d} \frac{\text{Num}^{\mu\nu\rho}(p_1, p_2, k) D_{\nu\rho}(k)}{[(k + p_1)^2 - m^2 + i\varepsilon][(p_2 - k)^2 - m^2 + i\varepsilon]}, \quad (2.1)$$

where $Q \equiv \sqrt{(p_1 + p_2)^2}$ and with the numerator,

$$\text{Num}^{\mu\nu\rho}(p_1, p_2, k) = -g^2 \bar{u}(p_1) \gamma^\nu (\not{p}_1 + \not{k} + m) \gamma^\mu (\not{p}_2 - \not{k} + m) \gamma^\rho v(p_2), \quad (2.2)$$

where m is the electron mass. The soft limit, where we take all components of the loop momentum $k^\mu \ll Q$, can be found by taking only the leading term of this integral as all components k^μ vanish. In this limit, the factors of \not{k} in the numerator are negligible along with any k^2 in the denominator. The contribution to the form factor in the soft limit is therefore

$$F_s^{(1),\mu}(Q, m^2) = -g^2 \int \frac{d^d k}{(2\pi)^d} D_{\nu\rho}(k) \left(\frac{1}{2k \cdot p_1 + i\varepsilon} \right) \left(\frac{1}{-2p_2 \cdot k + i\varepsilon} \right) \times \bar{u}(p_1) \gamma^\nu (\not{p}_1 + m) \gamma^\mu (\not{p}_2 + m) \gamma^\rho v(p_2). \quad (2.3)$$

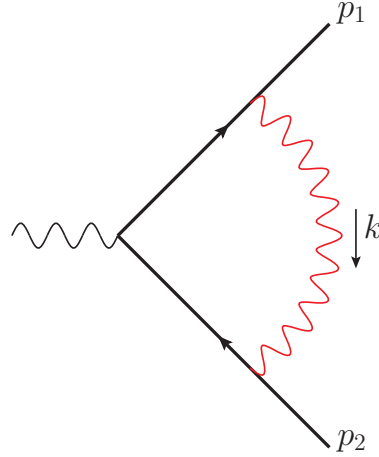


Figure 2.1: The one-loop correction to QED form factor

Further simplification can be found by application of the Clifford Algebra for the Dirac matrices, $\{\gamma^\mu, \gamma^\nu\} = 2g^{\mu\nu}$, along with the Dirac equations for fermion and anti-fermion spinors, $\bar{u}(p_1)(\not{p}_1 - m) = (\not{p}_2 + m)v(p_2) = 0$, giving

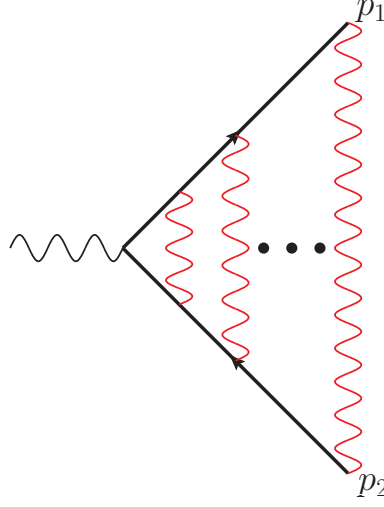
$$F_s^{(1),\mu}(Q, m^2) = -g^2 [\bar{u}(p_1)\gamma^\mu v(p_2)] \int \frac{d^d k}{(2\pi)^d} \left[D_{\nu\rho}(k) \right. \\ \left. \times \left(\frac{p_1^\nu}{k \cdot p_1 + i\varepsilon} \right) \left(\frac{p_2^\rho}{-p_2 \cdot k + i\varepsilon} \right) \right]. \quad (2.4)$$

A number of interesting observations can be made here. Firstly, we note the appearance of the tree-level form factor,

$$F^{(0),\mu}(Q, m^2) = \bar{u}(p_1)\gamma^\mu v(p_2), \quad (2.5)$$

indicating that the effects of the soft photon loop factorize from the finite, hard part of the interaction. Furthermore, the spinor structure of the amplitude has factorized from the soft component, along with any sensitivity to the scale of the hard momenta p_1 and p_2 . This reflects the fact that a soft photon cannot possibly change the momentum or spin of the hard particles from where it is emitted or absorbed.

Let us continue the QED example by considering multiple virtual emissions as shown in Fig. 2.2. When we have n photon loops, the emissions coming from the electron will contribute the following factors to the soft approximation of the

Figure 2.2: The n -loop ‘ladder’ diagram

amplitude,

$$\begin{aligned}
& g^n \frac{\bar{u}(p_1) \gamma^{\nu_1}(\not{p}_1 + m) \gamma^{\nu_2}(\not{p}_1 + m) \dots \gamma^{\nu_n}(\not{p}_1 + m)}{2p_1 \cdot k_1 \ 2p_1 \cdot (k_1 + k_2) \ \dots \ 2p_1 \cdot (k_1 + \dots + k_n)} \\
&= g^n \frac{\bar{u}(p_1) \not{p}_1^{\nu_1} \gamma^{\nu_2}(\not{p}_1 + m) \dots \gamma^{\nu_n}(\not{p}_1 + m)}{p_1 \cdot k_1 \ 2p_1 \cdot (k_1 + k_2) \ \dots \ 2p_1 \cdot (k_1 + \dots + k_n)} \\
&= g^n \frac{\bar{u}(p_1) \not{p}_1^{\nu_1} \not{p}_1^{\nu_2} \dots \not{p}_1^{\nu_n}}{p_1 \cdot k_1 \ p_1 \cdot (k_1 + k_2) \ \dots \ p_1 \cdot (k_1 + \dots + k_n)},
\end{aligned} \tag{2.6}$$

and similarly from the positron,

$$\begin{aligned}
& (-g)^n \frac{\gamma^{\rho_1}(\not{p}_2 + m) \gamma^{\rho_2}(\not{p}_2 + m) \dots v(p_2)}{2p_2 \cdot k_1 \ 2p_2 \cdot (k_1 + k_2) \ \dots \ 2p_2 \cdot (k_1 + \dots + k_n)} \\
&= (-g)^n \frac{\not{p}_2^{\rho_1} \not{p}_2^{\rho_2} \dots \not{p}_2^{\rho_n} v(p_2)}{p_2 \cdot k_1 \ p_2 \cdot (k_1 + k_2) \ \dots \ p_2 \cdot (k_1 + \dots + k_n)}.
\end{aligned} \tag{2.7}$$

However these give only one of the contributions to the n -loop form factor, specifically the ladder-like diagram (Fig. 2.2),

$$\begin{aligned}
F_{s,\text{ladder}}^{(n),\mu}(Q, m^2) &= (-g^2)^n F^{(0),\mu}(Q, m^2) \prod_{j=1}^n \left[\int \frac{d^d k_j}{(2\pi)^d} \right] \left\{ \right. \\
&\quad \times \not{p}_1^{\nu_1} \not{p}_1^{\nu_2} \dots \not{p}_1^{\nu_n} \not{p}_2^{\rho_1} \not{p}_2^{\rho_2} \dots \not{p}_2^{\rho_n} \\
&\quad \times D_{\nu_1 \rho_1}(k_1) D_{\nu_2 \rho_2}(k_2) \dots D_{\nu_n \rho_n}(k_n)
\end{aligned} \tag{2.8}$$

$$\left. \begin{aligned} & \times \frac{1}{p_1 \cdot k_1 p_1 \cdot (k_1 + k_2) \dots p_1 \cdot (k_1 + \dots + k_n)} \\ & \times \frac{1}{p_2 \cdot k_1 p_2 \cdot (k_1 + k_2) \dots p_2 \cdot (k_1 + \dots + k_n)} \end{aligned} \right\}.$$

To obtain the remaining $(n! - 1)$ diagrams, we can simply permute the order of attachments along one of the external particles, making use of the fact that we can simply relabel the integration variables k_i , and so,

$$\begin{aligned} F_s^{(n),\mu}(Q, m^2) &= (-g^2)^n F^{(0),\mu}(Q, m^2) \prod_{j=1}^n \left[\int \frac{d^d k_j}{(2\pi)^d} \right] \left\{ \right. \\ & \times p_1^{\nu_1} p_1^{\nu_2} \dots p_1^{\nu_n} p_2^{\rho_1} p_2^{\rho_2} \dots p_2^{\rho_n} \\ & \times D_{\nu_1 \rho_1}(k_1) D_{\nu_2 \rho_2}(k_2) \dots D_{\nu_n \rho_n}(k_n) \\ & \times \frac{1}{p_1 \cdot k_1 p_1 \cdot (k_1 + k_2) \dots p_1 \cdot (k_1 + \dots + k_n)} \\ & \left. \times \sum_{\pi} \frac{1}{p_2 \cdot k_{\pi(1)} p_2 \cdot (k_{\pi(1)} + k_{\pi(2)}) \dots p_2 \cdot (k_{\pi(1)} + \dots + k_{\pi(n)})} \right\}, \end{aligned} \quad (2.9)$$

where π are the permutations of the set $(1, 2, \dots, n)$. Here we may make use of the so-called *eikonal identity*

$$\sum_{\pi} \frac{1}{p \cdot k_{\pi(1)} p \cdot (k_{\pi(1)} + k_{\pi(2)}) \dots p \cdot (k_{\pi(1)} + \dots + k_{\pi(n)})} = \prod_i \frac{1}{p \cdot k_i}, \quad (2.10)$$

causing a dramatic simplification of the integrand,

$$\begin{aligned} F_s^{(n),\mu}(Q, m^2) &= (-g^2)^n F^{(0),\mu}(Q, m^2) \prod_{j=1}^n \left[\int \frac{d^d k_j}{(2\pi)^d} \right] \left\{ \right. \\ & \times p_1^{\nu_1} p_1^{\nu_2} \dots p_1^{\nu_n} p_2^{\rho_1} p_2^{\rho_2} \dots p_2^{\rho_n} \\ & \times D_{\nu_1 \rho_1}(k_1) D_{\nu_2 \rho_2}(k_2) \dots D_{\nu_n \rho_n}(k_n) \\ & \times \frac{1}{p_1 \cdot k_1 p_1 \cdot (k_1 + k_2) \dots p_1 \cdot (k_1 + \dots + k_n)} \\ & \left. \times \prod_i \frac{1}{p_2 \cdot k_i} \right\}. \end{aligned} \quad (2.11)$$

By summing over permutations of the attachments on the other line, we can utilize Eq. (2.10) again, but we must account for the over-counting that this will

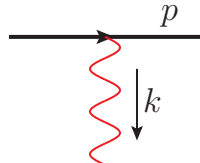
introduce. Having already generated all of the diagrams by permuting the soft photon attachments along one of the external particles, doing so on the other will introduce an additional instance of each diagram, requiring a compensating factor of $1/n!$. Hence,

$$\begin{aligned}
 F_s^{(n),\mu}(Q, m^2) &= (-g^2)^n F^{(0),\mu}(Q, m^2) \frac{1}{n!} \prod_{j=1}^n \left[\int \frac{d^d k_j}{(2\pi)^d} \right] \left\{ \right. \\
 &\quad \times p_1^{\nu_1} p_1^{\nu_2} \dots p_1^{\nu_n} p_2^{\rho_1} p_2^{\rho_2} \dots p_2^{\rho_n} \\
 &\quad \times D_{\nu_1 \rho_1}(k_1) D_{\nu_2 \rho_2}(k_2) \dots D_{\nu_n \rho_n}(k_n) \prod_i \frac{1}{p_1 \cdot k_i} \\
 &\quad \left. \times \sum_{\pi} \frac{1}{p_1 \cdot k_{\pi(1)} p_1 \cdot (k_{\pi(1)} + k_{\pi(2)}) \dots p_1 \cdot (k_{\pi(1)} + \dots + k_{\pi(n)})} \right\} \\
 &= \frac{1}{n!} (g^2)^n F^{(0),\mu}(Q, m^2) \\
 &\quad \times \prod_{i=1}^n \left[\int \frac{d^d k_i}{(2\pi)^d} \left(\frac{p_1^{\nu_i}}{p_1 \cdot k_i} \right) \left(\frac{-p_2^{\rho_i}}{p_2 \cdot k_i} \right) D_{\nu_i \rho_i}(k_i) \right] \\
 &= F^{(0),\mu}(Q, m^2) \frac{1}{n!} \left[g^2 \int \frac{d^d k}{(2\pi)^d} \left(\frac{p_1^{\nu}}{p_1 \cdot k} \right) \left(\frac{-p_2^{\rho}}{p_2 \cdot k} \right) D_{\nu \rho}(k) \right]^n,
 \end{aligned} \tag{2.12}$$

which permits the same factorized form as seen in Eq. (2.4). Additionally, in this form we reveal another helpful property of IR singularities; that is, they exponentiate. If we sum over all numbers of gluon emissions, n from 0 to ∞ , we find,

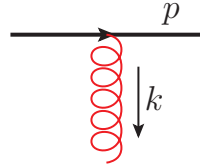
$$F_s^{\mu}(Q, m^2) = F^{(0),\mu}(Q, m^2) \exp \left(g^2 \int \frac{d^d k}{(2\pi)^d} \left(\frac{p_1^{\nu}}{p_1 \cdot k} \right) \left(\frac{-p_2^{\rho}}{p_2 \cdot k} \right) D_{\nu \rho}(k) \right). \tag{2.13}$$

The procedure we have carried out above is an example of what is known as the *eikonal approximation* for the amplitude which can be generated from the eikonal Feynman rules in an abelian theory,



$$\longrightarrow -ig \frac{p^{\mu}}{p \cdot k} = -ig \frac{\beta^{\mu}}{\beta \cdot k}, \tag{2.14}$$

or similarly in a non-abelian theory,



$$\longrightarrow -ig_s T^a \frac{p^\mu}{p \cdot k} = -ig_s T^a \frac{\beta^\mu}{\beta \cdot k}, \quad (2.15)$$

where the colour generator T^a is in the same representation as the emitting particle and we have defined the scaleless velocity $\beta = p/\Lambda$, for some arbitrary scale Λ , reflecting the scale invariance of the IR contribution to the amplitude. In terms of these Feynman rules we can rewrite Eq. (2.13),

$$F_s^\mu(Q, m^2) = \underbrace{F^{(0),\mu}(Q, m^2)}_{\text{hard}} \times \underbrace{\exp \left(\text{triangle diagram with wavy line} \right)}_{\text{soft}}, \quad (2.16)$$

illustrating both the factorization and exponentiation of IR singularities.

Through both factorization (Sec. 2.2) and exponentiation (Sec. 2.3), the task of computing the IR singularities is greatly simplified. Firstly, factorization permits us to compute the IR singularities without the overburdening complications of a complete multi-loop amplitude calculation – allowing us to study higher loop-orders and with greater generality than would otherwise be possible. Furthermore, exponentiation allows us to compute only a subset of the eikonal diagrams at each order but in doing so obtain the full IR singular contribution. In the case above this is particularly dramatic as we are able to give the IR singular contribution from an infinite set of diagrams by carrying out a simple one-loop integral.

However, whilst a neat illustration of the concepts we will discuss below, the above example is hardly the complete picture, primarily because the example above assumes an abelian theory. In a non-abelian theory such as QCD where ordering of emissions along particle lines matters, the exponent is not so simple, though IR singularities in such theories do indeed factorize [80, 94–99] and exponentiate [90–92]. Moreover, if we consider amplitudes with more than two hard, colour-charged, external particles then non-trivial colour flows are possible,

further complicating matters. A final point to note here is that we have not yet considered the possibility of particles interacting away from the Wilson lines. In theories such as QCD where gluon self interaction is present, as well as the possibility of interaction with vacuum fermions in both abelian and non-abelian theories, such diagrams will contribute to the exponent and so must be taken into account.

In the rest of this chapter, we shall review these properties, introducing the concepts and notation which will be required to discuss recent advances in the computation of IR singularities in non-abelian gauge theories. We begin in Sec. 2.2 by discussing in greater detail factorization and define the *soft function* which shall be the subject of this thesis. In Sec. 2.3 we will provide a brief overview of non-abelian exponentiation and discuss the form of the soft function exponent in terms of *webs*. We then cover the renormalization of the soft function in Sec. 2.4, introducing the much studied *soft anomalous dimension* and in this context frame the remaining chapters of this thesis. Sec. 2.5 explains how to put into practice these concepts with the computation of the one-loop web and an example of a two-loop subtracted web before reviewing the framework built around *multiple-polylogarithms* which shall be used extensively in Ch. 3 and Ch. 4.

2.2 Factorization

Through the uncertainty principle we see that gluons with vanishing momenta have infinite Compton wavelength. Thus, it is impossible for such gluons to resolve the underlying hard interaction from where the high energy partons originate. This fact permits the study of IR singularities in isolation, as we shall do throughout this thesis. The concept is formalized through the factorization theorem developed in Refs. [80, 94–99], the results of which will be described in this section, and which generalizes the factorization shown explicitly in the previous section.

We will be focusing on non-abelian gauge theories in which there is a crucial difference between amplitudes with two and those with several colour charged, hard, external particles. In the case where there are only two colour-charged external particles, there is only one possible colour flow. On the other hand, amplitudes containing more than two coloured external particles permit

multiple possible colour flows and so the amplitude $\mathcal{M}_{\{\alpha_i\}}$, where $\{\alpha_i\}$ are the n colour indices belonging to arbitrary representations of the gauge group, can be decomposed onto a basis of colour tensors,

$$\mathcal{M}_{\{\alpha_i\}} = \sum_L^N (c_L)_{\{\alpha_i\}} \mathcal{M}_L, \quad (2.17)$$

where N is the number of irreducible representations of the gauge group that can be constructed with the given particles, and $(c_L)_{\{\alpha_i\}}$ is a basis of N independent colour tensors.

It is known [80, 94–99] that n -external particle, fixed-angle¹ scattering amplitudes factorize such that,

$$\begin{aligned} \mathcal{M}_L(p_i/\mu, \alpha_s(\mu^2), r_S, r_C) &= S_{LK}(\beta_i \cdot \beta_j, \alpha_s(\mu^2), r_S, r_C) \\ &\times H_K\left(\frac{p_i \cdot p_j}{\mu^2}, \frac{p_i \cdot n_i}{\sqrt{n_i^2}}, \alpha_s(\mu^2)\right) \\ &\times \prod_i \frac{J_i\left(\frac{(p_i \cdot n_i)^2}{n_i^2}, \alpha_s(\mu^2), r_S, r_C\right)}{\mathcal{J}_i\left(\frac{(\beta_i \cdot n_i)^2}{n_i^2}, \alpha_s(\mu^2), r_S, r_C\right)}, \end{aligned} \quad (2.18)$$

where S_{LK} , the soft function, will contain all soft and overlapping soft+collinear divergences of the amplitude; the jet functions J_i contain the collinear singularities arising from each of the external particles indexed by i , along with the corresponding soft+collinear region; and the hard function, H_K , which is finite after renormalization of the theory. This alone would over-count the soft+collinear regions, which are present both in the soft and jet functions, and so we account for this with the ‘eikonal jets’, \mathcal{J}_i . These capture the overlapping soft+collinear information contained within their corresponding jet function. Also used in this expression are the renormalization scale, μ , as well as r_S and r_C , the soft and collinear regulators respectively, which shall be discussed in more detail below. As we can see, such a factorization would capture all of the leading IR singular regions discussed in Ch. 1. Written in this way we see that the hard function is a vector in the space of colour flows, the components of which are mixed by the soft function which itself is a colour space matrix. This is a

¹Meaning that the ratios of all kinematic invariants are of order one.

Representation	Initial/Final-state	T^a
Quark (Fundamental)	Initial	$-t_{\beta\alpha}^a$
Quark (Fundamental)	Final	$t_{\alpha\beta}^a$
Anti-quark (Anti-fundamental)	Initial	$t_{\alpha\beta}^a$
Anti-quark (Anti-fundamental)	Final	$-t_{\beta\alpha}^a$
Gluon (Adjoint)	Initial	if_{cab}
Gluon (Adjoint)	Final	if_{cab}

Table 2.1: Interpretation of the notation T^a in Yang-Mills theory. t^a are the fundamental representation generators and f_{cab} the $SU(N)$ structure constants.

key difference between the two-line case in which the colour flow decomposition, Eq. (2.17), is trivial, and will have consequences when we later consider non-abelian exponentiation and renormalization.

In order to formalize the constituents of Eq.(2.18) we must first introduce the key ingredient of the factorized amplitude; that is, the Wilson line,

$$\Phi_{\beta_i}(b, a) = \mathcal{P} \exp \left(ig_s \int_a^b ds \beta_i \cdot A(s\beta_i) \right). \quad (2.19)$$

Here g_s is the renormalized coupling, β_i is the Wilson line's scaleless velocity and $A^\mu(x) = A^{a,\mu}(x)T^a$ is the gauge field with T^a a generator of the gauge group in the representation of the corresponding parton i (see Tab. 2.1 for interpretation of this notation for the generators in Yang-Mills). The path ordering operator, \mathcal{P} , prescribes ordering of the generators (gluon emissions) along the path of the Wilson line. Eq. (2.19) can be construed as the gauge phase along the direction of the hard emitting partons, therefore it contains only the information which can be resolved by soft gluons emitted from said hard partons, being inherently scale invariant by re-parametrization of the integral, and scalar therefore lacking dependence on the parton's spin.

Eq. (2.18) relies on the fact that by replacing all hard partons of the amplitude by Wilson lines [27] in the same representation as each parton and in the direction $\beta_i = p_i/Q$, for some arbitrary scale Q , we will reproduce the eikonal approximation of the amplitude as outlined in Sec. 2.1. We can consider the Wilson lines in S as corresponding to the classical trajectories of the n partons, emanating from a hard interaction vertex at the origin. For now, let us assume that all of the external hard particles are massless, $\beta_i^2 = 0$, so that collinear

singularities are present. Using this replacement we can define the soft function for an n -point amplitude as the vacuum expectation value of a product of n Wilson lines²,

$$(c_L)_{\{\alpha_i\}} S_{LK}(\beta_i \cdot \beta_j, \alpha_s(\mu^2), r_S, r_C) = \sum_{\{\eta_k\}} \langle 0 | \left[\prod_i^n \Phi_{\beta_i}(0, \infty)_{\alpha_k, \eta_k} \right] | 0 \rangle (c_K)_{\{\eta_k\}}, \quad (2.20)$$

which will contain all soft and soft+collinear singularities of the amplitude regularized by a combination of r_S and r_C , the soft and collinear regulators respectively. It is possible to regularize both by dimensional regularization, though this is not mandatory and in fact it often proves useful to introduce a separate collinear regulator leaving only the soft singularities in the dimensional regularization parameter.

In order to see that Eq. (2.20) does indeed reproduce the soft component of the amplitude, we can Fourier transform the gauge field in the exponent of the Wilson lines,

$$\begin{aligned} i \int dx^\mu A_\mu(x) &= \int \frac{d^d k}{(2\pi)^d} \beta^\mu \tilde{A}_\mu(k) i \int ds e^{i(s\beta \cdot k + i\varepsilon)} \\ &= \int \frac{d^d k}{(2\pi)^d} \tilde{A}_\mu(k) \beta^\mu \left[-\frac{e^{i(s\beta \cdot k + i\varepsilon)}}{\beta \cdot k + i\varepsilon} \right]_0^\infty \\ &= \int \frac{d^d k}{(2\pi)^d} \tilde{A}_\mu(k) \left(\frac{\beta^\mu}{\beta \cdot k + i\varepsilon} \right) \end{aligned} \quad (2.21)$$

which reproduces the eikonal Feynman rule for the emission of a soft gauge field from a hard particle, Eq. (2.15).

Furthermore we define the jet functions, for example we consider an outgoing quark with momentum p_i ,

$$\bar{u}(p_i) J_i \left(\frac{(p_i \cdot n_i)^2}{n_i^2}, \alpha_s(\mu^2), r_S, r_C \right) = \langle p_i | \bar{\psi}(0) \Phi_{n_i}(0, -\infty) | 0 \rangle, \quad (2.22)$$

where we have also introduced an auxiliary Wilson line in the direction n_i as a source of virtual gluons. A sensible convention is to choose $n_i^2 \neq 0$ to avoid

²We have chosen as a matter of convention to have all Wilson lines incoming to the cusp at which they meet at the origin.

spurious collinear poles, however the amplitude must be insensitive to these auxiliary Wilson lines and therefore any dependence upon n_i will cancel between the jet and eikonal functions. The eikonal jet then can simply be seen as the eikonal approximation of the jet function,

$$\mathcal{J}_i\left(\frac{(\beta_i \cdot n_i)^2}{n_i^2}, \alpha_s(\mu^2), r_S, r_C\right) = \langle 0 | \Phi_{\beta_i}(0, -\infty) \otimes \Phi_{n_i}(0, -\infty) | 0 \rangle, \quad (2.23)$$

which, as mentioned above, exists purely to remove the double counting of all singularities which are not generated by regions of loop phase space purely collinear to the parton i .

If we were to reverse our condition on the mass of the external particles and so instead stipulate $\beta_i^2 \neq 0$ for every i , we will no longer have collinear divergences (following the discussion in Ch. 1). In this case, the jet functions will contain only soft divergences, implying that all of their singularities can be determined through their eikonal approximation. Thus, the ratio J_i/\mathcal{J}_i is finite to all orders and so we absorb this finite factor into the hard function. Having fewer singular regions naturally results in a simpler factorization of the amplitude,

$$\mathcal{M}_L = S_{LK}(\gamma_{ij}, \alpha_s(\mu^2), r_S) \tilde{H}_K\left(\frac{p_i \cdot p_j}{\mu^2}, \frac{p_i \cdot n_i}{\sqrt{n_i^2}}, \alpha_s(\mu^2)\right), \quad (2.24)$$

where we have defined the cusp angle,

$$\gamma_{ij} = \frac{2\beta_i \cdot \beta_j}{\sqrt{\beta_i^2 \beta_j^2}}. \quad (2.25)$$

Given that in the example above, Sec. 2.1, we chose not to neglect the electron mass, the factorized form we found in Eq. (2.13) demonstrates precisely the form of Eq. (2.24), though clearly the abelian analogue in which the soft and hard functions are scalar, given that the gauge group structure is trivial.

Clearly, it is not the case in QCD that all external particles can be considered massive. Not only is it possible for hard gluons to emit soft gluons, but also the light quarks are effectively massless at the energy scales produced in modern collider experiments. Despite this, the approach we will adopt is to assert that all $\beta_i^2 \neq 0$. We do this to avoid the UV+collinear mixed region from which the singularities will ruin the multiplicative renormalizability of the soft function. We

$$S_{\text{QED}} = \exp \left(\begin{array}{c} \text{---} \\ \diagup \quad \diagdown \\ \bullet \quad \text{---} \\ \diagdown \quad \diagup \\ \text{---} \end{array} + \begin{array}{c} \text{---} \\ \diagup \quad \diagdown \\ \bullet \quad \text{---} \\ \diagdown \quad \diagup \\ \text{---} \end{array} + \begin{array}{c} \text{---} \\ \diagup \quad \diagdown \\ \bullet \quad \text{---} \\ \diagdown \quad \diagup \\ \text{---} \end{array} + \dots \right)$$

Figure 2.3: Diagrammatic exponentiation of the soft function in an abelian theory. Only ‘connected’ diagrams contribute.

will return to this issue in Sec. 2.4.1 after introducing the renormalization of the non-null soft function.

To then recover the singularities of physical amplitudes in QCD with massless (or approximately massless) particles, we can consider the ‘tilt’ off the lightcone, β_i^2 , as the collinear regulator, r_C , and so the collinear poles will be recovered as logarithmic singularities as $\beta_i^2 \rightarrow 0$ in the soft and jet functions as found in equation (2.18). Moreover, through this strategy we also solve more general problems, including massive quark production where some β_i^2 remain non-zero.

2.3 Exponentiation and Webs

Having now factorized the singularities of our amplitude in accordance with Eqs. (2.18) and (2.24) we will focus on the properties of the soft function, S . While, naturally, any quantity can be written as the exponential of its logarithm, we found in the example of Sec. 2.1 that the exponent of the e^+e^- form-factor soft-function has a diagrammatic interpretation in terms of the eikonal Feynman rules, Eq. (2.14); for example the subset of diagrams shown in Fig. 2.3. It was first discovered that this was the case in the context of abelian theories in Ref. [100] before being proven to hold in non-abelian theories through what is known as the *non-abelian exponentiation theorem* in Refs. [90–92]. This was recently generalized to the multiparton case [61]. In this section, we shall focus on diagrammatic exponentiation in non-abelian theories and in doing so will introduce the key quantities which we shall study throughout the remainder of the thesis, namely webs.

Let us first restrict ourselves to only two Wilson lines. In the abelian case, the exponent is composed of only the connected diagrams at each order [90–92],

$$S_{\text{QCD}} = \exp \left(\begin{array}{c} \text{---} \\ \diagup \quad \diagdown \\ \bullet \\ \diagdown \quad \diagup \\ \text{---} \end{array} + \begin{array}{c} \text{---} \\ \diagup \quad \diagdown \\ \bullet \\ \diagdown \quad \diagup \\ \text{---} \end{array} + \begin{array}{c} \text{---} \\ \diagup \quad \diagdown \\ \bullet \\ \diagdown \quad \diagup \\ \text{---} \end{array} + \begin{array}{c} \text{---} \\ \diagup \quad \diagdown \\ \bullet \\ \diagdown \quad \diagup \\ \text{---} \end{array} + \dots \right)$$

Figure 2.4: Diagrammatic exponentiation of the soft function in a non-abelian theory. Note the appearance of diagrams such as the second which would be ‘disconnected’ in an abelian theory.

known as webs. To be specific, what we mean by connected in this context is that if we ignore the Wilson lines, the diagram remains one connected piece. All unconnected diagrams are then reproduced as powers of the connected diagrams in expansion of exponential, which is fairly simple to see in an abelian theory given that ordering on the Wilson lines is immaterial. This can be seen by repeating the application of the eikonal identity to diagrams with bubbles and will exponentiate in the same manner as before [100]. Affairs are made more difficult when we begin to consider multiple photon attachments to a single fermion loop, though there exist now several proofs of their exponentiation through more elegant means [56, 101].

As we have stated, the exponentiation observed in the example of Sec. 2.1 extends to the non-abelian case [90–92]. However, given that in a non-abelian theory ordering of emissions on the lines must be taken into account, the webs cannot simply be the connected graphs. In Fig. 2.4 we see the exponent contains diagrams such as the ‘X’ graph, which in the abelian sense are disconnected. One important point to note here is that while the diagrams of Fig. 2.4 do correspond to their respective kinematic factors, they appear with an exponentiated colour factor (ECF) which would normally belong to the fully connected webs at the same order. For this reason they are often referred to as the maximally non-abelian colour factors and this result is referred to as the *non-abelian exponentiation theorem* [90–92].

Moreover, if we extend to non-abelian multiparton scattering³ many more clearly disconnected diagrams appear, for example those shown in Fig. 2.7. The

³In an abelian theory the extension to the multiparton case is trivial. Since ordering on the lines is irrelevant, the multiline singularities are given by a product of two line soft functions depending upon each cusp angle in turn.

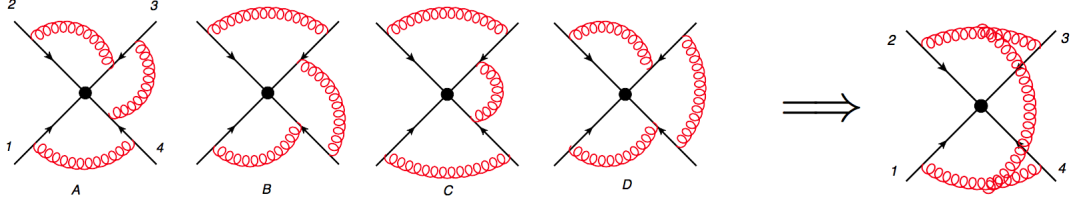


Figure 2.5: (1,2,2,1) web and associated exponentiated colour factor represented by the rightmost diagram.

multiparton extension of the non-abelian exponentiation theorem [61] implies that ECFs of multiline webs correspond to the colour factors of fully connected multiline graphs, for example the web and accompanying ECF shown in Fig. 2.5. The exponent can therefore be written as a sum over diagrams, D , with kinematic factors $\mathcal{F}(D)$ and ECFs $\tilde{C}(D)$ in terms of multiparton webs, W_i such that

$$S = \exp \left(\sum_i W_i \right) \quad (2.26)$$

where we define a web according to [56]

$$W_i = \sum_{D \in W_i} \mathcal{F}(D) \tilde{C}(D) = \sum_{D, D' \in W_i} \mathcal{F}(D) R_{DD'}^{(W_i)} C(D'). \quad (2.27)$$

Here, D and D' index the diagrams contributing to a web, which differ only by permutation of ordering of emissions on the Wilson lines⁴, and $C(D')$ is the diagrammatic colour factor belonging to diagram D' . The *web mixing matrix*, $R_{DD'}^{(W)}$, is a combinatorial object which determines the precise combination of ECFs with which a kinematic factor will appear. These matrices can be computed through the methodology of Ref. [56], and through these studies it has been proven to satisfy some useful properties [56, 57, 59, 93], the principal of which for our purposes is *idempotence* [56, 57]. This means that for any web mixing matrix R ,

$$R_{DE} = \sum_{D'} R_{DD'} R_{D'E}, \quad \forall D, E. \quad (2.28)$$

All idempotent matrices are diagonalizable and have eigenvalues 0, 1. Therefore,

⁴For example, as in diagrams A, B, C, D in Fig. 2.5

R can be seen as a projection operator with only those colour factors which appear in the exponent corresponding to the eigenvalue 1 eigenvectors. Those colour factors corresponding to eigenvalue 0 eigenvectors are reproduced by products of lower order webs in the expansion of the exponential [56].

Using the idempotence property, a web W , connecting L Wilson lines, can be conveniently expressed as

$$W = \sum_{j=1}^r \left(\sum_D \mathcal{F}(D) Y_{D,j}^{-1} \right) \left(\sum_{D'} Y_{j,D'} C(D') \right) = \sum_{j=1}^r \mathcal{F}_{W,j} c_j^{(L)}, \quad (2.29)$$

where r is the rank of R (which is always smaller than its dimension d) and Y is the diagonalizing matrix, $YRY^{-1} = \text{diag}(\lambda_1, \lambda_2, \dots, \lambda_d)$, with $\lambda_i = 1$ for $i \leq r$ and $\lambda_i = 0$ otherwise. Thus the first r eigenvectors of R , all corresponding to unit eigenvalue, determine r linear combinations of colour factors, $c_j^{(L)} = \sum_{D'} Y_{j,D'} C(D')$, each of which is associated with a particular linear combination of kinematic integrals $\mathcal{F}_{W,j} = \sum_D \mathcal{F}(D) Y_{D,j}^{-1}$ formed out of the diagrams in the web.

2.4 Renormalization of multiparton webs

Returning to the one loop example of Sec. 2.1, after applying the eikonal approximation, resulting in Eq. (2.4), power counting reveals something which at first seems surprising. In the UV limit, $k^\mu \rightarrow \infty$, the superficial degree of divergence, $D = d - 4$, implies a logarithmic UV divergence despite the fact that the theory is already renormalized. Consequently we must separately renormalize the soft function. This arises due to the scale invariance we introduce through the eikonal approximation, which removes the distinction between UV and IR and so we must expect there to be some mapping between these UV poles and the original IR poles of our amplitude. Moreover, we cannot expect the UV region of the eikonal diagrams to have physical significance of their own given that the eikonal limit is expressly soft.

To carry out this renormalization, we will make a distinction between dimensional regularization regularizing the IR singularities, $\epsilon_{\text{IR}} < 0$ and the UV,

$\epsilon_{UV} > 0$ and so allowing us to define a renormalized soft function,

$$S_{\text{ren}}(\gamma_{ij}, \alpha_s(\mu_R^2), \epsilon_{\text{IR}}, \mu) = S(\gamma_{ij}, \alpha_s(\mu_R^2), \epsilon_{\text{IR}}, \epsilon_{UV}) Z(\gamma_{ij}, \alpha_s(\mu_R^2), \epsilon_{UV}, \mu), \quad (2.30)$$

relying on the multiplicative renormalizability of products of non-null Wilson lines [28–31]. We shall call this *cusplike renormalization*, introducing the renormalization scale μ .

In pure dimensional regularization however, all scaleless integrals vanish. To illustrate this, consider the logarithmically divergent, two-dimensional integral $\int_{-\infty}^{\infty} d^2k/k^2$. Clearly this integral does not depend upon the scale of k . If we were to impose dimensional regularization on this integral yielding $\int d^d k/k^2$, with $d = 2 - \epsilon$ we must expect a result proportional to $s^{-\epsilon}(1/\epsilon + \mathcal{O}(\epsilon^0))$ where s has the same dimension as k . As no such quantity is present, the only conclusion can be that the integral vanishes. Also note that γ_{ij} , as defined in Eq. (2.25), is a scaleless quantity resulting in the vanishing of all contributions to the soft function exponent at all orders. Imposing this on Eq. (2.30) confirms our intuitive identification of the cusp UV singularities with the IR singularities,

$$S_{\text{ren}}(\gamma_{ij}, \alpha_s(\mu_R^2), \epsilon_{\text{IR}}, \mu) = Z(\gamma_{ij}, \alpha_s(\mu_R^2), \epsilon_{UV}, \mu), \quad (2.31)$$

and so through Eq. (2.24), can determine the IR singularities of the non-lightlike amplitude,

$$\mathcal{M} = Z(\gamma_{ij}, \alpha_s(\mu_R^2), \epsilon_{UV}, \mu) \tilde{H}(p_i, \alpha_s(\mu^2)), \quad (2.32)$$

by renormalizing the Wilson line correlator, as has been utilized by multiple authors [3, 27, 58, 77, 102, 103]. To continue with this analysis we must introduce further regulation to make a clear separation between the UV and IR, and to introduce a scale so that contributions to the soft function exponent are non-vanishing in dimensional regularization. Rewriting Eq. (2.30) with an IR regulator⁵ associated with the scale m ,

$$S_{\text{ren}}(\gamma_{ij}, \alpha_s(\mu^2), m) = S(\gamma_{ij}, \alpha_s(\mu^2), \epsilon, m) Z(\gamma_{ij}, \alpha_s(\mu^2)), \quad (2.33)$$

⁵In Sec. 2.5 we shall introduce the particular regulation scheme which shall be used throughout the thesis.

with $\epsilon > 0$ regulating the UV cusp singularities. We now introduce the *soft anomalous dimension*, Γ , through the renormalization group equation,

$$\frac{d}{d \log \mu} Z(\gamma_{ij}, \alpha_s(\mu^2), \epsilon) = -Z(\gamma_{ij}, \alpha_s(\mu^2), \epsilon) \Gamma(\gamma_{ij}, \alpha_s(\mu^2)), \quad (2.34)$$

which depends upon the renormalization scale only through the running coupling after we choose to identify the two renormalization scales $\mu_R = \mu$. Furthermore, by inverting Eq. (2.30),

$$S(\gamma_{ij}, \alpha_s(\mu_R^2), \epsilon_{\text{IR}}, \epsilon_{\text{UV}}) = S_{\text{ren}}(\gamma_{ij}, \alpha_s(\mu_R^2), \epsilon_{\text{IR}}, \mu) Z^{-1}(\gamma_{ij}, \alpha_s(\mu_R^2), \epsilon_{\text{UV}}, \mu) \quad (2.35)$$

and, noting that the unrenormalized soft function does not depend upon the cusp-renormalization scale, taking a derivative with respect to $\log \mu$ yields,

$$0 = \frac{dS_{\text{ren}}}{d \log \mu} Z^{-1} + S_{\text{ren}} \frac{dZ^{-1}}{d \log \mu} \quad (2.36)$$

which after rearranging Eq. (2.34),

$$\Gamma = -Z^{-1} \frac{dZ}{d \log \mu} = \frac{dZ^{-1}}{d \log \mu} Z, \quad (2.37)$$

and substituting into Eq. (2.36) we find,

$$\Gamma = -S_{\text{ren}}^{-1} \frac{dS_{\text{ren}}}{d \log \mu}. \quad (2.38)$$

An important conclusion that we can draw from Eq. (2.38) is that Γ is finite in four dimensions, given that S_{ren} is UV finite by definition and because Eq. (2.34) makes it clear that Γ cannot depend on the IR regulator. Furthermore, after the identification of the renormalization scales, Γ depends on μ only through the d -dimensional, renormalized coupling and so in its perturbative expansion,

$$\Gamma(\gamma_{ij}, \alpha_s(\mu^2)) = \sum_{n=1}^{\infty} \alpha_s^n(\mu^2) \Gamma^{(n)}(\gamma_{ij}), \quad (2.39)$$

the dependence upon μ factorizes. Thus, all of the UV poles of Z (and therefore IR poles of S_{ren}) are generated by the integral over the running coupling in the

solution of Eq. (2.34),

$$Z(\gamma_{ij}, \alpha_s(\mu^2, \epsilon), \epsilon) = \exp \left(-\frac{1}{2} \sum_{n=1}^{\infty} \int_0^{\mu^2} \frac{d\xi^2}{\xi^2} \alpha_s^n(\xi^2, \epsilon) \Gamma^{(n)}(\gamma_{ij}) \right), \quad (2.40)$$

where we have made explicit the dependence of the running coupling upon the dimensional regularization parameter.

Note as well that the ordering on the right-hand side of Eq. (2.34) is important: both Z and Γ are matrix valued, and therefore do not commute in general. The solution of Eq. (2.34) can be written in accordance with Eq. (2.40), as in Ref. [58],

$$\begin{aligned} Z(\alpha_s, \epsilon) = \exp \left\{ \alpha_s \frac{1}{2\epsilon} \Gamma^{(1)} + \alpha_s^2 \left(\frac{1}{4\epsilon} \Gamma^{(2)} - \frac{b_0}{4\epsilon^2} \Gamma^{(1)} \right) \right. \\ + \alpha_s^3 \left(\frac{1}{6\epsilon} \Gamma^{(3)} + \frac{1}{48\epsilon^2} [\Gamma^{(1)}, \Gamma^{(2)}] - \frac{1}{6\epsilon^2} (b_0 \Gamma^{(2)} + b_1 \Gamma^{(1)}) + \frac{b_0^2}{6\epsilon^3} \Gamma^{(1)} \right) \\ + \alpha_s^4 \left(\frac{1}{8\epsilon} \Gamma^{(4)} + \frac{1}{48\epsilon^2} [\Gamma^{(1)}, \Gamma^{(3)}] - \frac{b_0}{8\epsilon^2} \Gamma^{(3)} + \frac{1}{8\epsilon^2} \left(\frac{b_0^2}{\epsilon} - b_1 \right) \Gamma^{(2)} \right. \\ \left. \left. - \frac{1}{8\epsilon^2} \left(\frac{b_0^3}{\epsilon^2} - \frac{2b_0 b_1}{\epsilon} + b_2 \right) \Gamma^{(1)} - \frac{b_0}{48\epsilon^3} [\Gamma^{(1)}, \Gamma^{(2)}] \right) + \mathcal{O}(\alpha_s^5) \right\}, \end{aligned} \quad (2.41)$$

where we did not display the dependence on γ_{ij} for simplicity, we expanded the soft anomalous dimension $\Gamma(\alpha_s)$ in powers of α_s , and b_n is the n^{th} -order coefficient of the β -function. As discussed already extensively in Refs. [58, 60], the matrix nature of $\Gamma^{(n)}$ entails the presence of higher-order poles in the exponent of Eq. (2.41), involving commutators of lower-order contributions, even in a conformal theory where $\beta(\alpha_s) = 0$. At $\mathcal{O}(\alpha_s^n)$, the genuinely new information enters in the coefficient of the single $1/\epsilon$ pole, $\Gamma^{(n)}$. This can be directly computed from the unrenormalized webs as follows. First, one may write the unrenormalized soft function as

$$S(\alpha_s, \epsilon) = \exp \left[w(\alpha_s, \epsilon) \right] = \exp \left[\sum_{n=1}^{\infty} \sum_{k=-n}^{\infty} \alpha_s^n \epsilon^k w^{(n,k)} \right], \quad (2.42)$$

where $w = \sum_i W_i$, with webs W_i as defined in Eq. (2.27), and we again omitted for simplicity the dependence on γ_{ij} and on the IR regulator m : the dependence on m will in any case cancel at the level of the anomalous dimension. Note that, while the physically relevant matrix Z is a pure counterterm, *i.e.* it contains

only poles in ϵ , the IR-regularized, unrenormalized correlator S has also non-singular dependence on ϵ , which plays a non-trivial role. Indeed, in the notation of Eq. (2.42), the first few perturbative coefficients of the soft anomalous dimensions can be written as [58]

$$\begin{aligned}
 \Gamma^{(1)} &= -2w^{(1,-1)}, \\
 \Gamma^{(2)} &= -4w^{(2,-1)} - 2[w^{(1,-1)}, w^{(1,0)}], \\
 \Gamma^{(3)} &= -6w^{(3,-1)} + \frac{3}{2}b_0[w^{(1,-1)}, w^{(1,1)}] \\
 &\quad + 3[w^{(1,0)}, w^{(2,-1)}] + 3[w^{(2,0)}, w^{(1,-1)}] \\
 &\quad + [w^{(1,0)}, [w^{(1,-1)}, w^{(1,0)}]] - [w^{(1,-1)}, [w^{(1,-1)}, w^{(1,1)}]], \\
 \Gamma^{(4)} &= -8w^{(4,-1)} + \frac{4}{3}b_0^2[w^{(1,2)}, w^{(1,-1)}] + b_0\left(-2[w^{(2,1)}, w^{(1,-1)}] \right. \\
 &\quad - \frac{8}{3}[w^{(1,1)}, w^{(2,-1)}] + [w^{(1,1)}, [w^{(1,0)}, w^{(1,-1)}]] \\
 &\quad \left. - \frac{2}{3}[w^{(1,0)}, [w^{(1,-1)}, w^{(1,1)}]] + \frac{4}{3}[w^{(1,-1)}, [w^{(1,-1)}, w^{(1,2)}]]\right) \\
 &\quad + \frac{4}{3}b_1[w^{(1,-1)}, w^{(1,1)}] + 4[w^{(1,0)}, w^{(3,-1)}] + 4[w^{(3,0)}, w^{(1,-1)}] \\
 &\quad + 4[w^{(2,0)}, w^{(2,-1)}] + 2[w^{(1,1)}, [w^{(2,-1)}, w^{(1,-1)}]] \\
 &\quad + \frac{8}{3}[w^{(1,-1)}, [w^{(1,1)}, w^{(2,-1)}]] - \frac{4}{3}[w^{(2,0)}, [w^{(1,0)}, w^{(1,-1)}]] \\
 &\quad - \frac{4}{3}[w^{(1,0)}, [w^{(2,0)}, w^{(1,-1)}]] + \frac{4}{3}[w^{(1,-1)}, [w^{(2,1)}, w^{(1,-1)}]] \\
 &\quad - \frac{4}{3}[w^{(1,0)}, [w^{(1,0)}, w^{(2,-1)}]] - \frac{1}{3}[w^{(1,-1)}, [w^{(1,-1)}, [w^{(1,0)}, w^{(1,1)}]]] \\
 &\quad - \frac{1}{3}[w^{(1,-1)}, [w^{(1,0)}, [w^{(1,-1)}, w^{(1,1)}]]] + [w^{(1,0)}, [w^{(1,-1)}, [w^{(1,-1)}, w^{(1,1)}]]] \\
 &\quad + \frac{1}{3}[w^{(1,0)}, [w^{(1,0)}, [w^{(1,0)}, w^{(1,-1)}]]] - \frac{1}{3}[w^{(1,-1)}, [w^{(1,-1)}, [w^{(1,-1)}, w^{(1,2)}]]],
 \end{aligned} \tag{2.43}$$

which is sufficient to calculate the soft anomalous dimension up to four-loops. Notice that the exponent $w(\alpha_s, \epsilon)$ in Eq. (2.42) is given by a sum of regularized webs w_i . Similarly, all commutator subtraction in Eq. (2.43) can be organized on a web-by-web basis: one must subtract from each web all appropriate commutators constructed from subdiagrams of the diagrams comprising the original web. The contributions to the soft anomalous dimension are then given by the simple pole of the chosen web, plus all simple-pole contributions from the commutator

counterterms⁶. This combination of simple poles was called a *subtracted web* in [60]. For example, at the three-loop level subtracted webs have the structure

$$\begin{aligned} \overline{w}^{(3)} &= w^{(3,-1)} - \frac{1}{2} [w^{(1,0)}, w^{(2,-1)}] - \frac{1}{2} [w^{(2,0)}, w^{(1,-1)}] \\ &\quad - \frac{1}{6} [w^{(1,0)}, [w^{(1,-1)}, w^{(1,0)}]] - \frac{1}{6} [w^{(1,-1)}, [w^{(1,1)}, w^{(1,-1)}]] . \end{aligned} \quad (2.44)$$

with β -function contributions appearing in webs with UV subdivergences corresponding to the renormalization of the strong coupling (e.g. webs containing bubble subdiagrams). While the separate contributions of non-subtracted webs and the corresponding commutator counterterms have higher-order UV poles, making them sensitive to the infrared regulator used to calculate the integrals, subtracted webs, which directly contribute to the soft anomalous dimension $\Gamma^{(n)}$, are free of these artifacts [60]. A further consequence of this is that the coefficients $w^{(n,k)}$ for $-n < k < -1$ are expressible in terms of commutators of lower order webs [58]. For example,

$$w^{(3,-2)} \Big|_{\beta_n=0} = \frac{1}{6} [w^{(2,-1)}, w^{(1,-1)}] . \quad (2.45)$$

Subtracted webs are the direct analogue of the webs appearing in colour-singlet two-line correlators, as originally defined in [90–92], which individually have just a single UV pole.

2.4.1 Aside: correlators of lightlike Wilson lines

We shall now briefly discuss the computation of webs with strictly lightlike Wilson lines ($\beta_i^2 = 0$). One may be tempted, since most scattering at hadron colliders occurs between gluons and light quarks, to compute the soft function in the absence of the collinear regulation we have applied above. Indeed, this greatly simplifies the integrals involved and some recent work in this direction Ref. [53] has proposed a scheme to compute the lightlike, two-line exponent. However, in doing so one replaces complexity of the integrand, as found in the collinear regulated soft function, with conceptual complexity in the computation of the lightlike soft function. Principally this is caused by the failing of the multiplicative

⁶Note that the commutators also involve coefficients of positive powers of ϵ in the lower order webs. The overall power of ϵ associated with each commutator is, however, ϵ^{-1} .

renormalizability of the soft function, Eq. (2.31), due to the mixed UV+collinear region [36].

Despite this lack of renormalizability, evolution equations can be written for lightlike correlators [36] and a soft anomalous dimension defined and recent efforts have put forward a potential framework for the determination of the leading poles [53]. The lightlike soft anomalous dimension has been shown to have a highly constrained form, leading to the famous dipole formula [77, 79], which may have violations starting at three loops [82, 89]. However, without the constraints that renormalizability places on this anomalous dimension, such as those found in the collinear regulated case [58], it is unclear how one might define a regulator independent framework for the computation of this anomalous dimension in terms of webs. This is especially true when we move to multiparton scattering, where the notion of subtracted webs becomes key to a diagrammatic determination of the soft anomalous dimension. Without these constraints to rely on, a representation such as Eq. (2.43) has yet to be found.

In light of these facts, and in spite of the increase in computational difficulty, it seems that the best way to attempt a computation of the lightlike, multiparton soft anomalous dimension is best approached through an asymptotic lightlike limit of the collinear regulated approach we adopt in this thesis. This has been applied to the two-loop multiparton case [66] and recently also to three loops [89].

2.5 Computing web kinematics

Having reviewed the prescription through which the coefficients of the soft anomalous dimension perturbative expansion can be determined by the Laurent series of the given webs at that order, in this section we go on to review how such calculations are carried out in practice and the resulting analytic structure. We shall also highlight some properties of webs that will be useful in the coming chapters, as well as the mathematical concepts which come into play. We do this by going through in some detail the computation of two subtracted webs: the one-loop web, and the (1,2,1) subtracted web. The notation (n_1, n_2, \dots) indicates the number of gluon attachments to each Wilson line (n_1 attachments to the first, n_2 to the second and so on). Where this is ambiguous, the particular web in question will be made explicit contextually. This example will allow us to

illustrate some of the key results of [60] regarding the general analytic structure of webs and will demonstrate the particular integral parametrization which we generalize in Ch. 3 and use again in Ch. 4.

We first consider the one-loop contribution to the soft function, as discussed in Sec. 2.1, however having first Fourier transformed to configuration space in which we shall see our problem is more naturally described. Before this, we must first make explicit the IR regulator which we introduced in Sec. 2.4 when renormalizing the soft function.

We desire a regulator which will preserve the symmetries of the problem, in particular the invariance under rescaling of the Wilson line velocities $\beta_i^\mu \rightarrow \kappa \beta_i^\mu$, and so will follow [58] by introducing an exponential damping factor to the Wilson line integrals, Eq. (2.19),

$$\Phi_{\beta_i}^{(m)} = \mathcal{P} \exp \left[ig\mu^\epsilon \int_0^\infty d\lambda \beta_i \cdot A(\lambda\beta_i) e^{-im\lambda\sqrt{\beta_i^2 - i\epsilon}} \right], \quad (2.46)$$

so that one recovers the unregulated Wilson line as $m \rightarrow 0$. With this definition, the correlator S is finite in $d = 4 - 2\epsilon$, for $\epsilon > 0$: potential collinear divergences are again regulated by keeping $\beta_i^2 \neq 0$; infrared divergences are regulated by the exponential cut-off m , and ultraviolet divergences show up as poles in ϵ as $\epsilon \rightarrow 0^+$.

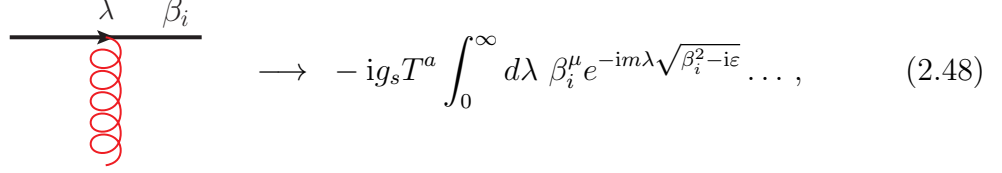
As discussed in Ref. [60], the $i\epsilon$ -prescription in Eq. (2.46) ensures convergence at $\lambda \rightarrow \infty$. We can see this by noting that $\beta_i^2 - i\epsilon = |\beta_i^2| \exp(-i\theta)$ with $\theta > 0$. Then for time-like lines $\theta \rightarrow 0^+$ giving $-im\lambda\sqrt{\beta_i^2 - i\epsilon} = -im\lambda\sqrt{|\beta_i^2|}(1 - i\epsilon/2)$, while for space-like lines $\theta \rightarrow \pi$ ($\theta < \pi$) yielding $-im\lambda\sqrt{\beta_i^2 - i\epsilon} = -im\lambda\sqrt{-\beta_i^2}(-i)$.

The IR regularized soft function,

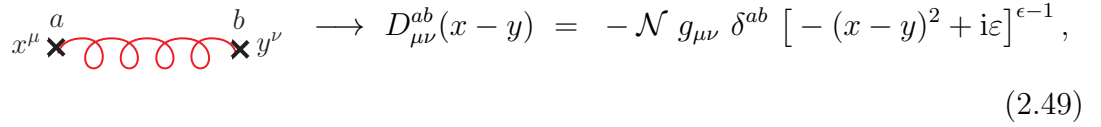
$$S\left(\gamma_{ij}, \alpha_s(\mu^2), \epsilon, \frac{m}{\mu}\right) = \left\langle \prod_i \Phi_{\beta_i}^{(m)}(0, \infty) \right\rangle_0, \quad (2.47)$$

will therefore have corrections described by the following configuration-space

Feynman rules (we choose throughout the thesis to work in Feynman gauge):



$$\longrightarrow -ig_s T^a \int_0^\infty d\lambda \beta_i^\mu e^{-im\lambda\sqrt{\beta_i^2 - i\epsilon}} \dots, \quad (2.48)$$



$$\longrightarrow D_{\mu\nu}^{ab}(x-y) = -\mathcal{N} g_{\mu\nu} \delta^{ab} [-(x-y)^2 + i\epsilon]^{\epsilon-1}, \quad (2.49)$$

where a, b are adjoint colour indices and,

$$\mathcal{N} = \frac{\Gamma(1-\epsilon)}{4\pi^{2-\epsilon}}, \quad (2.50)$$

which is the more natural form in which to express eikonal contributions since the Wilson lines follow the *straight* classical trajectories of the hard partons, thus reducing the emission vertex position integrals to a single dimension. For example, following [58], the one-loop web Fig. 2.6, where we choose for now to have all β_i space-like for convenience⁷, is given in configuration-space by

$$w^{(1)}(\gamma_{12}) = (-i)^2 4\pi T_1^a T_2^b \int_0^\infty d\lambda_1 d\lambda_2 \beta_1^\mu \beta_2^\nu D_{\mu\nu}^{ab}(\lambda_1\beta_1 - \lambda_2\beta_2) \times e^{-im(\lambda_1\sqrt{-\beta_1^2} + \lambda_2\sqrt{-\beta_2^2})}, \quad (2.51)$$

where summation over the adjoint colour indices is implicit. By rescaling $\tilde{\lambda}_i = \lambda_i\sqrt{-\beta_i^2}$ followed by,

$$\begin{pmatrix} \tilde{\lambda}_1 \\ \tilde{\lambda}_2 \end{pmatrix} \longrightarrow \sigma \begin{pmatrix} x \\ 1-x \end{pmatrix}, \quad \sigma \in (0, \infty), x \in (0, 1), \quad (2.52)$$

⁷We could similarly have chosen to take the Wilson lines to be timelike, $\beta_i^2 > 0$ for all i . Note that in this case the $-i\epsilon$ prescription is important for the IR regulator, and it can be implemented by taking $m \rightarrow m - i\epsilon$, ending up with the same final result.

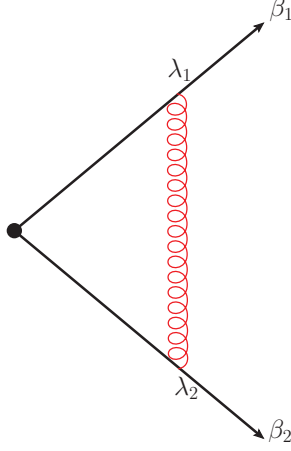


Figure 2.6: The one-loop web, $w^{(1)}$, found in the familiar cusp anomalous dimension (see e.g. Ref. [3])

for which the Jacobian $\det[\mathcal{J}] = \sigma$, we obtain

$$w^{(1)}(\gamma_{12}) = 2\pi \mathcal{N} T_1^a T_2^a \int_0^\infty d\sigma \sigma^{2\epsilon-1} e^{-m\sigma} \int_0^1 dx \gamma_{12} P_\epsilon(x, \gamma_{12}), \quad (2.53)$$

where we have introduced,

$$P_\epsilon(x, \gamma_{ij}) = [x^2 + (1-x)^2 - \gamma_{ij}x(1-x)]^{\epsilon-1}, \quad (2.54)$$

which is related to the propagator through the above rescaling, and depending upon the angle

$$\gamma_{ij} \equiv \frac{2\beta_i \cdot \beta_j + i\epsilon}{\sqrt{\beta_i^2 - i\epsilon} \sqrt{\beta_j^2 - i\epsilon}}, \quad (2.55)$$

which we introduced in Eq. (2.25), though here we have specified how the kinematic invariants should be analytically continued as described in Ref. [60].

This parametrization of the integrals can be interpreted geometrically by first inverting Eq. (2.52),

$$\sigma = \tilde{\lambda}_1 + \tilde{\lambda}_2, \quad x = \frac{\tilde{\lambda}_1}{\tilde{\lambda}_1 + \tilde{\lambda}_2}, \quad (2.56)$$

where we can see that σ encodes the total distance of the diagram from the cusp

so giving the cusp UV divergence at $\sigma \rightarrow 0$ and the IR singularity (regulated by m) at $\sigma \rightarrow \infty$, while x can be interpreted as the *tilt* of the diagram with $x = 0$ at $\tilde{\lambda}_1 = 0$, $x = 1$ at $\tilde{\lambda}_2 = 0$ and $x = 1/2$ at $\tilde{\lambda}_1 = \tilde{\lambda}_2$. This particular parametrization will reappear in every web example found throughout this thesis, in particular it will be generalized to n -loop webs in Ch. 3 and then applied to several three loop, and four loop examples. In Ch. 4 it will again return in the study of webs containing three gluon vertices.

Continuing with Eq. (2.53), we can use the integral identities

$$\int_0^\infty d\sigma \sigma^{p\epsilon-1} e^{-\sigma X} = X^{-p\epsilon} \Gamma(p\epsilon) \quad (2.57)$$

and

$$\int_0^1 dx P_\epsilon(x, \gamma_{ij}) = {}_2F_1\left(1, 1 - \epsilon; \frac{3}{2}; \frac{1}{2} + \frac{\gamma_{ij}}{4}\right), \quad (2.58)$$

which comes from the integral representation of the Gaussian hypergeometric function,

$${}_2F_1(a, b; c; z) = \frac{\Gamma(c)}{\Gamma(b)\Gamma(c-b)} \int_0^1 dt t^{b-1} (1-t)^{c-b-1} (1-tz)^{-a} \quad (2.59)$$

after $t = 4x(1-x)$, therefore giving the all-order-in- ϵ result for the one-loop web:

$$w^{(1)}(\gamma_{12}) = -2\pi T_1^a T_2^a \left(\frac{\mu^2}{m^2}\right)^\epsilon \mathcal{N}_{\gamma_{12}} {}_2F_1\left(1, 1 - \epsilon; \frac{3}{2}; \frac{1}{2} + \frac{\gamma_{12}}{4}\right). \quad (2.60)$$

Given however that to compute the anomalous dimension coefficients, $\Gamma^{(n)}$, we need the coefficients of the Laurent series of the web in the dimensional regularization parameter, $w^{(n,k)}$, it is far more typical and far more convenient not to attempt an all-order-in- ϵ computation of webs, such as was possible for $w^{(1)}$. Instead, we write webs in a form such that the coefficients of their ϵ Laurent expansion can be individually integrated order-by-order. To do so, we first introduce kinematic variables α_{ij} which in terms of γ_{ij} are given by,

$$\alpha_{ij} = \frac{1 - \sqrt{\frac{\gamma_{ij}+2}{\gamma_{ij}-2}}}{1 + \sqrt{\frac{\gamma_{ij}+2}{\gamma_{ij}-2}}}, \quad \text{or} \quad \gamma_{ij} = -\alpha_{ij} - \frac{1}{\alpha_{ij}}, \quad (2.61)$$

which were shown in Ref. [60] to more naturally describe the analytic and asymptotic behaviour of webs, and especially subtracted webs. We rephrase our integrals in terms of these kinematic variables by defining the functions,

$$p_\epsilon(x, \alpha_{ij}) = p_0(x, \alpha_{ij}) (q(x, \alpha_{ij}))^\epsilon, \quad (2.62)$$

$$q(x, \alpha_{ij}) = (x^2 + (1-x)^2 + (\alpha_{ij} + 1/\alpha_{ij})x(1-x)), \quad (2.63)$$

where

$$p_0(x, \alpha) = - \left(\alpha + \frac{1}{\alpha} \right) \frac{1}{q(x, \alpha)} = r(\alpha) \left[\frac{1}{x - \frac{1}{1-\alpha}} - \frac{1}{x + \frac{\alpha}{1-\alpha}} \right], \quad (2.64)$$

and we have defined the rational function

$$r(\alpha) = \frac{1 + \alpha^2}{1 - \alpha^2}. \quad (2.65)$$

Written in these terms the one-loop web,

$$w^{(1)}(\gamma_{12}) = T_1^a T_2^a \kappa \Gamma(2\epsilon) \int_0^1 dx p_\epsilon(x, \alpha_{12}), \quad (2.66)$$

where we have introduced

$$\kappa \equiv -\frac{1}{2\pi^{1-\epsilon}} \left(\frac{\mu^2}{m^2} \right)^\epsilon \Gamma(1-\epsilon). \quad (2.67)$$

If we were now to expand Eq. (2.66) our series would be muddled by superfluous terms proportional to the Euler-Mascheroni constant, γ_E , and logarithms of π which as we will soon see must cancel in subtracted webs. A simplification can be achieved by rescaling⁸ the renormalization scale

$$\mu^2 \rightarrow \tilde{\mu}^2 = \mu^2 \pi e^{-\gamma_E}. \quad (2.68)$$

We do this because, knowing that the overall UV pole at l -loops is contained within $\Gamma(2l\epsilon)$ accompanied by a factor of κ^l , and since it is possible to show using

⁸Note that this clearly differs from the standard modified minimal subtraction scheme where $\mu_{\overline{\text{MS}}}^2 = \mu^2 e^{\gamma_E}/4\pi$

the product representations

$$\Gamma(z) = \frac{e^{-\gamma_E z}}{z} \prod_{k=1}^{\infty} \left(1 + \frac{z}{k}\right)^{-1} e^{\frac{z}{k}}, \quad (2.69)$$

and

$$\Gamma(1+z) = e^{-\gamma_E z} \sqrt{\frac{\pi z}{\sin(\pi z)}} \prod_{k=1}^{\infty} \exp\left(-\frac{\zeta(2k+1)z^{2k+1}}{2k+1}\right), \quad (2.70)$$

that $(e^{\epsilon\gamma_E}\Gamma(1-\epsilon))^l\Gamma(2l\epsilon)$ is free from γ_E , then by making this rescaling we replace κ with

$$\tilde{\kappa} \equiv -\frac{1}{2\pi} \left(\frac{\tilde{\mu}^2}{m^2}\right)^\epsilon e^{\epsilon\gamma_E} \Gamma(1-\epsilon), \quad (2.71)$$

and the expansion of our webs will be free from γ_E and $\log \pi$. While it may seem strange that we are able to change the apparent results of our webs through a change of scheme, recall that from the discussion of Sec. 2.4 we find that $\Gamma^{(n)}$ cannot carry any dependence upon μ and so our choice of scheme will not affect the subtracted webs and therefore, naturally, the soft anomalous dimension itself.

In this way we can write the expansion of the one-loop web,

$$\begin{aligned} w^{(1)}(\gamma_{12}) &= -\frac{1}{4\pi} T_1^a T_2^a \int_0^1 dx p_0(x, \alpha_{12}) \\ &\times \left\{ \frac{1}{\epsilon} + \left[\log q(x, \alpha_{12}) + \log\left(\frac{\tilde{\mu}^2}{m^2}\right) \right] + \mathcal{O}(\epsilon) \right\}, \end{aligned} \quad (2.72)$$

from which we integrate the leading pole (found in the familiar cusp anomalous dimension, see e.g. Ref. [3]),

$$\begin{aligned} w^{(1,-1)}(\alpha_{12}) &= -\frac{1}{4\pi} T_1^a T_2^a \int_0^1 dx p_0(x, \alpha_{12}) \\ &= -\frac{1}{2\pi} T_1^a T_2^a r(\alpha_{ij}) \log(\alpha_{12}). \end{aligned} \quad (2.73)$$

Although the one-loop anomalous dimension, $\Gamma^{(1)}$ from Eq. (2.43), needs only Eq. (2.73), if we look at the higher order terms, $\Gamma^{(n)}$ with $n > 1$, we see that the subtraction terms (commutators) depend upon higher-order in ϵ terms in the

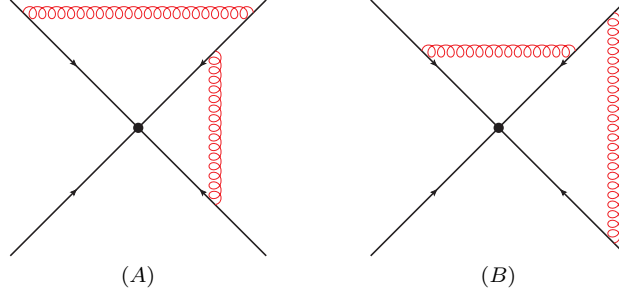


Figure 2.7: Diagrams contributing to the (1,2,1) web through the combination given in Eq. (2.74)

expansion of lower-order webs (in the α_s expansion). Let us now take a look at an example of a subtracted web, illustrating the process of their calculation, with the (1,2,1) web [60, 67–70] – Fig. 2.7. From Ref. [56] we find that the (1,2,1) web is given by the combination,

$$w_{(1,2,1)}^{(2)} = \frac{1}{2} \left(C(A) - C(B) \right) \left(\mathcal{F}_{(1,2,1)}^{(2)}(A) - \mathcal{F}_{(1,2,1)}^{(2)}(B) \right) \quad (2.74)$$

from the web mixing matrix,

$$R^{(1,2,1)} = \frac{1}{2} \begin{pmatrix} 1 & -1 \\ -1 & 1 \end{pmatrix}. \quad (2.75)$$

Using the configuration space Feynman rules given above (recalling that the Wilson lines are path ordered inwards towards the cusp by convention),

$$\begin{aligned} w_{(1,2,1)}^{(2)} &= \frac{1}{2} (T_1^a T_2^a T_2^c T_3^c - T_1^a T_2^c T_2^a T_3^c) (4\pi)^2 (i\mu^\epsilon)^4 (-\mathcal{N})^2 \int_0^\infty ds_1 dt_1 ds_2 dt_2 \\ &\times \beta_1 \cdot \beta_2 \beta_2 \cdot \beta_3 \left[- (s_1 \beta_1 - t_1 \beta_2)^2 \right]^{\epsilon-1} \left[- (s_2 \beta_2 - t_2 \beta_3)^2 \right]^{\epsilon-1} \\ &\times e^{-m \left(s_1 \sqrt{-\beta_1^2} + s_2 \sqrt{-\beta_2^2} + t_1 \sqrt{-\beta_2^2} + t_2 \sqrt{-\beta_3^2} \right)} \\ &\times \left(\theta(t_1 - s_2) - \theta(s_2 - t_1) \right), \end{aligned} \quad (2.76)$$

where for convenience we have once again chosen space-like β_i . Scaling out the factors of $\sqrt{-\beta_i^2}$, $\sigma_1 = s_1 \sqrt{-\beta_1^2}$, $\sigma_2 = s_2 \sqrt{-\beta_2^2}$, $\tau_1 = t_1 \sqrt{-\beta_2^2}$, and $\tau_2 = t_2 \sqrt{-\beta_3^2}$,

and then applying Eq. (2.52) to the parameter pairs (σ_1, τ_1) and (σ_2, τ_2) ,

$$\begin{pmatrix} \sigma_1 \\ \tau_1 \end{pmatrix} \longrightarrow \xi_1 \begin{pmatrix} x \\ 1-x \end{pmatrix}, \quad \begin{pmatrix} \sigma_2 \\ \tau_2 \end{pmatrix} \longrightarrow \xi_2 \begin{pmatrix} y \\ 1-y \end{pmatrix}, \quad (2.77)$$

$$\begin{aligned} w_{(1,2,1)}^{(2)} &= -\frac{i}{8} f^{abc} T_1^a T_2^b T_3^c (4\pi)^2 \mu^{4\epsilon} \mathcal{N}^2 \int_0^\infty d\xi_1 d\xi_2 (\xi_1 \xi_2)^{2\epsilon-1} e^{-m(\xi_1 + \xi_2)} \\ &\times \int_0^1 dx dy \gamma_{12} P_\epsilon(x, \gamma_{12}) \gamma_{23} P_\epsilon(y, \gamma_{23}) \\ &\times [\theta(\xi_1(1-x) - \xi_2 y) - \theta(\xi_2 y - \xi_1(1-x))]. \end{aligned} \quad (2.78)$$

In doing so we have almost factorized the scale from the propagators, as in $w^{(1)}$, though at this point only from the sub-diagrams. Thus the scale integrals are still convoluted by the Heaviside functions. To completely factorize the scale, and in doing so obtain the overall UV pole, we can apply once more the transformation Eq. (2.52),

$$\begin{pmatrix} \xi_1 \\ \xi_2 \end{pmatrix} \longrightarrow \chi \begin{pmatrix} z \\ 1-z \end{pmatrix}, \quad (2.79)$$

which, after changing scheme to that defined by Eq. (2.68) and performing the χ integral, gives

$$\begin{aligned} w_{(1,2,1)}^{(2)} &= -i f^{abc} T_1^a T_2^b T_3^c \tilde{\kappa}^2 \Gamma(4\epsilon) \\ &\times \int_0^1 dx dy p_\epsilon(x, \alpha_{12}) p_\epsilon(y, \alpha_{23}) \phi_{(1,2,1)}(x, y, \epsilon). \end{aligned} \quad (2.80)$$

where we have introduced the *web kernel*,

$$\begin{aligned} \phi_{(1,2,1)}(x, y, \epsilon) &= \frac{1}{2} \int_0^1 dz (z(1-z))^{2\epsilon-1} \\ &\times \left[\theta\left(\frac{z}{1-z} - \frac{y}{1-x}\right) - \theta\left(\frac{y}{1-x} - \frac{z}{1-z}\right) \right], \end{aligned} \quad (2.81)$$

in which we have made explicit the dependence upon the dimensional regularization parameter since this object will in general contain the UV sub-divergences

of the web diagrams. This can be evaluated by use of the integral identities,

$$\begin{aligned} \int_0^1 db b^{-1+q\epsilon}(1-b)^{-1+p\epsilon} \theta\left(A - \frac{b}{1-b}\right) \\ = \frac{1}{q\epsilon} A^{q\epsilon} {}_2F_1\left((p+q)\epsilon, q\epsilon; 1+q\epsilon; -A\right), \end{aligned} \quad (2.82)$$

and

$$\begin{aligned} \int_0^1 db b^{-1+q\epsilon}(1-b)^{-1+p\epsilon} \theta\left(\frac{b}{1-b} - A\right) \\ = \frac{1}{p\epsilon} A^{-p\epsilon} {}_2F_1\left((p+q)\epsilon, p\epsilon; 1+p\epsilon; -1/A\right), \end{aligned} \quad (2.83)$$

which leads us to express

$$\begin{aligned} \phi_{(1,2,1)}(x, y, \epsilon) = \frac{1}{2} \left[\frac{1}{2\epsilon} \left(\frac{y}{1-x}\right)^{-2\epsilon} {}_2F_1\left(4\epsilon, 2\epsilon; 1+2\epsilon; \frac{y}{1-x}\right) \right. \\ \left. - \frac{1}{2\epsilon} \left(\frac{y}{1-x}\right)^{2\epsilon} {}_2F_1\left(4\epsilon, 2\epsilon; 1+2\epsilon; \frac{y}{1-x}\right) \right]. \end{aligned} \quad (2.84)$$

Separating this expression into the individual diagram kernels such that $\phi_{(1,2,1)} = \phi_{(1,2,1),A}/2 - \phi_{(1,2,1),B}/2$ we find a further UV pole in both $\phi_{(1,2,1),A}$ and $\phi_{(1,2,1),B}$ caused by the shrinking of the individual sub-diagrams to the cusp. These combine with the overall UV singularity generated by $\Gamma(4\epsilon)$ in Eq. (2.80) to produce a double pole. However, as explained in [58], the leading singularity beyond one-loop, $w^{(n,-n)}$, is proportional to the one-loop single pole and β_0 , the leading coefficient of the β -function. Since this web does not have any UV subdivergences which would correspond to the renormalization of α_s it will not contribute to terms proportional to β -function coefficients and therefore $w_{(1,2,1)}^{(2,-2)} = 0$. We can confirm this by taking the Laurent expansion of Eq. (2.84).

Rather than directly integrate Eq. (2.80) after substituting the expansion of Eq. (2.84), it was shown in Ref. [60] that if we expand before carrying out the final integrations we obtain simplifications at the level of the subtracted web integrand, the most obvious of which is that we needn't do work to integrate terms proportional to $\log(\tilde{\mu}^2/m^2)$ given that we know these must cancel. There are further, more surprising, simplifications which shall be discussed below.

As we discussed in Sec. 2.4, we construct the contribution of the (1,2,1) web

to $\Gamma^{(2)}$, Eq. (2.43), through subtracted webs of the form

$$\bar{w}_{(1,2,1)}^{(2)} = w_{(1,2,1)}^{(2,-1)} + \frac{1}{2} [w^{(1,-1)}, w^{(1,0)}], \quad (2.85)$$

or more specifically, recalling that $w^{(1)} = \sum_{(i,j)} w^{(1)}(\gamma_{ij})$ over each independent angle γ_{ij} between the Wilson lines, we can specify the contribution from the particular (1,2,1) web shown in Fig. 2.7,

$$\begin{aligned} \bar{w}_{(1,2,1)}^{(2)}(\gamma_{12}, \gamma_{23}) &= w_{(1,2,1)}^{(2,-1)}(\gamma_{12}, \gamma_{23}) + \frac{1}{2} [w^{(1,-1)}(\gamma_{12}), w^{(1,0)}(\gamma_{23})] \\ &\quad + \frac{1}{2} [w^{(1,-1)}(\gamma_{23}), w^{(1,0)}(\gamma_{12})], \end{aligned} \quad (2.86)$$

where the one-loop webs, $w^{(1)}$, correspond to the sub-diagrams in the web $w_{(1,2,1)}^{(2)}(\gamma_{12}, \gamma_{23})$. Rather than obtaining expressions for $w^{(1,-1)}$ and $w^{(1,0)}$ directly from Eq. (2.60), it will benefit us to instead substitute the expansion of Eq. (2.66) along with the expansion of the web kernel, Eq. (2.84), obtained by using the result of Ref. [104],

$${}_2F_1(4\epsilon, 2\epsilon; 1 + 2\epsilon; z) = 1 + 8\epsilon^2 \text{Li}_2(z) + \mathcal{O}(\epsilon^3), \quad (2.87)$$

into Eq. (2.85) and so

$$\bar{w}_{(1,2,1)}^{(2)} = i f^{abc} T_1^a T_2^b T_3^c \left(\frac{1}{4\pi} \right)^2 \int_0^1 dx dy p_0(x, \alpha_{12}) p_0(y, \alpha_{23}) \mathcal{G}_{(1,2,1)}(x, y), \quad (2.88)$$

where the subtracted web kernel is

$$\mathcal{G}_{(1,2,1)}(x, y) = \log \left(\frac{q(x, \alpha)}{x^2} \right) - \log \left(\frac{q(y, \alpha_{23})}{y^2} \right). \quad (2.89)$$

The subtracted web, Eq. (2.88), satisfies the condition put on $\Gamma^{(n)}$ (see Sec. 2.4), and therefore $\bar{w}^{(n)}$, that it be independent of the renormalization scale and the IR regulator, m . Furthermore, it demonstrates the seemingly general properties of this particular class of webs uncovered in Ref. [60], chiefly that they factorize into sums of products of functions of a single angle, and that (in this case trivially) their integrands contain only logarithms with polylogarithms being completely absent.

We call webs of the form discussed in this section multiple-gluon-exchange-

webs (MGEWs), meaning those webs in which gluons are exchanged directly between Wilson lines without any intervening three- or four-gluon-vertices found in the diagrams of the last line of Eq. (2.99). MGEWs will be the topic of Ch. 3, in which we shall further explore and expand upon their conjectured properties.

2.6 Webs and polylogarithms

It is now possible to integrate Eq. (2.88) which naturally falls into so-called ‘ $d\log$ ’ form, meaning that is written as integrals over a linear denominator (see Eq. (2.64)) multiplying logarithms (in more complicated examples $d\log$ form extends to polylogarithmic integrands also). We refrain from giving its precise result here, which shall appear in Ch. 3, and instead provide a more general discussion which will be applicable at higher orders where matters are naturally less simple and in doing so will introduce the functions and their properties which shall be applied in the coming chapters.

To see what this means in practice we first consider a class of functions known as *multiple-polylogarithms* (MPLs) defined recursively by the iterated integral [105, 106]

$$G(a_1, a_2, \dots, a_n; z) = \int_0^1 \frac{dt}{t - a_1} G(a_2, \dots, a_n; t), \quad (2.90)$$

with initial condition $G(x) = G(; x) = 1$ but with the stipulation that $G(; 0) = 0$ to avoid a spurious end-point singularity (though this makes sense given that $\int_0^0 \dots$ must vanish). The number of iterated integrals used to generate an MPL from this initial condition is known as its *weight*, or equivalently the function $G(a_1, \dots, a_n; z)$ has weight n . The weight of a product of MPLs is equal to the sum of their individual weights. Special values of this very general class of polylogarithms relates to the more familiar classical polylogarithms, for example

$$G(\mathbf{0}_n; x) = \frac{1}{n!} \log^n x, \quad (2.91)$$

$$G(\mathbf{a}_n; x) = \frac{1}{n!} \log^n \left(1 - \frac{x}{a} \right), \quad (2.92)$$

$$G(\mathbf{0}_{n-1}, a; x) = -\text{Li}_n \left(\frac{x}{a} \right), \quad (2.93)$$

where \mathbf{a}_k is the k -tuple $\overbrace{(a, a, \dots, a)}^k$.

One particular property of MPLs which has seen much use in modern literature (and will be relied upon several times during this thesis) is that, by virtue of their iterated integral structure, they satisfy the properties of a *Hopf Algebra* [107–109]. While we will not be able to discuss this in detail here, it has been well reviewed in Refs. [109–111]. In essence, this means that there exists a *coproduct* [107] which maps a given MPL to a tensor product of lower weight MPLs. It is sufficient for our purposes to note that the maximal iteration of the coproduct maps MPLs onto a tensor product of only logarithms which retains a great deal of information about the original function. This object is known as the function’s *symbol* [107, 108, 110, 112, 113], for example we give the symbol of some classical polylogarithms:

$$\mathcal{S} \left[\frac{1}{n!} \log^n x \right] = \underbrace{x \otimes x \otimes \dots \otimes x}_n, \quad (2.94)$$

$$\mathcal{S} [\text{Li}_n(x)] = -(1-x) \otimes \underbrace{x \otimes x \otimes \dots \otimes x}_{n-1}, \quad (2.95)$$

and in general the symbol satisfies the properties:

$$\dots \otimes (a \cdot b) \otimes \dots = \dots \otimes a \otimes \dots + \dots \otimes b \otimes \dots, \quad (2.96)$$

$$\dots \otimes \rho_n \otimes \dots = 0, \quad (2.97)$$

where ρ_n is an n -th root of unity, i.e. their entries behave as logarithms and indeed in the language of the coproduct will be found in the literature written as $\log a_1 \otimes \dots \otimes \log a_n$. However it is a standard convention to suppress the logs in the context of the symbol map. One further complication to discuss is that the symbol is defined ‘modulo $i\pi$ ’ meaning

$$\dots \otimes i\pi \otimes \log a_i \otimes \dots = 0 \quad (2.98)$$

thus it is insensitive to the logarithmic discontinuity of its entries. Note that we have included the log notation in Eq. (2.98) only for clarity and will be adopting the standard symbol notation from here. Working modulo $i\pi$ is done to avoid a contradiction in taking the symbol of zeta values; more information can be

found in Ref. [111]. One of the symbol's most frequent uses is in finding often complicated relations between high weight MPLs which becomes simply linear algebra when mapped into symbols. Further applications of the symbol and more generally the coproduct technology can be found in the study of the analytic and differential structure of Feynman integrals [114].

It is now well established that many Feynman integrals can be expressed in terms of MPLs⁹ multiplying rational functions of kinematic invariants. For such integrals, the general procedure for their computation would be to find a parametrization in which at least one of the integration parameters, t say, is linear in the denominator and any MPLs in the integrand can be written such that its arguments are rational functions of t . The symbol map can then be used to find relations between the MPLs of the integrand, which in general can depend on t through any of their arguments, and MPLs of the form $G(\dots; t)$ where t appears only in the final entry (along with MPLs that do not depend on t at all). It will then be possible to apply the definition Eq. (2.90) to produce higher weight MPLs, and the process can be repeated.

This does, however, rely upon a property of the particular examples which we have considered in this chapter (and many other Feynman integrals), known as *linear reducibility* [117]. A given integral is said to be linearly reducible if the above procedure can be carried out for each parameter integral without non-trivial changes of variables. However, for our purposes we shall widen this definition to what would more precisely be called ‘linear reducibility up to diffeomorphisms,’ meaning that we call a Feynman integral linearly reducible if there exists a parametrization in which this procedure is possible. The examples that we are considering in this section, and in the following chapter, naturally fall into the ‘ $d \log$ ’ form in which linear reducibility is trivially found and so these can immediately be integrated to MPLs. However, it must be noted that the problem of showing that a given Feynman integral is linearly reducible, and finding the appropriate parametrization, is in general unsolved and has been the topic of recent study [117, 118]. We shall encounter this difficulty again in Ch. 4.

The functions resulting from the integration of subtracted webs also satisfy

⁹There is evidence to suggest that as one computes deeper into the perturbation series, the Feynman integrals encountered fall within a more general class of functions, of which MPLs are a subset. Principally discussed is the ‘sunrise diagram’ which is expressible in terms of *elliptic polylogarithms*, e.g. Ref. [115]. These functions are not well understood and are a topic of much interest (see e.g. Ref. [116]).

strict constraints [60] on their *symbol alphabet*¹⁰, which when expressed in terms of the variables α_{ij} is simply $\{\alpha_{ij}, \eta_{ij} = \alpha_{ij}/1 - \alpha_{ij}^2\}$. We shall revisit all of the special properties of MGEWs in Ch. 3 of which they shall be the focus.

2.7 Outlook

From this chapter we conclude that IR singularities of amplitudes can be obtained from subtracted webs which are computed in practice through two separate calculations. Their colour factors are determined by the specific combination of diagrammatic colour factors along with the requisite combinatorial coefficients obtained using, for example, the replica trick from the work of Refs. [56, 61]. This is subject to a choice of basis (see Eq. (2.29) and Refs. [56, 57, 61, 93] for more details) for which we shall use that provided by Ref. [61]. Web kinematic factors are then given by the combination of diagrammatic eikonal kinematic factors with the combinatorial factors in the chosen basis. The integrals are then performed as detailed in Sec. 2.5 by factorizing the ‘scale’ from the propagators, obtaining a web kernel multiplying an overall UV divergent ($\epsilon \rightarrow 0^+$) gamma function. The single pole of the Laurent series of this integral is then combined with the commutators of the expansions of lower order webs providing the subtracted webs from which we construct the anomalous dimension in terms of the MPLs into which they integrate.

At present, the multiparton soft anomalous dimension in general kinematics is known in a non-abelian theory to only two loops [66], and in the colour singlet, two-line case to three loops in the recent work of Refs. [50, 52, 63]. In the asymptotic lightlike limit ($\beta_i^2 \rightarrow 0$ or equivalently $\alpha_{ij} \rightarrow 0$), a result has recently been given in Ref. [89] for the full three-loop, multiparton soft anomalous dimension. Building on the recent work of Refs. [56, 58, 60, 61], our goal in this thesis is to push towards a determination of the three-loop, multiparton soft anomalous dimension of non-abelian gauge theories in general kinematics. We can best understand the task at hand by looking at a diagrammatic sketch of the

¹⁰A *symbol alphabet* gives the allowed entries of the symbol. For example, a symbol alphabet of $\{a, b\}$ permits functions whose symbols are a linear combination of $a \otimes a$, $b \otimes b$, $a \otimes b$ and $b \otimes a$

three-loop anomalous dimension,

$$\begin{aligned}
 \Gamma^{(3)} \sim & \underbrace{\text{[Diagram 1]} + \text{[Diagram 2]} + (\text{two and three lines})}_{\text{MGEWs - Ch. 3}} \\
 & + \underbrace{\text{[Diagram 3]} + (\text{two and three lines})}_{\text{Three gluon vertices - Ch. 4}} \\
 & + \underbrace{\text{[Diagram 4]} + \text{[Diagram 5]} + (\text{two and three lines})}_{\text{connected - future...}} .
 \end{aligned} \tag{2.99}$$

The diagrams in Eq. (2.99) should be interpreted as representing the corresponding subtracted webs to which they contribute. Following from this, the layout of the thesis will be as follows: Ch. 3 will continue the discussion of MGEWs started in Sec. 2.5, based on our paper of the same name [1] and will compute the remaining undetermined three-line webs required for $\Gamma^{(3)}$ along with more general results which carry further into the perturbative series; in Ch. 4 we begin a study of webs containing three gluon vertices (for example, those in the second line of Eq. (2.99)) and in particular we consider the four line (1,1,1,2) web depicted above; in Ch. 5 we conclude with a look at the future of web calculations and consider the work which still remains to be done to determine the three loop soft anomalous dimension in general kinematics.

This partitioning of the three-loop soft anomalous dimension is made to collect subtracted webs by difficulty of the requisite integrals, which increases with the number of three- and four-gluon vertices composing the connected sub-diagrams. These collections are not, however, gauge invariant alone. After imposing colour

conservation,

$$\sum_{i=1}^N T_i^a = 0 \quad (2.100)$$

where N is the number of Wilson lines and T_i^a are the generators of $SU(N_c)$ discussed further in the following chapter, the gauge-invariant anomalous dimension is formed by the sum over all of the subtracted webs at the desired order in α_s . At three loops, this is the sum over all the sum over all four-, three- and two-line subtracted webs which can be collected by colour factor in the basis of Ref. [61] as follows,

$$\begin{aligned} \Gamma_4^{(3)} = & -f^{ade} f^{bce} \sum_{(i,j,k,l)} T_i^a T_j^b T_k^c T_l^d F_{4;1}^{(3)}(\alpha_{ij}, \alpha_{ik}, \alpha_{il}, \alpha_{jk}, \alpha_{jl}, \alpha_{kl}) \\ & -f^{abe} f^{cde} \sum_{(i,j,k,l)} T_i^a T_j^b T_k^c T_l^d F_{4;2}^{(3)}(\alpha_{ij}, \alpha_{ik}, \alpha_{il}, \alpha_{jk}, \alpha_{jl}, \alpha_{kl}), \end{aligned} \quad (2.101)$$

$$\begin{aligned} \Gamma_3^{(3)} = & -f^{ace} f^{bde} \sum_{(i,j,k)} \{T_i^a, T_i^b\} T_j^c T_k^d F_{3;1}^{(3)}(\alpha_{ij}, \alpha_{ik}, \alpha_{jk}) \\ & -f^{cae} f^{bde} \sum_{(i,j,k)} T_i^a \{T_j^b, T_j^c\} T_k^d F_{3;2}^{(3)}(\alpha_{ij}, \alpha_{ik}, \alpha_{jk}) \\ & -f^{cbe} f^{ade} \sum_{(i,j,k)} T_i^a T_j^b \{T_k^c, T_k^d\} F_{3;3}^{(3)}(\alpha_{ij}, \alpha_{ik}, \alpha_{jk}) \\ & + i \frac{N_c^2}{2} f^{abc} \sum_{(i,j,k)} T_i^a T_j^b T_k^c F_{3;4}^{(3)}(\alpha_{ij}, \alpha_{ik}, \alpha_{jk}), \end{aligned} \quad (2.102)$$

$$\begin{aligned} \Gamma_2^{(3)} = & -f^{abe} f^{ecd} \sum_{(i,j)} \{T_i^a, T_i^b\} \{T_j^c, T_j^d\} F_{2;1}^{(3)}(\alpha_{ij}) \\ & + N_c^2 \sum_{(i,j)} T_i^a T_j^a F_{2;2}^{(3)}(\alpha_{ij}). \end{aligned} \quad (2.103)$$

From these, we can obtain the three-loop anomalous dimension through

$$\Gamma^{(n)} = \sum_{p=2}^{n+1} \Gamma_p^{(n)} \quad (2.104)$$

where $\Gamma_p^{(n)}$ is the contribution from webs correlating p Wilson lines. These are defined in terms of ordered sums,

$$\sum_{(i_1, \dots, i_p)} (\dots) \equiv \sum_{1 \leq i_1 < \dots < i_p \leq N} (\dots), \quad (2.105)$$

over colour tensors and their corresponding kinematic factor $F_{p;q}^{(n)}(\{\alpha_{ij}\})$, where n is again the loop order, p is the number of Wilson lines in the constituent webs and q indexes the colour factors, with the sums bounded above by $N -$ the number of total number of Wilson lines. The kinematic factors depend upon ${}_p C_2 = p!/(2!(p-2)!)$ kinematic variables, α_{ij} , defined in terms of the cusp angles in Eq. (2.61). They are composed of subtracted webs in accordance with the results of [61] with the two-line webs obtained from [64].

For the purpose of clarity, if we restrict to a process with four colour-charged, hard partons then Eq. (2.100) can be used to replace, for example, $T_4^a = -T_1^a - T_2^a - T_3^a$ in Eqs. (2.101), (2.102), (2.103). The four-line colour factors from Ref. [61] will thus mix with the basis of three-line colour factors. Similarly, the three-line colour factors which contain T_4^a will mix with the two-line colour factors. Therefore, the gauge invariant pieces are the independent colour factors after the application of Eq. (2.100) along with their corresponding kinematic factors, originating from two-, three- and four-line subtracted webs.

Chapter 3

Multiple Gluon Exchange Webs

3.1 Introduction

In this chapter, which is based on our paper Ref. [1], we will discuss in detail the simplest class of webs contributing to multiple Wilson line correlators, two examples of which we have already encountered in Sec. 2.5. These were dubbed *Multiple Gluon Exchange Webs* (MGEWs) in Ref. [60], where some of their properties were studied, and two non-trivial three-loop examples were computed. MGEWs can be characterized in general as those webs that arise when the Wilson line correlator is computed using only the quadratic part of the quantum Yang-Mills Lagrangian in the path integral. In diagrammatic terms, they consist of graphs where all gluons attach directly to the Wilson lines, with no interaction vertices located off the Wilson lines. The graphs generated in this way are abelian-like, in the sense that they would also appear in QED; however there is an essential difference between the two cases: in QED the order of emission from the Wilson lines is immaterial, and one can easily show that MGEWs collectively reconstruct powers of the one-loop result; indeed, according to the exponentiation theorem, MGE diagrams are not part of the exponent in QED. In contrast, in a non-abelian theory the ordering of gluon emission is crucial, and, as a consequence, MGEWs contribute to the exponent, where they collectively generate fully connected colour factors.

To recapitulate the discussion of Sec. 2.5, some key features of MGEWs were uncovered in Ref. [60], based on a general analysis of the structure of their kinematic integrals, along with some physically motivated considerations

concerning their analytic properties. Most notably, it was found that subtracted MGEWs can be expressed as sums of products of functions depending on individual cusp angles.

The results for the subtracted webs considered in Ref. [60] were expressed in terms of a highly constrained set of functions, consisting of products of polylogarithms, each depending on a single α_{ij} . The analytic structure of these functions has been elucidated using the symbol map (see Sec. 2.6): it was conjectured that the symbols of the functions entering subtracted MGEWs are built out of the restricted alphabet $\{\alpha_{ij}, \eta_{ij} \equiv \alpha_{ij}/(1 - \alpha_{ij}^2)\}$. This alphabet, in particular, realises crossing symmetry, which in this case is expressed by the reflection $\alpha_{ij} \rightarrow -\alpha_{ij}$.

The primary aim of this chapter is to study the all-order structure of MGEWs in further detail, and to test the conjectures of Ref. [60] in a broader range of examples. Specifically, the subset of webs computed in Ref. [60], connecting the maximal number of Wilson lines accessible at two and three loops, yields integrals which are less entangled than certain MGEWs connecting a smaller number of lines at the same order; the latter, more entangled ones, are computed and analysed here in order to confirm the conjectures. With the more complete understanding of MGEWs we gain here we are able to construct an ansatz for an all-order basis of functions. These are defined through *one-dimensional* integrals of powers of logarithms only. This yields a very restricted set of harmonic polylogarithms [119] satisfying the alphabet conjecture and other constraints. We show that this basis is sufficient to express all the subtracted webs we compute in a compact manner, and we argue that it should be sufficient for MGEWs at higher orders as well.

The structure of the chapter is as follows. In Sec. 3.2 we discuss the colour structure of webs using the effective vertex formulation developed in Ref. [61], and identify a new type of relations between webs comprising different numbers of Wilson lines, through a process of *collinear reduction*. Examples of this procedure will be given later on in the chapter, where it is used as a check of the results of specific webs. Then, in Sec. 3.3, we provide a general characterization of MGEWs: we give an integral representation valid for any web in this class, before subtraction, in terms of variables with a transparent physical interpretation, and we review the conjectures proposed in [60]. In Sec. 3.4, we explain how the basis

of functions for MGEWs is constructed, and provide the necessary definitions, which will be used in what follows to express the results of the various MGEWs we compute. In the subsequent sections, we provide explicit calculations of MGEWs to substantiate our arguments; the results are also important as ingredients for the computation of the soft anomalous dimension at three loops and beyond. In Sections 3.4.2 and 3.5 we consider three-loop webs connecting two and three Wilson lines: the two-line case, already studied in [52], is interesting in this context since it provides an example of maximal entanglement of gluon insertions at this order. The results of Sect. 3.5 constitute another significant step forward in constructing the complete three-loop soft anomalous dimension, as well as providing an interesting comparison with the four line case of Ref. [60]. In Sec. 3.6, we provide the complete calculation of a four-loop subtracted web, connecting five Wilson lines. The result is in complete agreement with the conjectured all-order properties of MGEWs. Finally, in Sec. 3.7, we show that a specific class of highly symmetric diagrams contributing to n -line webs can be explicitly computed for any n , obtaining a remarkably simple result that further substantiates our conjectures. This all-order calculation of kinematic factors further allows us to prove that a specific colour structure arising from these webs has a vanishing coefficient for any n . We discuss our results and conclude in Sec. 3.8, while some technical details concerning the calculation of the subtracted webs that we have presented are collected in appendices.

3.2 The colour structure of webs and collinear reduction

In order to compute the anomalous dimension coefficients at a given order using Eq. (2.43), one must classify the independent colour factors that arise, and then determine the contributions of every web to each colour factor. The first observation is that contributions to $\Gamma^{(n)}$ may involve up to $(n + 1)$ Wilson lines, namely

$$\Gamma^{(n)} = \sum_{k=2}^{n+1} \Gamma_k^{(n)}, \quad (3.1)$$

where, for example, $\Gamma_2^{(n)}$ are the coefficients of the cusp anomalous dimension. At three-loops, Ref. [60] computed MGEWs contributing to $\Gamma_4^{(3)}$, while in the present chapter we will compute those contributing to $\Gamma_k^{(3)}$ for $k \leq 3$. We will see below that certain contributions of webs that span a non-maximal number of Wilson lines, $k \leq n + 1$, can be deduced from webs that span a larger number of lines through a process we name *collinear reduction*.

As mentioned in Sec. 2.3, an important property of webs is that their colour factors $c_j^{(L)}$ correspond to connected graphs [61]. A convenient basis for these colour factors follows naturally from the effective vertex formalism developed in Ref. [61], and we will adopt this basis in the present chapter. In this formalism, $V_K^{(l)}$ is an effective vertex representing K gluon emissions from a given Wilson line l , and involving $K - 1$ nested commutators. In general, $V_K^{(l)}$ contains $(K - 1)!$ independent colour factors $C_{K,j}$, which are enumerated by the index j . For example, $V_2^{(l)}$, describing a double emission from Wilson line l , has a unique colour factor¹.

$$C_{2,1} = [T^a, T^b] = if^{abc}T^c, \quad (3.2)$$

while for $V_3^{(l)}$, describing triple emission from the Wilson line, there are two independent colour factors involving fully-nested commutators with different permutations,

$$C_{3,1} = [[T^a, T^b], T^c] = f^{abd}f^{dec}T^e, \quad (3.3)$$

$$C_{3,2} = [[T^a, T^c], T^b] = f^{acd}f^{deb}T^e; \quad (3.4)$$

the third permutation is related to the previous two by the Jacobi identity. Note that the attachment of the effective K -gluon-emission graph to the Wilson line involves a single generator. As an example of the effective vertex operators in action, consider again the (1,2,1) web of Sec. 2.5. Here, the only possible colour factor will come from the combination of effective vertices $V_1^{(1)} \cdot V_2^{(2)} \cdot V_1^{(3)}$ which from Eq. (3.2) results in $T_1^a (if^{abc}T_2^c) T_3^b = -if^{abc}T_1^a T_2^b T_3^c$ matching Eq. (2.80).

Recall that the diagrams we are considering (contributing to MGEWs) correspond to the emission of individual gluons directly from the Wilson line. Connected colour factors emerge from linear combinations of these diagrams:

¹We use the colour-insertion operator notation [16, 120] by which T_i^a represents a colour generator on Wilson line i (in the appropriate representation) with adjoint index a .

each effective vertex $V_K^{(l)}$ picks antisymmetric combinations of the corresponding K colour generators on line l , through $K - 1$ nested commutators. The effective vertex $V_K^{(l)}$ also associates with each colour factor $C_{K,j}$ a specific K -fold parameter integral along the Wilson line, involving Heaviside functions that determine the order of attachments of the K gluons to the Wilson line. Explicit expressions for these effective vertex integrals may be found in Ref. [61]. In the following, we will not make direct use of these integrals. Rather, we will use the fact that they end up generating linear combinations of Feynman integrals $\mathcal{F}(D)$ corresponding to the various diagrams D in the web: these are precisely the linear combinations appearing in Eq. (2.29), which are determined by the corresponding web mixing matrix. For specific webs, we shall use the results for the mixing matrices, and the corresponding eigenvectors entering Eq. (2.29), which are summarized in Appendix A of Ref. [61].

For our present purposes the vertex formalism will be useful in fixing the basis of colour factors $c_j^{(L)}$. We will further see that in this language one may readily identify relations between webs involving different numbers of Wilson lines L . As explained in Ref. [61], connected graphs in the vertex formalism may involve one or more effective vertices on each Wilson line. When a given line features several effective vertices, their order is taken to be fully symmetrised, defining

$$\{C_1 C_2 \dots C_n\}_+ \equiv \frac{1}{n!} \sum_{\pi \in S_n} C_{\pi_1} C_{\pi_2} \dots C_{\pi_n}. \quad (3.5)$$

A web is characterised by a fixed number of emissions, n_l , from line l . These n_l emissions may be distributed between different effective emission vertices, and different possibilities result in different web colour factors $c_j^{(L)}$. Some examples are provided by figures 3.8, 3.10 and 3.12 below. It should be noted that further multiplicity of the web colour factors originates in the fact that each vertex $V_K^{(l)}$ has $(K - 1)!$ different colour factors $C_{K,j}$ (as exemplified by Eq. (3.3) for $K = 3$). In general, web colour factors can be written in terms of the effective-vertex colour factors as

$$c_j^{(L)} = \prod_{l=1}^L \left\{ C_{K_1,j_1}^{(l)} C_{K_2,j_2}^{(l)} \dots C_{K_{n_l},j_{n_l}}^{(l)} \right\}_+, \quad (3.6)$$

where the product is an outer product between colour factors on different lines, and curly brackets indicate symmetrization, according to Eq. (3.5).

Our observation is as follows: contributions to the web in Eq. (2.29) in which a given line l contains $v_l > 1$ effective vertices can be related to webs with a larger number of Wilson lines, where line l is replaced by v_l collinear Wilson lines, each of which carries one of the v_l effective vertices. This conclusion follows from the fact that there is *no ordering* between the effective vertices, so the relevant Feynman integrals over the positions of these vertices all extend along the ray from the hard interaction to infinity. This is exactly what happens in the situation where these vertices appear on different Wilson lines. We note that in colour space the two situations are distinct, in the sense that the colour generators of vertices that occur on different lines carry different indices, while if they occur on the same line they must be in the same representation, and they multiply each other; according to the Feynman rules of Ref. [61], one then takes the symmetrized product as in Eq. (3.5).

This observation implies that one can make a precise identification between contributions corresponding to particular colour structures in webs involving different numbers of Wilson lines. Let us consider a simple case: consider a web with L Wilson lines, where two lines l_1 and l_2 feature, respectively, a single vertex each, $V_{K_1}^{(l_1)}$ and $V_{K_2}^{(l_2)}$; consider then the collinear limit, where the velocity vectors of the two lines coincide; this yields a contribution to the corresponding web with $L - 1$ Wilson lines, where the two vertices are placed on the same line, with the colour factor replacement

$$C_{K_1,j_1} \otimes C_{K_2,j_2} \otimes \dots \longrightarrow \{C_{K_1,j_1}, C_{K_2,j_2}\}_+ \otimes \dots, \quad (3.7)$$

where the dots stand for the contribution to the colour factor from the rest of the web, involving $L - 2$ Wilson lines. If the symmetry factor of the vertex diagram corresponding to the original graph differs from that of the final graph, this needs to be taken into account (an example will be given in Sec. 3.5). This process, which we call *collinear reduction*, may be generalised to the identification of multiple lines. As we will see in the following sections, it provides non-trivial checks of the final results for webs which span less than the maximal number of lines at a given order. A graphical illustration of this process can be found in Fig. 3.1.

A corollary to this result is that starting with webs that span the largest number of Wilson lines at a given order (at three loops these are the ones

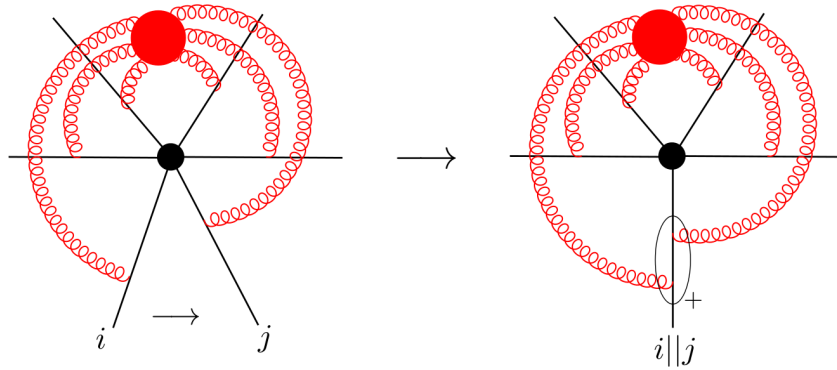


Figure 3.1: An illustration of collinear reduction from an n -line to an $(n - 1)$ -line web by identifying the lines labeled i and j . The encircled gluon–Wilson-line vertices with subscript $+$ indicates that after replacing $j \rightarrow i$ in the web colour factors, the anticommutator of the attachments is to be taken: $T_i^{\{a,b\}} = T_i^a T_i^b + T_i^b T_i^a$. The corresponding kinematic factors are determined by replacing $\beta_j \rightarrow \beta_i$ and multiplying by the appropriate symmetry factors.

connecting four legs, which were computed in Ref. [60]), and moving towards more entangled webs, where the same number of gluons connect fewer Wilson lines, the kinematic integrals corresponding to many of the colour factors $c_j^{(L)}$ in Eq. (2.29) would already be known in advance. In fact, the only contribution of a given MGEW with n_l attachments to leg l which cannot be deduced from other MGEWs in which the same number of gluons connects a larger number of Wilson lines, is the one corresponding to having a *single* effective vertex, $V_{n_l}^{(l)}$, on each line.

In the remainder of this chapter we focus on the calculation of the kinematic functions for MGEWs, whose study was started in [60]. We begin in the next section by discussing the general structure of these integrals.

3.3 General structure of MGEW integrals

Multiple gluon exchange webs are the simplest class of webs contributing to the multi-particle soft anomalous dimension. As mentioned above, despite the abelian-like appearance of their Feynman graphs, in a non-abelian gauge theory they contribute to the same colour structures as do fully connected webs containing the maximal number of gluon self-interactions. Understanding

MGEWs is therefore a necessary step to compute the soft anomalous dimension at high orders; on the other hand, the relative simplicity of MGEWs makes it possible to tackle multi-loop corrections, shedding light on the general structure of infrared singularities.

A simple way to characterize MGEWs is the following; they are the webs obtained when the Wilson line correlator in Eq. (2.47) is evaluated with a path integral in which the full gauge theory Lagrangian is replaced with its free counterpart, given by the set of terms that are quadratic in the gauge fields. One may write

$$S\left(\gamma_{ij}, \alpha_s(\mu), \epsilon, \frac{m_l}{\mu}\right)\Big|_{\text{MGEW}} \equiv \int [DA] \Phi_{\beta_1}^{(m)} \otimes \Phi_{\beta_2}^{(m)} \otimes \dots \otimes \Phi_{\beta_L}^{(m)} \exp\left\{i\mathbb{S}_0[A]\right\}, \quad (3.8)$$

where $\mathbb{S}_0[A]$ comprises the classical gauge kinetic term, and the quadratic contribution to the chosen gauge fixing (we will work in Feynman gauge). Terms quadratic in matter fields and ghost fields are not included. As a consequence, β -function contributions are absent in MGEWs, and we are effectively working in a conformally invariant sector of the theory, as we observed when considering the double pole in the (1,2,1) web in Sec. 2.5.

3.3.1 Feynman integral for a MGE diagram

It turns out to be possible to formally carry out a number of steps in the calculation of Feynman diagrams contributing to MGEWs in complete generality, as suggested in [60], by generalising the transformation, Eq. (2.52) found in the examples of Sec. 2.5. In order to do so we need to introduce a precise characterization of the gluon configuration for a generic MGEW diagram. First, we introduce an ordering in the set of L Wilson lines, $l = 1, \dots, L$. As an example, consider the diagram of Fig. 3.2, which is part of a (1,2,3,3,1) web. To further characterise a specific diagram in the web, we need to identify the order of gluon attachments to each Wilson line. Referring to Fig. 3.2, we introduce an ordering in the set of n gluons contributing to the chosen n -loop Feynman diagram in the following way: we consider each of the Wilson lines in turn according to the chosen order, moving along each line starting at the far end and reaching the origin; gluons are assigned the ordering with which they are encountered in this procedure. A given gluon k is counted only once, as it is first encountered. With

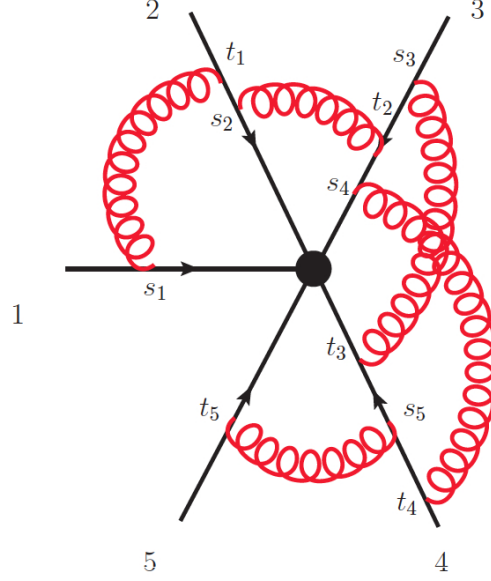


Figure 3.2: An example of a multiple gluon exchange diagram connecting five Wilson lines at five loops; it is part of the (1,2,3,3,1) web. The lines meet at a local effective vertex representing the hard interaction. For this diagram $\Theta_D[\{s_k, t_k\}] = \theta(t_1 > s_2)\theta(s_3 > t_2 > s_4)\theta(t_4 > s_5 > t_3)$.

this assignment, we say that the k -th gluon is emitted from the Wilson line in the direction $\beta_{i(k)}$ at point s_k , and is absorbed by the Wilson line in the direction $\beta_{f(k)}$ at point t_k . Using the coordinate space Feynman gauge gluon propagator, Eq. (2.49), and expanding the Wilson line operators in Eq. (2.46) in powers of the coupling, one easily finds that the most general n -gluon MGE Feynman diagram D , contributing to Eq. (3.8) at n loops, gives the kinematic factor

$$\begin{aligned}
 \mathcal{F}^{(n)}(D) &= \left(\mu^{2\epsilon} \frac{\Gamma(1-\epsilon)}{\pi^{1-\epsilon}} \right)^n \prod_{k=1}^n \beta_{i(k)} \cdot \beta_{f(k)} \int_0^\infty \prod_{k=1}^n ds_k dt_k \\
 &\times \Theta_D[\{s_k, t_k\}] \prod_{k=1}^n \left[-(\beta_{i(k)} s_k - \beta_{f(k)} t_k)^2 \right]^{-1+\epsilon} \\
 &\times \exp \left[-im \sum_{k=1}^n \left(s_k \sqrt{\beta_{i(k)}^2} - i\epsilon + t_k \sqrt{\beta_{f(k)}^2} - i\epsilon \right) \right].
 \end{aligned} \tag{3.9}$$

Clearly the ordering of the attachments of the gluons on each Wilson line is essential: it is given by the function $\Theta_D[\{s_k, t_k\}]$, which is a product of Heaviside functions assigned to each Wilson line, with $p - 1$ independent θ functions on a line with p gluon attachments².

Following Ref. [60], and the examples given in Sec. 2.5, we proceed by rescaling the Wilson line coordinates by defining³

$$\sigma_k = s_k \sqrt{-\beta_{i(k)}^2}, \quad \tau_k = t_k \sqrt{-\beta_{f(k)}^2}, \quad (3.10)$$

and furthermore we make an analogous transformation to Eq. (2.52) by writing

$$\sigma_k = x_k \lambda_k, \quad \tau_k = (1 - x_k) \lambda_k. \quad (3.11)$$

In this way, λ_k is a measure of the overall distance of the k -th gluon from the origin, whereas x_k is an ‘angular’ variable, measuring the degree of collinearity of the k -th gluon to either the emitting (as $x_k \rightarrow 1$) or the absorbing (as $x_k \rightarrow 0$) Wilson lines. In terms of these variables one finds

$$\begin{aligned} \mathcal{F}^{(n)}(D) &= \left(-\mu^{2\epsilon} \frac{\Gamma(1-\epsilon)}{2\pi^{1-\epsilon}} \right)^n \times \int_0^\infty \prod_{k=1}^n d\lambda_k \lambda_k^{-1+2\epsilon} e^{-m \sum_{k=1}^n \lambda_k} \\ &\times \int_0^1 \prod_{k=1}^n dx_k \gamma_k \left[-x_k^2 - (1-x_k)^2 + \gamma_k x_k (1-x_k) \right]^{-1+\epsilon} \Theta_D[\{x_k, \lambda_k\}], \end{aligned} \quad (3.12)$$

where $\gamma_k \equiv \gamma_{i(k),f(k)}$ is as defined in Eq. (2.55). Note that the distance variables λ_k have been scaled out of the propagators. We keep using the symbol Θ_D for the product of Heaviside functions, although now they are expressed in terms of the new variables.

To proceed we now extract from the diagram the overall UV singularity arising from the region where all gluons are emitted and absorbed very close to the origin. In order to do so, we change variable again expressing the λ_k ’s as

$$\lambda_k = (1 - y_{k-1}) \prod_{p=k}^n y_p, \quad (3.13)$$

²Notice that Eq. (3.10) applies also to the case of gluons being emitted and absorbed by the same Wilson line, corresponding to $i(k) = f(k)$, but we will not compute such webs here.

³We have once again chosen to work with timelike Wilson lines for simplicity. For a discussion of the analytic continuation see Sec. 2.5.

for $k = 1, \dots, n$, where we define $y_0 = 0$. Note that with this definition $\sum_{i=1}^k \lambda_i = \prod_{p=k}^n y_p$, and in particular the regulator in Eq. (3.12), which involves the sum of all the λ_i , depends only on y_n . The Jacobian of this change of variables is given by $J = \prod_k y_k^{k-1}$, so after performing the integral over y_n , equivalent to the χ integral from Eq. (2.79), and changing scheme to Eq. (2.68), we find

$$\begin{aligned} \mathcal{F}^{(n)}(D) &= \tilde{\kappa}^n \Gamma(2n\epsilon) \int_0^1 \prod_{k=1}^n dx_k \gamma_k \left[x_k^2 + (1-x_k)^2 - \gamma_k x_k(1-x_k) \right]^{-1+\epsilon} \\ &\quad \times \int_0^1 \prod_{k=1}^{n-1} dy_k (1-y_k)^{-1+2\epsilon} y_k^{-1+2k\epsilon} \Theta_D[\{x_k, y_k\}] \\ &= \tilde{\kappa}^n \Gamma(2n\epsilon) \int_0^1 \prod_{k=1}^n \left[dx_k p_\epsilon(x_k, \alpha_k) \right] \phi_D^{(n)}(x_i; \epsilon), \end{aligned} \quad (3.14)$$

where we defined the coefficient $\tilde{\kappa}$ in Eq. (2.71), as well as the function $p_\epsilon(x_k, \alpha_k)$ in Eq. (2.62) with $\gamma_k = -\alpha_k - 1/\alpha_k$ according to Eq. (2.61). We also give the n -th order generalisation of the web kernel,

$$\phi_D^{(n)}(x_i; \epsilon) = \int_0^1 \prod_{k=1}^{n-1} dy_k (1-y_k)^{-1+2\epsilon} y_k^{-1+2k\epsilon} \Theta_D[\{x_k, y_k\}], \quad (3.15)$$

an example of which is Eq. (2.84) for the (1,2,1) web. The analysis of Ref. [60] shows⁴ that $\phi_D^{(n)}(x_i; \epsilon)$ has a Laurent expansion in ϵ , $\phi_D^{(n)} = \sum_k \phi_D^{(n,k)} \epsilon^k$, where each term $\phi_D^{(n,k)}$ is a pure transcendental function of uniform weight $n-1+k$, containing logarithms and polylogarithms, as well as Heaviside functions depending on *ratios* of the variables x_i or $1-x_i$.

3.3.2 Feynman integral for a MGE web

The next observation [60] is that all diagrams D in a given web W have a common integral structure⁵ of the form of Eq. (3.14): assuming that in all diagrams $D \in W$

⁴Similar conclusions were reached in Ref. [52], working on two-line MGEWs and using different tools.

⁵It is important to note that in order to combine Feynman integrals corresponding to individual diagrams, as in Eq. (3.14), into the web Feynman integral, Eq. (3.17) below, one must use a common set of parameters, so that x_k is associated with a given cusp angle $\gamma_{i(k), f(k)}$ for all diagrams in the web. In practice one therefore selects one diagram D , based on which one defines the ordering of the gluons, as explained using the example of Fig. 3.2; for any other diagram in the web, one then uses the assigned order, where gluon k is always exchanged

gluon k is exchanged between the same pair of Wilson lines, such diagrams are only distinguished by the Heaviside functions $\Theta_D[\{x_k, y_k\}]$ representing the order of gluon attachments to the Wilson lines, hence they only differ by their kernels $\phi_D^{(n)}(x_i; \epsilon)$. Because a web W is defined as a linear combination of the contributing diagrams $D \in W$, one deduces that the web as a whole takes a form similar to Eq. (3.14), in the sense that they are both integrals over factors of $p_\epsilon(x_k, \alpha_k)$ multiplying hypergeometric kernels. To see this in more detail, recall that, according to Eq. (2.29), every web can contribute to different colour structures $c_j^{(L)}$ building up the anomalous dimension, $W = \sum_{j=1}^r \mathcal{F}_{W,j}^{(n)} c_j^{(L)}$, where the kinematic functions are specific linear combinations of the integrals corresponding to individual diagrams in the web,

$$\mathcal{F}_{W,j}^{(n)}(\alpha_{ij}, \epsilon) = \sum_{D \in W} Y_{D,j}^{-1} \mathcal{F}^{(n)}(D), \quad (3.16)$$

and where the numerical coefficients $Y_{D,j}^{-1}$ are fixed by the web mixing matrix. One concludes that the contribution of web W to the j -th colour structure is given by an integral similar to Eq. (3.14),

$$\mathcal{F}_{W,j}^{(n)}(\alpha_{ij}, \epsilon) = \tilde{\kappa}^n \Gamma(2n\epsilon) \int_0^1 \prod_{k=1}^n [dx_k p_\epsilon(x_k, \alpha_k)] \phi_{W,j}^{(n)}(x_i; \epsilon), \quad (3.17)$$

with a *web kernel* given by

$$\phi_{W,j}^{(n)}(x_i; \epsilon) = \sum_{D \in W} Y_{D,j}^{-1} \phi_D^{(n)}(x_i; \epsilon). \quad (3.18)$$

Before proceeding, it is useful to contrast non-abelian MGEWs with their much simpler abelian counterparts. According to the abelian exponentiation theorem only connected graphs enter the exponent, so in particular abelian MGEWs are not part of the exponent. Instead, they are reproduced by expanding the exponential involving a single exchange between each pair of Wilson lines. Because in the abelian theory ordering is immaterial, we simply sum all diagrams with *equal* weights. This sum must yield a product of the relevant one-loop

 between the same pair of Wilson lines.

integrals. The result can readily be verified from Eq. (3.14): indeed

$$\begin{aligned} \sum_{D \in W} \mathcal{F}^{(n)}(D) &= \tilde{\kappa}^n \Gamma(2n\epsilon) \int_0^1 \prod_{k=1}^n \left[dx_k p_\epsilon(x_k, \alpha_k) \right] \sum_{D \in W} \phi_D^{(n)}(x_i; \epsilon) \\ &= \left(\tilde{\kappa} \Gamma(2\epsilon) \right)^n \int_0^1 \prod_{k=1}^n \left[dx_k p_\epsilon(x_k, \alpha_k) \right], \end{aligned} \quad (3.19)$$

where in the second line we used the fact that the sum of Heaviside functions for a MGEW gives unity, so that one can use

$$\sum_{D \in W} \phi_D^{(n)}(x_i; \epsilon) = \int_0^1 \prod_{k=1}^{n-1} dy_k (1 - y_k)^{-1+2\epsilon} y_k^{-1+2k\epsilon} = \frac{(\Gamma(2\epsilon))^2}{\Gamma(2n\epsilon)}. \quad (3.20)$$

As expected, Eq. (3.19) is a product of one-loop integrals associated to the relevant cusp angles. The unweighted sum in Eq. (3.20) is a constraint on the web kernels of any non-abelian MGEW, providing a valuable check of explicit calculations in what follows.

3.3.3 Feynman integral for a MGE subtracted web

An important conclusion of the analysis in Ref. [60] is that the integration over the angular variables x_k in Eq. (3.17) is vastly simplified for subtracted webs. To this end, each web is expanded in powers of ϵ , as

$$W(\alpha_{ij}, \epsilon) = \alpha_s^n \sum_{k=-n}^{\infty} w^{(n,k)}(\alpha_{ij}) \epsilon^k, \quad (3.21)$$

and then, as discussed with Eq. (3.22) it is combined with the commutators of the webs composed by its subdiagrams, according to the pattern forming the anomalous dimension in Eq. (2.43). Then $\Gamma^{(n)} = -2n \sum_i \bar{w}_i^{(n)}$, the sum over all such subtracted webs. This step relies on the fact that the commutators build up the same colour factors and kinematic factors which also take the form of integrals over $p_0(x_i, \alpha_i)$ multiplying polylogarithmic kernels, as in Eq. (3.17). The $\mathcal{O}(\alpha^n, \epsilon^{-1})$ subtracted web can then be written as

$$\bar{w}^{(n)}(\alpha_k) = \left(\frac{1}{4\pi} \right)^n \sum_{j=1}^r c_j^{(L)} F_{W,j}^{(n)}(\alpha_k). \quad (3.22)$$

Using this notation, the subtracted web kinematic function $F_{W,j}^{(n)}$ can be written as

$$\begin{aligned}
 F_{W,j}^{(n)}(\alpha_i) &= \int_0^1 \left[\prod_{k=1}^n dx_k p_0(x_k, \alpha_k) \right] \mathcal{G}_{W,j}^{(n)}(x_i, \alpha_i) \\
 &= \left(\prod_{k=1}^n r(\alpha_k) \right) \int_0^1 \left[\prod_{k=1}^n dx_k \left(\frac{1}{x_k - \frac{1}{1-\alpha_k}} - \frac{1}{x_k + \frac{\alpha_k}{1-\alpha_k}} \right) \right] \mathcal{G}_{W,j}^{(n)}(x_i, \alpha_i) \\
 &\equiv \left(\prod_{k=1}^n r(\alpha_k) \right) G_{W,j}^{(n)}(\alpha_i), \tag{3.23}
 \end{aligned}$$

where in the first line we introduce the subtracted web kernel⁶ $\mathcal{G}_{W,j}^{(n)}$. This function contains the finite term⁷ of the web kernel $\phi_{W,j}^{(n)}(x_i; \epsilon)$, along with related terms from the commutators of the relevant subdiagrams; additional contributions occur due to (multiple) poles of $\phi_{W,j}^{(n)}(x_i; \epsilon)$, related to subdivergences, which are multiplied by appropriate powers of $\log q(x, \alpha)$ from the expansion in Eq. (2.62). For an example of this the reader is again directed to the (1,2,1) subtracted web example in Sec. 2.5. In the second expression in Eq. (3.23) we used the partial fraction form of p_0 introduced in Eq. (2.64), which places the x_k integrals in $d \log$ form as described in Sec. 2.6, owing also to the purely multiple-polylogarithmic content of $\mathcal{G}_{W,j}^{(n)}(x_i, \alpha_i)$ for MGEWs as demonstrated in Refs. [60]. This also fixes the rational function associated with the web, which is simply a factor of $r(\alpha_k)$, Eq. (2.65), for each gluon exchange. In the final expression in Eq. (3.23) all the x_k integrals are done, defining the function $G_{W,j}^{(n)}(\alpha_i)$.

As discussed in Ref. [60], remarkable simplifications occur at the level of Eq. (3.23). These can most easily be described through the properties of the subtracted web kernel $\mathcal{G}_{W,j}^{(n)}$: this function depends on its arguments only through powers of the logarithms, $\log(x_k)$, $\log(1 - x_k)$ and $\log q(x_k, \alpha_k)$, and through Heaviside functions involving ratios of the variables x_k . As integrals in the second line of Eq. (3.23) are of a $d \log$ form, the resulting function $G_{W,j}^{(n)}(\alpha_i)$ is a pure function of transcendental weight $2n - 1$. Subtracted multi-particle webs thus share the properties of two-parton webs described in Ref. [52]. It should be stressed, however, that the route by which one calculates multiparton webs is

⁶N.B. $G_{W,j}^{(n)}$ is distinct from $\mathcal{G}_{W,j}^{(n)}$, the subtracted web kernel, which is a component of the integrand of the former.

⁷Recall that $\phi_{W,j}^{(n)}(x_i; \epsilon)$ enters at $\mathcal{O}(\epsilon^{-1})$ due to the overall factor $\Gamma(2n\epsilon)$ in Eq. (3.17).

substantially different, due to the combinatorics associated with the non-trivial colour structure, and to the presence of subdivergences.

We emphasise that the absence of polylogarithms in $\mathcal{G}_{W,j}^{(n)}$ is rather surprising: recall that polylogarithms of weight $n - 1$ do occur in the $\mathcal{O}(\epsilon^0)$ term of the non-subtracted web kernel $\phi_{W,j}^{(n)}(x_i; \epsilon)$ which commonly contain, for example, Gaussian hypergeometric functions such as ⁸

$${}_2F_1(a\epsilon, b\epsilon; 1 + b\epsilon; z) = 1 - \sum_{i=2}^{\infty} (-\epsilon)^i \sum_{k=1}^{i-1} a^k b^{i-k} G(\mathbf{0}_{i-k}, \mathbf{1}_k; z). \quad (3.24)$$

Ref. [60] argued that these polylog cancellations (and the related analytic properties of $G_{W,j}^{(n)}(\alpha_i)$, which we describe below) are linked with the restoration of crossing symmetry. The latter is lost at the level of non-subtracted webs, due to the action of the IR regulator in the presence of UV subdivergences, but it is recovered for subtracted webs.

The most important consequence of the purely logarithmic nature of the subtracted web kernel is that the resulting integrated function, $G_{W,j}^{(n)}(\alpha_i)$, is a sum of products of polylogarithms, each depending on a single α_k variable. Furthermore, these polylogarithms are very specific; their symbol alphabet is restricted to α_k and $1 - \alpha_k^2$. The goal of the next section is to fully characterize these functions and obtain an explicit basis for them.

It should be stressed that the properties just described have been conjectured to be general, but they have not been proven. Specifically, all explicit calculations in Ref. [60] were of webs whose subtracted kernel is free of Heaviside functions, in which case the relation between the purely logarithmic nature of the kernel and the factorization property is obvious. Such a relation is less obvious when Heaviside functions occur in $\mathcal{G}_{W,j}^{(n)}$. The number of Heaviside functions appearing in a given subtracted web kernel depends on the level of entanglement of the web: webs spanning the maximal number, $n + 1$, of Wilson lines at n loops are not entangled (so there is no Heaviside function after performing the y_k integrals in Eq. (3.15)) while those connecting fewer Wilson lines are entangled by up to $n - 1$ Heaviside functions. A central goal of the present chapter is to verify that the factorization property does indeed hold even for entangled webs.

⁸ $G(a_1, \dots, a_n; z)$ here is the multiple-polylogarithm defined in Sec. 2.6.

3.4 A basis of functions for MGEWs

3.4.1 Constructing a basis

One of the conclusions of Ref. [60] is that the subtracted webs (1,2,2,1) and (1,1,1,3), connecting the maximum possible number of Wilson lines at three loops, can be written in terms of the simple set of integrals

$$\begin{aligned}
 R_0(\alpha) &= \frac{1}{r(\alpha)} \int_0^1 dx p_0(x, \alpha), \\
 \Sigma_2(\alpha) &= \frac{1}{2r(\alpha)} \int_0^1 dx p_0(x, \alpha) \log^2 \left(\frac{x}{1-x} \right), \\
 U_1(\alpha) &= \frac{1}{r(\alpha)} \int_0^1 dx p_0(x, \alpha) \log \left(\frac{q(x, \alpha)}{x^2} \right), \\
 U_2(\alpha) &= \frac{1}{4r(\alpha)} \int_0^1 dx p_0(x, \alpha) \log^2 \left(\frac{q(x, \alpha)}{x^2} \right),
 \end{aligned} \tag{3.25}$$

where $p_0(x, \alpha)$ is defined in Eq. (2.64) and $r(\alpha)$ in Eq. (2.65). These integrals have an integrand consisting only of logarithms, depend upon only a single cusp angle, and individually satisfy the alphabet constraints outlined above. It is natural to ask whether one may construct a basis for *all* MGEWs, given the requirements of the alphabet and factorization conjectures, and the limited range of elements entering the subtracted web kernel in Eq. (3.23), namely

$$\log \frac{q(x, \alpha)}{x^2} = \log \left(\frac{1}{x} + \alpha - 1 \right) + \log \left(\frac{1}{x} + \frac{1}{\alpha} - 1 \right) \tag{3.26}$$

and $\log \left(\frac{x}{1-x} \right)$. A first attempt could be to consider the set of functions

$$M_{k,m}(\alpha) = \frac{1}{r(\alpha)} \int_0^1 dx p_0(x, \alpha) \log^k \left(\frac{q(x, \alpha)}{x^2} \right) \log^{2m} \left(\frac{x}{1-x} \right), \tag{3.27}$$

with k and m non-negative integers (note that $q(x, \alpha)$ is symmetric under $x \rightarrow 1-x$, and odd powers of $\log \left(\frac{x}{1-x} \right)$ can be eliminated in terms of ones with even powers). The functions in Eq. (3.27) have uniform weight $2m + k + 1$, and they

satisfy the alphabet conjecture. In terms of these functions one finds

$$\begin{aligned} R_0(\alpha) &= M_{0,0}(\alpha), & U_1(\alpha) &= M_{1,0}(\alpha), \\ \Sigma_2(\alpha) &= \frac{1}{2}M_{0,1}(\alpha), & U_2(\alpha) &= \frac{1}{4}M_{2,0}(\alpha). \end{aligned} \quad (3.28)$$

At least through three loops, the basis of Eq. (3.27) is sufficient to describe MGEWs that connect the maximum number of Wilson lines at a given loop order. We now wish to check whether more entangled webs, which connect fewer lines, and thus may have leftover Heaviside functions in their subtracted web kernel \mathcal{G}_W , will belong to the span of this basis. To do this, we shall first consider the (2,2) web at two loops, and then the (3,3), (1,2,3), and (2,2,2) subtracted webs at three loops. The relevant combination of effective vertices are, respectively: $V_2^{(1)} \cdot V_2^{(2)}$, $V_3^{(1)} \cdot V_3^{(2)}$, $V_1^{(1)} \cdot V_2^{(2)} \cdot V_3^{(3)}$ and $V_2^{(1)} \cdot V_2^{(2)} \cdot V_2^{(3)}$.

Let us begin by considering the simplest example, the two-loop, two-line (2,2) web, which is of course well-known [3, 62]. This web contains two diagrams: the ladder (II) and the crossed (X) one. It is immediately evident, however, according to the definition of webs for the colour-singlet case [91, 92], that only the kinematic integral of the latter, shown in Fig. 3.3, contributes. The web therefore evaluates to

$$\begin{aligned} W_{(2,2)}^{(2)} &= [C(X) - C(II)] \mathcal{F}(X) = \frac{1}{2} [T_1^a, T_1^b] [T_2^b, T_2^a] \mathcal{F}(X) \\ &= \frac{N_c}{2} T_1 \cdot T_2 \mathcal{F}(X). \end{aligned} \quad (3.29)$$

A derivation of this result using the effective vertex formalism was given in Sec. 3 of Ref. [61], where it was shown that the only contribution arises from a double-emission vertex V_2 on each of the two Wilson lines, each vertex having a connected colour structure given by Eq. (3.2). We now proceed to consider the integral $\mathcal{F}(X)$. Specifically we will be interested in the simple pole of this function,

$$\mathcal{F}(X) = \left(\frac{\alpha_s}{4\pi} \right)^2 \left[\frac{1}{\epsilon} F_{(2,2)}^{(2)}(\alpha) + \mathcal{O}(\epsilon^0) \right], \quad (3.30)$$

which depends on a single kinematic variable, $\alpha_{12} \equiv \alpha$. In the notation of Eq. (3.9), one has four semi-infinite parameter integrals, two over s_1 and s_2 along line 1, and two over t_1 and t_2 along line 2, with the restrictions

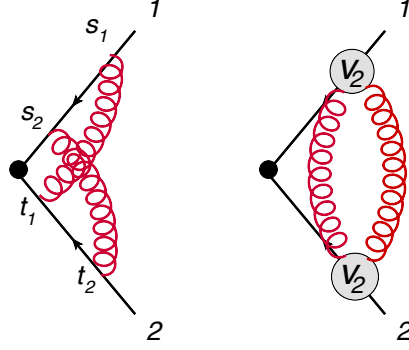


Figure 3.3: The two-loop crossed graph connecting two Wilson lines, and the corresponding effective vertex graph containing a double emission vertex V_2 on each of the two lines.

$\Theta_X = \theta(s_1 - s_2) \theta(t_2 - t_1)$. Following the steps leading to Eq. (3.23), we find

$$F_{(2,2)}^{(2)}(\alpha) = \int_0^1 dx_1 \int_0^1 dx_2 p_0(x_1, \alpha) p_0(x_2, \alpha) \mathcal{G}_{(2,2)}^{(2)}(x_1, x_2), \quad (3.31)$$

with the kernel

$$\mathcal{G}_{(2,2)}^{(2)}(x_1, x_2) = \theta(x_1 - x_2) \log \left(\frac{x_1}{1 - x_1} \frac{1 - x_2}{x_2} \right). \quad (3.32)$$

Using $p_0(1 - x, \alpha) = p_0(x, \alpha)$, we can write the kinematic factor in Eq. (3.31) as

$$F_{(2,2)}^{(2)}(\alpha) = 2 \int_0^1 dx_1 p_0(x_1, \alpha) \log \left(\frac{x_1}{1 - x_1} \right) \int_0^1 dx_2 p_0(x_2, \alpha) \theta(x_1 - x_2). \quad (3.33)$$

The second integral in Eq. (3.33) does not yield an expression of the form of Eq. (3.27), so we shall be forced to extend our basis. Let us proceed as follows.

First we define

$$\begin{aligned} \log \tilde{q}(x, \alpha) &\equiv \frac{1}{r(\alpha)} \int_0^1 dy p_0(y, \alpha) \theta(x - y) \\ &= \log \left(\frac{1}{x} + \alpha - 1 \right) - \log \left(\frac{1}{x} + \frac{1}{\alpha} - 1 \right). \end{aligned} \quad (3.34)$$

We may then extend our basis by defining the set of functions

$$M_{k,l,n}(\alpha) = \frac{1}{r(\alpha)} \int_0^1 dx p_0(x, \alpha) \log^k \left(\frac{q(x, \alpha)}{x^2} \right) \log^l \left(\frac{x}{1-x} \right) \log^n \tilde{q}(x, \alpha). \quad (3.35)$$

These functions have uniform weight $w = k + l + n + 1$, and we will see below that $M_{k,l,n}(\alpha)$ still gives rise to the required alphabet composed of α and $\eta = \alpha/(1 - \alpha^2)$. Clearly, these functions are consistent with our constraints. Note also that $\log \tilde{q}(x, \alpha)$ is a natural addition to the previous basis: as shown in Eq. (3.34), it is precisely the difference of the same two logarithms whose sum is given by the factor in Eq. (3.26). Notice also that $\log \tilde{q}(x, \alpha)$ and $r(\alpha)$ are odd under $\alpha \rightarrow 1/\alpha$, while the full result for every web must be even, because of the relation between α and γ . Therefore if this logarithm appears raised to an odd power, the symmetry in the corresponding contribution will have to be restored by some other factor in the result, for example a factor of $r(\alpha)$, or multiplication by another function of the basis also odd under the same transformation.

We can now revisit Eq. (3.33), and express the result for the (2,2) web in terms of the basis in Eq. (3.35), as

$$\overline{w}_{(2,2)}^{(2)} = \left(\frac{1}{4\pi} \right)^2 \frac{N_c}{2} T_1 \cdot T_2 F_{(2,2)}^{(2)}(\alpha), \quad F_{(2,2)}^{(2)}(\alpha) = 2r^2(\alpha) M_{0,1,1}(\alpha). \quad (3.36)$$

By using the explicit expression for the function $M_{0,1,1}(\alpha)$ given in Appendix A.1, we see that this result agrees with the calculation reported in [3, 62].

Having fixed the basis, we can readily express all previously computed subtracted webs in terms of the first few basis functions. To begin with, the functions in Eq. (3.25) can be expressed in terms of Eq. (3.35) as

$$\begin{aligned} R_0(\alpha) &= M_{0,0,0}(\alpha), & U_1(\alpha) &= M_{1,0,0}(\alpha), \\ \Sigma_2(\alpha) &= \frac{1}{2} M_{0,2,0}(\alpha), & U_2(\alpha) &= \frac{1}{4} M_{2,0,0}(\alpha). \end{aligned} \quad (3.37)$$

Further, the (1,2,1) subtracted web computed in Sec. 2.5 and in Refs. [60, 67–70] can be written as

$$\overline{w}_{(1,2,1)}^{(2,-1)} = -i f^{abc} T_i^a T_j^b T_k^c \left(\frac{1}{4\pi} \right)^2 \frac{1}{2} r(\alpha_{ij}) r(\alpha_{jk}) \quad (3.38)$$

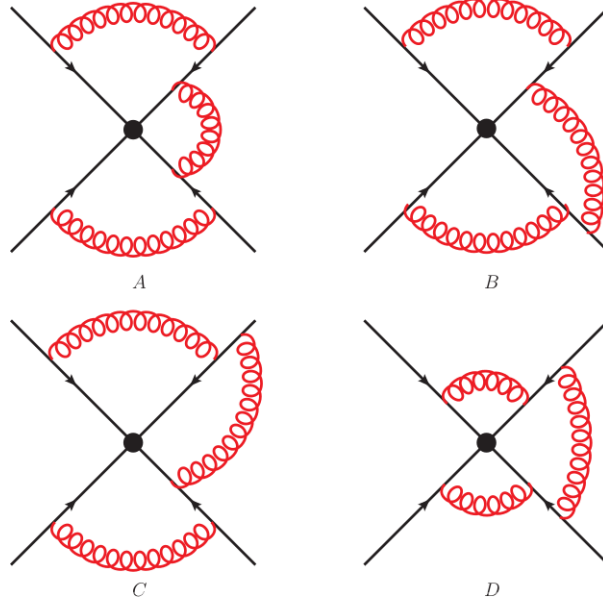


Figure 3.4: The (1,2,2,1) web, connecting four Wilson lines at three loops.

$$\times \left(M_{0,0,0}(\alpha_{ij})M_{1,0,0}(\alpha_{jk}) - M_{0,0,0}(\alpha_{jk})M_{1,0,0}(\alpha_{ij}) \right).$$

Next, the results of the (1,2,2,1) and (1,1,1,3) subtracted webs, computed in Ref. [60], can be expressed in the new basis as follows. For the (1,2,2,1) web of Fig. 3.4, whose colour structure in the effective vertex formalism is shown in Fig. 3.5, we find

$$\begin{aligned} \overline{w}_{(1,2,2,1)}^{(3)}(\alpha_{12}, \alpha_{23}, \alpha_{34}) &= -\frac{1}{6} f^{abe} f^{ecd} T_1^a T_2^b T_3^c T_4^d \left(\frac{1}{4\pi} \right)^3 \\ &r(\alpha_{12}) r(\alpha_{23}) r(\alpha_{34}) G_{(1,2,2,1)}(\alpha_{12}, \alpha_{23}, \alpha_{34}), \end{aligned} \quad (3.39)$$

where

$$\begin{aligned} G_{(1,2,2,1)}(\alpha_{12}, \alpha_{23}, \alpha_{34}) &= -\frac{1}{2} M_{2,0,0}(\alpha_{12})M_{0,0,0}(\alpha_{23})M_{0,0,0}(\alpha_{34}) \\ &- \frac{1}{2} M_{2,0,0}(\alpha_{34})M_{0,0,0}(\alpha_{12})M_{0,0,0}(\alpha_{23}) + M_{2,0,0}(\alpha_{23})M_{0,0,0}(\alpha_{12})M_{0,0,0}(\alpha_{34}) \\ &- M_{0,0,0}(\alpha_{12})M_{1,0,0}(\alpha_{23})M_{1,0,0}(\alpha_{34}) - M_{0,0,0}(\alpha_{34})M_{1,0,0}(\alpha_{12})M_{1,0,0}(\alpha_{23}) \\ &+ 2 M_{0,0,0}(\alpha_{23})M_{1,0,0}(\alpha_{12})M_{1,0,0}(\alpha_{34}) - 4 M_{0,2,0}(\alpha_{23})M_{0,0,0}(\alpha_{12})M_{0,0,0}(\alpha_{34}). \end{aligned} \quad (3.40)$$

For the (1,1,1,3) web, whose colour structure is depicted in Fig. 3.6, we find

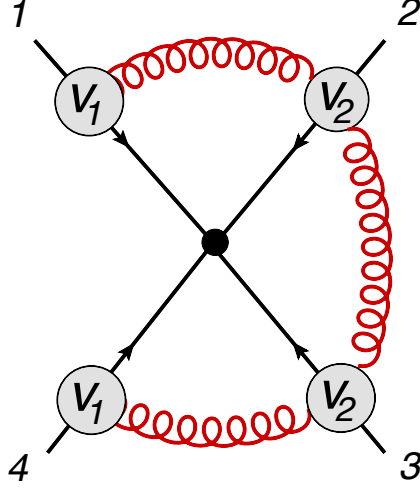


Figure 3.5: The (1,2,2,1) web in the effective vertex formalism.

$$\begin{aligned} \bar{w}_{(1,1,1,3)}^{(3)}(\alpha_{14}, \alpha_{24}, \alpha_{34}) &= -\frac{1}{6} T_1^a T_2^b T_3^c T_4^d \left(\frac{1}{4\pi} \right)^3 r(\alpha_{14}) r(\alpha_{24}) r(\alpha_{34}) \\ &\times \left[f^{ade} f^{ebc} G_{(1,1,1,3)}(\alpha_{14}, \alpha_{24}, \alpha_{34}) + f^{ace} f^{ebd} G_{(1,1,1,3)}(\alpha_{24}, \alpha_{14}, \alpha_{34}) \right], \end{aligned} \quad (3.41)$$

where

$$\begin{aligned} G_{(1,1,1,3)}(\alpha_{14}, \alpha_{24}, \alpha_{34}) &= \frac{1}{2} M_{2,0,0}(\alpha_{14}) M_{0,0,0}(\alpha_{24}) M_{0,0,0}(\alpha_{34}) \\ &+ \frac{1}{2} M_{2,0,0}(\alpha_{34}) M_{0,0,0}(\alpha_{14}) M_{0,0,0}(\alpha_{24}) - M_{2,0,0}(\alpha_{24}) M_{0,0,0}(\alpha_{14}) M_{0,0,0}(\alpha_{34}) \\ &+ M_{0,0,0}(\alpha_{14}) M_{1,0,0}(\alpha_{24}) M_{1,0,0}(\alpha_{34}) + M_{0,0,0}(\alpha_{34}) M_{1,0,0}(\alpha_{14}) M_{1,0,0}(\alpha_{24}) \\ &- 2 M_{0,0,0}(\alpha_{24}) M_{1,0,0}(\alpha_{14}) M_{1,0,0}(\alpha_{34}). \end{aligned} \quad (3.42)$$

We note that, while the weight of G_W is $2n - 1$, where W is an n -loop web, these webs span $n + 1$ Wilson lines, involving n individual gluons, each depending on a separate α_{ij} . Thus the weight w is partitioned so that each term involves a function of $w \geq 1$ for each of the n gluons. Consequently, we only encounter functions up to weight $w = n$. To explore the validity of the basis beyond weight three we need to either consider more entangled webs spanning fewer lines, where fewer, but higher weight functions enter, or explore higher loop corrections. In the following we will do both.

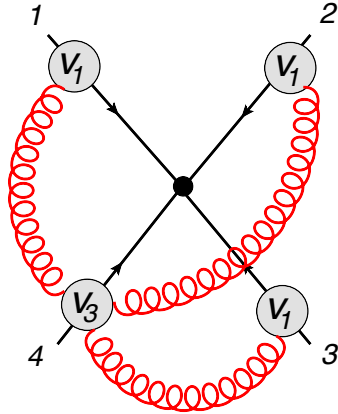


Figure 3.6: Effective vertex diagram for the (1,1,1,3) web.

As a first step, we need to generate the basis functions up to weight five (this will be sufficient for the calculations we present in this chapter). Before doing so, however, we must note that not all functions $M_{k,l,n}$ are independent, and we must discuss the relevant degeneracies. As an example, in the $n = 0$ case we find that

$$M_{k,2\lambda+1,0}(\alpha) = - \sum_{r=1}^k \binom{k}{r} 2^{r-1} M_{k-r,2\lambda+1+r,0}(\alpha), \quad (3.43)$$

so, for $n = 0$, we can recursively express all the functions with odd values of l , in terms of those with even values of l . Similarly, we can find relations in the general case $n \neq 0$, by considering the symmetry under $x \leftrightarrow 1 - x$. We verify that

$$\begin{aligned} M_{k,l,n}(\alpha) &= \frac{1}{r(\alpha)} \int_0^1 dx p_0(x, \alpha) (-1)^{l+n} \\ &\times \left[\log \left(\frac{q(x, \alpha)}{x^2} \right) + 2 \log \left(\frac{x}{1-x} \right) \right]^k \\ &\times \left[\log \left(\frac{x}{1-x} \right) \right]^l \left[\log(\tilde{q}(x, \alpha)) - 2 \log(\alpha) \right]^n. \end{aligned} \quad (3.44)$$

By expanding the integrand in Eq. (3.44) we obtain then the general relation

$$M_{k,l,n}(\alpha) = (-1)^{l+n} \sum_{r=0}^k \sum_{s=0}^n \binom{k}{r} \binom{n}{s} 2^{s+r} (-1)^s \log^s(\alpha) M_{k-r,l+r,n-s}(\alpha). \quad (3.45)$$

Once again, we can express $M_{k,l,n}$, with $l+n$ odd, in terms of the basis functions with $l+n$ even, and lower weights. Using these relations it is easy to derive the set of independent functions up to any desired weight. For example, at weight two, we have the relation

$$M_{0,0,1}(\alpha) = \frac{1}{2}M_{0,0,0}^2(\alpha), \quad (3.46)$$

and at weight three we find

$$\begin{aligned} M_{1,1,0}(\alpha) &= -M_{0,2,0}(\alpha), \\ M_{1,0,1}(\alpha) &= -M_{0,1,1}(\alpha) + \frac{1}{2}M_{0,0,0}(\alpha)M_{1,0,0}(\alpha). \end{aligned} \quad (3.47)$$

Using these relations to eliminate redundant entries, we give the basis functions up to weight five in Table 3.1. The table presents the symbol of each function, while explicit expressions in terms of classical and harmonic polylogarithms [119] are given in Appendix A.1. All functions have the required symbol alphabet; consequently, they can all be expressed in terms of harmonic polylogarithms with entries 0 and 1. A crucial question at this point is whether further extensions of our proposed basis will be required at higher orders, when more entangled webs are present. In the following, we present several examples of webs at three and four loops, providing evidence that the basis of functions in Eq. (3.35) is indeed sufficient. We begin by looking at the most entangled three-loop web, the (3,3) web involving only two Wilson lines.

3.4.2 Testing the basis: a three-loop, two-line web

In the colour singlet channel, the (3,3) web $W_{(3,3)}$ contributes to the three-loop cusp anomalous dimension, and it could easily be computed, for example, with the techniques of Ref. [52]. For open Wilson lines⁹, the only minor complication is that two independent colour structures arise, while of course the relevant kinematic integrals are the same. The diagrams contributing to $W_{(3,3)}$ are displayed in Fig. 3.7, and are denoted by (a) and (b) respectively. Using the

⁹‘Open’ here is used to distinguish this from the standard cusp configuration where the lines are considered closed into a Wilson loop at infinite distance from the cusp. In doing so one would impose colour conservation and the contributions from all but the most antisymmetric colour factors would cancel.

$M_{k,l,n}(\alpha)$		
w	Name	Symbol
1	$M_{0,0,0}$	$2(\otimes\alpha)$
2	$M_{1,0,0}$	$-4\alpha \otimes \eta$
3	$M_{0,0,2}$	$16\alpha \otimes \alpha \otimes \alpha$
	$M_{0,1,1}$	$-4\alpha \otimes \eta \otimes \alpha$
	$M_{0,2,0}$	$4\alpha \otimes \alpha \otimes \alpha$
	$M_{2,0,0}$	$16\alpha \otimes \eta \otimes \eta$
4	$M_{1,0,2}$	$-32\alpha \otimes \alpha \otimes \alpha \otimes \eta$
	$M_{1,1,1}$	$-16\alpha \otimes \alpha \otimes \alpha \otimes \alpha + 8\alpha \otimes \eta \otimes \alpha \otimes \eta + 8\alpha \otimes \eta \otimes \eta \otimes \alpha$
	$M_{1,2,0}$	$-8\alpha \otimes \alpha \otimes \alpha \otimes \eta - 8\alpha \otimes \eta \otimes \alpha \otimes \alpha$
	$M_{3,0,0}$	$-96\alpha \otimes \eta \otimes \eta \otimes \eta$
5	$M_{0,0,4}$	$768\alpha \otimes \alpha \otimes \alpha \otimes \alpha \otimes \alpha$
	$M_{0,1,3}$	$-96\alpha \otimes \alpha \otimes \alpha \otimes \eta \otimes \alpha - 96\alpha \otimes \alpha \otimes \eta \otimes \alpha \otimes \alpha - 96\alpha \otimes \eta \otimes \alpha \otimes \alpha \otimes \alpha$
	$M_{0,2,2}$	$96\alpha \otimes \alpha \otimes \alpha \otimes \alpha \otimes \alpha + 32\alpha \otimes \eta \otimes \alpha \otimes \eta \otimes \alpha$
	$M_{0,3,1}$	$-24\alpha \otimes \alpha \otimes \alpha \otimes \eta \otimes \alpha - 24\alpha \otimes \eta \otimes \alpha \otimes \alpha \otimes \alpha$
	$M_{0,4,0}$	$48\alpha \otimes \alpha \otimes \alpha \otimes \alpha \otimes \alpha$
	$M_{2,0,2}$	$128\alpha \otimes \alpha \otimes \alpha \otimes \eta \otimes \eta$
	$M_{2,1,1}$	$64\alpha \otimes \alpha \otimes \alpha \otimes \alpha \otimes \eta + 32\alpha \otimes \alpha \otimes \eta \otimes \alpha \otimes \alpha + 32\alpha \otimes \eta \otimes \alpha \otimes \alpha \otimes \alpha - 32\alpha \otimes \eta \otimes \alpha \otimes \eta \otimes \eta - 32\alpha \otimes \eta \otimes \eta \otimes \alpha \otimes \eta - 32\alpha \otimes \eta \otimes \eta \otimes \eta \otimes \alpha$
	$M_{2,2,0}$	$32\alpha \otimes \alpha \otimes \alpha \otimes \alpha \otimes \alpha + 32\alpha \otimes \alpha \otimes \alpha \otimes \eta \otimes \eta + 32\alpha \otimes \eta \otimes \alpha \otimes \alpha \otimes \eta + 32\alpha \otimes \eta \otimes \eta \otimes \alpha \otimes \alpha$
$M_{4,0,0}$	$768\alpha \otimes \eta \otimes \eta \otimes \eta \otimes \eta$	

Table 3.1: Symbols of all the linearly independent functions of the MGEW basis of Eq. (3.35) up to weight five. We use the shorthand notation $\eta = \alpha/(1 - \alpha^2)$.

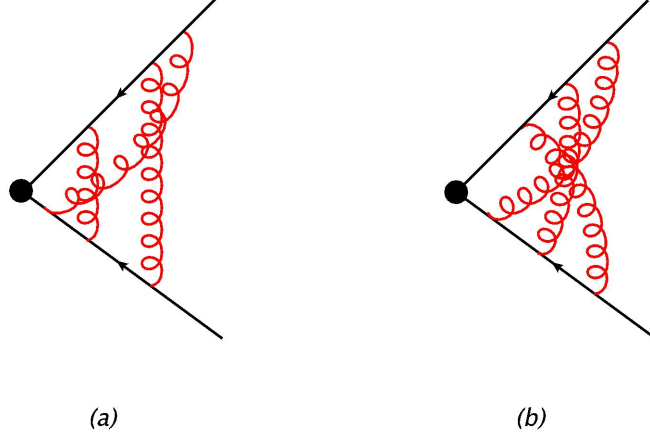


Figure 3.7: The two diagrams contributing to the (3,3) web at the three loop order. Diagram (a) has a twin under the symmetry swapping the two Wilson lines; its kinematic integral yields the same function as (a).

procedure outlined in Sec. 3.3, it is straightforward to evaluate the contributions of the two diagrams to the web. Since these diagrams are irreducible, they each have just a single UV pole, and we define

$$\begin{aligned}\mathcal{F}_a &= \left(\frac{\alpha_s}{4\pi}\right)^3 \left[\frac{1}{\epsilon} F_{(3,3),a}^{(3)} + \mathcal{O}(\epsilon^0) \right], \\ \mathcal{F}_b &= \left(\frac{\alpha_s}{4\pi}\right)^3 \left[\frac{1}{\epsilon} F_{(3,3),b}^{(3)} + \mathcal{O}(\epsilon^0) \right].\end{aligned}\quad (3.48)$$

In the absence of subdivergences (in the colour singlet case, each diagram separately is a ‘web’ in the sense of Refs. [91, 92]), no subtractions are needed. The entangled nature of the diagrams, which leads to the absence of subdivergences, also implies, however, that their contributions to the web kernel involve two Heaviside functions, as we shall see explicitly below.

For open Wilson lines, one finds that the (3,3) web involves two independent colour structures. Working in the effective colour vertex basis, the result can be written as

$$\overline{w}_{(3,3)}^{(3)}(\alpha) = \left(\frac{1}{4\pi}\right)^3 \frac{1}{4} \left[-f^{abe} f^{ecd} \{T_i^a, T_i^c\} \{T_j^b, T_j^d\} F_{(V_1 V_2)_+(V_1 V_2)_+}^{(3)}(\alpha) \right]$$

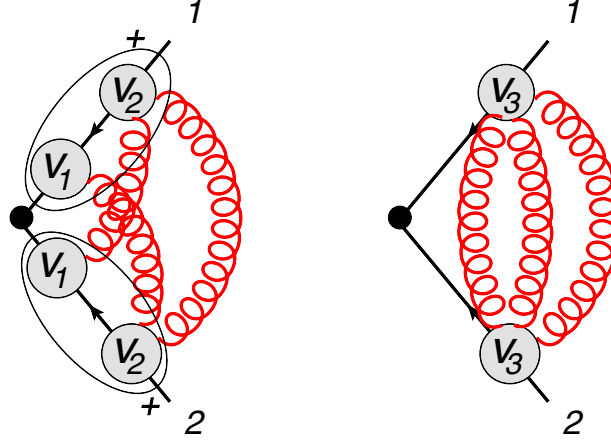


Figure 3.8: The elements of the (3,3) web in the effective vertex formalism. The diagram on the left hand side, where each Wilson line features a (symmetrized) pair of V_2 and V_1 vertices, can be obtained from the (1,2,2,1) web of Fig. 3.5 upon taking collinear limits, as explained in the text.

$$+ N_c^2 T_i \cdot T_j F_{V_3 V_3}^{(3)}(\alpha) \Big], \quad (3.49)$$

where the first term involves the symmetric combination of a single emission vertex and a double emission vertex on each line, while the second term has one triple emission vertex per line. These two colour structures are depicted in Fig. 3.8. The linear combinations of kinematic integrals corresponding to each colour structure can be easily computed from the corresponding web mixing matrix [61], and one finds

$$\begin{aligned} F_{(V_1 V_2)_+(V_1 V_2)_+}^{(3)}(\alpha) &= 2 F_{(3,3),a}^{(3)}(\alpha) + F_{(3,3),b}^{(3)}(\alpha), \\ F_{V_3 V_3}^{(3)}(\alpha) &= F_{(3,3),a}^{(3)}(\alpha) + \frac{3}{2} F_{(3,3),b}^{(3)}(\alpha), \end{aligned} \quad (3.50)$$

where $F_{(3,3),j}^{(3)}(\alpha)$ with $j = a, b$ denotes the contributions of the two diagrams in Fig. 3.7. Following the steps described in Sec. 3.3, we get

$$F_{(3,3),j}^{(3)}(\alpha) = \int_0^1 dx \int_0^1 dy \int_0^1 dz p_0(x, \alpha) p_0(y, \alpha) p_0(z, \alpha) \mathcal{G}_{(3,3),j}^{(3)}(x, y, z) \quad (3.51)$$

with the kernels

$$\begin{aligned}\mathcal{G}_{(3,3),a}^{(3)}(x,y,z) &= -\frac{4}{3}\log^2\left(\frac{x}{1-x}\frac{1-z}{z}\right)\theta(z-x)\theta(y-z), \\ \mathcal{G}_{(3,3),b}^{(3)}(x,y,z) &= -\frac{4}{3}\log\left(\frac{x}{1-x}\frac{1-y}{y}\right)\log\left(\frac{y}{1-y}\frac{1-z}{z}\right) \\ &\quad \times \theta(y-x)\theta(z-y).\end{aligned}\quad (3.52)$$

Using Eqs. (3.51) and (3.52) with the combination $F_{(V_1V_2)_+(V_1V_2)_+}^{(3)}(\alpha)$ from Eq. (3.50), yields

$$F_{(V_1V_2)_+(V_1V_2)_+}^{(3)}(\alpha) = -\frac{2}{3}r^3(\alpha)M_{0,2,0}(\alpha)M_{0,0,0}^2(\alpha), \quad (3.53)$$

which is the final answer for this component of the (3,3) web in Eq. (3.49).

According to the general reasoning outlined in Sec. 3.2, we expect this result to be reproduced by a two-fold collinear reduction process starting with the (1,2,2,1) web. Specifically, in Fig. 3.5 we must take Wilson line 1 to be collinear to Wilson line 3, and line 4 to be collinear to line 2. It is clear that in this limit the diagram degenerates to reproduce the first configuration in Fig. 3.8, provided we take the symmetrized product of the colour factors of the two vertices on each line according to Eq. (3.7). Considering Eq. (3.39), taking the limit requires identifying α_{12} and α_{34} with α_{23} , which we denote in the context of the (3,3) web as α . This yields

$$\begin{aligned}\bar{w}_{(1,2,2,1)}(\alpha_{12}, \alpha_{23}, \alpha_{34}) &\xrightarrow{1||3, 2||4} -\frac{1}{6}f_{abc}f_{cd}^e\frac{1}{2}\{T_1^a, T_1^c\}\frac{1}{2}\{T_2^b, T_2^d\} \\ &\quad \times \left(\frac{1}{4\pi}\right)^3 r^3(\alpha) G_{(1,2,2,1)}(\alpha, \alpha, \alpha),\end{aligned}\quad (3.54)$$

where $G_{(1,2,2,1)}(\alpha, \alpha, \alpha)$ was defined in Eq. (3.40). It is easy to check that this collinear reduction result exactly reproduces the first term in Eq. (3.49), with the kinematic function obtained in Eq. (3.53) through a direct calculation.

Notice that a direct calculation of the (subtracted) web yields in general a combination of polylogarithms that may not be immediately identified in terms of our basis functions. In order to express the results in terms of the basis, it is very useful to construct the symbol of the result, and then use the properties of

the symbol map [110, 113, 121], and more generally of the coproduct structure described in Ref. [109]. We emphasise that the use of these algebraic methods to manipulate polylogarithmic functions is merely an intermediate step, as the final goal is always to find the result for the subtracted web as an analytic function, written as a sum of products of basis elements $M_{k,l,n}$ with numerical rational coefficients. In the case of Eq. (3.53), the symbol is very simple

$$\mathcal{S} \left[\frac{1}{r^3(\alpha)} F_{(V_1 V_2)_+(V_1 V_2)_+}^{(3)}(\alpha) \right] = -\frac{640}{3} \alpha \otimes \alpha \otimes \alpha \otimes \alpha \otimes \alpha . \quad (3.55)$$

Note however that the identification of the result, at function level, in terms of the basis is not fully determined by the symbol: for example, in addition to the correct result in Eq. (3.53), $M_{0,0,0}^5(\alpha)$ also has a symbol proportional to Eq. (3.55). This illustrates the well known fact that the symbol is not sufficient to control lower-weight functions multiplied by transcendental constants such as $\zeta(n)$. Such terms however can be easily recovered using the coproduct technique, along with a numerical evaluation of the integrals [109, 110].

We can now turn to the more interesting case of the $V_3 \cdot V_3$ colour structure, which is novel, in the sense that it cannot be derived from collinear reduction of less entangled webs. It is not obvious a priori that our proposed basis suffices for this kinematic function, since now two integrals over the ‘propagator’ functions p_0 are cut off by the Heaviside functions appearing in Eq. (3.52). Having two Heaviside functions, this web is clearly more entangled than the ones considered so far, thus providing a non-trivial test of the generality of the basis.

It is not difficult to perform the required integrals, yielding, as expected, a combination of polylogarithms of uniform weight five. In order to map the result to our basis, we compute the symbol, which is given by

$$\mathcal{S} \left[\frac{1}{r^3(\alpha)} F_{V_3 V_3}^{(3)}(\alpha) \right] = -\frac{64}{3} \left[4 \left(\alpha \otimes \eta \otimes \eta \otimes \alpha \otimes \alpha + \alpha \otimes \eta \otimes \alpha \otimes \eta \otimes \alpha \right) - \alpha \otimes \alpha \otimes \alpha \otimes \alpha \otimes \alpha \right]. \quad (3.56)$$

Expressing the result in our basis is now an algebraic problem. We find that the $M_{k,l,n}$ basis is sufficient to express the $V_3 \cdot V_3$ function, and the resulting expression

is

$$\begin{aligned}
 F_{V_3 V_3}^{(3)}(\alpha) &= -\frac{4}{3} r^3(\alpha) \left[\frac{1}{4} M_{0,0,0}^2(\alpha) M_{2,0,0}(\alpha) - \frac{1}{4} M_{0,0,0}(\alpha) M_{1,0,0}^2(\alpha) \right. \\
 &\quad + M_{0,0,0}(\alpha) M_{1,1,1}(\alpha) - M_{0,1,1}(\alpha) M_{1,0,0}(\alpha) + \frac{3}{2} M_{0,2,2}(\alpha) \\
 &\quad \left. - \frac{1}{4} M_{0,0,0}^2(\alpha) M_{0,2,0}(\alpha) + \frac{1}{48} M_{0,0,0}^5(\alpha) \right]. \tag{3.57}
 \end{aligned}$$

For future reference, let us summarize the results we obtained for MGEWs in the two-line case, with arbitrary colour exchange at the cusp, at the level of the anomalous dimension. We find the following contribution from the webs,

$$\alpha_s \Gamma_2^{(1)}(\alpha) \Big|_{(1,1)} = \frac{\alpha_s}{\pi} T_1 \cdot T_2 r(\alpha) \log(\alpha) \tag{3.58a}$$

$$\alpha_s^2 \Gamma_2^{(2)}(\alpha) \Big|_{(2,2)} = -4 \left(\frac{\alpha_s}{4\pi} \right)^2 N_c T_1 \cdot T_2 r^2(\alpha) M_{0,1,1}(\alpha) \tag{3.58b}$$

$$\begin{aligned}
 \alpha_s^3 \Gamma_2^{(3)}(\alpha) \Big|_{(3,3)} &= -\frac{3}{2} \left(\frac{\alpha_s}{4\pi} \right)^3 \left[-f_{abe} f_{cd}^e \{T_1^a, T_1^c\} \{T_2^b, T_2^d\} F_{(V_1 V_2)_+(V_1 V_2)_+}^{(3)}(\alpha) \right. \\
 &\quad \left. + N_c^2 T_1 \cdot T_2 F_{V_3 V_3}^{(3)}(\alpha) \right], \tag{3.58c}
 \end{aligned}$$

with the two functions in the three-loop result given in Eqs. (3.53) and (3.57). The results agree with previous calculations. In particular, at the three-loop level, the result for the colour singlet projection of the (3,3) web can be read off from Eq. (28) in Ref. [49]: it is given by the coefficient of ξ^3 in that expression¹⁰. In order to project our result Eq. (3.49) onto the colour singlet case, we simply need to substitute $T_2 = -T_1$, which guarantees colour conservation at the cusp. The three-loop result is

$$\alpha_s^3 \Gamma_2^{(3)}(\alpha) \Big|_{(3,3)} = \frac{3}{2} \left(\frac{\alpha_s}{4\pi} \right)^3 N_c^2 C_R \left[\frac{1}{2} F_{(V_1 V_2)_+(V_1 V_2)_+}^{(3)}(\alpha) + F_{V_3 V_3}^{(3)}(\alpha) \right], \tag{3.59}$$

where C_R is the quadratic Casimir eigenvalue of representation R , corresponding

¹⁰The calculation in [49] is done for $\mathcal{N} = 4$ Super Yang-Mills theory, with supersymmetric Wilson lines, but one may extract the Yang-Mills limit by choosing the directions of the scalar fields in the internal space on the two Wilson lines to be perpendicular to each other, in which case ξ maps to our rational factor $r(\alpha)$. The highest power of $r(\alpha)$ is fully determined by MGEWs, and at three loops by the (3,3) web alone.

to $T_i \cdot T_i$. The result is in full agreement with Ref. [49].

3.5 Results for three-loop, three-line webs

In this section, we present the calculation of the three-loop, three-line webs of Figs. 3.9 and 3.11, and the corresponding contributions to the soft anomalous dimension. While the calculations are lengthy, they closely follow the steps described in Sec. 3.3: we can therefore concentrate on the results and on the role of the basis functions defined in Sec. 3.4 above. The most important intermediate steps are summarized in two appendices, Appendix A.2 for the (2,2,2) web and Appendix A.3 for the (1,2,3) web. We choose our conventions so that both webs connect lines 1, 2 and 3, counting clockwise from top-left in Figs. 3.9 and 3.11. A suitable basis for the colour factors of all three-loop three-line webs is [61]

$$\begin{aligned}
 c_1^{(3)} &= \{T_1^a, T_1^b\} [T_2^b, T_2^c] [T_3^a, T_3^c], \\
 c_2^{(3)} &= [T_1^a, T_1^b] \{T_2^b, T_2^c\} [T_3^a, T_3^c], \\
 c_3^{(3)} &= [T_1^a, T_1^b] [T_2^b, T_2^c] \{T_3^a, T_3^c\}, \\
 c_4^{(3)} &= [T_1^a, T_1^b] [T_2^b, T_2^c] [T_3^a, T_3^c].
 \end{aligned}
 \tag{3.60}$$

Note that terms with more than one anticommutator cannot occur because they would correspond to disconnected colour diagrams.

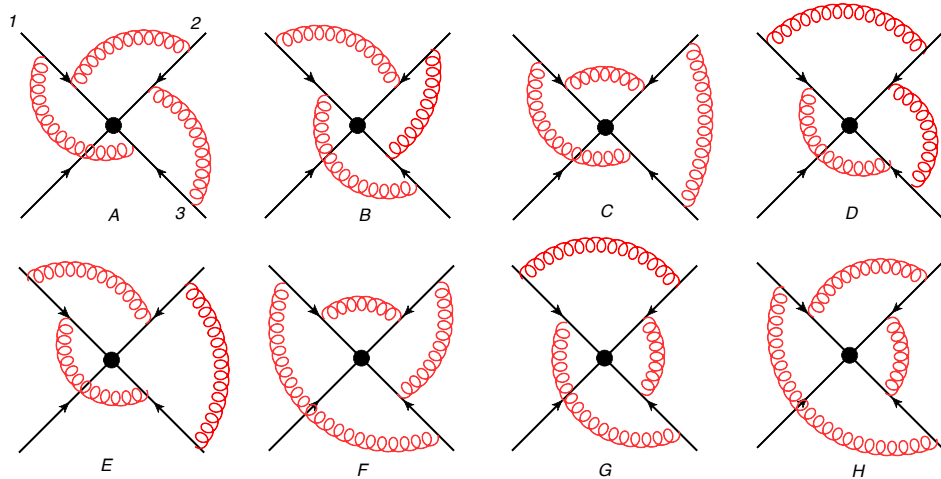


Figure 3.9: The (2,2,2) web connecting three Wilson lines at three-loop order.

3.5.1 The (2,2,2) web

The (2,2,2) web potentially contributes to all four colour factors in the basis of Eq. (3.60). As a consequence, one may write the unsubtracted web as

$$W_{(2,2,2)}(\alpha_{12}, \alpha_{23}, \alpha_{13}) = \sum_{i=1}^4 c_i^{(3)} \mathcal{F}_{(2,2,2);i}(\alpha_{12}, \alpha_{23}, \alpha_{13}, \epsilon). \quad (3.61)$$

The combinations of kinematic factors accompanying each colour factor are collected in Table 3.2. These form the web kernel, which is then combined with appropriate commutators, to form the subtracted web. We present the details of this calculation in appendix A.2, while here we discuss the results.

Using the specified colour basis the subtracted web takes the form

$$\bar{w}_{(2,2,2)}(\alpha_{12}, \alpha_{23}, \alpha_{13}) = \left(\frac{1}{4\pi}\right)^3 \sum_{i=1}^4 c_i^{(3)} F_{(2,2,2);i}(\alpha_{12}, \alpha_{23}, \alpha_{13}), \quad (3.62)$$

where

$$F_{(2,2,2);i}(\alpha_{12}, \alpha_{23}, \alpha_{13}) = \int_0^1 dx_1 dx_2 dx_3 p_0(x_1, \alpha_{12}) p_0(x_2, \alpha_{23}) p_0(x_3, \alpha_{13}) \\ \times \mathcal{G}_{(2,2,2);i}(x_1, x_2, x_3, \alpha_{12}, \alpha_{23}, \alpha_{13}). \quad (3.63)$$

The subtracted web kernels $\mathcal{G}_{(2,2,2);i}$, defined in Eq. (3.23), will be given below. We will see that the subtracted web kernels depend on their arguments via powers of logarithms only, as anticipated in Ref. [60]. This simple structure emerges through the cancellation of all polylogarithms amongst the various diagrams and commutators, when the subtracted web kernel is assembled (see for example Eq. (A.22) and Eqs. (A.27) through (A.29), respectively). This simplification is responsible for the factorized structure of the final result.

To express the subtracted web kernels in compact form, we define the logarithmic functions

$$L_{ij} \equiv \log\left(\frac{q(x_i, \alpha_{ij})}{x_i^2}\right); \quad R_i \equiv \log\left(\frac{x_i}{1-x_i}\right). \quad (3.64)$$

In terms of these functions, the subtracted web kernels associated to the first

Colour Factor	Kinematic Feynman Integral $\mathcal{F}_{(2,2,2),i}$
$c_1^{(3)}$	$\frac{1}{12}(-2A - 2B + C - 2D + E - 2F + G + H)$
$c_2^{(3)}$	$\frac{1}{12}(-2A - 2B - 2C + D + E + F - 2G + H)$
$c_3^{(3)}$	$\frac{1}{12}(2A + 2B - C - D + 2E - F - G + 2H)$
$c_4^{(3)}$	$\frac{1}{2}(-A + B)$

Table 3.2: Kinematic integral associated with each colour factor in the (2,2,2) web of Fig. 3.9, where $A \equiv \mathcal{F}(A)$ and similarly for B, C , etc.

three colour factors are

$$\begin{aligned}
 \mathcal{G}_{(2,2,2),1}^{(3)} &= \frac{1}{3} \left[R_2^2 - \frac{1}{4}L_{23}^2 + \frac{1}{8}L_{12}^2 + \frac{1}{8}L_{31}^2 + \frac{1}{4}L_{12}L_{23} - \frac{1}{2}L_{31}L_{12} + \frac{1}{4}L_{23}L_{31} \right], \\
 \mathcal{G}_{(2,2,2),2}^{(3)} &= \frac{1}{3} \left[R_3^2 - \frac{1}{4}L_{31}^2 + \frac{1}{8}L_{23}^2 + \frac{1}{8}L_{12}^2 + \frac{1}{4}L_{23}L_{31} - \frac{1}{2}L_{12}L_{23} + \frac{1}{4}L_{31}L_{12} \right], \\
 \mathcal{G}_{(2,2,2),3}^{(3)} &= -\frac{1}{3} \left[R_1^2 - \frac{1}{4}L_{12}^2 + \frac{1}{8}L_{23}^2 + \frac{1}{8}L_{31}^2 + \frac{1}{4}L_{31}L_{12} - \frac{1}{2}L_{23}L_{31} + \frac{1}{4}L_{12}L_{23} \right].
 \end{aligned} \tag{3.65}$$

As expected from Bose symmetry in Eq. (3.62), the three functions $\mathcal{G}_{(2,2,2),i}^{(3)}$ can be obtained from each other by permuting the relevant indices; the overall sign for $i = 3$ compared to $i = 1$ and 2 reflects the symmetry properties of the corresponding colour factors in Eq. (3.60) under cyclic permutations.

In contrast to Eq. (3.65), the contribution of the (2,2,2) web to the fully antisymmetric colour factor $c_4^{(3)}$ is found to vanish,

$$\mathcal{G}_{(2,2,2),4}^{(3)} = 0. \tag{3.66}$$

One sees explicitly that each subtracted web kernel consists of products of logarithms involving distinct kinematic invariants, consistent with the basis of functions defined in Sec. 3.4. It is now straightforward to integrate the results over the ‘angle’ parameters x_i . In line with Eq. (3.22), we denote the integrated coefficient of each colour factor (with factors of $(4\pi)^3$ removed) by $F_{(2,2,2),i}^{(3)}$; the result for the first kinematic factor is then

$$F_{(2,2,2),1}^{(3)}(\alpha_{12}, \alpha_{23}, \alpha_{13}) = \frac{1}{3} r(\alpha_{12})r(\alpha_{23})r(\alpha_{13}) \times$$

$$\begin{aligned}
 & \left[- M_{0,0,0}(\alpha_{12})M_{0,0,0}(\alpha_{13}) \left(\frac{1}{4} M_{2,0,0}(\alpha_{23}) - M_{0,2,0}(\alpha_{23}) \right) \right. \\
 & + \frac{1}{8} M_{0,0,0}(\alpha_{13})M_{0,0,0}(\alpha_{23})M_{2,0,0}(\alpha_{12}) \\
 & + \frac{1}{8} M_{0,0,0}(\alpha_{12})M_{0,0,0}(\alpha_{23})M_{2,0,0}(\alpha_{13}) \\
 & - \frac{1}{2} M_{0,0,0}(\alpha_{23})M_{1,0,0}(\alpha_{12})M_{1,0,0}(\alpha_{13}) \\
 & + \frac{1}{4} M_{0,0,0}(\alpha_{13})M_{1,0,0}(\alpha_{12})M_{1,0,0}(\alpha_{23}) \\
 & \left. + \frac{1}{4} M_{0,0,0}(\alpha_{12})M_{1,0,0}(\alpha_{13})M_{1,0,0}(\alpha_{23}) \right]. \tag{3.67}
 \end{aligned}$$

The second and third kinematic contributions may be obtained via

$$\begin{aligned}
 F_{(2,2,2),2}^{(3)}(\alpha_{12}, \alpha_{23}, \alpha_{13}) &= F_{(2,2,2),1}^{(3)}(\alpha_{23}, \alpha_{13}, \alpha_{12}), \\
 F_{(2,2,2),3}^{(3)}(\alpha_{12}, \alpha_{23}, \alpha_{13}) &= -F_{(2,2,2),1}^{(3)}(\alpha_{13}, \alpha_{12}, \alpha_{23}), \tag{3.68}
 \end{aligned}$$

as follows from the symmetry of the web, and the relabelling of the colour factors in Eq. (3.60). Finally, the fourth kinematic factor vanishes

$$F_{(2,2,2),4}^{(3)} = 0, \tag{3.69}$$

as is clear from the vanishing of the subtracted web kernel in Eq. (3.66). One may note that the subtracted kernels $\mathcal{G}_{(2,2,2),i}^{(3)}$ do not contain any Heaviside functions, despite the fact that individual diagrams (given in Appendix A.2) contain one for every Wilson line. As a consequence, only a subclass of the basis functions is relevant: those without any power of $\log \tilde{q}(x, \alpha)$.

Let us now discuss the collinear reduction process, following Sec. 3.2, in the context of the (2,2,2) web. We will see that the above results can be derived from the (1,2,2,1) web of Fig. 3.5. Indeed, upon taking external lines 1 and 4 to be collinear, one ends up with the diagram of Fig. 3.10(a), involving a symmetric combination of one-gluon vertices on line 1. Applying the collinear reduction according to Eq. (3.7), the colour factor corresponds to $c_1^{(3)}$ of Eq. (3.60).

Eqs. (3.39) and (3.40), with $\alpha_{34} \rightarrow \alpha_{13}$, then yield

$$\begin{aligned} \overline{w}_{(1,2,2,1)}^{(3)}(\alpha_{12}, \alpha_{23}, \alpha_{34}) &\longrightarrow -\frac{1}{6} f^{abe} f^{ecd} \frac{1}{2} \{T_1^a, T_1^d\} T_2^b T_3^c \left(\frac{1}{4\pi}\right)^3 & (3.70) \\ &\quad \times r(\alpha_{12}) r(\alpha_{23}) r(\alpha_{31}) G_{(1,2,2,1)}(\alpha_{12}, \alpha_{23}, \alpha_{31}) \\ &= -c_1^{(3)} \frac{1}{12} \left(\frac{1}{4\pi}\right)^3 r(\alpha_{12}) r(\alpha_{23}) r(\alpha_{31}) G_{(1,2,2,1)}(\alpha_{12}, \alpha_{23}, \alpha_{31}), \end{aligned}$$

which indeed agrees with Eq. (3.67). The contributions to the colour factors $c_2^{(3)}$

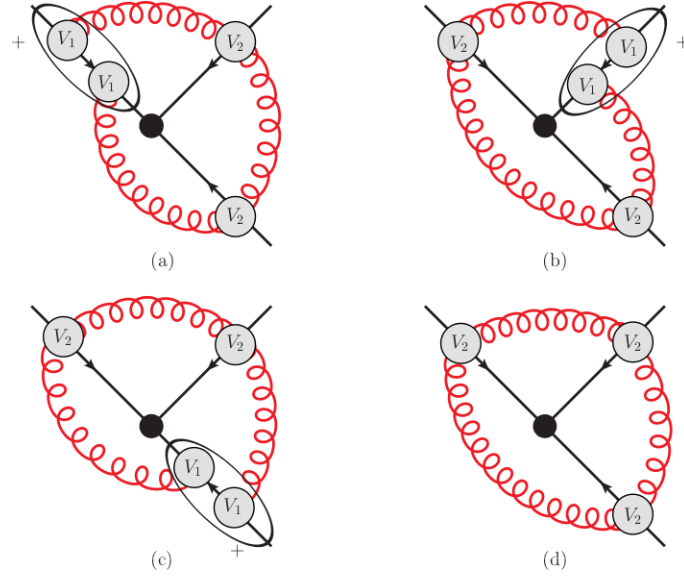


Figure 3.10: Effective vertex diagrams for the (2,2,2) web. The first three cases, a, b and c , can be obtained via collinear reduction from the (1,2,2,1) web of figure 3.5 and its permutations.

and $c_3^{(4)}$ arise from permuting external lines in Fig. 3.5, as was done in Eq. (3.68), so clearly these can also be obtained via collinear reductions of the (1,2,2,1) web. The only contribution that cannot be generated in this way is the effective vertex diagram of Fig. 3.10(d), which features a V_2 vertex on all three lines. As explained in Sec. 3.2, diagrams which feature a single effective vertex on each line constitute the genuinely new information in a given web, that cannot be obtained from collinear reductions of webs connecting more external lines. In

the present case, however, the colour factor of the diagram in Fig. 3.10(d) is the fully antisymmetric combination $c_4^{(3)}$, and we have seen above that the kinematic function associated with this colour structure vanishes. The reason for this is that the kinematic function associated with $c_4^{(3)}$ involves only diagrams A and B in Fig. 3.9, in the antisymmetric combination $\mathcal{F}(A) - \mathcal{F}(B)$. Diagrams A and B , which were referred to as *Escher staircase* diagrams in Ref. [56], are special for several reasons: they are highly symmetric, they are chirally opposed to each other, and they are fully irreducible: one cannot shrink any gluon to the origin without also pulling in the others. Therefore, they have no subdivergences, and they do not need any commutator counterterms. Thus their UV pole can be computed in isolation, yielding a regularization-independent result¹¹. Finally, we shall show below that their kinematic parts are equal, so that the antisymmetric combination vanishes.

In Sec. 3.7, we will be able to construct the kinematic integrals of the Escher staircases to all loop orders, and we will prove that a similar cancellation (though with slightly different mechanisms for even and odd numbers of gluons) happens for any number of gluons. More precisely, we will show that, out of $n + 1$ colour structures sampled by the $(\overbrace{2, 2, \dots, 2}^n)$ web, the only one which cannot be obtained from collinear reduction of $(1, \overbrace{2, 2, \dots, 2}^{n-1}, 1)$ webs, which corresponds to a product of n effective vertices of type V_2 , receives contributions only from the two Escher staircases which are present for any n , and these contributions cancel, so that the corresponding kinematic function vanishes. Note however that this discussion does not imply that staircase diagrams do not enter the exponent at all. Indeed, as can be seen in Table 3.2, they do contribute to the colour factors $c_i^{(3)}$, with $1 \leq i \leq 3$.

¹¹The first computation of the staircase diagram A of the (2,2,2) web in Fig. 3.9 was performed using a cutoff regularization in Ref. [52].

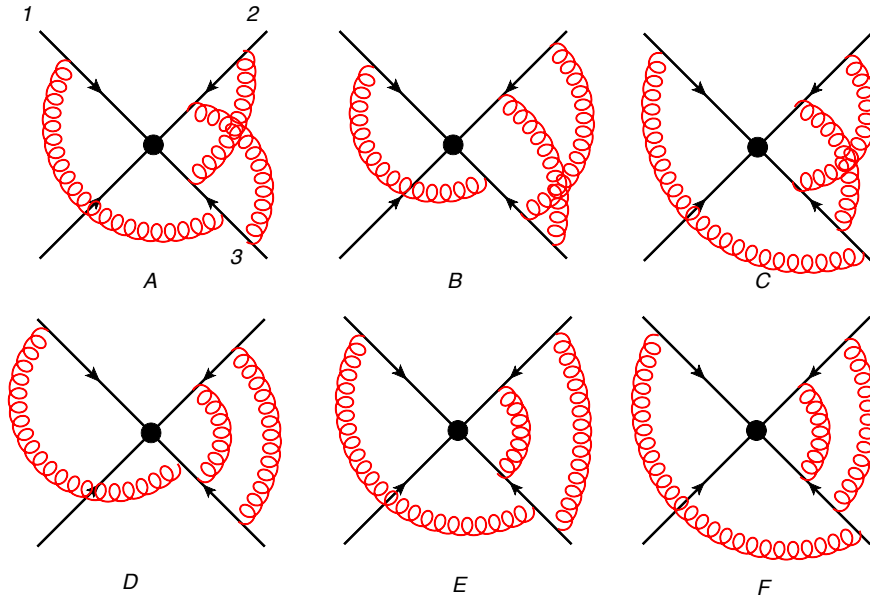


Figure 3.11: The (1,2,3) web connecting three Wilson lines at three-loop order.

3.5.2 The (1,2,3) web

In this section we focus on the (1,2,3) web of Fig. 3.11. Analogously to the (2,2,2) web of the previous section, one may write the unsubtracted web as

$$W_{(1,2,3)}(\alpha_{13}, \alpha_{23}) = \sum_{i=1}^4 c_i^{(3)} \mathcal{F}_{(1,2,3),i}(\alpha_{13}, \alpha_{23}, \epsilon) . \quad (3.71)$$

The combinations of kinematic functions of individual diagrams required for each colour factor are collected in Table 3.3, and the details of the calculation of the subtracted web may be found in Appendix A.3. Here we quote the results.

Note first that according to Table 3.3 this web, in the present basis, has no projection on the $c_1^{(3)}$ colour factor. We can therefore consider only the three components $c_i^{(3)}$ for $i = 2, 3, 4$. The subtracted web is given by

$$\bar{w}_{(1,2,3)}(\alpha_{13}, \alpha_{23}) = \left(\frac{1}{4\pi}\right)^3 \sum_{i=2}^4 c_i^{(3)} F_{(1,2,3),i}(\alpha_{13}, \alpha_{23}) , \quad (3.72)$$

Colour Factor	Kinematic Feynman Integral $\mathcal{F}_{(1,2,3),i}$
$c_1^{(3)}$	0
$c_2^{(3)}$	$\frac{1}{12}(2A - B - C - D + 2E - F)$
$c_3^{(3)}$	$-\frac{1}{12}(4A + B + C + D - 2E + F)$
$c_4^{(3)}$	$-\frac{1}{2}(B - C)$

Table 3.3: Kinematic Feynman integrals accompanying each connected colour factor for the (1,2,3) web of Fig. 3.11, where $A \equiv \mathcal{F}(A)$, etc.

where

$$F_{(1,2,3);i}(\alpha_{13}, \alpha_{23}) = \int_0^1 dx_1 dx_2 dx_3 p_0(x_1, \alpha_{13}) p_0(x_2, \alpha_{23}) p_0(x_3, \alpha_{23}) \times \mathcal{G}_{(1,2,3);i}(x_1, x_2, x_3, \alpha_{13}, \alpha_{23}, \alpha_{23}). \quad (3.73)$$

The subtracted kernels are

$$\begin{aligned} \mathcal{G}_{(1,2,3),2}^{(3)} &= \frac{1}{3} \left[\frac{1}{8} L_{13}^2 - \frac{1}{8} L_{23}^2 + \frac{1}{4} L_{23} L_{32} - \frac{1}{4} L_{13} L_{23} \right], \\ \mathcal{G}_{(1,2,3),3}^{(3)} &= -\frac{1}{3} \left[\frac{1}{4} L_{23} L_{13} - \frac{1}{4} L_{23} L_{32} + \frac{1}{8} L_{23}^2 - \frac{1}{8} L_{13}^2 - R_2^2 \right], \\ \mathcal{G}_{(1,2,3),4}^{(3)} &= \frac{2}{3} \theta(x_2 - x_3) \left[2 L_{13} R_2 + L_{23} (R_3 - R_2) \right. \\ &\quad \left. - \log^2 \left(\frac{x_2}{x_3} \right) + \log \left(\frac{x_2}{x_3} \right) \log \left(\frac{1 - x_2}{1 - x_3} \right) \right], \end{aligned} \quad (3.74)$$

where we used the definitions in Eq. (3.64). As a consequence of the presence of two entangled gluons spanning the cusp between lines 2 and 3, all subtracted kernels have a leftover Heaviside function; for the first two colour structures, it has been eliminated using symmetries of the integrand in the variables (x_1, x_2, x_3) , while this cannot be done for the coefficient of $c_4^{(3)}$. This notwithstanding, the final integration can be performed, and the result can be expressed in terms of our basis functions. Indeed, given the above subtracted kernels, we find

$$\begin{aligned} F_{(1,2,3),2}^{(3)}(\alpha_{13}, \alpha_{23}) &= \frac{1}{12} r(\alpha_{13}) r^2(\alpha_{23}) \left[\frac{1}{2} M_{2,0,0}(\alpha_{13}) M_{0,0,0}^2(\alpha_{23}) \right. \\ &\quad \left. - \frac{1}{2} M_{2,0,0}(\alpha_{23}) M_{0,0,0}(\alpha_{13}) M_{0,0,0}(\alpha_{23}) + M_{0,0,0}(\alpha_{13}) M_{1,0,0}^2(\alpha_{23}) \right] \end{aligned} \quad (3.75a)$$

$$\begin{aligned}
 & - M_{0,0,0}(\alpha_{23})M_{1,0,0}(\alpha_{13})M_{1,0,0}(\alpha_{23}) \Big], \\
 F_{(1,2,3),3}^{(3)}(\alpha_{13}, \alpha_{23}) &= -\frac{1}{12} r(\alpha_{13})r^2(\alpha_{23}) \left[-\frac{1}{2} M_{2,0,0}(\alpha_{13})M_{0,0,0}^2(\alpha_{23}) \right. \\
 & + \frac{1}{2} \left(M_{2,0,0}(\alpha_{23}) - 8M_{0,2,0}(\alpha_{23}) \right) M_{0,0,0}(\alpha_{13})M_{0,0,0}(\alpha_{23}) \\
 & \left. - M_{0,0,0}(\alpha_{13})M_{1,0,0}^2(\alpha_{23}) + M_{0,0,0}(\alpha_{23})M_{1,0,0}(\alpha_{13})M_{1,0,0}(\alpha_{23}) \right], \\
 F_{(1,2,3),4}^{(3)}(\alpha_{13}, \alpha_{23}) &= \frac{4}{3} r(\alpha_{13})r^2(\alpha_{23}) \left[M_{0,1,1}(\alpha_{23})M_{1,0,0}(\alpha_{13}) \right. \\
 & + \frac{1}{8} \left(M_{1,0,0}^2(\alpha_{23}) - M_{0,0,0}(\alpha_{23})M_{2,0,0}(\alpha_{23}) \right. \\
 & \left. \left. - \frac{1}{12} M_{0,0,0}^4(\alpha_{23}) + 2 M_{0,0,0}(\alpha_{23})M_{0,2,0}(\alpha_{23}) \right) M_{0,0,0}(\alpha_{13}) \right].
 \end{aligned} \tag{3.75b}$$

$$\tag{3.75c}$$

As for the (2,2,2) web, and the MGEWs discussed in the previous section, these results are fully consistent with our expectations: the kinematic functions entering the anomalous dimension take the form of a sum of products of polylogarithmic functions of individual cusp angles, consistently with the factorization conjecture of Ref. [60], and these functions all belong to the basis of Eq. (3.35). The way this is realised in the case of the (1,2,3) web is non-trivial: this web includes two cusp angles and these are entangled in individual diagrams due to three Heaviside functions. We find again that polylogarithms appear in the kernel of individual diagrams and in the unsubtracted web, but not in the subtracted web kernel. Furthermore, the only Heaviside function surviving in the subtracted web kernel $\mathcal{G}_{(1,2,3),4}^{(3)}$ in Eq. (3.74) relates two of the angular integrations associated with the same kinematic variable α_{23} , and therefore is consistent with the factorization property.

We conclude by discussing the constraints provided by collinear reduction. As for the (2,2,2) web discussed above, one may obtain certain components of the (1,2,3) web from collinear reductions of webs connecting four Wilson lines. Two of the three components of Eq. (3.72) can be obtained this way: the component associated with the colour factor $c_2^{(3)}$ corresponds, in the effective vertex description, to diagram (a) in Fig. 3.12, and can be obtained by collinear reduction from the (1,1,3,1) web, while the component associated with colour factor $c_3^{(3)}$ corresponds to diagram (b) in Fig. 3.12, and can be obtained by collinear reduction from the (1,2,2,1) web. The component of $c_4^{(3)}$ corresponds, in

turn, to diagram (c); since the latter has a single effective vertex on each line, it cannot be obtained through collinear reduction.

Let us now examine the two components that can be deduced from four-line webs. In the case of diagram (a) in Fig. 3.12, one may first permute lines 3 and 4 in the result of the (1,1,1,3) web, so that the line carrying the V_3 vertex will be line 3, matching our conventions for the (1,2,3) web. Following this permutation, we apply the collinear reduction by identifying line 4 with line 2. To match diagram (a) in Fig. 3.12 we must also include a symmetry factor¹² of $1/2$, associated with the exchange of the two gluons, both propagating between the V_3 vertex on line 3 and the V_1 vertices on line 2: this symmetry factor is absent in the original (1,1,3,1) web, where the two gluons attach to different lines. We thus get

$$\begin{aligned} \overline{w}_{(1,1,3,1)}^{(3)}(\alpha_{13}, \alpha_{23}, \alpha_{34}) &\xrightarrow{4||2} -\frac{1}{2} \cdot \frac{1}{6} T_1^a \frac{1}{2} \{T_2^b, T_2^d\} T_3^c \left(\frac{1}{4\pi}\right)^3 r(\alpha_{13}) r^2(\alpha_{23}) \\ &\quad \times \left[f^{ace} f^{ebd} G_{(1,1,1,3)}(\alpha_{13}, \alpha_{23}, \alpha_{23}) + f^{ade} f^{ebc} G_{(1,1,1,3)}(\alpha_{23}, \alpha_{13}, \alpha_{23}) \right] \\ &= -\frac{1}{6} T_1^a \frac{1}{2} \{T_2^b, T_2^d\} T_3^c \left(\frac{1}{4\pi}\right)^3 r(\alpha_{13}) r^2(\alpha_{23}) f^{ade} f^{ebc} G_{(1,1,1,3)}(\alpha_{23}, \alpha_{13}, \alpha_{23}) , \end{aligned} \quad (3.76)$$

where in the last line we kept only the second term, noting that the first vanishes owing to the contraction of the colour tensors. It is straightforward to check, using Eq. (3.42), that Eq. (3.76) reproduces the $c_2^{(3)}$ component of the (1,2,3) web in Eq. (3.72), with the kinematic function given by Eq. (3.75a).

Finally, consider diagram (b) in Fig. 3.12. This diagram can be obtained from the collinear reduction of the (1,2,2,1) web of Eq. (3.39) by identifying lines 3 and 1, and then renaming 4 as 1, to match our conventions for the (1,2,3) web. One finds

$$\begin{aligned} \overline{w}_{(1,2,2,1)}^{(3)}(\alpha_{12}, \alpha_{23}, \alpha_{34}) &\xrightarrow{1||3} -\frac{1}{6} f^{abe} f^{ecd} T_1^d T_2^b \frac{1}{2} \{T_3^a, T_3^c\} \left(\frac{1}{4\pi}\right)^3 \\ &\quad \times r^2(\alpha_{23}) r(\alpha_{13}) G_{(1,2,2,1)}(\alpha_{23}, \alpha_{23}, \alpha_{13}) . \end{aligned} \quad (3.77)$$

¹²For a detailed discussion of the Feynman rules in the vertex effective theory, see Ref. [61]. The specific example of the (1,2,3) web was also analysed there, see Eqs. (63) and (64).

One may verify, using Eq. (3.40), that this equation exactly reproduces Eq. (3.72), with the kinematic function given by Eq. (3.75b).

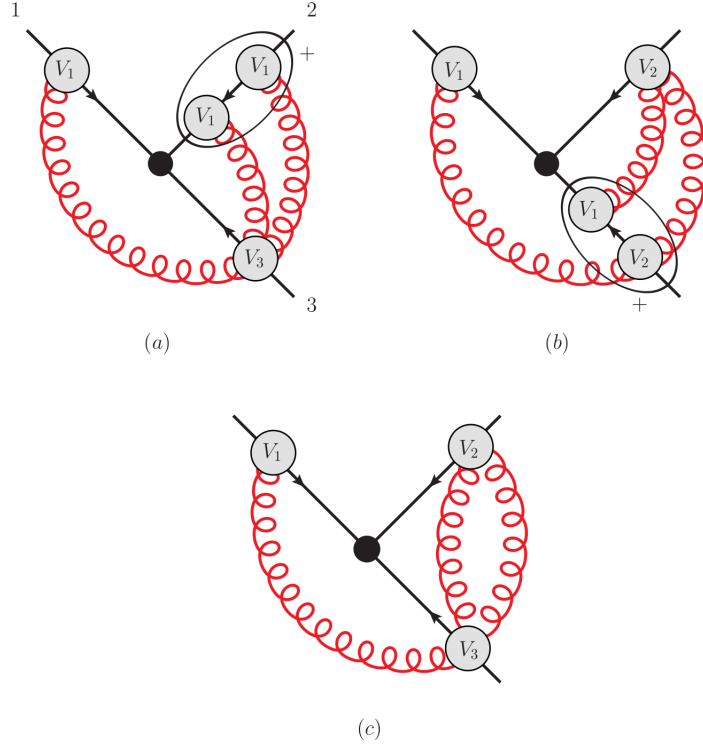


Figure 3.12: The three components of the (1,2,3) web using the effective vertex formalism. The components described by the two upper diagrams can be obtained via collinear reduction of: (a) the (1,1,3,1) web; (b) the (1,2,2,1) web. Diagram (c) shows the connected colour factor that features one vertex on each line and cannot be determined by collinear reduction.

In this section, we have calculated the three-loop, three-line MGEWs that are needed for the three-loop soft anomalous dimension. In the remainder of the chapter, we examine how the methods developed here, and in Ref. [60], can be applied beyond the three-loop order. We begin by studying a particular four-loop example in the following section.

3.6 A four-loop, five-line web

The method developed in Ref. [60] and in Sections 2.4-3.4 above allows us to compute high-order webs in the MGEW class with relatively little effort. It is then

worthwhile to look for interesting examples beyond three loops: this will provide non-trivial checks of our conjectures on the analytic structure of subtracted webs, and on the relevant basis of functions.

In this section, we present a complete calculation of a fully subtracted four-loop web. As our example, we choose to consider the (1,2,2,2,1) web, connecting five Wilson lines at four loops, and consisting of the diagrams depicted in Fig. 3.13. The (1,2,2,2,1) web is particularly interesting because of its simple colour structure, and because, spanning five legs, it will allow one to determine certain components of other webs at the same order, spanning a smaller number of Wilson lines but having more than one effective vertex on at least one line. Furthermore, the (1,2,2,2,1) web is the third member of the infinite series of MGEWs (1,2,2,⋯,2,1), connecting $n + 1$ lines at n loops. All the webs in this class have a single colour structure, and the general solution of the corresponding web mixing matrices for any n have been obtained using combinatorial methods in [59, 93], while the kinematic functions have been determined in [60] for the cases $n = 2, 3$. One may hope that a completely explicit answer for the first three elements of this collection could provide some insights for an all-order answer.

The pattern of subtractions at the four-loop level is particularly intricate, as can be seen from Eq. (2.43). For example, in the specific case of the web (1,2,2,2,1), we need to consider the commutators of the webs (1,2,2,1), (1,2,1) and (1,1) connecting the five lines. In this section we organize and discuss the result, while further details are given in Appendix A.4.

The first step in the construction of the subtracted web is the determination of the colour structure. In the case of the (1,2,2,2,1) web, depicted in Fig. 3.13, there is only one colour structure, which can be written in terms of ordinary colour generators as

$$c_1^{(5)} = T_1^a [T_2^a, T_2^b] [T_3^b, T_3^c] [T_4^c, T_4^d] T_5^d. \quad (3.78)$$

The corresponding combination of integrals can be constructed from the appropriate web mixing matrix, which is known [59]. Expressing the result in terms of the kinematic Feynman integrals of the individual diagrams in Fig. 3.13, one finds

$$\mathcal{F}_{(1,2,2,2,1),1}^{(4)}(\alpha_{ij}, \epsilon) = \frac{1}{24} [6 (\mathcal{F}^{(4)}(F) - \mathcal{F}^{(4)}(A)) + 2 (\mathcal{F}^{(4)}(C) + \mathcal{F}^{(4)}(D) + \mathcal{F}^{(4)}(E))]$$

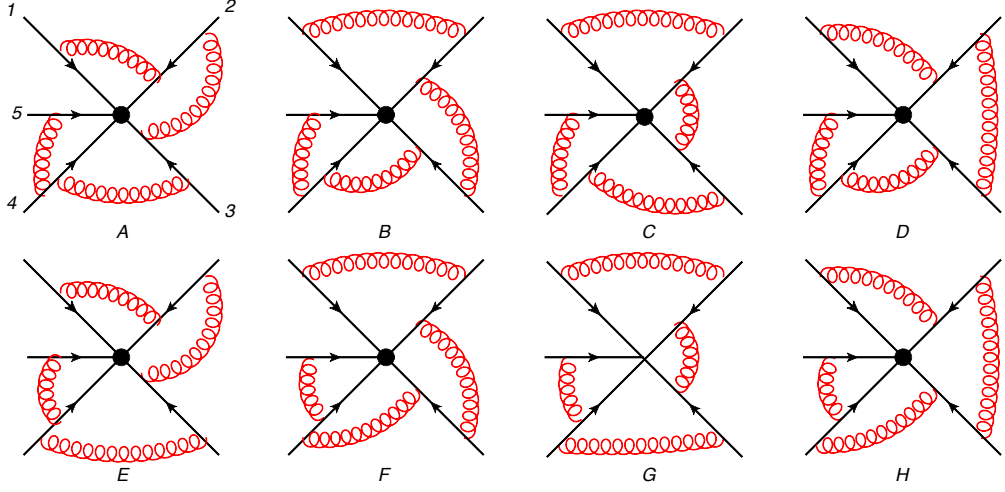


Figure 3.13: The (1,2,2,2,1) web connecting five Wilson lines at four loops.

$$-2 (\mathcal{F}^{(4)}(B) + \mathcal{F}^{(4)}(G) + \mathcal{F}^{(4)}(H))]. \quad (3.79)$$

It is convenient to work at the level of the integrand of the diagrams, by taking directly the combination in Eq. (3.79) of the functions $\phi_X^{(4)}$ given in Appendix A.4. The unsubtracted web is lengthy, and, much like the (1,2,2,1) web of Ref. [60], contains polylogarithms, so upon integration it does not yield a factorized function of the cusp angles, but rather a lengthy sum of MPLs involving different kinematic variables.

According to the factorization conjecture, we expect that the commutators of the webs at lower orders will cancel all the correlations between different cusp angles, as well as all polylogarithmic functions in the kernel. We find that indeed the integrand of the subtracted web becomes much simpler, and the integrated result is factorized as expected. The subtracted web kernel, in terms of the functions defined in Eq. (3.64), is given by

$$\begin{aligned} \mathcal{G}_{(1,2,2,2,1),1}^{(4)}(x_i, \alpha_i) &= -\frac{1}{144} \left\{ L_{12}^3 - 3L_{23}^3 + 3L_{34}^3 - L_{45}^3 \right. \\ &\quad + 3L_{12}^2 \left[L_{23} + L_{34} - 3L_{45} \right] - 3L_{45}^2 \left[L_{23} + L_{34} - 3L_{12} \right] \\ &\quad \left. + 3L_{23}^2 \left[L_{12} - 3L_{34} + 5L_{45} \right] - 3L_{34}^2 \left[L_{45} - 3L_{23} + 5L_{12} \right] \right\} \end{aligned} \quad (3.80)$$

$$\begin{aligned}
 & + 6 \left[L_{12}L_{23}L_{34} - 3L_{12}L_{23}L_{45} + 3L_{12}L_{34}L_{45} - L_{23}L_{34}L_{45} \right] \\
 & + 24 \left[R_2^2 \left(L_{12} + L_{23} + L_{34} - 3L_{45} \right) - R_3^2 \left(L_{23} + L_{34} + L_{45} - 3L_{12} \right) \right] \Big\}.
 \end{aligned}$$

By looking at the subtracted web kernel in Eq. (3.80), we immediately note that the result is already expressed in terms of the functions of the basis in Eq. (3.35). More precisely, the functions $M_{3,0,0}(\alpha_{ij})$ and $M_{1,2,0}(\alpha_{ij})$ at weight four are the only new functions appearing at this order. Upon performing the x_k integrals, and in the notations of Eq. (3.23), we find that the contribution of this web to the anomalous dimension is given by

$$\begin{aligned}
 F_{(1,2,2,2,1),1}^{(4)}(\alpha_{ij}) &= -\frac{1}{144} r(\alpha_{12})r(\alpha_{23})r(\alpha_{34})r(\alpha_{45}) \times \tag{3.81} \\
 & \times \left\{ \left[6 \left(M_{1,0,0}(\alpha_{12})M_{1,0,0}(\alpha_{23})M_{1,0,0}(\alpha_{34})M_{0,0,0}(\alpha_{45}) \right. \right. \right. \\
 & \quad \left. \left. \left. - 3M_{1,0,0}(\alpha_{12})M_{1,0,0}(\alpha_{23})M_{1,0,0}(\alpha_{45})M_{0,0,0}(\alpha_{34}) \right) \right. \right. \\
 & \quad \left. \left. + \left(M_{3,0,0}(\alpha_{12})M_{0,0,0}(\alpha_{45}) - 9M_{2,0,0}(\alpha_{12})M_{1,0,0}(\alpha_{45}) \right) M_{0,0,0}(\alpha_{23})M_{0,0,0}(\alpha_{34}) \right. \right. \\
 & \quad \left. \left. - 3 \left(M_{3,0,0}(\alpha_{23})M_{0,0,0}(\alpha_{34}) + 3M_{2,0,0}(\alpha_{23})M_{1,0,0}(\alpha_{34}) \right) M_{0,0,0}(\alpha_{12})M_{0,0,0}(\alpha_{45}) \right. \right. \\
 & \quad \left. \left. + 3M_{2,0,0}(\alpha_{12})M_{0,0,0}(\alpha_{45}) \left(M_{1,0,0}(\alpha_{23})M_{0,0,0}(\alpha_{34}) + M_{1,0,0}(\alpha_{34})M_{0,0,0}(\alpha_{23}) \right) \right. \right. \\
 & \quad \left. \left. + 3M_{2,0,0}(\alpha_{23})M_{0,0,0}(\alpha_{34}) \left(M_{1,0,0}(\alpha_{12})M_{0,0,0}(\alpha_{45}) + 5M_{1,0,0}(\alpha_{45})M_{0,0,0}(\alpha_{12}) \right) \right. \right. \\
 & \quad \left. \left. + 24M_{0,2,0}(\alpha_{23}) \left(M_{1,0,0}(\alpha_{12})M_{0,0,0}(\alpha_{34})M_{0,0,0}(\alpha_{45}) \right. \right. \right. \\
 & \quad \left. \left. \left. + M_{1,0,0}(\alpha_{34})M_{0,0,0}(\alpha_{12})M_{0,0,0}(\alpha_{45}) - 3M_{1,0,0}(\alpha_{45})M_{0,0,0}(\alpha_{12})M_{0,0,0}(\alpha_{34}) \right) \right. \right. \\
 & \quad \left. \left. \left. + 24M_{1,2,0}(\alpha_{23})M_{0,0,0}(\alpha_{12})M_{0,0,0}(\alpha_{34})M_{0,0,0}(\alpha_{45}) \right] \right. \right. \\
 & \quad \left. \left. - \left[(\alpha_{12} \leftrightarrow \alpha_{45}), (\alpha_{23} \leftrightarrow \alpha_{34}) \right] \right\}.
 \end{aligned}$$

As expected, we find a factorized function of uniform transcendental weight $w = 7$, expressed as a sum of products of our basis functions, each one depending on a single cusp angle, and satisfying the symbol conjecture. Through various

collinear limits, this will also yield information on other four-loop webs, involving less than five Wilson lines, but with more than one effective vertex on a given line.

3.7 The Escher Staircase and $(2, 2, \dots, 2)$ webs

In this section we will explore the flexibility and the reach of the formalism that we have developed above by computing a certain class of diagrams contributing to a specific series of MGEWs to all orders in perturbation theory. The results of the calculation are not of immediate physical relevance, since we will not be computing complete webs, much less subtracted webs, to all orders. Nevertheless, the calculation of these particular diagrams will allow us to prove a general statement about this series of webs. Moreover, the feasibility of this calculation suggests that all-order calculations of MGEWs are possible. In addition the simplicity of the result, which by itself is properly factorized into functions belonging to our basis, provides further evidence for our conjectures.

Following Ref. [56], we refer to the class of diagrams we will compute as Escher staircases. An example with $n = 6$ is displayed in Fig. 3.14. These diagrams are the most symmetric members of the n -loop $(2, 2, \dots, 2)$ webs: each such web contains 2^n diagrams, two of which are of the form we are studying, differing by clockwise or counterclockwise orientations. The staircase diagrams are particularly interesting, not only because of their graphical symmetry, but also because they do not have subdivergences, so they do not require commutator counterterms. As a consequence, they should satisfy the alphabet and factorization conjectures by themselves, and indeed we will find that they do. Interestingly, we also find that a non-trivial cancellation takes place when the kinematic factors of staircase diagrams are combined to build up contributions to the n -loop soft anomalous dimension. Indeed, as verified in Sec. 3.5.1 for the $(2,2,2)$ web, the two staircases are the only diagrams to contribute to the colour structure composed of only V_2 effective vertices, denoted by $c_4^{(3)}$ in Sec. 3.5.1. Their contributions to that colour structure however cancel exactly, as noted in Eq. (3.69). The $(2,2,2)$ staircases of course do contribute to the other three colour structures, $c_i^{(3)}$, with $i = 1, 2, 3$. One should keep in mind, however, that the kinematic functions of those colour structures can be obtained also from

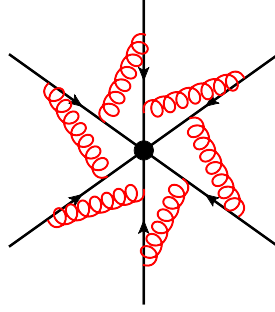


Figure 3.14: Example of an Escher staircase with six external legs. There are two staircases at arbitrary order, related by reflection.

collinear reduction of the $(1, 2, 2, 1)$ web. A similar story is played out for the $(2, 2, \dots, 2)$ web at arbitrary order, and we provide a general argument for this in what follows.

Turning now to the evaluation of the Escher staircase at n loops, we begin by noticing that the diagram kernel in Eq. (3.15) can be explicitly written down, for the staircase, as

$$\begin{aligned} \phi_S^{(n)}(x_i; \epsilon) &= \int_0^1 \prod_{k=1}^{n-1} dy_k (1 - y_k)^{-1+2\epsilon} y_k^{-1+2k\epsilon} \\ &\times \prod_{i=1}^n \theta \left[(1 - x_i) (1 - y_{i-1}) \prod_{j=i}^{n-1} y_j - x_{i+1} (1 - y_i) \prod_{j=i+1}^{n-1} y_j \right], \end{aligned} \quad (3.82)$$

where the i -th Heaviside function guarantees that the absorption point of gluon $i - 1$ is further away (along Wilson line i) than the emission point of gluon i . To properly define the product of θ functions, we set $1 - y_0 = 1 - y_n = 1$ when they occur, as well as $\prod_{j=n+1}^{n-1} y_j = \prod_{j=1}^{n-1} y_j$ in the last factor, and $\prod_{j=n}^{n-1} y_j = 1$ in the penultimate factor; similarly, we set $x_{n+1} = x_1$ when it occurs. To illustrate the notation, we write explicitly the products of θ functions for small n , as

$$\begin{aligned} n = 2 &\quad \rightarrow \quad \theta [(1 - x_1) y_1 - x_2 (1 - y_1)] \theta [(1 - x_2)(1 - y_1) - x_1 y_1], \\ n = 3 &\quad \rightarrow \quad \theta [(1 - x_1) y_1 y_2 - x_2 (1 - y_1) y_2] \\ &\quad \times \theta [(1 - x_2)(1 - y_1) y_2 - x_3 (1 - y_2)] \\ &\quad \times \theta [(1 - x_3)(1 - y_2) - x_1 y_1 y_2], \\ n = 4 &\quad \rightarrow \quad \theta [(1 - x_1) y_1 y_2 y_3 - x_2 (1 - y_1) y_2 y_3] \end{aligned} \quad (3.83)$$

$$\begin{aligned}
 & \times \theta [(1 - x_2)(1 - y_1) y_2 y_3 - x_3 (1 - y_2) y_3] \\
 & \times \theta [(1 - x_3)(1 - y_2) y_3 - x_4 (1 - y_3)] \\
 & \times \theta [(1 - x_4)(1 - y_3) - x_1 y_1 y_2 y_3] .
 \end{aligned}$$

Using the fact that $0 < x_i < 1$, and $0 < y_i < 1$, it is easy to realize that the θ functions are more naturally expressed by changing variables to $\xi_i \equiv y_i/(1 - y_i)$, so that $0 < \xi_i < \infty$. In this way one gets, for small n , factors of

$$\begin{aligned}
 n = 2 & \rightarrow \theta \left[\frac{x_2}{1 - x_1} < \xi_1 < \frac{1 - x_2}{x_1} \right] \theta \left[\frac{(1 - x_1)(1 - x_2)}{x_1 x_2} > 1 \right] , \\
 n = 3 & \rightarrow \theta \left[\frac{x_3}{1 - x_2} < \xi_2 < \frac{1 - x_3}{x_1 \xi_1} \right] \theta \left[\frac{x_2}{1 - x_1} < \xi_1 < \frac{(1 - x_2)(1 - x_3)}{x_1 x_3} \right] \\
 & \times \theta \left[\frac{(1 - x_1)(1 - x_2)(1 - x_3)}{x_1 x_2 x_3} > 1 \right] , \\
 n = 4 & \rightarrow \theta \left[\frac{x_4}{1 - x_3} < \xi_3 < \frac{(1 - x_4)(1 + \xi_1)}{x_1 \xi_1 \xi_2} \right] \\
 & \times \theta \left[\frac{x_3}{1 - x_2} < \xi_2 < \frac{(1 - x_3)(1 - x_4)}{x_1 x_4 \xi_1} \right] \\
 & \times \theta \left[\frac{x_2}{1 - x_1} < \xi_1 < \frac{(1 - x_2)(1 - x_3)(1 - x_4)}{x_1 x_3 x_4} \right] \\
 & \times \theta \left[\frac{(1 - x_1)(1 - x_2)(1 - x_3)(1 - x_4)}{x_1 x_2 x_3 x_4} > 1 \right] ,
 \end{aligned} \tag{3.84}$$

where we used the notation $\theta(a < x < b)$ to denote the product $\theta(b - x) \theta(x - a)$. Furthermore, the last θ function for each n must be present since the variables x_i must also later be integrated in the interval $0 < x_i < 1$; its meaning is clear: it distinguishes the ‘clockwise’ staircase diagram from the ‘counterclockwise’ one, which carries the complementary θ function. We define therefore

$$\theta_+(n) \equiv \theta \left(S_n(x_i) - 1 \right) \tag{3.85}$$

where

$$S_n(x_i) \equiv \prod_{i=1}^n \frac{1 - x_i}{x_i} . \tag{3.86}$$

The n -loop ‘clockwise’ staircase diagram carries a factor of $\theta_+(n)$, while its ‘counterclockwise’ image carries a factor of $\theta_-(n) = 1 - \theta_+(n)$. Upon further inspection of Eq. (3.84) one sees also that the ξ_i integrals are all bounded

from above and from below: since poles in ϵ could only arise from the limits $\xi_i \rightarrow \{0, \infty\}$, this implies, as expected, that the staircase graph has only a single overall UV divergence, given by $\Gamma(2n\epsilon)$ in Eq. (3.14), and no subdivergences. It is not difficult to work out the generalization to all n of the constraints in Eq. (3.84): one can then write Eq. (3.82) as

$$\begin{aligned} \phi_S^{(n)}(x_i; \epsilon) &= \int_0^\infty \prod_{k=1}^{n-1} d\xi_k (1 + \xi_k)^{-2(k+1)\epsilon} \xi_k^{-1+2k\epsilon} \Theta_S[\{x_k, \xi_k\}] \\ &= \theta_+(n) \int_{A_1}^{B_1} \frac{d\xi_1}{\xi_1} \int_{A_2}^{B_2(\xi_1)} \frac{d\xi_2}{\xi_2} \dots \int_{A_{n-1}}^{B_{n-1}(\xi_1, \xi_2, \dots, \xi_{n-2})} \frac{d\xi_{n-1}}{\xi_{n-1}} + \mathcal{O}(\epsilon). \end{aligned} \quad (3.87)$$

Importantly, the resulting integral is explicitly of a ‘ $d \log$ ’ form, in agreement with the considerations of Refs. [52, 60]. The remaining difficulty is that (also as expected) the integrals are nested and not completely factorized. One can however work out explicitly the limits of integration, generalizing Eq. (3.84). One finds

$$A_k = \frac{x_{k+1}}{1 - x_k}, \quad B_k(\xi_1, \dots, \xi_{k-1}) = \frac{\prod_{j=k+1}^n (1 - x_j) \prod_{j=1}^{k-2} (1 + \xi_j)}{\prod_{j=k+2}^{n+1} x_j \prod_{j=1}^{k-1} \xi_j}, \quad (3.88)$$

where we define $x_{n+1} = x_1$, and all products running over empty sets of integers are set equal to one. The final integration is now trivial, and one finds the remarkably simple result

$$\phi_S^{(n)}(x_i; 0) = \frac{1}{(n-1)!} \theta_+(n) \left(\log [S_n(x_i)] \right)^{n-1}. \quad (3.89)$$

The result is Bose symmetric and completely factorized, and, when integrated to give the kinematic function $\mathcal{F}^{(n)}(S)$ of Eq. (3.14), manifestly expressible in terms of our basis functions.

Note now that by sending $x_i \leftrightarrow 1 - x_i$ in Eq. (3.89), the result has the same form, but with a factor $(-1)^{n-1}$ from the power of the logarithm, and θ_+ replaced by θ_- . Denoting the clockwise and anticlockwise staircase diagrams by S_+ and S_- respectively, one thus finds

$$\mathcal{F}(S_+) = (-1)^{n-1} \mathcal{F}(S_-). \quad (3.90)$$

This leads to the cancellation observed at three loops ($n = 3$) in Sec. 3.5.1: the two staircase diagrams have identical kinematic factors, which however combine to form the coefficient of the colour structure $c_3^{(4)}$ with the same weight and opposite signs. Since the other diagrams in the $(2,2,2)$ web do not contribute to $c_3^{(4)}$, the corresponding coefficient vanishes. We now demonstrate that a similar argument applies in an arbitrary $(2, 2, \dots, 2)$ web.

Let us define a colour basis for n -loop webs connecting n lines, generalising the three-loop basis of Eq. (3.60). The requirement in constructing this basis is that it should allow one to express all the colour components of the $(2,2,\dots,2)$ web. The dimension of this basis is¹³ $n + 1$, and its elements have a transparent interpretation (see Fig. 3.10 for the three-loop case) upon considering the $(2,2,\dots,2)$ web in the effective vertex formalism of Ref. [61]: $c_i^{(n)}$ ($1 \leq i \leq n$) is the colour factor one obtains upon having two V_1 vertices on line i , corresponding to an anticommutator of colour generators, and a V_2 vertex, corresponding to a commutator, on all the other lines, yielding

$$c_i^{(n)} = [T_1^{a_1}, T_1^{a_2}] [T_2^{a_2}, T_2^{a_3}] \dots \{T_i^{a_i}, T_i^{a_{i+1}}\} \dots [T_{n-1}^{a_{n-1}}, T_{n-1}^{a_n}] [T_n^{a_n}, T_n^{a_1}]. \quad (3.91)$$

Finally, the $(n + 1)$ -th basis element is the fully antisymmetric colour factor corresponding to a V_2 vertex on each of the lines,

$$c_{n+1}^{(n)} = [T_1^{a_1}, T_1^{a_2}] [T_2^{a_2}, T_2^{a_3}] \dots [T_{n-1}^{a_{n-1}}, T_{n-1}^{a_n}] [T_n^{a_n}, T_n^{a_1}]. \quad (3.92)$$

It is this latter component of the $(2, 2, \dots, 2)$ web that will receive a contribution from the kinematic integrals of the staircase diagrams only, which will ultimately turn out to vanish. First, one notes that the fact that staircase diagrams are irreducible means that the web mixing matrix has the generic form

$$\begin{pmatrix} 1 & 0 & \dots \\ 0 & 1 & \dots \\ 0 & 0 & \dots \\ \vdots & \vdots & \dots \\ 0 & 0 & \dots \end{pmatrix},$$

¹³This is the rank of the mixing matrix of the $(2,2,\dots,2)$ web, as proved in Theorem 8.2 of Ref. [59].

where the first two columns arise from the staircase diagrams. This form follows from the replica trick analysis of Ref. [56], which dictates that the exponentiated colour factor of diagram D receives no contributions from diagrams D' which are more reducible (less irreducible) than D . From the above form, it then follows that any such mixing matrix has right-eigenvectors¹⁴ of the form

$$\begin{pmatrix} a & b & 0 & 0 & \dots & 0 \end{pmatrix}, \quad (3.93)$$

for arbitrary a and b . Two special cases are $a = \pm b = 1$, corresponding to the symmetric and antisymmetric combinations of S_+ and S_- . These combinations are special in that they have definite parity under a “flipping transformation” that interchanges all pairs of gluons on all lines simultaneously. Such a transformation exchanges $S_+ \rightarrow S_-$, and so the symmetric (anti-symmetric) combination has flipping parity $+$ ($-$) respectively. The contribution from the entire web must be invariant under this transformation, as it maps the total web to itself. Given that the basis of colour factors in Eqs. (3.91) and (3.92) is linearly independent, each separate colour factor multiplied by the corresponding kinematic function must also be invariant under the flipping transformation. The basis we have chosen is particularly convenient in this regard, as each colour factor has a definite flipping parity: $(-1)^{n-1}$ for $c_i^{(n)}$ ($1 \leq i \leq n$) and $(-1)^n$ for the fully antisymmetric colour factor $c_{n+1}^{(n)}$. One then finds that the contribution to the latter colour factor contains the combination

$$c_{n+1}^{(n)} [\mathcal{F}(S_+) - \mathcal{F}(S_-) + \dots],$$

for odd n , and

$$c_{n+1}^{(n)} [\mathcal{F}(S_+) + \mathcal{F}(S_-) + \dots],$$

for even n , where the ellipsis in each case denotes possible contributions from non-staircase diagrams. In fact, such contributions are not present, which can be seen as follows. At the n -loop order, there are $n + 1$ colour factors, n of which have parity $(-1)^{n-1}$, and only one of which has parity $(-1)^n$. It follows that of the $(n + 1)$ right eigenvectors with eigenvalue 1, n must correspond to kinematic functions with flipping parity $(-1)^{n-1}$, and only one to parity $(-1)^n$. Since we

¹⁴Right eigenvectors of the mixing matrix correspond to $Y_{D,j}^{-1}$ in Eq. (2.29), dictating the linear combination of integrals associated with a given connected colour factor c_j .

know that the eigenvector of Eq. (3.93) with $a = (-1)^n b$ has parity $(-1)^n$, this must be the only possibility, and there can be no other contributions. Having established Eq. (3.90) above, this completes the proof that the contribution to the fully antisymmetric colour factor from the $(2, 2, \dots, 2)$ web vanishes.

Returning to consider the $(2, 2, \dots, 2)$ n -th order web as a whole, we now see that all of its non-vanishing components belong to the colour structures in Eq. (3.91), where one of the lines features an anticommutator of two V_1 emission vertices. This means that it may be determined from the corresponding n -loop $n + 1$ line $(1, 2, 2, \dots, 2, 1)$ web through collinear reduction, just as the $(2, 2, 2)$ web was obtained from the $(1, 2, 2, 1)$ web in Eq. (3.39). Specifically, at four-loops we essentially have the result for the $(2, 2, 2, 2)$ web based on the calculation of the $(1, 2, 2, 2, 1)$ web in Sec. 3.6.

In this section, we have shown that is possible to calculate a particular type of web diagram to all orders in perturbation theory. As seen from the explicit calculations of other webs, the computations for diagrams with subdivergences are considerably more intricate, and further technical developments will be needed before a complete calculation of an all-order class of subtracted webs can be completed. The present example however testifies to the underlying simplicity of the structure of MGEWs, and suggests that the problem of computing this class of webs might at some point be completely solved.

3.8 Conclusion

In this chapter, based on Ref. [1], we have extended the programme of Refs. [56, 58, 60, 61], which established a diagrammatic approach for studying IR singularities in QCD scattering amplitudes (see also [122, 123]). We have done this by computing the UV singularities of products of semi-infinite Wilson lines in terms of webs. In the multi-line case, webs are sets of diagrams, each closed under the group of gluon permutations on the Wilson lines, whose contribution to the *exponent* of the Wilson line correlator consists of a sum of terms, each involving a fully connected colour factor multiplying a linear combination of Feynman integrals of diagrams belonging to the set. As explained in detail in Refs. [58, 60, 61], and reviewed in Sec. 2.4, each web contains UV subdivergences in general, which must be removed by appropriate counterterms

involving commutators of subdiagrams. This makes the case of multi-leg scattering qualitatively different to the familiar case of a Wilson loop; we call the combination of an unrenormalised web and its counterterms a *subtracted web*.

Specifically, we have focused on the contribution to the soft anomalous dimension from diagrams consisting of multiple gluon exchanges between the Wilson lines. These Multiple Gluon Exchange Webs (MGEWs) are the simplest diagrams at any given order; however, they also contain the highest number of UV subdivergences. Thus, the web language, coupled with a suitable IR regulator for calculating individual diagrams, is extremely useful in order to cleanly isolate their contribution to the soft anomalous dimension.

MGEWs connecting four Wilson lines at three-loop order were already considered in Ref. [60], which also analysed the analytic structure of MGEWs in general. It was conjectured that: (i) the contributions of MGEWs to the soft anomalous dimension take the form of sums of products of polylogarithmic functions, each involving a single cusp angle; (ii) the symbol alphabet of these functions consists of $\{\alpha_{ij}, \alpha/(1 - \alpha_{ij}^2)\}$, where α_{ij} is defined in Eq. (2.61) related to the cusp angle at which the Wilson lines i and j meet.

We provided significant additional evidence supporting these conjectures. Moreover, we took a step forward in understanding MGEWs by constructing a basis of functions, motivated by the alphabet conjecture as well as specific calculations, that we conjecture can be used to express MGEWs connecting any number of Wilson lines at arbitrary order in perturbation theory. The basis $M_{k,l,n}(\alpha)$, is defined in Eq. (3.35) as a single parameter integral over the gluon emission angle. The integrand consists of a product of three types of logarithms (depending on the gluon emission angle and the corresponding cusp angle) raised to non-negative integer powers k, l and n , respectively. The basis functions are consistent with the alphabet conjecture, and they are conveniently characterised by their symbols; these are listed in Table 3.1 up to weight five. The functions may also be explicitly evaluated in terms of Harmonic polylogarithms with indices 0 and 1: all independent functions up to weight five are listed in Appendix A.1. The three logarithms appearing in the integrands of $M_{k,l,n}(\alpha)$ have been identified in two-loop calculations of the (2,2) and (1,2,1) webs, where functions up to weight three appear, that is $M_{k,l,n}(\alpha)$ with $k + n + l \leq 2$. The basis passed all tests at three loops, where basis elements up to weight five appear, corresponding to

$k + n + l \leq 4$. These tests include the four-line webs of Ref. [60], namely the (1,2,2,1) and (1,1,1,3) webs, the three-line webs of Sec. 3.5 above, namely the (2,2,2) and (1,2,3) webs, as well as the two-line (3,3) web of Sec. 3.4.2. Further tests are provided by the five-line four-loop (1,2,2,2,1) web computed in Sec. 3.6, and by the all order analysis of the Escher Staircase diagrams and the (2,2,...,2) webs in Sec. 3.7. Note however that the above statements are valid only in the Feynman gauge given that even the sum MGEWs over all MGEWs at a given order is not gauge invariant. Thus we can expect that there exist gauges mixing contributions from MGEWs and fully connected diagrams which we do not expect to be completely described by these basis functions alone.

We also discovered a procedure for deriving collinear reduction relations between webs connecting different numbers of Wilson lines. These relations, which we briefly summarize below, are discussed in more detail in Sec. 3.2, and then illustrated in several examples throughout the chapter. The idea is formulated using the effective vertex language of Ref. [61], which provides a convenient colour basis for webs. In this language, the emission of K gluons from a Wilson line, associated with a tree-graph colour factor (a fully nested commutator) is described by an effective vertex V_K . Considering a given web, different components may be described as connected graphs made out of such vertices, as shown for example in Figs. 3.8, 3.10 and 3.12. These graphs may in general feature one or more effective vertices on a given line. However, when multiple vertices appear on a line, they are not ordered: the integrals range over the entire Wilson line independently of each other, and in the colour factor one takes the symmetric combination of all possible orderings. As a consequence, the calculation of such a graph maps directly into the calculation of a graph where the Wilson line that features several vertices is replaced by a set of collinear lines, each featuring only one of these vertices. The upshot is that starting with a web that features a single effective vertex on each line, one may deduce various components of webs connecting fewer Wilson lines, but featuring more than one vertex on some of the lines. Collinear reduction provides stringent checks of the two- and three-line webs we have computed: it allowed us to determine one of the two components of the (3,3) web in Eq. (3.54), and the entire (2,2,2) web in Eq. (3.70), from the (1,2,2,1) web, as well as two of the three components of the (1,2,3) web in Eqs. (3.77) and (3.76), using, respectively, the (1,2,2,1) and

(1,1,3,1) webs. We note that the only colour component that cannot be deduced by collinear reduction for the (1,2,3) web is the one corresponding to the fully antisymmetric colour factor $c_4^{(3)}$ in Eq. (3.60). Given that the same diagrams enter both the components that can be deduced by collinear reduction and those that cannot, webs connecting less than the maximal number of lines at a given order are strongly constrained, providing us with high confidence in the results presented above.

As an additional check on the basis of functions we propose, as well as to illustrate the power and general applicability of the web language, we have also calculated the (1,2,2,2,1) four-loop web, and the Escher Staircase diagrams to arbitrary order in perturbation theory. The latter enter the $(2,2,\dots,2)$ web, and are especially simple because they do not contain UV subdivergences. Furthermore, we were able to show that the component corresponding to the fully antisymmetric colour factor of the $(2,2,\dots,2)$ web vanishes. This was proven using the fact that this colour structure is associated exclusively with the Escher Staircase diagrams, and these two diagrams are related by a parity transformation as in Eq. (3.90). The conclusion is rather striking: the entire contribution of the $(2,2,\dots,2)$ web family to the exponent can be deduced from the corresponding $(1,2,2,\dots,2,1)$ webs through collinear reduction. Specifically, at four loops, the result for the $(2,2,2,2)$ web can be directly read off the results of Sec. 3.6 for the $(1,2,2,2,1)$ web.

The analysis and explicit calculations which we have performed promote our understanding of an entire class of contributions to the renormalisation of Wilson line correlators. The progress achieved in understanding the analytic properties of the result [60], and the specific class of functions by which they may be expressed, is a step towards translating the entire calculation of an arbitrary MGEW into a combinatorial problem: given the factorization conjecture and the basis of functions, along with the expected transcendental weight, one may write down an ansatz for the answer where only rational numerical coefficients need to be fixed. This, along with the progress already made on webs [56, 58, 61] and their combinatorics [57, 59, 93] may facilitate all-order calculations in the future.

The results presented in this chapter also constitute a further step forward in assembling all necessary ingredients for the soft anomalous dimension of massive partons at three-loop order. In order to complete this programme, one needs to

include MGEWs in which gluons can be emitted and absorbed from the same Wilson line. Furthermore, one needs to include diagrams containing a single three-gluon vertex off the Wilson lines, which shall be the topic of the next chapter, and the fully connected graphs – appearing on the last line of Eq. (2.99).

Chapter 4

Webs Containing Three-Gluon Vertices

Having studied MGEWs in depth in the previous chapter, and having developed a general procedure for their computation, we will turn our attention to the next class of webs in the three-loop soft anomalous dimension. This class consists of webs whose diagrams contain a single three-gluon vertex subgraph connecting directly to (three or fewer) Wilson lines – such as those in Figs. 4.1 and 4.2. Specifically, in this chapter we shall aim to compute the (1,1,1,2) web, Fig. 4.2, which contains a three-gluon vertex between three lines, convoluted with a single gluon exchange with a fourth line which is the simplest of the three-loop examples in this class. This chapter is based on work which shall form part of a planned publication, Ref. [2].

At present, the only multi-line web containing a three-gluon vertex that has been computed in general kinematics is the two-loop, three-line diagram [68], Fig. 4.1. In this case, the integrand is seemingly complex (in comparison with the two-loop MGEWs),

$$\begin{aligned} w_{3g}^{(2)}(\alpha_{23}, \alpha_{24}, \alpha_{34}) &= c^{(2)}(4\pi)^2(-i\mathcal{N})^3\mu^{4\epsilon} \int_0^\infty ds_2 ds_3 ds_4 \int d^d z e^{-m(s_2\sqrt{-\beta_2^2} + s_3\sqrt{-\beta_3^2} + s_4\sqrt{-\beta_4^2})} \\ &\times \frac{\beta_2^\mu \beta_3^\nu \beta_4^\rho}{g_s} \Gamma_{\mu'\nu'\rho'}(s_2\beta_2, s_3\beta_3, s_4\beta_4) [D_{\mu\mu'}(s_2\beta_2 - z) D_{\nu\nu'}(s_3\beta_3 - z) D_{\rho\rho'}(s_4\beta_4 - z)], \end{aligned} \tag{4.1}$$

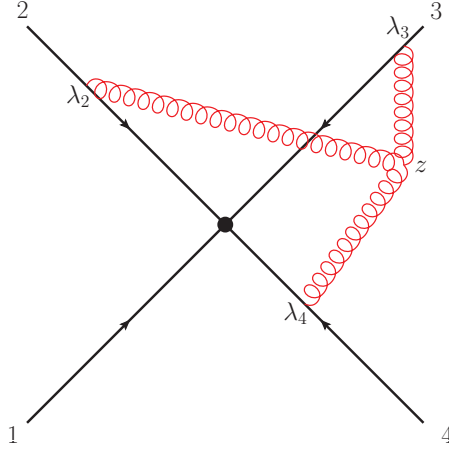


Figure 4.1: Two-loop diagram which gives the web $w_{3g}^{(2)}$, three-gluon vertex between three Wilson lines.

where the colour factor is

$$c^{(2)} = if^{abc}T_1^a T_2^b T_3^c, \quad (4.2)$$

and where the configuration space three-gluon vertex rule is

$$\begin{aligned} \frac{1}{g_s} \Gamma_{\mu'\nu'\rho'}(x_1, x_2, x_3) = & -i \left[g_{\mu'\nu'} \left(\frac{\partial}{\partial(x_1^{\rho'} - z^{\rho'})} - \frac{\partial}{\partial(x_2^{\rho'} - z^{\rho'})} \right) \right. \\ & + g_{\nu'\rho'} \left(\frac{\partial}{\partial(x_2^{\mu'} - z^{\mu'})} - \frac{\partial}{\partial(x_3^{\mu'} - z^{\mu'})} \right) \\ & \left. + g_{\mu'\rho'} \left(\frac{\partial}{\partial(x_3^{\nu'} - z^{\nu'})} - \frac{\partial}{\partial(x_1^{\nu'} - z^{\nu'})} \right) \right]. \end{aligned} \quad (4.3)$$

However, it belies a remarkably simple solution in terms of MGEW basis functions, Eq. (3.35),

$$\begin{aligned} w_{3g}^{(2,-1)}(\alpha_{23}, \alpha_{24}, \alpha_{34}) = & -c^{(2)} \left(\frac{1}{4\pi} \right)^2 \frac{1}{4} \left[r(\alpha_{23}) M_{0,0,0}(\alpha_{23}) (M_{0,0,0}^2(\alpha_{34}) - M_{0,0,0}^2(\alpha_{24})) \right. \\ & + r(\alpha_{24}) M_{0,0,0}(\alpha_{24}) (M_{0,0,0}^2(\alpha_{23}) - M_{0,0,0}^2(\alpha_{34})) \\ & \left. + r(\alpha_{34}) M_{0,0,0}(\alpha_{34}) (M_{0,0,0}^2(\alpha_{24}) - M_{0,0,0}^2(\alpha_{23})) \right]. \end{aligned} \quad (4.4)$$

We wish to extend our knowledge further into the class of single three-gluon

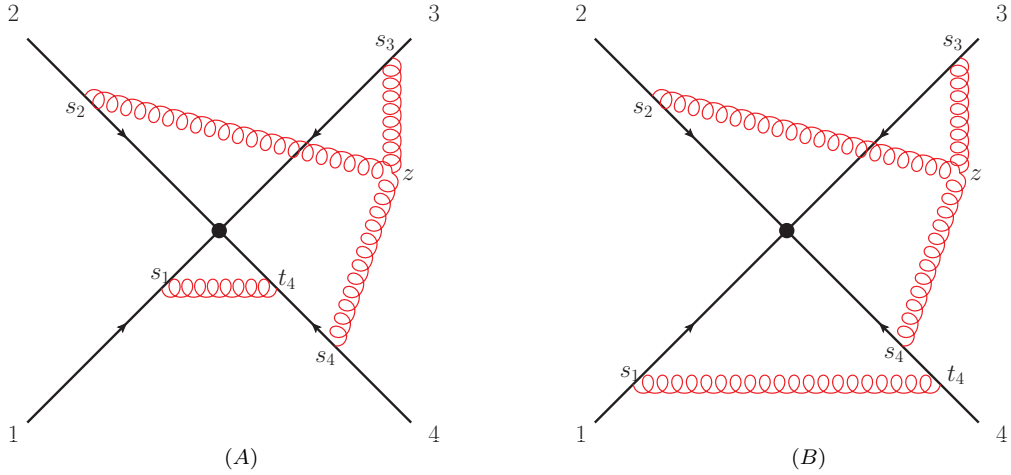


Figure 4.2: Diagrams contributing to the $(1,1,1,2)$ web through the combination given in Eq. (4.5)

vertex containing webs and in doing so, not only be able to move a step closer to the three-loop soft anomalous dimension, but also to reveal general properties of these subtracted webs which can be used to aid in future calculations.

In particular, it will be interesting to see whether the dramatic simplification seen in $w_{3g}^{(2,-1)}$ carries into the rest of the class and if they can be expressed in terms of the MGEW basis functions. If this is the case, then one expects that Eq. (4.1), the $(1,1,1,2)$, and related webs must be expressible through some parametrization which makes this simplicity manifest. Finding such a representation may lead to a procedure for their calculation in a manner similar to the treatment of MGEWs above in Ch. 3, and would likely be beneficial to our study of the far more difficult, fully connected webs – for example the last line in Eq. (2.99). To make such advances we need further data regarding the solution of this intermediary class.

The layout of this chapter is as follows. In Sec. 4.1 we study the kinematic factor of the $(1,1,1,2)$ subtracted web and discuss the methodologies available with which it may be computed. We consider the possibility of a direct integration through the methodology outlined in Sec. 2.6, though we find that a feasible choice is to obtain a least-squares fit of a physically constrained ansatz which we justify will be composed of sums of products of MGEW basis functions. This is attempted using data obtained by numerically integrating the $(1,1,1,2)$ integrals. As an illustrative example, and a benchmark, in Sec. 4.2 we generate such an

ansatz for the two-loop three-gluon vertex diagram, Eq. (4.1), and achieve a fit which reproduces Eq. (4.4). In Sec. 4.3 we return to the integrals obtained in Sec. 4.1 and an ansatz is produced and constrained with the requisite symmetries. We then make an attempt at numerically fixing the ansatz parameters.

4.1 Studying the (1,1,1,2) subtracted web

To begin, we shall construct the subtracted web and study its integrand. From [61] we see that the (1,1,1,2) web contains only a single colour factor,

$$w_{(1,1,1,2)}^{(3)} = -f^{ade} f^{bce} T_1^a T_2^b T_3^c T_4^d \frac{1}{2} \left(-\mathcal{F}_{(1,1,1,2); A}^{(3)} + \mathcal{F}_{(1,1,1,2); B}^{(3)} \right), \quad (4.5)$$

where $\mathcal{F}_{(1,1,1,2); A}^{(3)}$ and $\mathcal{F}_{(1,1,1,2); B}^{(3)}$ are the kinematic factors corresponding to diagrams A and B respectively from Fig. 4.2. Choosing again to work with space-like Wilson lines¹, the overall kinematic factor for the web,

$$\begin{aligned} \mathcal{F}_{(1,1,1,2)}^{(3)} &= \frac{1}{2} \left(-\mathcal{F}_{(1,1,1,2); A} + \mathcal{F}_{(1,1,1,2); B} \right) \\ &= i(4\pi)^3 \mathcal{N}^4 \mu^{6\epsilon} \int_0^\infty ds_1 ds_2 ds_3 ds_4 dt_4 \int d^d z \beta_1^\mu \beta_2^\nu \beta_3^\rho \beta_4^\sigma \beta_4^\delta \\ &\quad \times \frac{1}{g_s} \Gamma_{\nu'\rho'\sigma'}(s_2\beta_2, s_3\beta_3, s_4\beta_4) \left[D_{\mu\mu'}(s_2\beta_2 - z) D_{\nu\nu'}(s_3\beta_3 - z) \right. \\ &\quad \times \left. D_{\rho\rho'}(s_4\beta_4 - z) \right] D_{\mu\delta}(s_1\beta_1 - t_4\beta_4) \left\{ \frac{\theta(t_4 - s_4) - \theta(s_4 - t_4)}{2} \right\} \\ &\quad \times e^{-m(s_1\sqrt{-\beta_1^2} + s_2\sqrt{-\beta_2^2} + s_3\sqrt{-\beta_3^2} + t_4\sqrt{-\beta_4^2} + s_4\sqrt{-\beta_4^2})}. \end{aligned} \quad (4.6)$$

The factor $1/g_s$ in Eq. (4.6) accounts for the corresponding factor in Eq. (4.3) and is necessary as we have factorized the strong coupling from the web coefficients, $w^{(n,k)}$, according to Eq. (2.42). As was the case of the MGEWs in Sec. 2.5 and Sec. 3.3.1, it will benefit us to make the change of variables $s_i \rightarrow \sigma_i/\sqrt{-\beta_i^2}$, $t_4 \rightarrow \tau_4/\sqrt{-\beta_4^2}$, followed by

$$\begin{pmatrix} \sigma_2 \\ \sigma_3 \\ \sigma_4 \end{pmatrix} \longrightarrow \lambda \begin{pmatrix} x_2 \\ x_3 \\ x_4 \end{pmatrix}, \quad \begin{pmatrix} \sigma_1 \\ \tau_4 \end{pmatrix} \longrightarrow \sigma \begin{pmatrix} a \\ 1 - a \end{pmatrix}, \quad (4.7)$$

¹See Sec. 2.5 for further discussion.

where $\lambda, \sigma \in (0, \infty)$, $a \in (0, 1)$ and $\sum_i x_i = 1$, preceding

$$\begin{pmatrix} \lambda \\ \sigma \end{pmatrix} \longrightarrow \rho \begin{pmatrix} b \\ 1-b \end{pmatrix}, \quad \rho \in (0, \infty), b \in (0, 1). \quad (4.8)$$

Once again we can interpret the $\rho \rightarrow 0$ limit geometrically as both sub-diagrams simultaneously shrinking to the cusp, resulting in an overall UV pole in $\epsilon \rightarrow 0^+$. Conversely, $\rho \rightarrow \infty$ is the IR limit, regularized by the exponential regulator with scale m . Carrying out the ρ integral therefore yields,

$$\begin{aligned} \mathcal{F}_{(1,1,1,2)}^{(3)} &= -\frac{i}{g_s} (4\pi)^3 \mathcal{N}^4 \mu^{6\epsilon} \frac{1}{4} \frac{\Gamma(6\epsilon)}{m^{6\epsilon}} \int_0^1 dx_2 dx_3 dx_4 dadb \\ &\quad \delta\left(1 - \sum_i x_i\right) b^{-1+2\epsilon} (1-b)^{-1+4\epsilon} \int d^d \widehat{z} \widehat{\beta}_2^\nu \widehat{\beta}_3^\rho \widehat{\beta}_4^\sigma \gamma_{14} P_\epsilon(a, \gamma_{14}) \\ &\quad \Gamma_{\nu'\rho'\sigma'}(x_2 \widehat{\beta}_2, x_3 \widehat{\beta}_3, x_4 \widehat{\beta}_4) \left[D_{\mu\mu'}(x_2 \widehat{\beta}_2 - \widehat{z}) D_{\nu\nu'}(x_3 \widehat{\beta}_3 - \widehat{z}) D_{\rho\rho'}(x_4 \widehat{\beta}_4 - \widehat{z}) \right] \\ &\quad \left(\theta\left(\frac{b}{1-b} - \frac{x_4}{1-a}\right) - \theta\left(\frac{x_4}{1-a} - \frac{b}{1-b}\right) \right), \end{aligned} \quad (4.9)$$

where we have also had to scale $z^\mu \rightarrow \lambda \widehat{z}^\mu$, and

$$\widehat{\beta}_i^\mu = \frac{\beta_i^\mu}{\sqrt{-\beta_i^2}}. \quad (4.10)$$

Noticing that,

$$\frac{\partial}{\partial(x_i^\mu - z^\mu)} \left[-(x_i - z)^2 \right]^{\epsilon-1} = \frac{\partial}{\partial x_i^\mu} \left[-(x_i - z)^2 \right]^{\epsilon-1} \quad (4.11)$$

we can rewrite the kinematic factor,

$$\begin{aligned} \mathcal{F}_{(1,1,1,2)}^{(3)} &= -\frac{1}{4} (4\pi)^3 \mathcal{N}^4 \left(\frac{\mu^2}{m^2} \right)^{3\epsilon} \Gamma(6\epsilon) \int_0^1 dx_2 dx_3 dx_4 dadb \\ &\quad \delta\left(1 - \sum_i x_i\right) b^{-1+2\epsilon} (1-b)^{-1+4\epsilon} \\ &\quad \Gamma_{3g} \left[\int d^d \widehat{z} D(x_2 \widehat{\beta}_2 - \widehat{z}) D(x_3 \widehat{\beta}_3 - \widehat{z}) D(x_4 \widehat{\beta}_4 - \widehat{z}) \right] \\ &\quad \gamma_{14} P_\epsilon(a, \gamma_{14}) \left(\theta\left(\frac{b}{1-b} - \frac{x_4}{1-a}\right) - \theta\left(\frac{x_4}{1-a} - \frac{b}{1-b}\right) \right), \end{aligned} \quad (4.12)$$

defining,

$$\begin{aligned} \Gamma_{3g} = & \frac{\gamma_{23}}{2} \widehat{\beta}_4^\mu \left(\frac{\partial}{\partial x_2 \widehat{\beta}_2^\mu} - \frac{\partial}{\partial x_3 \widehat{\beta}_3^\mu} \right) + \frac{\gamma_{34}}{2} \widehat{\beta}_2^\mu \left(\frac{\partial}{\partial x_3 \widehat{\beta}_3^\mu} - \frac{\partial}{\partial x_4 \widehat{\beta}_4^\mu} \right) \\ & + \frac{\gamma_{24}}{2} \widehat{\beta}_3^\mu \left(\frac{\partial}{\partial x_4 \widehat{\beta}_4^\mu} - \frac{\partial}{\partial x_2 \widehat{\beta}_2^\mu} \right). \end{aligned} \quad (4.13)$$

We note here that though we have factored out the overall UV divergence corresponding to the shrinking of all sub-diagrams to the cusp in Eq. (4.12), there remains a further sub-divergence resulting from the UV limit of the innermost sub-diagrams of Fig. 4.2. This will manifest as a double pole after carrying out the divergent b integral, which itself can be interpreted as the relative distance of the sub-diagrams to the cusp.

Considering in isolation the \widehat{z} integral,

$$\int d^d \widehat{z} \frac{1}{(- (x_2 \widehat{\beta}_2 - \widehat{z})^2)^{1-\epsilon} (- (x_3 \widehat{\beta}_3 - \widehat{z})^2)^{1-\epsilon} (- (x_4 \widehat{\beta}_4 - \widehat{z})^2)^{1-\epsilon}}, \quad (4.14)$$

shifting $\widehat{z} \rightarrow \widehat{z} + x_4 \widehat{\beta}_4$ and introducing the dual-space momenta,

$$p_1^\mu = x_2 \widehat{\beta}_2^\mu - x_4 \widehat{\beta}_4^\mu, \quad p_2^\mu = x_3 \widehat{\beta}_3^\mu - x_2 \widehat{\beta}_2^\mu, \quad p_3^\mu = x_4 \widehat{\beta}_4^\mu - x_3 \widehat{\beta}_3^\mu, \quad (4.15)$$

we find that this is nothing other than a scalar triangle, Fig. 4.3. In this case with three external masses and no internal masses,

$$T(d, \nu_1, \nu_2, \nu_3; p_i^2) = e^{\epsilon \gamma_E} \int \frac{d^d z}{i\pi^{d/2}} \frac{1}{(- (z - p_1)^2)^{\nu_1} (- (z + p_3)^2)^{\nu_2} (- z^2)^{\nu_3}}. \quad (4.16)$$

Such scalar integrals have been studied extensively [124–126], and have been solved in d dimensions and for suitable powers of the propagators to all orders in the dimensional regularization parameter [124], in terms of Appell hypergeometric functions of the type F_4 (see Appendix B for a brief review of this result). In the case of Eq. (4.14) where we are in $4 - 2\epsilon$ dimensions with all propagators raised to the power $1 - \epsilon$, we find a special case of the result in which the F_4 functions

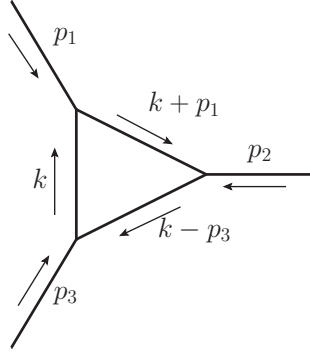


Figure 4.3: Scalar triangle with three external masses

reduce to simpler Gaussian hypergeometric functions allowing us to write,

$$\begin{aligned}
 & T(4 - 2\epsilon, 1 - \epsilon, 1 - \epsilon, 1 - \epsilon; p_i^2) \\
 &= \frac{e^{\epsilon\gamma_E}}{\Gamma^3(1 - \epsilon)\Gamma(1 + \epsilon)} (p_1^2)^{\frac{\epsilon}{2}} (p_2^2)^{\frac{\epsilon}{2}} (p_3^2)^{\epsilon-1} \\
 & \left[u^{\frac{\epsilon}{2}} v^{\frac{\epsilon}{2}} \Gamma(1 + \epsilon) \Gamma^2(-\epsilon) (1 - x)(1 - y) {}_2F_1\left(1, 1 - \epsilon, 1 + \epsilon, xy\right) \right. \\
 & + u^{\frac{\epsilon}{2}} v^{-\frac{\epsilon}{2}} \Gamma(1 - \epsilon) \Gamma(\epsilon) \Gamma(-\epsilon) (1 - y) {}_2F_1\left(1, 1 - \epsilon, 1 + \epsilon, -x \frac{1 - y}{1 - x}\right) \\
 & + u^{-\frac{\epsilon}{2}} v^{\frac{\epsilon}{2}} \Gamma(1 - \epsilon) \Gamma(\epsilon) \Gamma(-\epsilon) (1 - x) {}_2F_1\left(1, 1 - \epsilon, 1 + \epsilon, -y \frac{1 - x}{1 - y}\right) \\
 & \left. + u^{-\frac{\epsilon}{2}} v^{-\frac{\epsilon}{2}} \Gamma(1 - 2\epsilon) \Gamma(1 - \epsilon) \Gamma^2(-\epsilon) (1 - x)^{1-2\epsilon} (1 - y)^{1-2\epsilon} (1 - xy)^{-1+2\epsilon} \right], \quad (4.17)
 \end{aligned}$$

where

$$u = p_1^2/p_3^2 = -\frac{x}{(1-x)(1-y)} \quad \text{and} \quad v = p_2^2/p_3^2 = -\frac{y}{(1-x)(1-y)}. \quad (4.18)$$

We shall soon make use of this result in determining the appropriate methodology to be applied in completing the integration of the subtracted (1,1,1,2) web, as well as for numerical checks.

Returning now to Eq. (4.12), we can substitute Eq. (4.16), along with the Gaussian hypergeometric function integral representations, Eqs. (2.82) and (2.83),

to produce

$$\begin{aligned}
 \mathcal{F}_{(1,1,1,2)}^{(3)} &= \frac{1}{2} \Omega \Gamma(6\epsilon) \int_0^1 dx_2 dx_3 dx_4 da \delta\left(1 - \sum_i x_i\right) \\
 &\times \Gamma_{3g} \left[T(4 - 2\epsilon, 1 - \epsilon, 1 - \epsilon, 1 - \epsilon) \right] \\
 &\times \gamma_{14} P_\epsilon(a, \gamma_{14}) \left[\frac{1}{4\epsilon} \left(\frac{x_4}{1-a} \right)^{-4\epsilon} {}_2F_1 \left(6\epsilon, 4\epsilon, 1 + 4\epsilon, -\frac{1-a}{x_4} \right) \right. \\
 &\left. - \frac{1}{2\epsilon} \left(\frac{x_4}{1-a} \right)^{2\epsilon} {}_2F_1 \left(6\epsilon, 2\epsilon, 1 + 2\epsilon, -\frac{x_4}{1-a} \right) \right], \quad (4.19)
 \end{aligned}$$

where we have defined the prefactor

$$\Omega = \left(\frac{1}{2\pi} \right)^3 \left(\frac{\tilde{\mu}^2}{m^2} \right)^{3\epsilon} e^{2\epsilon\gamma_E} \Gamma^4(1 - \epsilon). \quad (4.20)$$

We are now prepared to obtain the Laurent expansion for the web written in terms of a two-dimensional parameter integral over derivatives of the scalar triangle. Given that the scalar triangle is finite in four dimensions we can write its expansion,

$$\begin{aligned}
 T(4 - 2\epsilon, 1 - \epsilon, 1 - \epsilon, 1 - \epsilon; p_i^2) &= T^{(0)}(p_1^2, p_2^2, p_3^2) + \epsilon T^{(1)}(p_1^2, p_2^2, p_3^2) \\
 &+ \mathcal{O}(\epsilon^2), \quad (4.21)
 \end{aligned}$$

and so the Laurent series expansion of $\mathcal{F}_{(1,1,1,2)}^{(3)}$ will be given by the integral,

$$\begin{aligned}
 \mathcal{F}_{(1,1,1,2)}^{(3)} &= \frac{2}{3} \left(\frac{1}{4\pi} \right)^3 \int_0^1 dx_2 dx_3 dx_4 da \delta\left(1 - \sum_i x_i\right) p_0(a, \alpha_{14}) \left[-\frac{1}{4\epsilon} \Gamma_{3g}[T^{(0)}] \right. \\
 &- \frac{1}{4} \Gamma_{3g}[T^{(0)}] \left(\log(q(a, \alpha_{14})) + 8 \log\left(\frac{x_4}{1-a}\right) \right. \\
 &\left. \left. + 3 \log\left(\frac{\mu^2}{m^2}\right) \right) - \frac{1}{4} \Gamma_{3g}[T^{(1)}] \right] + \mathcal{O}(\epsilon^2). \quad (4.22)
 \end{aligned}$$

The coefficient of the single pole, $w_{(1,1,1,2)}^{(3,-1)}$ will form the primary part of the subtracted (1,1,1,2) web (defined according to Eq. (2.44)),

$$\bar{w}_{(1,1,1,2)}^{(3)}(\alpha_{23}, \alpha_{24}, \alpha_{34}, \alpha_{14}) = w_{(1,1,1,2)}^{(3,-1)}(\alpha_{23}, \alpha_{24}, \alpha_{34}, \alpha_{14})$$

$$\begin{aligned}
 & -\frac{1}{2} [w_{3g}^{(2,0)}(\alpha_{23}, \alpha_{24}, \alpha_{34}), w^{(1,-1)}(\alpha_{14})] \\
 & +\frac{1}{2} [w_{3g}^{(2,-1)}(\alpha_{23}, \alpha_{24}, \alpha_{34}), w^{(1,0)}(\alpha_{14})],
 \end{aligned} \tag{4.23}$$

with $w_{3g}^{(2)}$ as defined in Eq. (4.1) and $w^{(1)}$, the one-loop diagram as reviewed in Sec. 2.5. Diagrammatically, the subtracted web, Eq. (4.23), can be represented with

$$\begin{aligned}
 \overline{w}_{(1,1,1,2)}^{(3)}(\alpha_{23}, \alpha_{24}, \alpha_{34}, \alpha_{14}) = & \frac{1}{2} \left(\begin{array}{c} \text{Diagram 1} \\ \text{Diagram 2} \end{array} \right)^{(-1)} \\
 & -\frac{1}{2} \left[\begin{array}{c} \text{Diagram 3} \\ \text{Diagram 4} \end{array} \right]^{(0)}, \quad \text{Diagram 5}^{(-1)} \\
 & +\frac{1}{2} \left[\begin{array}{c} \text{Diagram 6} \\ \text{Diagram 7} \end{array} \right]^{(-1)}, \quad \text{Diagram 8}^{(0)},
 \end{aligned} \tag{4.24}$$

where the superscript bracketed numbers beside diagrams indicate the relevant coefficient in their Laurent expansion. We can again identify the d -dimensional position integral for the three-gluon vertex in the two-loop diagram by substituting Eq. (4.16) into Eq. (4.1),

$$\begin{aligned}
 w_{3g}^{(2)}(\alpha_{23}, \alpha_{24}, \alpha_{34}) = & -c^{(2)} \left(\frac{1}{4\pi} \right)^2 \int_0^1 dx_2 dx_3 dx_4 \delta(1 - \sum_i x_i) \\
 & \times \left[\frac{1}{\epsilon} \Gamma_{3g}[T^{(0)}] + \Gamma_{3g}[T^{(1)}] - 2\Gamma_{3g}[T^{(0)}] \log \left(\frac{\mu^2}{m^2} \right) \right] \\
 & + \mathcal{O}(\epsilon).
 \end{aligned} \tag{4.25}$$

A check of our web Laurent expansion, Eq. (4.22), is provided by the double pole, $w^{(3,-2)}$, which can be written as a commutator of lower order webs [58]. Precisely that is,

$$w^{(3,-2)}(\alpha_{14}, \alpha_{23}, \alpha_{24}, \alpha_{34}) = \frac{1}{6} [w_{3g}^{(2,-1)}(\alpha_{23}, \alpha_{24}, \alpha_{34}), w^{(1,-1)}(\alpha_{14})]. \tag{4.26}$$

It is simple to show from the $SU(N)$ colour algebra that,

$$[c^{(2)}(234), c^{(1)}(14)] = -f^{ade} f^{bce} T_1^a T_2^b T_3^c T_4^d, \quad (4.27)$$

where $c^{(2)}(ijk)$ and $c^{(1)}(ij)$ are the colour factors of the $w_{3g}^{(3)}$ web, Eq. (4.2), and one-loop web, Eq. (2.60), respectively. Consequently, by taking the coefficient of the ϵ^{-1} pole in Eq. (2.73) and Eq. (4.25) into Eq. (4.26) we obtain,

$$w^{(3,-2)}(\alpha_{14}, \alpha_{23}, \alpha_{24}, \alpha_{34}) = -\frac{c_1^{(4)}}{6} \int_0^1 dx_2 dx_3 dx_4 da \delta(1 - \sum_i x_i) \left(\frac{1}{16\pi^2} \Gamma_{3g}[T^{(0)}] \right) \left(\frac{1}{4\pi} p_0(a, \alpha_{14}) \right), \quad (4.28)$$

matching exactly the leading singular term in Eq. (4.22). With this check in hand, we now substitute the relevant coefficients in Eqs. (2.60), (4.22), (4.25) and (4.27) into Eq. (4.23), leading to the (1,1,1,2) subtracted web,

$$\bar{w}_{(1,1,1,2)}^{(3)} = \frac{2}{3} \left(\frac{1}{4\pi} \right)^3 c_1^{(4)} \int_0^1 dx_2 dx_3 dx_4 da \delta(1 - \sum_i x_i) p_0(a, \alpha_{14}) \left[\Gamma_{3g}[T^{(1)}] - \left(4 \log x_4 + \log \left(\frac{q(a, \alpha_{14})}{a^2} \right) \right) \Gamma_{3g}[T^{(0)}] \right]. \quad (4.29)$$

Here, we have written the a integral in a manner which makes clear its solution in terms of MGEW basis functions (Eq. (3.35)),

$$\bar{w}_{(1,1,1,2)}^{(3)} = \frac{2}{3} \left(\frac{1}{4\pi} \right)^3 c_1^{(4)} \int_0^1 dx_2 dx_3 dx_4 \delta(1 - \sum_i x_i) p_0(a, \alpha_{14}) \left[\frac{1}{2} M_{0,0,0}(\alpha_{14}) \Gamma_{3g}[T^{(1)}] \right. \quad (4.30)$$

$$\left. - \left(2M_{0,0,0}(\alpha_{14}) \log x_4 + M_{1,0,0}(\alpha_{14}) \right) \Gamma_{3g}[T^{(0)}] \right], \quad (4.31)$$

which we separate into the two integrals,

$$t_0(\alpha_{23}, \alpha_{24}, \alpha_{34}) = \int_0^1 dx_2 dx_3 dx_4 \delta(1 - \sum_j x_j) \Gamma[T^{(0)}] \quad (4.32)$$

and

$$t_1(\alpha_{23}, \alpha_{24}, \alpha_{34}) = \int_0^1 dx_2 dx_3 dx_4 \delta\left(1 - \sum_j x_j\right) \left(\Gamma_{3g}[T^{(1)}] - 4 \log(x_4) \Gamma_{3g}[T^{(0)}] \right), \quad (4.33)$$

so that

$$\begin{aligned} \bar{w}_{(1,1,1,2)}^{(3)}(\alpha_{14}, \alpha_{23}, \alpha_{24}, \alpha_{34}) &= \frac{c_1^{(4)}}{3} \left(\frac{1}{4\pi} \right)^3 r(\alpha_{14}) \left(M_{0,0,0}(\alpha_{14}) t_1(\alpha_{23}, \alpha_{24}, \alpha_{34}) \right. \\ &\quad \left. - 2M_{1,0,0}(\alpha_{14}) t_0(\alpha_{23}, \alpha_{24}, \alpha_{34}) \right). \end{aligned} \quad (4.34)$$

We can apply consistency checks to Eq. (4.31) by taking into account physical constraints on the anomalous dimension coefficients, $\Gamma^{(n)}$, and accordingly on $\bar{w}^{(n)}$. Given that $\Gamma^{(n)}$ must be independent of the renormalization scale, $\tilde{\mu}$, the $\log(\tilde{\mu}^2/m^2)$ term in Eq. (4.22) must cancel with corresponding terms from the commutators in Eq. (4.23) (see Sec. 2.4 and Ref. [58]). This mirrors the dependence upon the scale m from the exponential regulator which, since it regulates the IR, should not appear in the renormalization factor and thus must not be present in subtracted webs. Indeed, both of these properties are apparent in Eq. (4.31). As a further check, the appearance of α_{14} through MGEW basis functions in the subtracted web required a non-trivial combination of subtraction commutator terms and the web coefficient.

The former of these integrals, Eq. (4.32), has already been computed as part of $w_{3g}^{(2,-1)}$. We see from Eq. (4.1),

$$w_{3g}^{(2,-1)}(\alpha_{23}, \alpha_{24}, \alpha_{34}) = -c^{(2)} \left(\frac{1}{4\pi} \right)^2 t_0(\alpha_{23}, \alpha_{24}, \alpha_{34}), \quad (4.35)$$

which from Eq. (4.4) requires

$$\begin{aligned} t_0(\alpha_{23}, \alpha_{24}, \alpha_{34}) &= \frac{1}{4} \left[r(\alpha_{23}) M_{0,0,0}(\alpha_{23}) (M_{0,0,0}^2(\alpha_{34}) - M_{0,0,0}^2(\alpha_{24})) \right. \\ &\quad \left. + r(\alpha_{24}) M_{0,0,0}(\alpha_{24}) (M_{0,0,0}^2(\alpha_{23}) - M_{0,0,0}^2(\alpha_{34})) \right. \\ &\quad \left. + r(\alpha_{34}) M_{0,0,0}(\alpha_{34}) (M_{0,0,0}^2(\alpha_{24}) - M_{0,0,0}^2(\alpha_{23})) \right]. \end{aligned} \quad (4.36)$$

Eq. (4.33), however, remains to be integrated. Firstly, let us consider the most direct approach, that is to attempt to write the integrand in $d \log$ form such that its representation in terms of generalized polylogarithms is made explicit, as outlined in Sec. 2.6. One possible order of integration is to substitute the corresponding terms in the ϵ expansion of Eq. (4.17) for $T^{(0)}$ and $T^{(1)}$ (see Appendix B for more details) leaving only the integrals over x_1 , x_2 and x_3 , though constrained by the delta function. Despite the fact that such a low dimensional integral leaves us tantalizingly close, this route has thus far failed to yield a result. This is due to the complexity of the arguments of the resulting polylogarithms in the integrand, the dependence on x_1, x_2 arising through the non-rational variables

$$z = \frac{1}{2}(1 + u - v + \sqrt{\lambda(1, u, v)}), \quad \bar{z} = \frac{1}{2}(1 + u - v - \sqrt{\lambda(1, u, v)}), \quad (4.37)$$

where λ denotes the Källén function,

$$\lambda(a, b, c) = a^2 + b^2 + c^2 - 2ab - 2ac - 2bc. \quad (4.38)$$

The precise results in terms of polylogarithms for $T^{(0)}$ and $T^{(1)}$ can be found in Appendix B.

Solving the scalar triangles first is only one of several possible orders of integration. A more amenable representation comes from writing the scalar triangle as a Feynman parameter integral,

$$\begin{aligned} T(d, \nu_1, \nu_2, \nu_3; p_i^2) &= e^{\gamma_E \epsilon} \frac{\Gamma(\nu - d/2)}{\Gamma(\nu_1)\Gamma(\nu_2)\Gamma(\nu_3)} \int_0^1 dy_2 dy_3 dy_4 \delta\left(1 - \sum_j y_j\right) \\ &\times y_2^{\nu_1-1} y_3^{\nu_2-1} y_4^{\nu_3-1} (y_2 + y_3 + y_4)^{\nu-d} \\ &\times (p_1^2 y_2 y_3 + p_2^2 y_3 y_4 + p_3^2 y_2 y_4)^{d/2-\nu}, \end{aligned} \quad (4.39)$$

where $\nu = \nu_1 + \nu_2 + \nu_3$, giving a representation for the integrals

$$\begin{aligned} t_0(\alpha_{23}, \alpha_{24}, \alpha_{34}) &= \int_0^1 \left[\prod_{j=2}^3 dx_j dy_j \right] \delta\left(1 - \sum_j x_j\right) \delta\left(1 - \sum_j y_j\right) \\ &\times \frac{1}{y_2 + y_3 + y_4} \Gamma_{3g} \left[\frac{1}{p_1^2 y_2 y_3 + p_2^2 y_3 y_4 + p_3^2 y_2 y_4} \right], \end{aligned} \quad (4.40)$$

$$\begin{aligned}
 t_1(\alpha_{23}, \alpha_{24}, \alpha_{34}) &= \int_0^1 \left[\prod_{j=2}^3 dx_j dy_j \right] \delta\left(1 - \sum_j x_j\right) \delta\left(1 - \sum_j y_j\right) \\
 &\times \frac{1}{y_2 + y_3 + y_4} \Gamma_{3g} \left[\frac{1}{p_1^2 y_2 y_3 + p_2^2 y_3 y_4 + p_3^2 y_2 y_4} \right. \\
 &\times \left. \left\{ 4 \log x_4 + \log(y_2 + y_3 + y_4) + \log y_2 + \log y_3 \right. \right. \\
 &\left. \left. + \log y_4 - 2 \log(p_1^2 y_2 y_3 + p_2^2 y_3 y_4 + p_3^2 y_2 y_4) \right\} \right]. \quad (4.41)
 \end{aligned}$$

At present, while we expect that the t_1 integral is almost certainly expressible in terms of MPLs, it seems that Eq. (4.41) is not directly linearly reducible and we have been unable thus far to find a parametrization which allows its direct integration through the methodology outlined in Sec. 2.6. Moreover, we have attempted to extend the work of Ref. [70] in which a class of so-called *conformal gauges* is derived which exploit the particular constraints on gluon polarization in eikonal diagrams to eliminate diagrams containing three- or four-gluon-vertices connecting directly to Wilson lines. This leads to a particularly substantial simplification at two loops in the computation of Eq. (4.1) since $\Gamma_3^{(2)}$ contains only this web and the (1,2,1). $w_{3g}^{(2,-1)}$ can then be recovered as the difference between $\Gamma_3^{(2)}$ in the two gauges and, as it turns out, $w_{3g}^{(2,-1)}$ then appears as simply a new term in the conformal gauge subtraction terms for the (1,2,1) MGEW. However we were unable, despite significant effort, to recover the (1,1,1,2) from a calculation in this gauge at three loops. The additional complication comes from the fully connected double three-gluon vertex diagram² which remains undetermined in the (far simpler) Feynman gauge and does not vanish in the conformal gauges.

This leads us to instead consider alternative numerical methods. Fortunately, when written in the form of Eq. (4.34), we see that the dependence upon α_{14} factorizes such that remaining integrals depend upon only the three angles α_{23} , α_{24} , α_{34} . Therefore, t_1 cannot depend on kinematics through more complicated variables, such as *conformal invariant cross-ratios*,

$$\rho_{ijkl} = \frac{\beta_i \cdot \beta_j \beta_k \cdot \beta_l}{\beta_i \cdot \beta_k \beta_j \cdot \beta_l}, \quad (4.42)$$

or, in other words, there are no new multiparton thresholds in this web and so we can apply the same physical constraints as were applied to MGEWs in Ref. [60],

²The first diagram in the last line of Eq. (2.99).

and further explored in Ch. 3, which heavily restrict the symbol alphabet. As was the case in MGEWs, as well as $w_{3g}^{(2,-1)}$, where it is possible to impose the symbol alphabet constraints, webs have been expressible as sums of products of the basis functions, Eq. (3.35), and the rational factor $r(\alpha_{ij}) = (1 + \alpha_{ij}^2)/(1 - \alpha_{ij}^2)$.

This is in contrast to the fully connected webs at three loops, the double three-gluon vertex and four-gluon-vertex diagrams (see the last line of Eq. (2.99)), which should be expected to carry kinematic dependence both through α_{ij} and ρ_{ijkl} , as observed in their lightlike limit [89]. This gives further thresholds in limits of ρ_{ijkl} implying an enriched symbol alphabet. Hence, we cannot expect such webs to be expressible in terms of the MGEW basis functions alone.

Our approach then is as follows: we shall use the above arguments to produce an ansatz for t_1 in terms of the basis functions, Eq. (3.35), constrain this ansatz with the physical symmetries of the diagrams and then, by numerically evaluating the integrals of Eq. (4.41) at random values of the angles α_{ij} , we should be able to obtain a numerical least-squares fit for the ansatz parameters to this data.

4.2 Fitting the two-loop web

As a check of the methodology which we shall soon apply to the t_1 integral, and as an illustration, we begin by building and fitting an ansatz for t_0 , Eq. (4.40) obtaining Eq. (4.36). From the same considerations as applied to the (1,1,1,2) discussion above, t_0 will carry kinematic dependence only through α_{ij} , not through conformal invariant cross-ratios. It also must carry the full weight of the $w_{3g}^{(2)}$ and so will be of uniform weight three.

Additionally, we must determine where the rational factors $r(\alpha_{ij})$ can appear. For this we turn to the $\alpha_{ij} \rightarrow 1/\alpha_{ij}$ symmetry which the web must possess given the relation $\gamma_{ij} = -\alpha_{ij} - 1/\alpha_{ij}$. Under this transformation from Eq. (3.35) we find,

$$\begin{aligned}
 M_{k,l,n}(1/\alpha) &= -\frac{1}{r(\alpha)} \int_0^1 dx p_0(x, \alpha) \left[\log^k \left(\frac{q(x, \alpha)}{x^2} \right) \log^l \left(\frac{x}{1-x} \right) \right. \\
 &\quad \left. \times \left(-\log \tilde{q}(x, \alpha) \right)^n \right] \\
 &= (-1)^{n+1} M_{k,l,n}(\alpha),
 \end{aligned} \tag{4.43}$$

and so basis functions with an even power of $\log(\tilde{q}(x, \alpha))$ must appear with another odd function. This can be either another odd basis function or a factor of $r(\alpha)$. All possible weight-three products of basis functions, and the requisite factors of $r(\alpha_{ij})$, are given in Tab. 4.1. We thus find a twenty-five parameter ansatz for t_0 ,

$$\begin{aligned}
 t_0 = & \lambda_1 M_{0,1,1}(\alpha_{23}) + \lambda_2 M_{2,0,0}(\alpha_{23})r(\alpha_{23}) + \lambda_3 M_{0,0,0}^3(\alpha_{23})r(\alpha_{23}) \\
 & + \lambda_4 M_{0,0,0}(\alpha_{23})M_{1,0,0}(\alpha_{23}) + \lambda_5 M_{0,1,1}(\alpha_{24}) + \lambda_6 M_{2,0,0}(\alpha_{24})r(\alpha_{24}) \\
 & + \lambda_7 M_{0,0,0}^3(\alpha_{24})r(\alpha_{24}) + \lambda_8 M_{0,0,0}(\alpha_{24})M_{1,0,0}(\alpha_{24}) + \lambda_9 M_{0,1,1}(\alpha_{34}) \\
 & + \lambda_{10} M_{2,0,0}(\alpha_{34})r(\alpha_{34}) + \lambda_{11} M_{0,0,0}^3(\alpha_{34})r(\alpha_{34}) + \lambda_{12} M_{0,0,0}(\alpha_{34})M_{1,0,0}(\alpha_{34}) \\
 & + \lambda_{13} M_{0,0,0}^2(\alpha_{23})M_{0,0,0}(\alpha_{24})r(\alpha_{24}) + \lambda_{14} M_{1,0,0}(\alpha_{23})r(\alpha_{23})M_{0,0,0}(\alpha_{24})r(\alpha_{24}) \\
 & + \lambda_{15} M_{0,0,0}^2(\alpha_{23})M_{0,0,0}(\alpha_{34})r(\alpha_{34}) + \lambda_{16} M_{1,0,0}(\alpha_{23})r(\alpha_{23})M_{0,0,0}(\alpha_{34})r(\alpha_{34}) \\
 & + \lambda_{17} M_{0,0,0}^2(\alpha_{24})M_{0,0,0}(\alpha_{34})r(\alpha_{34}) + \lambda_{18} M_{1,0,0}(\alpha_{24})r(\alpha_{24})M_{0,0,0}(\alpha_{34})r(\alpha_{34}) \\
 & + \lambda_{19} M_{0,0,0}(\alpha_{23})r(\alpha_{23})M_{0,0,0}^2(\alpha_{24}) + \lambda_{20} M_{0,0,0}(\alpha_{23})r(\alpha_{23})M_{1,0,0}(\alpha_{24})r(\alpha_{24}) \\
 & + \lambda_{21} M_{0,0,0}(\alpha_{23})r(\alpha_{23})M_{0,0,0}^2(\alpha_{34}) + \lambda_{22} M_{0,0,0}(\alpha_{23})r(\alpha_{23})M_{1,0,0}(\alpha_{34})r(\alpha_{34}) \\
 & + \lambda_{23} M_{0,0,0}(\alpha_{24})r(\alpha_{24})M_{0,0,0}^2(\alpha_{34}) + \lambda_{24} M_{0,0,0}(\alpha_{24})r(\alpha_{24})M_{1,0,0}(\alpha_{34})r(\alpha_{34}) \\
 & + \lambda_{25} M_{0,0,0}(\alpha_{23})r(\alpha_{23})M_{0,0,0}(\alpha_{24})r(\alpha_{24})M_{0,0,0}(\alpha_{34})r(\alpha_{34})
 \end{aligned} \tag{4.44}$$

for which we can now attempt to find a numerical fit of the parameters λ_i . Of course, this ansatz could be constrained further by imposing the antisymmetry under exchanging any two of the external lines inherent to the three-gluon vertex rule, Eq. (4.13). Doing so reduces Eq. (4.44) to a two parameter, completely antisymmetric ansatz,

$$\begin{aligned}
 t_0 = & \rho_1 \left[r(\alpha_{23})r(\alpha_{24}) \left(M_{0,0,0}(\alpha_{23})M_{1,0,0}(\alpha_{24}) - M_{1,0,0}(\alpha_{23})M_{0,0,0}(\alpha_{24}) \right) \right. \\
 & + r(\alpha_{23})r(\alpha_{34}) \left(-M_{0,0,0}(\alpha_{23})M_{1,0,0}(\alpha_{34}) + M_{1,0,0}(\alpha_{23})M_{0,0,0}(\alpha_{34}) \right) \\
 & \left. + r(\alpha_{24})r(\alpha_{34}) \left(-M_{1,0,0}(\alpha_{24})M_{0,0,0}(\alpha_{34}) + M_{0,0,0}(\alpha_{24})M_{1,0,0}(\alpha_{34}) \right) \right] \\
 & + \rho_2 \left[r(\alpha_{23})M_{0,0,0}(\alpha_{23}) \left(M_{0,0,0}^2(\alpha_{34}) - M_{0,0,0}^2(\alpha_{24}) \right) \right. \\
 & \left. + r(\alpha_{24})M_{0,0,0}(\alpha_{24}) \left(M_{0,0,0}^2(\alpha_{23}) - M_{0,0,0}^2(\alpha_{34}) \right) \right]
 \end{aligned} \tag{4.45}$$

$$+ r(\alpha_{34})M_{0,0,0}(\alpha_{34})(M_{0,0,0}^2(\alpha_{24}) - M_{0,0,0}^2(\alpha_{23})) \Big].$$

However, the (1,1,1,2) web, and thus the t_1 integral, has fewer constraints from such physical symmetries, and is of higher weight, leading to a greater number of allowed ansatz terms. We therefore choose to fit Eq. (4.44), the larger ansatz for t_0 , providing a better benchmark for the techniques we shall apply to t_1 in the next section.

The algorithms we have chosen to achieve this are available within *Mathematica* [127], namely `NIntegrate` for numerically evaluating t_0 over a random set of cusp angles, and `NMinimize` for finding a least-squares fit to this data for the ansatz parameters. For t_0 and t_1 , the parameter controlling the termination of the numerical integration is `NIntegrate`'s `MaxErrorIncreases` which indicates the number of iterations of the integration algorithm in which the global error increases after the region contributing the most to the global error is bisected [128]. These data will be used to generate a chi-squared to be minimized with respect to the ansatz parameters using `NMinimize`.

The results of the fit for the parameters λ_i of Eq. (4.44) can be found in full in Appendix C. Fig. 4.4 shows typical examples of these plots when a stable fit is obtained. Here, the horizontal axes indicate the size of the dataset used for the least-squares fit and, as we would expect, we find that with increasing number of data we have an increasingly accurate approximation for the parameters, matching Eq. (4.4). In order to obtain an error estimate, we take the maximum of the differences between the values obtained for the integral at different values

$f_1(\alpha_1)$	$f_2(\alpha_2)$	$f_3(\alpha_3)$
$M_{0,1,1}(\alpha_1)$	•	•
$M_{2,0,0}(\alpha_1) r(\alpha_1)$	•	•
$M_{0,0,0}^3(\alpha_1) r(\alpha_1)$	•	•
$M_{1,0,0}(\alpha_1)M_{0,0,0}(\alpha_1)$	•	•
$M_{0,0,0}^2(\alpha_1)$	$M_{0,0,0}(\alpha_2) r(\alpha_2)$	•
$M_{1,0,0}(\alpha_1) r(\alpha_1)$	$M_{0,0,0}(\alpha_2) r(\alpha_2)$	•
$M_{0,0,0}(\alpha_1) r(\alpha_1)$	$M_{0,0,0}(\alpha_2) r(\alpha_2)$	$M_{0,0,0}(\alpha_3) r(\alpha_3)$

Table 4.1: Building ansatz terms for t_0 . All products of basis functions at weight three with factors of $r(\alpha)$ necessary to ensure $\alpha \rightarrow 1/\alpha$ symmetry. A ‘•’ indicates no contribution from functions of additional angles.

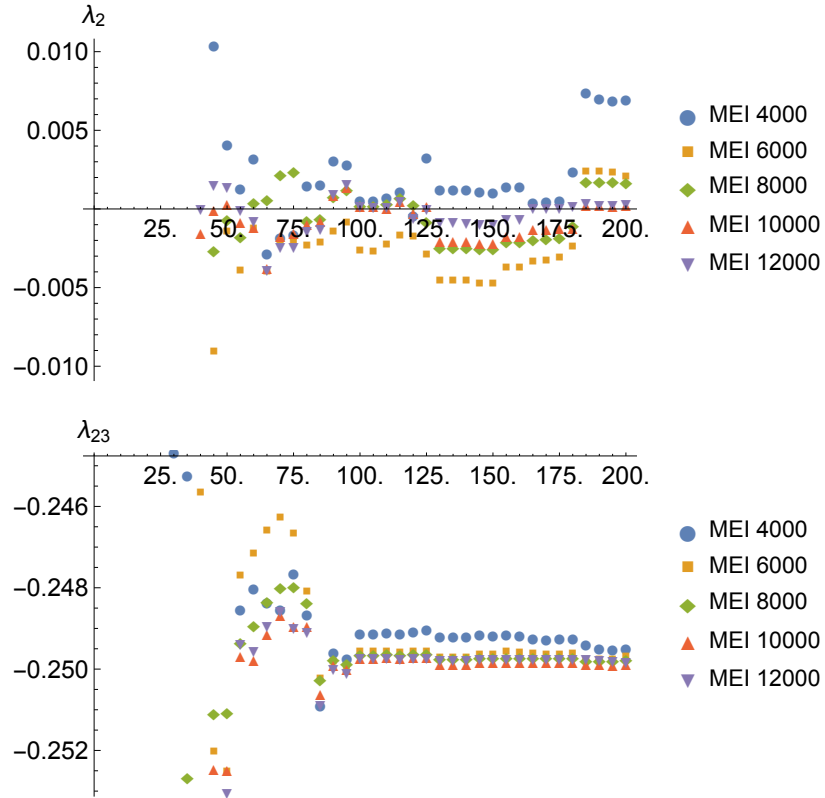


Figure 4.4: Parameter fits for the t_0 ansatz. Horizontal axis indicates size of dataset in units of (number of points)/5. Vertical axis indicates fit value for corresponding parameter. The value of `MaxErrorIncreases` (MEI) used in integrating the data is indicated.

of `MaxErrorIncreases`, which is used to weight the fitting³. In this way, we find the parameters as given in Tab. 4.2, with a chi-squared per degree of freedom for the fit of 0.2 for `MaxErrorIncreases` set at 12000. We also see from Fig. 4.4 that increasing `MaxErrorIncreases` produces a more stable fit therefore giving us a handle on the numerical inaccuracies. Hence we can conclude, given our argument that t_1 can be expressed in terms of the MGEW basis functions, that we should be able to obtain a fit for an ansatz in precisely the same manner as was possible above.

³This estimate for the errors ranges from $\sim 10^{-3}$ to $\sim 10^{-7}$ in both t_0 and t_1

Parameter	Fit value	Actual Value
λ_1	0.00243317	0
λ_2	0.000348412	0
λ_3	0.0000506619	0
λ_4	-0.0000677252	0
λ_5	-0.00714523	0
λ_6	-0.00144551	0
λ_7	0.0000414581	0
λ_8	0.000304069	0
λ_9	0.00419044	0
λ_{10}	0.00129946	0
λ_{11}	-0.000103559	0
λ_{12}	-0.0000427786	0
λ_{13}	0.250014	1/4
λ_{14}	0.0000334599	0
λ_{15}	-0.249766	-1/4
λ_{16}	0.000428478	0
λ_{17}	0.249952	1/4
λ_{18}	-0.0000788383	0
λ_{19}	-0.24995	-1/4
λ_{20}	0.000104371	0
λ_{21}	0.249761	1/4
λ_{22}	-0.000436145	0
λ_{23}	-0.24982	-1/4
λ_{24}	0.000357652	0
λ_{25}	$6.5024760773516825 \times 10^{-6}$	0

Table 4.2: Fit parameters from ansatz, Eq. (4.44), for t_0 , Eq. (4.4), obtained using a least-squares fit with 200 points of numerical data obtained with `MaxErrorIncreases` set at 12000. Gives a chi-squared per degree of freedom of 0.2. Actual values obtained from direct calculation, Eq. (4.4).

$f_1(\alpha_1)$	$f_2(\alpha_2)$	$f_3(\alpha_3)$
$M_{3,0,0}(\alpha_1)r(\alpha_1)$	•	•
$M_{1,2,0}(\alpha_1)r(\alpha_1)$	•	•
$M_{1,0,2}(\alpha_1)r(\alpha_1)$	•	•
$M_{1,1,1}(\alpha_1)$	•	•
$M_{2,0,0}(\alpha_1)M_{0,0,0}(\alpha_1)$	•	•
$M_{0,2,0}(\alpha_1)M_{0,0,0}(\alpha_1)$	•	•
$M_{0,1,1}(\alpha_1)M_{0,0,0}(\alpha_1)r(\alpha_1)$	•	•
$M_{1,0,0}^2(\alpha_1)$	•	•
$M_{1,0,0}(\alpha_1)M_{0,0,0}^2(\alpha_1)r(\alpha_1)$	•	•
$M_{0,0,0}^4(\alpha_1)$	•	•
$M_{2,0,0}(\alpha_1)r(\alpha_1)$	$M_{0,0,0}(\alpha_2)r(\alpha_2)$	•
$M_{0,2,0}(\alpha_1)r(\alpha_1)$	$M_{0,0,0}(\alpha_2)r(\alpha_2)$	•
$M_{0,1,1}(\alpha_1)$	$M_{0,0,0}(\alpha_2)r(\alpha_2)$	•
$M_{1,0,0}(\alpha_1)r(\alpha_1)$	$M_{1,0,0}(\alpha_2)r(\alpha_2)$	•
$M_{1,0,0}(\alpha_1)r(\alpha_1)$	$M_{0,0,0}^2(\alpha_2)$	•
$M_{1,0,0}(\alpha_1)M_{0,0,0}(\alpha_1)$	$M_{0,0,0}(\alpha_2)r(\alpha_2)$	•
$M_{1,0,0}(\alpha_1)r(\alpha_1)$	$M_{0,0,0}(\alpha_2)r(\alpha_2)$	$M_{0,0,0}(\alpha_3)r(\alpha_3)$
$M_{0,0,0}^3(\alpha_1)r(\alpha_1)$	$M_{0,0,0}(\alpha_2)r(\alpha_2)$	•
$M_{0,0,0}^2(\alpha_1)$	$M_{0,0,0}^2(\alpha_2)$	•
$M_{0,0,0}^2(\alpha_1)$	$M_{0,0,0}(\alpha_2)r(\alpha_2)$	$M_{0,0,0}(\alpha_3)r(\alpha_3)$

Table 4.3: Weight four terms for t_1 ansatz. A ‘•’ indicates no contribution from functions of additional angles.

4.3 Fitting the three-loop (1,1,1,2) integral

Let us now build an ansatz for t_1 , conjecturing that it will be described by basis functions and $r(\alpha_{ij})$. Knowing that the web will be of uniform weight five and that t_1 appears along with a factor of $M_{0,0,0}(\alpha_{14})$, itself weight one, then t_1 must carry uniform weight four. Hence, the ansatz will be a linear combination of the products of basis functions in Tab. 4.3, including the factors of $r(\alpha_{ij})$ required to ensure $\alpha_{ij} \rightarrow 1/\alpha_{ij}$ symmetry. Furthermore, we may constrain the ansatz with the antisymmetry of the three-gluon vertex operator, Eq. (4.13), under exchanging any two external lines. Unlike the two-loop three-gluon vertex however, in this case we have antisymmetry only under exchanging lines two and three due to the additional single gluon exchange between lines one and four, which breaks the further antisymmetry found in $w_{3g}^{(2)}$.

Tabs. 4.4, 4.5 and 4.6 give the combinations of these weight four terms which

satisfy the symmetry constraints outlined above, and are separated by the number of rational factors $r(\alpha_{ij})$ with which they appear. Given that the only constraint which we have under exchange of external lines is $2 \leftrightarrow 3$, corresponding to the replacement $\alpha_{24} \leftrightarrow \alpha_{34}$ while α_{23} remains unchanged, we build the terms by listing all possible functions in which α_{23} can appear in the first column. The second column contains the antisymmetric combination of basis functions depending on the remaining two angles. This results in a forty parameter ansatz which is written in full in Appendix D.

$f(\alpha_{23})$	$g(\alpha_{24}, \alpha_{34})$
•	$(M_{0,0,0}^2(a_{24}) - M_{0,0,0}^2(a_{34}))(M_{0,0,0}^2(a_{24}) + M_{0,0,0}^2(a_{34}))$
•	$M_{0,0,0}(a_{24})M_{0,2,0}(a_{24}) - M_{0,0,0}(a_{34})M_{0,2,0}(a_{34})$
•	$M_{0,0,0}(a_{24})M_{2,0,0}(a_{24}) - M_{0,0,0}(a_{34})M_{2,0,0}(a_{34})$
•	$M_{0,0,0}^4(a_{24}) - M_{0,0,0}^4(a_{34})$
•	$M_{1,0,0}^2(a_{24}) - M_{1,0,0}^2(a_{34})$
•	$M_{1,1,1}(a_{24}) - M_{1,1,1}(a_{34})$
$M_{0,0,0}^2(a_{23})$	$M_{0,0,0}^2(a_{24}) - M_{0,0,0}^2(a_{34})$

Table 4.4: t_1 ansatz terms with no rational factor $r(\alpha_{ij})$. A ‘•’ indicates no contribution from functions of additional angles.

$f(\alpha_{23})$	$g(\alpha_{24}, \alpha_{34})$
•	$(M_{0,0,0}(a_{24})M_{0,0,0}^3(a_{34}) - M_{0,0,0}^3(a_{24})M_{0,0,0}(a_{34}))r(a_{24})r(a_{34})$
•	$(M_{0,0,0}(a_{24})M_{0,2,0}(a_{34}) - M_{0,0,0}(a_{34})M_{0,2,0}(a_{24}))r(a_{24})r(a_{34})$
•	$(M_{0,0,0}(a_{24})M_{2,0,0}(a_{34}) - M_{0,0,0}(a_{34})M_{2,0,0}(a_{24}))r(a_{24})r(a_{34})$
$M_{0,0,0}(a_{23})r(a_{23})$	$(M_{0,0,0}^2(a_{24}) + M_{0,0,0}^2(a_{34}))(M_{0,0,0}(a_{24})r(a_{24}) - M_{0,0,0}(a_{34})r(a_{34}))$
$M_{0,0,0}(a_{23})r(a_{23})$	$(M_{0,0,0}^2(a_{24}) - M_{0,0,0}^2(a_{34}))(M_{0,0,0}(a_{24})r(a_{24}) + M_{0,0,0}(a_{34})r(a_{34}))$
$M_{0,0,0}(a_{23})r(a_{23})$	$M_{0,0,0}(a_{24})M_{0,0,0}^2(a_{34})r(a_{24}) - M_{0,0,0}^2(a_{24})M_{0,0,0}(a_{34})r(a_{34})$
$M_{0,0,0}(a_{23})r(a_{23})$	$M_{0,0,0}^3(a_{24})r(a_{24}) - M_{0,0,0}^3(a_{34})r(a_{34})$
$M_{0,0,0}(a_{23})r(a_{23})$	$M_{0,2,0}(a_{24})r(a_{24}) - M_{0,2,0}(a_{34})r(a_{34})$
$M_{0,0,0}(a_{23})r(a_{23})$	$M_{2,0,0}(a_{24})r(a_{24}) - M_{2,0,0}(a_{34})r(a_{34})$
$M_{0,0,0}(a_{23})^3r(a_{23})$	$M_{0,0,0}(a_{24})r(a_{24}) - M_{0,0,0}(a_{34})r(a_{34})$
$M_{0,2,0}(a_{23})r(a_{23})$	$M_{0,0,0}(a_{24})r(a_{24}) - M_{0,0,0}(a_{34})r(a_{34})$
$M_{2,0,0}(a_{23})r(a_{23})$	$M_{0,0,0}(a_{24})r(a_{24}) - M_{0,0,0}(a_{34})r(a_{34})$
$M_{1,0,0}(a_{23})r(a_{23})$	$M_{1,0,0}(a_{24})r(a_{24}) - M_{1,0,0}(a_{34})r(a_{34})$
$M_{0,0,0}(a_{23})r(a_{23})$	$(M_{0,0,0}(a_{34})M_{1,0,0}(a_{24}) - M_{0,0,0}(a_{24})M_{1,0,0}(a_{34}))r(a_{24})r(a_{34})$

Table 4.5: t_1 ansatz terms with two and three rational factors $r(\alpha_{ij})$. A ‘•’ indicates no contribution from functions of additional angles.

$f(\alpha_{23})$	$g(\alpha_{24}, \alpha_{34})$
•	$(M_{0,1,1}(a_{24}) + M_{0,1,1}(a_{34}))(M_{0,0,0}(a_{24})r(a_{24}) - M_{0,0,0}(a_{34})r(a_{34}))$
•	$(M_{0,1,1}(a_{24}) - M_{0,1,1}(a_{34}))(M_{0,0,0}(a_{24})r(a_{24}) + M_{0,0,0}(a_{34})r(a_{34}))$
•	$(M_{0,0,0}(a_{24})M_{1,0,0}(a_{24}) + M_{0,0,0}(a_{34})M_{1,0,0}(a_{34}))(M_{0,0,0}(a_{24})r(a_{24}) - M_{0,0,0}(a_{34})r(a_{34}))$
•	$(M_{0,0,0}(a_{24})M_{1,0,0}(a_{24}) - M_{0,0,0}(a_{34})M_{1,0,0}(a_{34}))(M_{0,0,0}(a_{24})r(a_{24}) + M_{0,0,0}(a_{34})r(a_{34}))$
•	$M_{0,0,0}(a_{24})M_{0,1,1}(a_{34})r(a_{24}) - M_{0,0,0}(a_{34})M_{0,1,1}(a_{24})r(a_{34})$
•	$M_{0,0,0}(a_{24})M_{0,1,1}(a_{24})r(a_{24}) - M_{0,0,0}(a_{34})M_{0,1,1}(a_{34})r(a_{34})$
•	$(M_{0,0,0}^2(a_{24}) + M_{0,0,0}^2(a_{34}))(M_{1,0,0}(a_{24})r(a_{24}) - M_{1,0,0}(a_{34})r(a_{34}))$
•	$(M_{0,0,0}^2(a_{24}) - M_{0,0,0}^2(a_{34}))(M_{1,0,0}(a_{24})r(a_{24}) + M_{1,0,0}(a_{34})r(a_{34}))$
•	$M_{0,0,0}^2(a_{34})M_{1,0,0}(a_{24})r(a_{24}) - M_{0,0,0}^2(a_{24})M_{1,0,0}(a_{34})r(a_{34})$
•	$M_{0,0,0}^2(a_{24})M_{1,0,0}(a_{24})r(a_{24}) - M_{0,0,0}^2(a_{34})M_{1,0,0}(a_{34})r(a_{34})$
•	$M_{1,0,2}(a_{24})r(a_{24}) - M_{1,0,2}(a_{34})r(a_{34})$
•	$M_{1,2,0}(a_{24})r(a_{24}) - M_{1,2,0}(a_{34})r(a_{34})$
•	$M_{3,0,0}(a_{24})r(a_{24}) - M_{3,0,0}(a_{34})r(a_{34})$
$M_{0,0,0}(a_{23})r(a_{23})$	$M_{0,1,1}(a_{24}) - M_{0,1,1}(a_{34})$
$M_{0,0,0}(a_{23})r(a_{23})$	$M_{0,0,0}(a_{24})M_{1,0,0}(a_{24}) - M_{0,0,0}(a_{34})M_{1,0,0}(a_{34})$
$M_{0,0,0}^2(a_{23})$	$M_{1,0,0}(a_{24})r(a_{24}) - M_{1,0,0}(a_{34})r(a_{34})$
$M_{1,0,0}(a_{23})r(a_{23})$	$M_{0,0,0}^2(a_{24}) - M_{0,0,0}^2(a_{34})$
$M_{0,1,1}(a_{23})$	$M_{0,0,0}(a_{24})r(a_{24}) - M_{0,0,0}(a_{34})r(a_{34})$
$M_{0,0,0}(a_{23})M_{1,0,0}(a_{23})$	$M_{0,0,0}(a_{24})r(a_{24}) - M_{0,0,0}(a_{34})r(a_{34})$

Table 4.6: t_1 ansatz terms with one rational factor $r(\alpha_{ij})$. A ‘•’ indicates no contribution from functions of additional angles.

A fit is obtained using the methodology outlined in Sec. 4.2, that is, using `NMinimize` to minimize the chi-squared with respect to the ansatz parameters, λ_i , obtained from numerical data which is provided by applying `NIntegrate` to t_1 , Eq. (4.33). In this case we shall again use `NIntegrate`'s 'GlobalAdaptive' strategy and 'MultiDimensionalRule' integration rule at various values of `MaxErrorIncreases`. An error estimate is obtained by taking the maximum of the differences between the result of this integration at the differing values of `MaxErrorIncreases`.

The sample plots in Fig. 4.5, show the fit values for their respective parameters on the vertical axis, and the size of the data set on the horizontal axis. Unlike the corresponding plots for t_0 , Fig. 4.4, we see here an unstable fit for t_1 . The values of the parameters change drastically as the number of data increases rather than settling to a rational value. We can see similar behaviour in the t_0 fitting, Fig. 4.4, using data obtained with the lower values of `MaxErrorIncreases`. Also, if we eliminate a parameter which is approximately zero according to the fit shown in Tab. 4.7, we expect that the remaining parameters will shift slightly towards their actual rational values and the chi-squared will decrease. However, if we do so for λ_{39} we obtain the fit in Tab. 4.8 which bears no resemblance to Tab. 4.7. Furthermore, rather than falling, the already extremely large chi-squared per degree of freedom rises from 9.67×10^7 to 1.44×10^8 . In the conclusions below we shall discuss possible causes for the issues above and work ongoing to obtain a result for the (1,1,1,2) subtracted web.

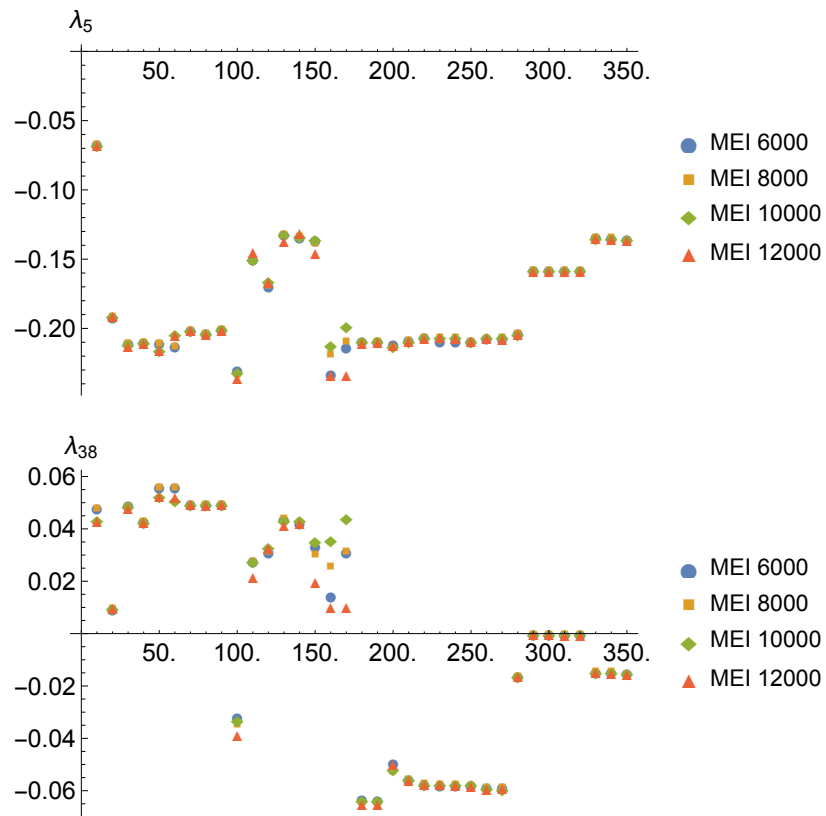


Figure 4.5: Example of t_1 parameter fits. Horizontal axis indicates size of dataset. Vertical axis indicates fit value for corresponding parameter. The value of MaxErrorIncreases (MEI) used in integrating the data is indicated.

Parameter	Fit value	Parameter	Fit value
λ_1	-0.112113	λ_{21}	-0.0576135
λ_2	-0.0986314	λ_{22}	0.018717
λ_3	0.0275748	λ_{23}	-0.0566518
λ_4	-0.0426735	λ_{24}	-0.287824
λ_5	-0.136046	λ_{25}	0.026475
λ_6	-0.0286221	λ_{26}	0.0373178
λ_7	-0.109038	λ_{27}	0.128883
λ_8	-0.0177893	λ_{28}	-0.0753646
λ_9	0.0926251	λ_{29}	-0.105511
λ_{10}	-0.129871	λ_{30}	-0.0319839
λ_{11}	0.0617089	λ_{31}	0.00778212
λ_{12}	-0.265696	λ_{32}	-0.115078
λ_{13}	-0.0330709	λ_{33}	0.0656556
λ_{14}	-0.0939348	λ_{34}	-0.0329081
λ_{15}	-0.112931	λ_{35}	-0.0752321
λ_{16}	-0.136939	λ_{36}	-0.176888
λ_{17}	-0.198864	λ_{37}	0.0742235
λ_{18}	0.0367732	λ_{38}	-0.0153439
λ_{19}	-0.00354897	λ_{39}	0.000257854
λ_{20}	0.059384	λ_{40}	-0.127847

Table 4.7: Fit parameters from ansatz, Eq. (D.1), for t_1 , Eq. (4.41), obtained using a least-squares fit with 350 points of numerical data obtained with `MaxErrorIncreases` set at 12000. Gives a very high chi-squared per degree of freedom of 9.67×10^7 .

Parameter	Fit value
λ_1	-0.170715
λ_2	0.0295372
λ_3	-0.185356
λ_4	0.0338624
λ_5	-0.176151
λ_6	-0.0681446
λ_7	-0.107208
λ_8	-0.207936
λ_9	0.00978535
λ_{10}	-0.0682999
λ_{11}	0.0812123
λ_{12}	-0.0836554
λ_{13}	-0.0979989
λ_{14}	-0.250069
λ_{15}	0.0798778
λ_{16}	-0.102344
λ_{17}	-0.188995
λ_{18}	-0.13967
λ_{19}	-0.020149
λ_{20}	-0.0356646

Parameter	Fit value
λ_{21}	-0.141209
λ_{22}	-0.18176
λ_{23}	0.0222813
λ_{24}	-0.166805
λ_{25}	-0.0998812
λ_{26}	0.0934013
λ_{27}	0.00991889
λ_{28}	-0.260759
λ_{29}	-0.0108505
λ_{30}	-0.108596
λ_{31}	-0.255557
λ_{32}	0.056411
λ_{33}	-0.0524971
λ_{34}	-0.0414136
λ_{35}	0.0359645
λ_{36}	-0.117621
λ_{37}	-0.00595601
λ_{38}	-0.0695166
λ_{40}	0.0153481

Table 4.8: Fit parameters from ansatz, Eq. (D.1) with $\lambda_{39} \rightarrow 0$. This is obtained using a least-squares fit with 350 points of numerical data obtained with `MaxErrorIncreases` set at 12000. Gives a very high chi-squared per degree of freedom of 1.44×10^8 . Note that the values differ substantially from Tab. 4.7 indicating instability of the fit.

4.4 Conclusions

We have begun a study of webs containing a single three-gluon vertex with the simplest diagram of this class, namely the (1,1,1,2) web, Fig. 4.2. While we are as yet unable to find a solution to the required integrals, we have identified several attractive directions to pursue which will hopefully in the near future lead to a determination of this web in general kinematics. We find that the (1,1,1,2) web can be written as a linear combination of the integrals t_0 , Eq. (4.40), and t_1 , Eq. (4.41). t_0 is known from the computation of the two-loop, three-line, three-gluon vertex web, Eq. (4.4), while t_1 , which involves integrating over the external momenta of a three mass triangle at order ϵ , remains to be determined.

We adopted several approaches towards the computation of this integral, both analytic and numeric. A direct analytic integration remains elusive as it is not clear if the integrals are linearly reducible and we have thus far been unable to find a parametrization in which it satisfies this property. Moreover, considerable effort was directed towards extending the application of so-called *conformal gauges* [70] to three loops, given their success in greatly simplifying the calculation of $w_{3g}^{(2)}$. We found no means by which to recover the Feynman gauge (1,1,1,2) result from the calculation of $\Gamma^{(3)}$ in this gauge without computing the far more difficult, fully connected, double three-gluon vertex diagram which remains unknown in general kinematics, even in the Feynman gauge.

We propose instead to numerically fit this integral to an ansatz. Given that, as shown above, dependence upon the kinematic variable α_{14} factorizes and so t_1 is a function of the remaining three variables α_{23} , α_{24} and α_{34} , then it cannot depend on more complicated kinematic variables such as conformal invariant cross-ratios. Therefore it is subject to the symbol alphabet constraints [60], as were the MGEWs of Ch. 3, and so we argue that it is likely expressible in terms of the MGEW basis functions, Eq. (3.35), and the rational function $r(\alpha) = (1 + \alpha^2)/(1 - \alpha^2)$. This allows us to write a forty parameter ansatz, Eq. (D.1), found in Appendix D, which is constrained with the available physical (anti-) symmetries.

Before moving on to the three-loop (1,1,1,2), we began by building an ansatz for t_0 , from the two-loop $w_{3g}^{(2)}$, composed of all possible weight three products of basis functions, with factors of $r(\alpha)$ present where necessary to give the requisite $\alpha \rightarrow 1/\alpha$ symmetry. This provided a twenty-five parameter ansatz, Eq. (4.44). Eq. (4.40) was then numerically evaluated at random

values of α_{23} , α_{24} and α_{34} to provide numerical data with which to fit the ansatz parameters. This was accomplished using Mathematica's `NIntegrate` function with the 'GlobalAdaptive' strategy and 'MultidimensionalRule' integration rule. The termination of the integration algorithm is controlled by the `MaxErrorIncreases` parameter⁴, which we demonstrated gives control over the numerical errors. An estimate for the integration error was obtained by taking the maximum of the difference between the integration results at various values of `MaxErrorIncreases`. A fit was obtained using the `NMinimize` function to minimize the chi-squared of this ansatz and data with respect to the ansatz parameters, resulting in Tab. 4.2 in good agreement with Eq. (4.36).

At present, work is ongoing to find a fit for the forty parameters of the ansatz for t_1 . The lack of convergence we see in Sec. 4.3 could be caused by a combination of the size of our very large, forty dimensional, parameter space with insufficiently precise numerics (as stated above, at present we are only able to obtain an accuracy of between $\sim 10^{-3}$ and $\sim 10^{-7}$ in both t_0 and t_1). If this is the case then, even through we may have an ansatz which will correctly fit the function for suitable values of λ_i , the minimization algorithm may not be able to discern the global minimum from the multitude of local minima in the chi-squared as a function of these parameters. Another explanation could be that our ansatz is simply not large enough to describe the function. A possible extension would be to allow rational factors of the form $r^n(\alpha_{ij})$ for $n > 1$, or even to allow additional rational factors such as $\alpha/(1 - \alpha^2)$ which have been known to occur in computation of the cusp [64], however it is not clear if such functions arise in $\Gamma_i^{(n)}$ for $i = n$ in the former case and $i > 2$ in the latter. We must now improve the precision of the numerical integration in order to either confirm the ansatz above and determine the rational parameters, or to be able to fit an even larger set of parameters for an expanded ansatz.

Work is currently on-going in this direction: we hope to improve the precision of the numerical integrals by studying the integrand to see if numerical inaccuracies are being generated by large cancelling terms or integrable singularities, particularly at the boundaries of the integration region as can often be the case with Feynman parameter type integrals. Furthermore, we are investigating physical constraints which can be imposed on the ansatz parameters, for example

⁴See above for a definition.

the limit where all of the Wilson lines are taken lightlike ($\beta_i^2 \rightarrow 0$), which may be obtained through the Mellin-Barnes asymptotics applied in Ref. [89]. We are also considering other packages to handle the numerical integration and fitting to see if better performance can be obtained.

Moreover, we are continuing to pursue an analytic computation of t_1 by making use of modern tools being developed for the evaluation of multiloop Feynman integrals. For example, we are working towards an application of the *compatibility graph* method of Ref. [117] – which is implemented in the package `HyperInt` [129] for Maple – to test linear reducibility of the integral or to search for parametrizations in which it satisfies this property. Beyond this, the application of integration by parts reduction [130] and the differential equation methods [131–136] have garnered much interest in the recent literature and have generated success in several recent multiloop calculations. It is possible that such approaches may yet yield results in the webs containing single three-gluon vertices and beyond.

Chapter 5

Conclusions and Outlook

In this thesis we have studied infrared singularities in gauge theories, focussing particularly on multiparton amplitudes in non-abelian theories such as QCD. We have discussed the factorization of the soft singularities from the hard and jet components of amplitudes [80, 94–99], and their mapping to the UV divergences of Wilson lines correlators [3, 27–32]. We have also seen that the logarithm of such correlators is described by the soft anomalous dimension matrix which has a diagrammatic interpretation in terms of subtracted webs [56, 58, 61, 90–92]. Throughout we have stressed the distinction between the IR singularities of two-parton and multiparton amplitudes, the latter of which has a far richer structure [56, 58–61, 93], though is commensurately more difficult to compute.

Presently, the IR singularities of non-abelian theories in the multiparton case are known only to two loops in general kinematics [67–69], and recently this was advanced to three loops in the lightlike limit where all of the Wilson lines are taken asymptotically close to the lightcone. With only two Wilson lines, results have been obtained at three loops [63, 64] and some preliminary analysis exists at four loops [50, 52]. Our goal then in this thesis was to push toward a calculation of the three-loop soft anomalous dimension matrix, building upon contemporary progress in understanding and computing multiparton webs [56, 58–61, 93]. The webs contributing to the three-loop soft anomalous dimension can be broken into three classes, given in order of the computational difficulty they present: the multiple gluon exchange webs (MGEWs), webs containing single three-gluon-vertex subgraphs, and fully connected webs.

In Ch. 3 we built upon the work of Ref. [60] in which the structure of MGEWs

was studied. MGEWs are defined as those webs containing only gluon exchanges directly between Wilson lines with no intervening three- or four-gluon-vertices, or fermion/gluon/ghost bubble insertions. These are the simplest of webs given that they effectively exist in a conformally invariant sector of the theory [58], and naturally permit a factorized structure which lends itself to integration procedure outlined in Sec. 2.6. Owing to this, their form appears highly constrained: their subtracted web kernels are conjectured to be free from anything other than logarithms, and they can be written as sums of products of functions depending upon only a single cusp angle each. These functions are themselves strongly constrained by physical considerations and have an incredibly simple symbol alphabet [60]. We were able to take this remarkable simplification further by demonstrating that the MGEWs we have computed thus far can be written in terms of a simple basis of functions, described by a single dimensional integral over only logarithms, and depending on a single angle. We conjectured that this basis will describe MGEWs to all orders, and provided evidence for this and the other aforementioned conjectures, by computing the remaining three-loop MGEWs and even a four-loop example. We went on to demonstrate the utility of the framework we have built around this class of webs by providing some all-order results for particular web families. Moreover, we discovered a new relation between webs correlating different numbers of Wilson lines in the form of a collinear reduction. Identifying two lines in an n line web, we demonstrate, reproduces a particular colour and corresponding kinematic factor for a specific $n - 1$ line web.

Ch. 4 focussed on multiparton webs containing a single three-gluon-vertex, a class in which only a single example [68] has so far been obtained away from the lightlike limit, that is the three-gluon-vertex web between three lines, $w_{3g}^{(2)}$. This example is only at two loops and exhibits a significant simplification in comparison to what one might expect considering its integrand. Clearly, more data is required regarding webs of this class to see if such simplifications continue, and if some general procedure for their computation can be constructed, as was achieved for MGEWs [1, 60]. The next in this class is the (1,1,1,2) web in which the two-loop subdiagram is convoluted with a single gluon exchange with a fourth line. We began by constructing the (1,1,1,2) subtracted web and studying its integrand in detail. We found that it can be expressed as a two dimensional parameter integral over a one-loop, three mass triangle with no internal masses,

and that the dependence upon the angle correlated by the single gluon exchange can be factorized. The remaining integral therefore cannot depend on kinematic invariants through conformal invariant cross ratios and so we argue will be subject to the same constraints as were applied to MGEWs in Ref. [60]. This provides the same symbol alphabet and factorization constraints and led us to conjecture that the $(1,1,1,2)$ web can also be expressed in terms of the MGEW basis functions we found in Ch. 3. We investigated several approaches for a direct analytic evaluation of the integrals, and a generalization of the method found in Ref. [70] involving specialised gauge transformations to obtain the two loop three-gluon-vertex web, neither of which yielded a result. We instead, for the reasons outlined above, generated an ansatz for the $(1,1,1,2)$ in terms of MGEW basis functions and attempted to find a numerical least-squares fit for its forty parameters. This work is still ongoing and so we presented results for a successful test fit of $w_{3g}^{(2)}$ from an ansatz of MGEW basis functions, and preliminary results for a fit of the $(1,1,1,2)$, demonstrating the need for higher precision numerical evaluations of the integrals which we are currently in progress.

To conclude, the three-loop soft anomalous dimension in general kinematics remains undetermined with the major barrier being the fully connected graphs. We have made progress in understanding the intermediary class webs consisting of lower order connected subgraphs convoluted with MGEW-like single gluon exchanges, however these integrals also remain problematic beyond the simplest of examples, or simplifying kinematic limits. In fact, even at two loops the computation of the three-gluon-vertex web, $w_{3g}^{(2)}$, is laborious without relying on specialised gauges such as the conformal gauges described in Ref. [70]. These gauges, unfortunately, appear to lose their utility at three loops where, again, the fully connected diagrams remain uncomputed. However, in recent years there has been a wealth of new tools and techniques developed collaboratively by the amplitudes and mathematics communities, e.g. Refs. [109, 110, 117, 129–137]. These have significantly driven forward our ability to compute and understand Feynman integrals, and the space of functions onto which they map. We are confident that these developments, along with data regarding the properties of webs such as the $(1,1,1,2)$, will shed light onto the remaining challenges at three loops and beyond. As we continue to better understand the structure of webs and the functions involved in such calculations, more and more classes of webs

will become computationally procedural. In achieving this we shall be able not only to compute IR singularities deeper within the perturbative series, but also will continue to provide insights into the structure of gauge theory amplitudes and the physical processes to which they pertain.

Appendix A

Multiple Gluon Exchange Webs

A.1 Basis Functions

In this appendix we list the explicit expressions for the basis functions defined in Eq. (3.35), in terms of polylogarithms and harmonic polylogarithms, up to transcendental weight five. Harmonic polylogarithms are defined as in [119].

- Weight one.

$$M_{0,0,0}(\alpha) = 2 \log(\alpha). \quad (\text{A.1})$$

- Weight two.

$$M_{1,0,0}(\alpha) = 2 \text{Li}_2(\alpha^2) + 4 \log(\alpha) \log(1 - \alpha^2) - 2 \log^2(\alpha) - 2 \zeta(2). \quad (\text{A.2})$$

- Weight three.

$$M_{0,0,2}(\alpha) = \frac{8}{3} \log^3(\alpha), \quad (\text{A.3})$$

$$M_{0,1,1}(\alpha) = 2 \text{Li}_3(\alpha^2) - 2 \log(\alpha) \left[\text{Li}_2(\alpha^2) + \frac{\log^2(\alpha)}{3} + \zeta(2) \right] - 2 \zeta(3), \quad (\text{A.4})$$

$$M_{0,2,0}(\alpha) = \frac{2}{3} \log^3(\alpha) + 4 \zeta(2) \log(\alpha), \quad (\text{A.5})$$

$$\begin{aligned}
 M_{2,0,0}(\alpha) &= -4 \left[\text{Li}_3(\alpha^2) + 2\text{Li}_3(1 - \alpha^2) \right] - 8 \log(1 - \alpha^2) \log^2(\alpha) \\
 &\quad + \frac{8}{3} \log^3(\alpha) + 8 \zeta(2) \log(\alpha) + 4 \zeta(3).
 \end{aligned} \tag{A.6}$$

- Weight four.

$$\begin{aligned}
 M_{3,0,0}(\alpha) &= 12 \left[\text{Li}_4(\alpha^2) - 4 \text{Li}_4(1 - \alpha^2) \right] - 24 S_{2,2}(\alpha^2) \\
 &\quad - 24 \log(1 - \alpha^2) \text{Li}_3(\alpha^2) - 24 \log^2(1 - \alpha^2) \log^2(\alpha) \\
 &\quad + 16 \log(1 - \alpha^2) \log^3(\alpha) - 4 \log^4(\alpha) \\
 &\quad - 24 \zeta(2) \log(\alpha) \log \left[\frac{\alpha}{(1 - \alpha^2)^2} \right] \\
 &\quad + 24 \zeta(3) \log[\alpha(1 - \alpha^2)] - 6 \zeta(4),
 \end{aligned} \tag{A.7}$$

$$\begin{aligned}
 M_{1,2,0}(\alpha) &= 4 \text{Li}_4(\alpha^2) - 4 \log(\alpha) \text{Li}_3(\alpha^2) + 2 \log^2(\alpha) \text{Li}_2(\alpha^2) \\
 &\quad + \frac{4}{3} \log^3(\alpha) \log(1 - \alpha^2) - \frac{2}{3} \log^4(\alpha) \\
 &\quad + \zeta(2) \left[8 \log(\alpha) \log(1 - \alpha^2) + 4 \text{Li}_2(\alpha^2) - 6 \log^2(\alpha) \right] \\
 &\quad + 4 \zeta(3) \log(\alpha) - 14 \zeta(4),
 \end{aligned} \tag{A.8}$$

$$\begin{aligned}
 M_{1,0,2}(\alpha) &= 4 \text{Li}_4(\alpha^2) - 8 \log(\alpha) \text{Li}_3(\alpha^2) + 8 \log^2(\alpha) \text{Li}_2(\alpha^2) \\
 &\quad + \frac{16}{3} \log^3(\alpha) \log(1 - \alpha^2) - \frac{4}{3} \log^4(\alpha) - 4 \zeta(4),
 \end{aligned} \tag{A.9}$$

$$\begin{aligned}
 M_{1,1,1}(\alpha) &= -4 \text{Li}_4(\alpha^2) + 4 S_{2,2}(\alpha^2) + 2 \log \left[\alpha(1 - \alpha^2)^2 \right] \text{Li}_3(\alpha^2) \\
 &\quad + 4 \log(\alpha) \text{Li}_3(1 - \alpha^2) \\
 &\quad - \frac{4}{3} \log(\alpha)^2 \log(1 - \alpha^2) \left[\log(\alpha) - 3 \log(1 - \alpha^2) \right] \\
 &\quad - 8 \zeta(2) \log(\alpha) \log(1 - \alpha^2) - 2 \zeta(3) \log \left[\alpha(1 - \alpha^2)^2 \right] + 3 \zeta(4).
 \end{aligned} \tag{A.10}$$

- Weight five

$$M_{0,0,4}(\alpha) = \frac{32}{5} \log^5(\alpha), \quad (\text{A.11})$$

$$\begin{aligned} M_{4,0,0}(\alpha) = & 48 H_{0,0,0,1,0}(\alpha^2) + 96 H_{1,0,0,1,0}(\alpha^2) + 96 H_{0,1,0,1,0}(\alpha^2) \\ & + 48 H_{0,0,1,0,0}(\alpha^2) + 96 H_{0,0,1,1,0}(\alpha^2) + 192 H_{1,1,0,1,0}(\alpha^2) \\ & + 96 H_{1,0,1,0,0}(\alpha^2) + 192 H_{1,0,1,1,0}(\alpha^2) + 48 H_{0,1,0,0,0}(\alpha^2) \\ & + 96 H_{0,1,1,0,0}(\alpha^2) + 192 H_{0,1,1,1,0}(\alpha^2) + 48 H_{1,0,0,0,0}(\alpha^2) \\ & + 96 H_{1,1,0,0,0}(\alpha^2) + 192 H_{1,1,1,0,0}(\alpha^2) + 384 H_{1,1,1,1,0}(\alpha^2) \quad (\text{A.12}) \\ & + \frac{32}{5} \log^5(\alpha) + 64 \zeta(2) \log^3\left(\frac{\alpha}{1-\alpha^2}\right) \\ & - 96 \zeta(3) \left[\zeta(2) + \log^2\left(\frac{\alpha}{1-\alpha^2}\right) \right] \\ & + 432 \zeta(4) \log \frac{\alpha}{1-\alpha^2} - 144 \zeta(5), \end{aligned}$$

$$M_{0,4,0}(\alpha) = \frac{2}{5} \log^5(\alpha) + 8 \zeta(2) \log^3(\alpha) + 84 \zeta(4) \log(\alpha), \quad (\text{A.13})$$

$$\begin{aligned} M_{0,1,3}(\alpha) = & -6 H_{0,0,0,1,0}(\alpha^2) - 6 H_{0,0,1,0,0}(\alpha^2) - 6 H_{0,1,0,0,0}(\alpha^2) \\ & - \frac{12}{5} \log^5(\alpha) - 8 \zeta(2) \log^3(\alpha) - 12 \zeta(3) \log^2(\alpha) \quad (\text{A.14}) \\ & - 12 \zeta(4) \log(\alpha) - 12 \zeta(5), \end{aligned}$$

$$\begin{aligned} M_{0,3,1}(\alpha) = & -\frac{3}{2} \left[H_{0,0,0,1,0}(\alpha^2) + H_{0,1,0,0,0}(\alpha^2) \right] - \frac{2}{5} \log^5(\alpha) \\ & + 6 \zeta(2) \left[-\log^3(\alpha) - 2 \log(\alpha) \text{Li}_2(\alpha^2) + 2 \text{Li}_3(\alpha^2) \right] \\ & - 6 \zeta(3) \log^2(\alpha) - 42 \zeta(4) \log(\alpha) - 12 \zeta(2) \zeta(3) - 12 \zeta(5), \quad (\text{A.15}) \end{aligned}$$

$$\begin{aligned}
M_{2,2,0}(\alpha) = & 4 H_{0,0,0,1,0}(\alpha^2) + 4 H_{1,0,0,1,0}(\alpha^2) + 4 H_{0,0,1,1,0}(\alpha^2) \\
& + 4 H_{1,0,0,0,0}(\alpha^2) + 4 H_{1,1,0,0,0}(\alpha^2) + 2 H_{0,1,0,0,0}(\alpha^2) \\
& + 2 H_{0,0,1,0,0}(\alpha^2) + \frac{16}{15} \log^5(\alpha) \\
& + 8 \zeta(2) \left[\log^2(\alpha) \left(2 \log(\alpha) - 3 \log(1 - \alpha^2) \right) \right. \\
& \quad \left. - \log(\alpha) \operatorname{Li}_2(\alpha^2) - 2 \operatorname{Li}_3(1 - \alpha^2) \right] \\
& + 4 \zeta(3) \left[2 \operatorname{Li}_2(\alpha^2) + \log(\alpha) \left(4 \log(1 - \alpha^2) - 3 \log(\alpha) \right) \right] \\
& + 2 \zeta(4) \left[67 \log(\alpha) - 8 \log(1 - \alpha^2) \right] - 16 \zeta(5),
\end{aligned} \tag{A.16}$$

$$\begin{aligned}
M_{2,0,2}(\alpha) = & 8 H_{0,1,0,0,0}(\alpha^2) + 8 H_{1,0,0,0,0}(\alpha^2) + 16 H_{1,1,0,0,0}(\alpha^2) \\
& + \frac{16}{15} \log^5(\alpha) + 16 \zeta(4) \log\left(\frac{\alpha}{1 - \alpha^2}\right) \\
& + 16 \zeta(2)\zeta(3) - 8 \zeta(5),
\end{aligned} \tag{A.17}$$

$$\begin{aligned}
M_{2,1,1}(\alpha) = & -4 H_{0,0,0,1,0}(\alpha^2) - 8 H_{1,0,0,1,0}(\alpha^2) - 8 H_{0,1,0,1,0}(\alpha^2) \\
& - 2 H_{0,0,1,0,0}(\alpha^2) - 8 H_{0,0,1,1,0}(\alpha^2) - 8 H_{1,1,0,1,0}(\alpha^2) \\
& - 4 H_{1,0,1,0,0}(\alpha^2) - 8 H_{1,0,1,1,0}(\alpha^2) - 4 H_{0,1,0,0,0}(\alpha^2) \\
& - 4 H_{0,1,1,0,0}(\alpha^2) - 8 H_{0,1,1,1,0}(\alpha^2) - 4 H_{1,1,0,0,0}(\alpha^2) + \frac{4}{15} \log^5(\alpha) \\
& - 8 \zeta(2) \left[\log(\alpha) \left(2 \operatorname{Li}_2(\alpha^2) + \log^2(1 - \alpha^2) \right) - \operatorname{Li}_3(\alpha^2) \right] \\
& - 4 \zeta(3) \left[3 \log^2(\alpha) + 2 \log^2(1 - \alpha^2) - 2 \log(\alpha) \log(1 - \alpha^2) \right] \\
& - 6 \zeta(4) \left[5 \log(\alpha) - 2 \log(1 - \alpha^2) \right] - 8 \zeta(2)\zeta(3) - 20 \zeta(5),
\end{aligned} \tag{A.18}$$

$$\begin{aligned}
M_{0,2,2}(\alpha) &= 2 H_{0,0,0,1,0}(\alpha^2) + 4 H_{0,1,0,1,0}(\alpha^2) + 2 H_{0,1,0,0,0}(\alpha^2) \\
&+ \frac{16}{15} \log^5(\alpha) + 8 \zeta(2) \left[\log^3(\alpha) + \log(\alpha) \text{Li}_2(\alpha^2) - \text{Li}_3(\alpha^2) \right] \\
&+ 8 \zeta(3) \left[\log^2(\alpha) + \text{Li}_2(\alpha^2) \right] + 22 \zeta(4) \log(\alpha) + 8 \zeta(2) \zeta(3) + 8 \zeta(5).
\end{aligned} \tag{A.19}$$

A.2 Calculation of the (2,2,2) web

In this appendix, we provide more details regarding the calculation of the (2,2,2) web, the results of which are presented in Sec. 3.5.1.

A.2.1 Unsubtracted web

The general method for calculating a given web diagram has been presented in Sec. 3.3. Here we present the kernels, defined in Eq. (3.14) and Eq. (3.15), for each diagram appearing in the (2,2,2) web. To simplify our notations slightly, we relabel the variables used in Sec. 3.5.1 as $\{x_1, x_2, x_3\} \rightarrow \{x, y, z\}$. Applying the relevant definitions to the kinematic factor of diagrams A and B in Fig. 3.9 one finds,

$$\phi_A^{(3)}(x, y, z; \epsilon) = \phi_B^{(3)}(x, y, z; \epsilon) = \frac{1}{4} \log^2 \left[\frac{x}{1-x} \frac{y}{1-y} \frac{z}{1-z} \right] + \mathcal{O}(\epsilon), \tag{A.20}$$

where we used Eqs. (2.71) and (2.62). Note that it is necessary to use the symmetry of the function to remove the factor,

$$\theta_+(n=3) = \theta \left(\frac{1-x}{x} \frac{1-y}{y} \frac{1-z}{z} > 1 \right). \tag{A.21}$$

The other diagrams in Fig. 3.9 have subdivergences, therefore the kernels have to be computed including higher orders in their ϵ expansion. For example, from diagram C one finds

$$\begin{aligned}
\phi_C^{(3)}(x, y, z; \epsilon) &= \frac{1}{8\epsilon^2} \left\{ 1 + 2\epsilon \log \left[\frac{(1-y)^2(1-z)}{z^2x} \right] + \epsilon^2 \left[24 \text{Li}_2 \left(-\frac{1-y}{z} \right) \right. \right. \\
&\left. \left. + 2 \log^2 \left(\frac{(1-y)^2(1-z)}{z^2x} \right) - 2 \log^2 \left(\frac{(1-x)(1-y)(1-z)}{xyz} \right) \right] \right\}
\end{aligned}$$

$$+ \mathcal{O}(\epsilon^3) \Big\}. \quad (\text{A.22})$$

The remaining web kernel contributions can then be found by permuting the variables x , y and z in the integrand, with the results

$$\begin{aligned} \phi_D^{(3)}(x, y, z; \epsilon) &= \phi_C^{(3)}(z, x, y; \epsilon), \\ \phi_E^{(3)}(x, y, z; \epsilon) &= \phi_C^{(3)}(x, z, y; \epsilon), \\ \phi_F^{(3)}(x, y, z; \epsilon) &= \phi_C^{(3)}(y, x, z; \epsilon), \\ \phi_G^{(3)}(x, y, z; \epsilon) &= \phi_C^{(3)}(z, y, x; \epsilon), \\ \phi_H^{(3)}(x, y, z; \epsilon) &= \phi_C^{(3)}(y, z, x; \epsilon). \end{aligned} \quad (\text{A.23})$$

From these functions one can compute the unsubtracted web,

$$W_{(2,2,2)} = \sum_{j=1}^4 c_j^{(3)} \mathcal{F}_{(2,2,2);j}^{(3)}, \quad (\text{A.24})$$

using Eq. (3.16) and taking the specific coefficients $Y_{X,j}^{-1}$ given in Table 3.2. One finds

$$\begin{aligned} \mathcal{F}_{(2,2,2),j}^{(3)} &= \kappa^3 \Gamma(6\epsilon) \int_0^1 dx dy dz p_\epsilon(x, \alpha_{12}) p_\epsilon(y, \alpha_{23}) p_\epsilon(z, \alpha_{13}) \sum_{X \in (2,2,2)} Y_{X,j}^{-1} \phi_X^{(3)}(x, y, z; \epsilon) \\ &= \kappa^3 \Gamma(6\epsilon) \int_0^1 dx dy dz p_\epsilon(x, \alpha_{12}) p_\epsilon(y, \alpha_{23}) p_\epsilon(z, \alpha_{13}) \phi_{(2,2,2),j}^{(3)}(x, y, z; \epsilon). \end{aligned} \quad (\text{A.25})$$

A.2.2 Subtracted web

As explained in Sec. 2.4, the anomalous dimension is obtained from subtracted webs. Thus the single pole of Eq. (A.25) must be combined with suitable subtraction terms, consisting of commutators of lower-order webs, as prescribed in Eq. (2.44). Recall that simplifications occur [60] when this subtraction is performed under the integral over variables (x, y, z) corresponding to the gluon emission angles. In particular, the symbol alphabet and factorization constraints which allow us to use the basis of functions introduced in Sec. 3.4 only apply to

the subtracted web. Consider then the integrand of Eq. (2.44),

$$\bar{w}_{(2,2,2),i}^{(3,-1)} = \left(\frac{1}{4\pi}\right)^3 \int_0^1 dx dy dz p_0(x, \alpha_{12}) p_0(y, \alpha_{23}) p_0(z, \alpha_{13}) \left(\mathcal{G}_{0,i} + \sum_k \Delta \mathcal{G}_{k,i} \right), \quad (\text{A.26})$$

where we defined $\mathcal{G}_{0,i}$ as the contribution proportional to $c_i^{(3)}$ from the unsubtracted web, obtained by expanding the integrand of Eq. (A.25); $\Delta \mathcal{G}_{k,i}$, in turn, are the contributions from the commutators of lower order webs to this colour factor, where k runs over the relevant commutator terms in Eq. (2.44) (note that $\Delta \mathcal{G}_{k,i}$ include the numerical factors appearing there). We recall that each of these contributions to $\mathcal{G}_{(2,2,2),i}$ depends on x, y and z as well as on $q(x, \alpha_{12}), q(y, \alpha_{23})$ and $q(z, \alpha_{13})$. Using the lower-order web results collected in Ref. [60], the contributions to the integrand of $\bar{w}_{(2,2,2)}^{(3)}$ multiplying the colour factor $c_1^{(3)}$ are

$$\begin{aligned} \Delta \mathcal{G}_{[w^{(1,0)}, w^{(2,-1)}], 1} &= \frac{1}{4} \left[\log [q(x, \alpha_{12})] \log \left(\frac{y}{z}\right) \right. \\ &\quad \left. - \log [q(z, \alpha_{13})] \log \left(\frac{x}{y}\right) \right], \\ \Delta \mathcal{G}_{[w^{(2,0)}, w^{(1,-1)}], 1} &= -\frac{1}{2} \left[\text{Li}_2 \left(-\frac{y}{z}\right) - \text{Li}_2 \left(-\frac{z}{y}\right) \right. \\ &\quad + \text{Li}_2 \left(-\frac{y}{x}\right) - \text{Li}_2 \left(-\frac{x}{y}\right) \\ &\quad + \frac{1}{2} \log \left(\frac{y}{z}\right) (\log [q(y, \alpha_{23})] + \log [q(z, \alpha_{13})]) \\ &\quad \left. - \frac{1}{2} \log \left(\frac{x}{y}\right) (\log [q(x, \alpha_{12})] + \log [q(y, \alpha_{23})]) \right], \\ \Delta \mathcal{G}_{[w^{(1,0)}, [w^{(1,-1)}, w^{(1,0)}], 1} &= -\frac{1}{12} \left[\log [q(x, \alpha_{12})] \log [q(y, \alpha_{23})] \right. \\ &\quad \left. + \log [q(z, \alpha_{13})] \log [q(y, \alpha_{23})] - 2 \log [q(z, \alpha_{13})] \log [q(x, \alpha_{12})] \right], \\ \Delta \mathcal{G}_{[w^{(1,-1)}, [w^{(1,1)}, w^{(1,-1)}], 1} &= -\frac{1}{24} \left[\log^2 [q(z, \alpha_{13})] - 2 \log^2 [q(y, \alpha_{23})] \right. \\ &\quad \left. + \log^2 [q(x, \alpha_{12})] \right]. \end{aligned} \quad (\text{A.27})$$

The contributions to the coefficient of the colour factor $c_2^{(3)}$ are

$$\begin{aligned}
\Delta\mathcal{G}_{[w^{(1,0)},w^{(2,-1)}],2} &= \frac{1}{4} \left[-\log [q(x, \alpha_{12})] \log \left(\frac{y}{z} \right) + \log [q(y, \alpha_{23})] \log \left(\frac{z}{x} \right) \right], \\
\Delta\mathcal{G}_{[w^{(2,0)},w^{(1,-1)}],2} &= -\frac{1}{2} \left[\text{Li}_2 \left(-\frac{z}{x} \right) - \text{Li}_2 \left(-\frac{x}{z} \right) + \text{Li}_2 \left(-\frac{z}{y} \right) - \text{Li}_2 \left(-\frac{y}{z} \right) \right. \\
&\quad \left. + \frac{1}{2} \log \left(\frac{z}{x} \right) (\log [q(z, \alpha_{13})] + \log [q(x, \alpha_{12})]) \right. \\
&\quad \left. - \frac{1}{2} \log \left(\frac{y}{z} \right) (\log [q(y, \alpha_{23})] + \log [q(z, \alpha_{13})]) \right], \\
\Delta\mathcal{G}_{[w^{(1,0)},[w^{(1,-1)},w^{(1,0)}]],2} &= -\frac{1}{12} \left[\log [q(x, \alpha_{12})] \log [q(z, \alpha_{13})] \right. \\
&\quad \left. + \log [q(z, \alpha_{13})] \log [q(y, \alpha_{23})] - 2 \log [q(y, \alpha_{23})] \log [q(x, \alpha_{12})] \right], \\
\Delta\mathcal{G}_{[w^{(1,-1)},[w^{(1,1)},w^{(1,-1)}]],2} &= -\frac{1}{24} \left[\log^2 [q(y, \alpha_{23})] - 2 \log^2 [q(z, \alpha_{13})] \right. \\
&\quad \left. + \log^2 [q(x, \alpha_{12})] \right]. \tag{A.28}
\end{aligned}$$

Finally, the contributions to the coefficient of the colour factor $c_3^{(3)}$ are found to be

$$\begin{aligned}
\Delta\mathcal{G}_{[w^{(1,0)},w^{(2,-1)}],3} &= \frac{1}{4} \left[-\log [q(z, \alpha_{13})] \log \left(\frac{x}{y} \right) \right. \\
&\quad \left. + \log [q(y, \alpha_{23})] \log \left(\frac{z}{x} \right) \right], \\
\Delta\mathcal{G}_{[w^{(2,0)},w^{(1,-1)}],3} &= -\frac{1}{2} \left[\text{Li}_2 \left(-\frac{z}{x} \right) - \text{Li}_2 \left(-\frac{x}{z} \right) \right. \\
&\quad \left. + \text{Li}_2 \left(-\frac{y}{x} \right) - \text{Li}_2 \left(-\frac{x}{y} \right) \right. \\
&\quad \left. + \frac{1}{2} \log \left(\frac{z}{x} \right) (\log [q(z, \alpha_{13})] + \log [q(x, \alpha_{12})]) \right. \\
&\quad \left. - \frac{1}{2} \log \left(\frac{x}{y} \right) (\log [q(x, \alpha_{12})] + \log [q(y, \alpha_{23})]) \right], \tag{A.29} \\
\Delta\mathcal{G}_{[w^{(1,0)},[w^{(1,-1)},w^{(1,0)}]],3} &= \frac{1}{12} \left[\log [q(x, \alpha_{12})] \log [q(y, \alpha_{23})] \right. \\
&\quad \left. + \log [q(z, \alpha_{13})] \log [q(x, \alpha_{12})] - 2 \log [q(y, \alpha_{23})] \log [q(z, \alpha_{13})] \right], \\
\Delta\mathcal{G}_{[w^{(1,-1)},[w^{(1,1)},w^{(1,-1)}]],3} &= \frac{1}{24} \left[\log^2 [q(z, \alpha_{13})] - 2 \log^2 [q(x, \alpha_{12})] \right. \\
&\quad \left. + \log^2 [q(y, \alpha_{23})] \right].
\end{aligned}$$

There are no commutator counterterms contributing to the fully antisymmetric colour factor $c_4^{(3)}$, as there are no colour factors of lower order webs that commute to produce the desired structure. This is consistent with the fact that the kinematic function associated with $c_4^{(3)}$ involves only staircase diagrams, which are irreducible, and as such do not contain subdivergences.

Combining all terms, using appropriate dilogarithm identities, and the symmetry of $p_0(x, \alpha)$ under $x \leftrightarrow 1 - x$, and finally using the definition given in Eq. (3.35), one finds the results presented in Eqs. (3.67) and (3.69). As a check of these results, one may verify that the $\mathcal{O}(\epsilon^{-2})$ pole of the (2,2,2) web vanishes, according to the web consistency relation discussed in Ref. [58],

$$w^{(3,-2)}|_{\beta_0=0} = -\frac{1}{6} [w^{(1,-1)}, w^{(2,-1)}] . \quad (\text{A.30})$$

As a further check, the sum of all web diagrams must give a product of one-loop graphs, in accordance with Eq. (3.19). We have explicitly confirmed that both of these criteria are satisfied.

A.3 Calculation of the (1,2,3) web

The calculation of the (1,2,3) web, shown in Fig. 3.11, proceeds similarly to the (2,2,2) case considered in the previous Appendix.

A.3.1 Unsubtracted web

Using the method of Sec. 3.3, the result for the contribution to the web kernel $\phi_{(1,2,3)}^{(3)}$ from diagram A is

$$\phi_A^{(3)} = \frac{1}{4} \log^2 \left[\frac{y(1-x)}{x(1-y)} \right] . \quad (\text{A.31})$$

Carrying out a similar exercise for the other diagrams of the (1,2,3) web gives the results

$$\begin{aligned} \phi_B^{(3)} = & \frac{1}{8\epsilon^2} \theta(x-y) \left(\frac{1-x}{z} \right)^{2\epsilon} \left[\left(\frac{1-y}{1-x} \right)^{4\epsilon} - \left(\frac{y}{x} \right)^{4\epsilon} \right. \\ & \left. + 24\epsilon^2 \left(\text{Li}_2 \left(-\frac{x}{y} \right) - \text{Li}_2 \left(-\frac{y}{x} \right) \right) + \mathcal{O}(\epsilon^3) \right] , \end{aligned}$$

$$\begin{aligned}
\phi_C^{(3)} &= \frac{1}{2\epsilon} \theta(x-y) \left[\frac{\Gamma(2\epsilon)\Gamma(4\epsilon)}{\Gamma(6\epsilon)} - \frac{1}{2\epsilon} \left(\frac{1-y}{z} \right)^{2\epsilon} \right] \left[\left(\frac{1-y}{1-x} \right)^{2\epsilon} - \left(\frac{y}{x} \right)^{2\epsilon} \right], \\
\phi_D^{(3)} &= \frac{1}{8\epsilon^2} \left(\frac{1-y}{z} \right)^{2\epsilon} \left[\theta(y-x) \left(\frac{x}{y} \right)^{4\epsilon} + \theta(x-y) \left(\frac{1-x}{1-y} \right)^{4\epsilon} \right. \\
&\quad \left. + 24\epsilon^2 \theta(y-x) \text{Li}_2 \left(-\frac{x}{y} \right) + 24\epsilon^2 \theta(x-y) \text{Li}_2 \left(-\frac{1-x}{1-y} \right) + \mathcal{O}(\epsilon^3) \right], \\
\phi_E^{(3)} &= \frac{1}{8\epsilon^2} \left\{ \theta(x-y) \left[2 \left(\frac{1-x}{z} \right)^{2\epsilon} \left(\frac{1-y}{1-x} \right)^{-2\epsilon} - \left(\frac{1-y}{z} \right)^{2\epsilon} \left(\frac{1-y}{1-x} \right)^{-4\epsilon} \right] \right. \\
&\quad \left. + \theta(y-x) \left[2 \left(\frac{1-x}{z} \right)^{2\epsilon} \left(\frac{y}{x} \right)^{-2\epsilon} - \left(\frac{1-y}{z} \right)^{2\epsilon} \left(\frac{y}{x} \right)^{-4\epsilon} \right] \right. \\
&\quad \left. + 24\epsilon^2 \text{Li}_2 \left(-\frac{1-x}{z} \right) + \mathcal{O}(\epsilon^3) \right\}, \tag{A.32} \\
\phi_F^{(3)} &= \frac{1}{2\epsilon} \left\{ \theta(x-y) \left(\frac{1-y}{1-x} \right)^{-2\epsilon} \left[\frac{\Gamma(4\epsilon)\Gamma(2\epsilon)}{\Gamma(6\epsilon)} \left(1 + 8\epsilon^2 \text{Li}_2 \left(-\frac{1-x}{1-y} \right) \right) \right. \right. \\
&\quad \left. \left. - \frac{1}{2\epsilon} \left(\frac{1-x}{z} \right)^{2\epsilon} \left(1 + 12\epsilon^2 \text{Li}_2 \left(-\frac{1-x}{1-y} \right) \right) \right] \right. \\
&\quad \left. + \theta(y-x) \left(\frac{y}{x} \right)^{-2\epsilon} \left[\frac{\Gamma(4\epsilon)\Gamma(2\epsilon)}{\Gamma(6\epsilon)} \left(1 + 8\epsilon^2 \text{Li}_2 \left(-\frac{x}{y} \right) \right) - \frac{1}{2\epsilon} \left(\frac{1-x}{z} \right)^{2\epsilon} \right. \right. \\
&\quad \left. \left. \times \left(1 + 12\epsilon^2 \text{Li}_2 \left(-\frac{x}{y} \right) \right) \right] - 6\epsilon \left(\frac{1-x}{z} \right)^{2\epsilon} \text{Li}_2 \left(-\frac{1-x}{z} \right) + \mathcal{O}(\epsilon^2) \right\}.
\end{aligned}$$

These expressions must of course be expanded in powers of ϵ , up to $\mathcal{O}(\epsilon^0)$. Notice that there is a difference with respect to the (2,2,2) web, in that Heaviside functions survive in the integrand. This can ultimately be traced to the fact that the (1,2,3) web contains a crossed-gluon pair spanning a single cusp angle, and a Heaviside function is needed in order to implement the crossing condition. From Eq. (A.32), the unsubtracted web

$$W_{(1,2,3)} = \sum_{j=1}^4 c_j^{(3)} \mathcal{F}_{(1,2,3),j}^{(3)} \tag{A.33}$$

is obtained through Eq. (3.16) by taking the specific coefficients $Y_{X,j}^{-1}$ given in table 3.3, as

$$\begin{aligned} \mathcal{F}_{(1,2,3),j}^{(3)} &= \kappa^3 \Gamma(6\epsilon) \int_0^1 dx dy dz p_\epsilon(x, \alpha_{23}) p_\epsilon(y, \alpha_{23}) p_\epsilon(z, \alpha_{13}) \sum_{X \in (1,2,3)} Y_{X,j}^{-1} \phi_X^{(3)}(x, y, z; \epsilon) \\ &= \kappa^3 \Gamma(6\epsilon) \int_0^1 dx dy dz p_\epsilon(x, \alpha_{23}) p_\epsilon(y, \alpha_{23}) p_\epsilon(z, \alpha_{13}) \phi_{(1,2,3),j}^{(3)}(x, y, z; \epsilon), \end{aligned} \quad (\text{A.34})$$

where we recall that the contribution to the $i = 1$ colour component vanishes. In the following we compute the (1,2,3) subtracted web for $i = 2, 3$ and 4.

A.3.2 Subtracted web

As for the (2,2,2) web, it is useful to collect results for the subtraction terms separated according to the colour factor they contribute to. We once again split the subtracted web kernel into contributions from the unsubtracted web, $\mathcal{G}_{0,i}$ originating in the expansion of the integrand in Eq. (A.34), and the commutators of lower order webs, $\Delta\mathcal{G}_{j,i}$, so that the coefficient of the colour factors $c_i^{(3)}$ can be written as

$$\overline{w}_{(1,2,3),i}^{(3,-1)} = \left(\frac{1}{4\pi}\right)^3 \int_0^1 dx dy dz p_0(x, \alpha_{23}) p_0(y, \alpha_{23}) p_0(z, \alpha_{13}) \left(\mathcal{G}_{0,i} + \sum_k \Delta\mathcal{G}_{k,i} \right). \quad (\text{A.35})$$

We recall that each of these contributions to $\mathcal{G}_{(1,2,3),i}$ depends on x, y and z as well as on $q(x, \alpha_{23}), q(y, \alpha_{23})$ and $q(z, \alpha_{13})$. We will see that after cancellations only logarithmic dependence on these arguments will survive. The results of the commutators with the colour factors $c_i^{(3)}$ with $i = 2$ and 3 are

$$\begin{aligned} \Delta\mathcal{G}_{[w^{(1,0)}, w^{(2,-1)}], i} &= \frac{1}{4} \log\left(\frac{x}{z}\right) \log[q(y, \alpha_{23})], \\ \Delta\mathcal{G}_{[w^{(2,0)}, w^{(1,-1)}], i} &= -\frac{1}{2} \left[\text{Li}_2\left(-\frac{x}{z}\right) - \text{Li}_2\left(-\frac{z}{x}\right) \right. \\ &\quad \left. + \frac{1}{2} \log\left(\frac{x}{z}\right) \left(\log[q(x, \alpha_{23})] + \log[q(z, \alpha_{13})] \right) \right], \\ \Delta\mathcal{G}_{[w^{(1,0)}, [w^{(1,-1)}, w^{(1,0)}]], i} &= -\frac{1}{12} \log[q(x, \alpha_{23})] \left(\log[q(y, \alpha_{23})] - \log[q(z, \alpha_{13})] \right), \end{aligned}$$

$$\Delta\mathcal{G}_{[w^{(1,-1)},[w^{(1,1)},w^{(1,-1)}],i]} = -\frac{1}{24} \left(\log^2 [q(z, \alpha_{13})] - \log^2 [q(x, \alpha_{23})] \right). \quad (\text{A.36})$$

Finally, there are contributions to the fully antisymmetric colour factor $c_4^{(3)}$, given by

$$\begin{aligned} \Delta\mathcal{G}_{[w^{(1,0)},w^{(2,-1)}],4} &= \theta(x-y) \log\left(\frac{y}{x}\right) \log[q(z, \alpha_{13})], & (\text{A.37}) \\ \Delta\mathcal{G}_{[w^{(2,0)},w^{(1,-1)}],4} &= -\theta(x-y) \left[4 \text{Li}_2\left(-\frac{y}{x}\right) + \log^2\left(\frac{y}{x}\right) + 2\zeta(2) \right. \\ &\quad \left. - \log\left(\frac{x}{y}\right) \left(\log[q(x, \alpha_{23})] + \log[q(y, \alpha_{23})] \right) \right]. \end{aligned}$$

This colour factor had no commutator contributions in the (2,2,2) case, as discussed above. In this case they can be generated due to the fact that one of the lower order webs contains a crossed gluon pair. Combining, as prescribed by Eq. (2.44), the non-subtracted web and the commutator counterterms, one finds again that the integrated results can be expressed using the basis functions of Eq. (3.35), and they are given in Eq. (3.75). Finally, as for the (2,2,2) web, we have verified the cancellation of the double pole, and also the abelian sum rule given in Eq. (3.19).

A.4 Calculation of the (1,2,2,2,1) web

A.4.1 Unsubtracted web

In this appendix we write the integrand $\phi_X^{(4)}$ for each diagram X of the (1,2,2,2,1) unsubtracted web. We begin by noting that the diagrams of Fig. 3.13 are pairwise related by a symmetry under permutations mapping a clockwise orientation into an anticlockwise one, thus swapping lines $1 \leftrightarrow 5$ along with $2 \leftrightarrow 4$. Because of this symmetry argument, we need to report only four out of the eight diagram kernels, while the remaining ones can be obtained through

$$\phi_X^{(4)}(x_1, x_2, x_3, x_4) = \phi_{X'}^{(4)}(1-x_4, 1-x_3, 1-x_2, 1-x_1), \quad (\text{A.38})$$

where X and X' are any two diagrams related to each other by the symmetry. In order to express the results in compact form, it is useful to define the function

$$\mathcal{L}_3(a, b, -x) = a b \left(\log(x) \operatorname{Li}_2(-x) - \operatorname{Li}_3(-x) \right) + b^2 S_{1,2}(-x), \quad (\text{A.39})$$

which arises in the expansion of integrals of the form

$$\begin{aligned} I(m, n; a, \epsilon) &\equiv \int_0^a d\zeta \zeta^{-1+m\epsilon} (1 + \zeta)^{-n\epsilon} \\ &= \frac{a^{m\epsilon}}{m\epsilon} + n\epsilon \operatorname{Li}_2(-a) + \epsilon^2 \mathcal{L}_3(m, n, -a) + \mathcal{O}(\epsilon^3), \end{aligned} \quad (\text{A.40})$$

as well as the integral

$$\begin{aligned} \mathcal{I}_3(a, b) &= \int_0^a \frac{d\zeta}{\zeta} \left[\operatorname{Li}_2(-b(1 + \zeta)) - \operatorname{Li}_2(-b) \right] = \int_0^b \frac{d\zeta}{\zeta} \operatorname{Li}_2\left(-b \frac{\zeta}{1 + \zeta}\right) \\ &= \log(1 + b) \operatorname{Li}_2(-a) - G\left(0, -1, -\frac{1 + b}{b}; a\right), \end{aligned} \quad (\text{A.41})$$

where $G(a_1, \dots, a_n; z)$ is the generalised polylogarithm defined by the iterated integral [109]

$$G(a_1, \dots, a_n; z) = \int_0^z \frac{dt}{t - a_1} G(a_2, \dots, a_n; t), \quad (\text{A.42})$$

with $G(z) = 1$ and $a_i, z \in \mathbb{C}$. Using these definitions, the results for the first four diagrams in Fig. 3.13 are given by

$$\begin{aligned} \phi_A^{(4)}(x_i; \epsilon) &= \frac{1}{48\epsilon^3} \left(\frac{x_4}{1 - x_3} \right)^{6\epsilon} \left(\frac{x_3}{1 - x_2} \right)^{4\epsilon} \left(\frac{x_2}{1 - x_1} \right)^{2\epsilon} \\ &\quad + \frac{1}{\epsilon} \left(\frac{x_3}{1 - x_2} \right)^{4\epsilon} \left(\frac{x_2}{1 - x_1} \right)^{2\epsilon} \operatorname{Li}_2\left(-\frac{x_4}{1 - x_3}\right) \\ &\quad + 4 \mathcal{I}_3\left(\frac{x_3}{1 - x_2}, \frac{x_4}{1 - x_3}\right) + \frac{1}{8} \mathcal{L}_3\left(6, 8, -\frac{x_4}{1 - x_3}\right), \end{aligned} \quad (\text{A.43})$$

$$\begin{aligned} \phi_B^{(4)}(x_i; \epsilon) &= -\frac{1}{48\epsilon^3} \left(\frac{1 - x_3}{x_4} \right)^{2\epsilon} \left(\frac{1 - x_2}{x_3} \right)^{4\epsilon} \left(\frac{1 - x_1}{x_2} \right)^{6\epsilon} \\ &\quad + \frac{1}{12\epsilon^3} \left(\frac{1 - x_2}{x_3} \right)^{2\epsilon} \left(\frac{1 - x_1}{x_2} \right)^{4\epsilon} + \frac{2}{\epsilon} \left(\frac{1 - x_2}{x_3} \right)^{2\epsilon} \operatorname{Li}_2\left(-\frac{1 - x_1}{x_2}\right) \end{aligned}$$

$$\begin{aligned}
 & -\frac{\zeta(2)}{\epsilon} \left(\frac{1-x_2}{x_3}\right)^{2\epsilon} \left(\frac{1-x_1}{x_2}\right)^{4\epsilon} \\
 & -\frac{1}{\epsilon} \left(\frac{1-x_3}{x_4}\right)^{2\epsilon} \left(\frac{1-x_2}{x_3}\right)^{4\epsilon} \text{Li}_2\left(-\frac{1-x_1}{x_2}\right) + \frac{1}{3} \mathcal{L}_3\left(4, 6, -\frac{1-x_1}{x_2}\right) \\
 & -\frac{1}{8} \mathcal{L}_3\left(6, 8, -\frac{1-x_1}{x_2}\right) + 8\zeta(3),
 \end{aligned} \tag{A.44}$$

$$\begin{aligned}
 \phi_D^{(4)}(x_i; \epsilon) &= \frac{1}{6\epsilon^3} \left(\frac{1-x_2}{x_3}\right)^{2\epsilon} \left(\frac{1-x_1}{x_2}\right)^{-2\epsilon} + \frac{2}{\epsilon} \left(\frac{1-x_1}{x_2}\right)^{-2\epsilon} \text{Li}_2\left(-\frac{1-x_2}{x_3}\right) \\
 & -\frac{1}{16\epsilon^3} \left(\frac{1-x_3}{x_4}\right)^{2\epsilon} \left(\frac{1-x_2}{x_3}\right)^{4\epsilon} \left(\frac{1-x_1}{x_2}\right)^{-2\epsilon} + \frac{2}{\epsilon} \left(\frac{1-x_2}{x_3}\right)^{2\epsilon} \text{Li}_2\left(-\frac{x_2}{1-x_1}\right) \\
 & -\frac{2}{\epsilon} \left(\frac{1-x_3}{x_4}\right)^{2\epsilon} \left(\frac{1-x_1}{x_2}\right)^{-2\epsilon} \text{Li}_2\left(-\frac{1-x_2}{x_3}\right) - \frac{2\zeta(2)}{\epsilon} \left(\frac{1-x_2}{x_3}\right)^{2\epsilon} \left(\frac{1-x_1}{x_2}\right)^{-2\epsilon} \\
 & -\frac{1}{\epsilon} \left(\frac{1-x_3}{x_4}\right)^{2\epsilon} \left(\frac{1-x_2}{x_3}\right)^{4\epsilon} \text{Li}_2\left(-\frac{x_2}{1-x_1}\right) \\
 & +\frac{1}{3} \mathcal{L}_3\left(2, 6, -\frac{x_2}{1-x_1}\right) + \frac{1}{3} \mathcal{L}_3\left(2, 6, -\frac{1-x_2}{x_3}\right) - \frac{1}{4} \mathcal{L}_3\left(4, 8, \frac{1-x_2}{x_3}\right) \\
 & -\frac{1}{8} \mathcal{L}_3\left(2, 8, \frac{x_2}{1-x_1}\right) - 4\mathcal{I}_3\left(\frac{1-x_3}{x_4}, \frac{1-x_2}{x_3}\right) + 16\zeta(3),
 \end{aligned} \tag{A.45}$$

$$\begin{aligned}
 \phi_E^{(4)}(x_i; \epsilon) &= \frac{1}{16\epsilon^3} \left(\frac{x_2}{1-x_1}\right)^{2\epsilon} \left(\frac{x_3}{1-x_2}\right)^{4\epsilon} \left(\frac{1-x_3}{x_4}\right)^{2\epsilon} \\
 & +\frac{2}{\epsilon} \left(\frac{x_2}{1-x_1}\right)^{2\epsilon} \left(\frac{1-x_3}{x_4}\right)^{2\epsilon} \text{Li}_2\left(-\frac{x_3}{1-x_2}\right) \\
 & +\frac{1}{\epsilon} \left(\frac{x_2}{1-x_1}\right)^{2\epsilon} \left(\frac{x_3}{1-x_2}\right)^{4\epsilon} \text{Li}_2\left(-\frac{1-x_3}{x_4}\right) \\
 & -4\text{Li}_{1,2}\left(-\frac{1-x_3}{x_4}\right) - 4\log\left(\frac{x_3}{1-x_2}\right) \text{Li}_2\left(-\frac{1-x_3}{x_4}\right) \\
 & +\frac{1}{8} \mathcal{L}_3\left(2, 8, -\frac{1-x_3}{x_4}\right) + \frac{1}{4} \mathcal{L}_3\left(4, 8, -\frac{x_3}{1-x_2}\right) \\
 & +4\mathcal{I}_3\left(\frac{x_2}{1-x_1}, \frac{x_3}{1-x_2}\right) - 4\mathcal{I}_3\left(\frac{1-x_3}{x_4}, \frac{1-x_2}{x_3}\right),
 \end{aligned} \tag{A.46}$$

where, as above, these expressions must be expanded to order $\mathcal{O}(\epsilon^0)$. The remaining four diagrams can be obtained using symmetry, as

$$\begin{aligned}
\phi_C^{(4)}(x_1, x_2, x_3, x_4; \epsilon) &= \phi_B^{(4)}(1 - x_4, 1 - x_3, 1 - x_2, 1 - x_1; \epsilon), \\
\phi_F^{(4)}(x_1, x_2, x_3, x_4; \epsilon) &= \phi_A^{(4)}(1 - x_4, 1 - x_3, 1 - x_2, 1 - x_1; \epsilon), \\
\phi_G^{(4)}(x_1, x_2, x_3, x_4; \epsilon) &= \phi_D^{(4)}(1 - x_4, 1 - x_3, 1 - x_2, 1 - x_1; \epsilon), \\
\phi_H^{(4)}(x_1, x_2, x_3, x_4; \epsilon) &= \phi_E^{(4)}(1 - x_4, 1 - x_3, 1 - x_2, 1 - x_1; \epsilon).
\end{aligned} \tag{A.47}$$

A.4.2 Subtracted web

The subtracted (1,2,2,2,1) web involves a sum of commutators of lower-order webs, comprising subdiagrams of the original unsubtracted web, and given in Eq. (2.43). The relevant webs are the (1,1) one-loop web, which is needed to $\mathcal{O}(\epsilon^2)$ and can be taken from Ref. [60], the (1,2,1) two-loop web, which is needed to $\mathcal{O}(\epsilon)$, and the (1,2,2,1) three-loop web, which is needed to $\mathcal{O}(\epsilon^0)$. The commutators of these webs have precisely the same colour structure $c_1^{(4)}$ as the non-subtracted (1,2,2,2,1) three-loop web. In order to complete the calculation, we list here the kernels for the (1,2,2,1) and the (1,2,1) webs, in a form which is appropriate to be expanded to the relevant order.

The non-subtracted (1,2,2,1) web [60] is given by the combination

$$\phi_{(1,2,2,1)}^{(3)} = \frac{1}{6} \left(\phi_A^{(3)} - 2\phi_B^{(3)} - 2\phi_C^{(3)} + \phi_D^{(3)} \right), \tag{A.48}$$

where the diagrams are labelled as in Fig. 3.4. The expansions of the kinematic integrands $\phi_X^{(3)}$ up to $\mathcal{O}(\epsilon)$ can be obtained from

$$\begin{aligned}
\phi_A^{(3)}(x_i; \epsilon) &= B(2\epsilon, 4\epsilon) \left[B(2\epsilon, 2\epsilon) - \frac{1}{2\epsilon} \left(\frac{1-x_2}{x_3} \right)^{2\epsilon} \right. \\
&\quad \left. - 4\epsilon \operatorname{Li}_2 \left(-\frac{1-x_2}{x_3} \right) - \epsilon^2 \mathcal{L}_3 \left(2, 4, -\frac{1-x_2}{x_3} \right) \right] \\
&\quad - \frac{1}{2\epsilon} \left(\frac{x_1}{x_2} \right)^{2\epsilon} \left[B(2\epsilon, 4\epsilon) - \frac{1}{2\epsilon} \left(\frac{1-x_2}{x_3} \right)^{2\epsilon} \right. \\
&\quad \left. - 6\epsilon \operatorname{Li}_2 \left(-\frac{1-x_2}{x_3} \right) - \epsilon^2 \mathcal{L}_3 \left(2, 6, -\frac{1-x_2}{x_3} \right) \right]
\end{aligned}$$

$$-6 \epsilon \mathcal{I}_3 \left(\frac{x_2}{x_1}, \frac{x_3}{1-x_2} \right), \quad (\text{A.49})$$

$$\begin{aligned} \phi_B^{(3)}(x_i; \epsilon) &= \frac{1}{2\epsilon} \left(\frac{x_2}{x_1} \right)^{2\epsilon} \left[B(2\epsilon, 4\epsilon) - \frac{1}{2\epsilon} \left(\frac{1-x_2}{x_3} \right)^{2\epsilon} \right. \\ &\quad \left. - 6 \epsilon \text{Li}_2 \left(-\frac{1-x_2}{x_3} \right) - \epsilon^2 \mathcal{L}_3 \left(-\frac{1-x_2}{x_3} \right) \right] \\ &\quad + 6 \epsilon \mathcal{I}_3 \left(\frac{x_2}{x_1}, \frac{x_3}{1-x_2} \right), \end{aligned} \quad (\text{A.50})$$

$$\begin{aligned} \phi_D^{(3)}(x_i; \epsilon) &= \frac{1}{2\epsilon} \left(\frac{x_2}{x_1} \right)^{2\epsilon} \left[\frac{1}{2\epsilon} \left(\frac{1-x_2}{x_3} \right)^{2\epsilon} + 6\epsilon \text{Li}_2 \left(-\frac{1-x_2}{x_3} \right) + \epsilon^2 \mathcal{L}_3 \left(2, 6, -\frac{1-x_2}{x_3} \right) \right] \\ &\quad + 3 \text{Li}_2 \left(-\frac{x_2}{x_1} \right) - 6\epsilon \left[\mathcal{I}_3 \left(\frac{x_2}{x_1}, \frac{x_3}{1-x_2} \right) + \text{Li}_{1,2} \left(-\frac{x_2}{x_1} \right) \right] + \frac{\epsilon}{2} \mathcal{L}_3 \left(2, 6, -\frac{x_2}{x_1} \right). \end{aligned} \quad (\text{A.51})$$

Again, we observe that diagram B and diagram C are related by the exchange of the gluon labels. We obtain diagram C by means of the relation

$$\phi_C^{(3)}(x_1, x_2, x_3; \epsilon) = \phi_B^{(3)}(x_3, 1-x_2, x_1; \epsilon). \quad (\text{A.52})$$

We finally need the integrand of the non-subtracted two-loop (1,2,1) web. It is given by

$$\begin{aligned} \phi_{(1,2,1)}^{(2)}(x_1, x_2) &= \frac{1}{4\epsilon} \left[\left(\frac{x_1}{x_2} \right)^{2\epsilon} - \left(\frac{x_2}{x_1} \right)^{2\epsilon} \right] + 2\epsilon \left[\text{Li}_2 \left(-\frac{x_1}{x_2} \right) - \text{Li}_2 \left(-\frac{x_2}{x_1} \right) \right] \\ &\quad + \frac{\epsilon^2}{2} \left[\mathcal{L}_3 \left(2, 4, -\frac{x_1}{x_2} \right) - \mathcal{L}_3 \left(2, 4, -\frac{x_2}{x_1} \right) \right]. \end{aligned} \quad (\text{A.53})$$

Note that, as in all other cases we examined, both the unsubtracted webs and the lower-order webs entering Eq. (2.43) are not factorised integrals, because the functions \mathcal{I}_3 , \mathcal{L}_3 and the other polylogarithms entering the web depend on ratios of different integration variables x_i . All such functions, however, cancel in the sum in Eq. (2.43), and the resulting expression for the integrand is factorised, as reported in the text, Eq. (3.80).

Appendix B

Triangle Integrals

In [124], the authors study a class of scalar triangles with three external masses and no internal masses, in d dimensions and with general ¹ powers of the propagators, $\nu_1, \nu_2, \nu_3 > 0$,

$$T(d, \nu_1, \nu_2, \nu_3; p_i^2) = e^{\gamma_E \epsilon} \int \frac{d^d z}{i\pi^{d/2}} \frac{1}{(-z^2)^{\nu_1} (-(z-p_1)^2)^{\nu_2} (-(z+p_3)^2)^{\nu_3}}, \quad (\text{B.1})$$

where the definition of the momenta can be inferred from figure B.1, with $\sum_i p_i = 0$.

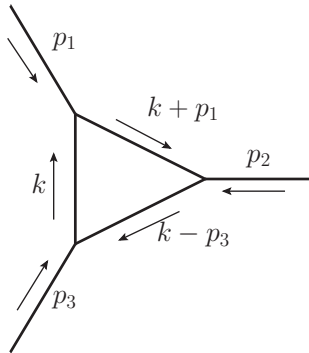


Figure B.1: Scalar triangle with three external masses, massless propagators to power of $1 - \epsilon$.

They show that they can be written as a one dim integral over a hypergeo-

¹This is naturally restricted to $\nu_1, \nu_2, \nu_3 < 0$ since if at least one of $\nu_i < 0$ then the integral reduces to bubbles.

metric function,

$$\begin{aligned}
T(d, \nu_1, \nu_2, \nu_3; p_i^2) &= e^{\gamma_{\mathbb{E}} \epsilon} \frac{\Gamma(\nu - d/2) \Gamma(n/2 - \nu_3)}{\Gamma(\nu_1) \Gamma(\nu_2) \Gamma(d/2)} (p_1^2)^{d/2 - \nu} \\
&\times \int_0^1 d\xi \xi^{d/2 - \nu_1 - \nu_3 - 1} (1 - \xi)^{d/2 - \nu_2 - \nu_3 - 1} \\
&\times {}_2F_1\left(\nu_3, \nu - d/2; d/2; 1 - \frac{(1 - \xi)p_3^2 + \xi p_2^2}{\xi(1 - \xi)p_1^2}\right) \quad (\text{B.2})
\end{aligned}$$

where $\nu = \nu_1 + \nu_2 + \nu_3$, and then by expressing the hypergeometric function through its Mellin-Barnes representation,

$${}_2F_1(a, b; c; z) = \frac{\Gamma(c)}{\Gamma(a)\Gamma(b)} \frac{1}{2\pi i} \int_{-i\infty}^{i\infty} ds (-z)^s \frac{\Gamma(-s)\Gamma(a+s)\Gamma(b+s)}{\Gamma(c+s)}, \quad (\text{B.3})$$

they are able to use the fact that ${}_2F_1$ is an analytical function to close the contour to the right and so write the integral as a sum over the poles of the gamma functions. Using the relation between ${}_2F_1$ and the Appell F_4 hypergeometric functions,

$$F_4(\alpha, \beta, \gamma, \delta; x, xy) = \sum_{j=0}^{\infty} \frac{x^j}{j!} \frac{(\alpha)_j (\beta)_j}{(\gamma)_j} {}_2F_1(-j, 1 - \gamma - j; \delta; y) \quad (\text{B.4})$$

where the Pochhammer symbol,

$$(\alpha)_j = \frac{\Gamma(\alpha + j)}{\Gamma(\alpha)}, \quad (\text{B.5})$$

to perform this sum, they can conclude that,

$$\begin{aligned}
T(d, \nu_1, \nu_2, \nu_3; p_i^2) &= \frac{e^{\gamma_{\mathbb{E}} \epsilon}}{\Gamma(\nu_1) \Gamma(\nu_2) \Gamma(\nu_3) \Gamma(d - \nu)} \\
&\times \left[(p_3^2)^{-\nu_1} (p_2^2)^{d/2 - \nu_2 - \nu_3} \Gamma(\nu_2 + \nu_3 - d/2) \Gamma(d/2 - \nu_1 - \nu_3) \Gamma(d/2 - \nu_2) \right. \\
&\times \Gamma(\nu_1) F_4(\mu, d/2 - \nu_2, \nu_1 + \nu_3 - d/2 + 1, d/2 - \nu_2 - \nu_3 + 1; u, v) \\
&+ (p_3^2)^{-\nu_2} (p_1^2)^{d/2 - \nu_1 - \nu_3} \Gamma(\nu_1 + \nu_3 - d/2) \Gamma(d/2 - \nu_2 - \nu_3) \Gamma(d/2 - \nu_1) \\
&\times \Gamma(\nu_2) F_4(\nu_2, d/2 - \nu_1, d/2 - \nu_1 - \nu_3 + 1, \nu_2 + \nu_3 - d/2 + 1; u, v) \\
&+ (p_3^2)^{d/2 - \nu} \Gamma(d/2 - \nu_1 - \nu_3) \Gamma(d/2 - \nu_2 - \nu_3) \Gamma(\nu - d/2) \\
&\left. \times \Gamma(\nu_3) F_4(\nu_3, \nu - d/2, \nu_1 + \nu_3 - d/2 + 1, \nu_2 + \nu_3 - d/2 + 1; u, v) \right]
\end{aligned}$$

$$\begin{aligned}
& + (p_3^2)^{\nu_3-d/2} (p_1^2)^{d/2-\nu_1-\nu_3} (p_2^2)^{d/2-\nu_2-\nu_3} \\
& \times \Gamma(\nu_2 + \nu_3 - d/2) \Gamma(\nu_1 + \nu_3 - d/2) \Gamma(d - \nu) \Gamma(d/2 - \nu_3) \\
& \times F_4(d - \nu, d/2 - \nu_3, d/2 - \nu_1 - \nu_3 + 1, d/2 - \nu_2 - \nu_3 + 1; u, v) \Big].
\end{aligned}$$

In special cases these functions reduce to simpler ${}_2F_1$ hypergeometric functions through the following identities,

$$\begin{aligned}
F_4\left(\alpha, \beta, \alpha, \beta; -\frac{x}{(1-x)(1-y)}; -\frac{y}{(1-x)(1-y)}\right) \\
= \frac{(1-x)^\beta (1-y)^\alpha}{1-xy}, \tag{B.6}
\end{aligned}$$

$$\begin{aligned}
F_4\left(\alpha, \beta, \beta, \beta; -\frac{x}{(1-x)(1-y)}; -\frac{y}{(1-x)(1-y)}\right) \\
= (1-x)^\alpha (1-y)^\alpha {}_2F_1(\alpha, 1 + \alpha - \beta; \beta; xy), \tag{B.7}
\end{aligned}$$

$$\begin{aligned}
F_4\left(\alpha, \beta, 1 + \alpha - \beta, \beta; -\frac{x}{(1-x)(1-y)}; -\frac{y}{(1-x)(1-y)}\right) \\
= (1-y)^\alpha {}_2F_1\left(\alpha, \beta; 1 + \alpha - \beta; -\frac{x(1-y)}{1-x}\right), \tag{B.8}
\end{aligned}$$

combined with the symmetry properties under exchange of indices,

$$F_4(\alpha, \alpha', \gamma, \gamma'; u, v) = F_4(\alpha', \alpha, \gamma, \gamma'; u, v) = F_4(\alpha, \alpha', \gamma', \gamma; v, u), \tag{B.9}$$

and so, when $d = 4 - 2\epsilon$ and $\nu_1 = \nu_2 = \nu_3 = 1 - \epsilon$,

$$T(4 - 2\epsilon, 1 - \epsilon, 1 - \epsilon, 1 - \epsilon; p_i^2) \tag{B.10}$$

$$\begin{aligned}
& = \frac{e^{\gamma_E \epsilon}}{\Gamma^3(1 - \epsilon) \Gamma(1 + \epsilon)} (p_1^2)^{\frac{\epsilon}{2}} (p_2^2)^{\frac{\epsilon}{2}} (p_3^2)^{\epsilon-1} \\
& \left[u^{\frac{\epsilon}{2}} v^{\frac{\epsilon}{2}} \Gamma(1 + \epsilon) \Gamma^2(-\epsilon) (1-x)(1-y) {}_2F_1\left(1, 1 - \epsilon, 1 + \epsilon, xy\right) \right. \\
& + u^{\frac{\epsilon}{2}} v^{-\frac{\epsilon}{2}} \Gamma(1 - \epsilon) \Gamma(\epsilon) \Gamma(-\epsilon) (1-y) {}_2F_1\left(1, 1 - \epsilon, 1 + \epsilon, -x \frac{1-y}{1-x}\right) \\
& \left. + u^{-\frac{\epsilon}{2}} v^{\frac{\epsilon}{2}} \Gamma(1 - \epsilon) \Gamma(\epsilon) \Gamma(-\epsilon) (1-x) {}_2F_1\left(1, 1 - \epsilon, 1 + \epsilon, -y \frac{1-x}{1-y}\right) \right] \tag{B.11}
\end{aligned}$$

$$+ u^{-\frac{\epsilon}{2}} v^{-\frac{\epsilon}{2}} \Gamma(1-2\epsilon) \Gamma(1-\epsilon) \Gamma^2(-\epsilon) (1-x)^{1-2\epsilon} (1-y)^{1-2\epsilon} (1-xy)^{-1+2\epsilon} \Big].$$

We can therefore give expressions for the coefficients $T^{(0)}$ and $T^{(1)}$ of $T = T^{(0)} + \epsilon T^{(1)} + \mathcal{O}(\epsilon^2)$,

$$\begin{aligned} T^{(0)} = & \frac{\pi^2}{48p_3^2} \frac{(1-x)(1-y)}{1-xy} \left[\pi^2 - 3\log^2(1-x) - 3\log^2(1-y) \right. \\ & + 3\log(1-y)\log(-y) + 6\log(1-x)\log(1-y) + 3\log(-x)\log(-y) \\ & - 3\log(-x)\log(1-y) - 3\log(1-x)\log(-y) + 3\log(1-x)\log(-x) \\ & \left. - 6\text{Li}_2\left(-x\frac{1-y}{1-x}\right) - 6\text{Li}_2\left(-y\frac{1-x}{1-y}\right) + \text{Li}_2(xy) \right] \end{aligned} \quad (\text{B.12})$$

and

$$T^{(1)} = \widehat{T}^{(1)} + \frac{1}{2} \log\left(p_1^2 p_2^2 (p_3^2)^2\right) T^{(0)}, \quad (\text{B.13})$$

where

$$\begin{aligned} \widehat{T}^{(1)} = & \frac{1}{p_3^2} \frac{(1-x)(1-y)}{1-xy} \left[\text{Li}_2\left(-\frac{x(y-1)}{x-1}\right) \log\left(\frac{u}{v}\right) \right. \\ & - (\text{Li}_2(xy) - \zeta_2) \log(uv) - \log\left(\frac{u}{v}\right) \text{Li}_2\left(-\frac{(x-1)y}{y-1}\right) \\ & - 4\text{Li}_3\left(\frac{xy-1}{x-1}\right) - 2\text{Li}_3\left(-\frac{x(y-1)}{x-1}\right) - 4\text{Li}_3\left(\frac{xy-1}{y-1}\right) \\ & - 2\text{Li}_3\left(-\frac{(x-1)y}{y-1}\right) + 2\text{Li}_3(xy) + 4\text{Li}_3(1-xy) \\ & + \log(u)\log(v)\log\left(\frac{(1-x)(1-y)}{(1-xy)^2}\right) + 2\log(u)\log(1-x)\log(1-y) \\ & - 4\log(u)\log(1-x)\log(1-xy) + 2\log(u)\log^2(1-x) \\ & + 2\log(v)\log(1-x)\log(1-y) - 4\log(v)\log(1-y)\log(1-xy) \\ & + 2\log(v)\log^2(1-y) - 2\log^2(1-x)\log\left(-\frac{x(y-1)}{x-1}\right) \\ & + 4\log^2(1-x)\log(1-y) + 4\log(1-x)\log^2(1-y) \\ & - 2\log\left(-\frac{x(y-1)}{x-1}\right)\log^2(1-xy) - 2\log\left(-\frac{(x-1)y}{y-1}\right)\log^2(1-xy) \\ & \left. + 2\log(xy)\log^2(1-xy) - 2\log^2(1-y)\log\left(-\frac{(x-1)y}{y-1}\right) \right] \end{aligned}$$

$$\begin{aligned}
& + 4 \log(1-x) \log\left(-\frac{x(y-1)}{x-1}\right) \log(1-xy) \\
& - 8 \log(1-x) \log(1-y) \log(1-xy) \\
& + 4 \log(1-y) \log\left(-\frac{(x-1)y}{y-1}\right) \log(1-xy) + 2\zeta_3 \Big], \tag{B.14}
\end{aligned}$$

For convenience, we have expressed these functions in terms of the variables

$$x = -\frac{\bar{z}}{1-\bar{z}}, \quad y = -\frac{1-z}{z}, \tag{B.15}$$

where

$$z = \frac{1}{2}(1+u-v+\sqrt{\lambda(1,u,v)}), \quad \bar{z} = \frac{1}{2}(1+u-v-\sqrt{\lambda(1,u,v)}), \tag{B.16}$$

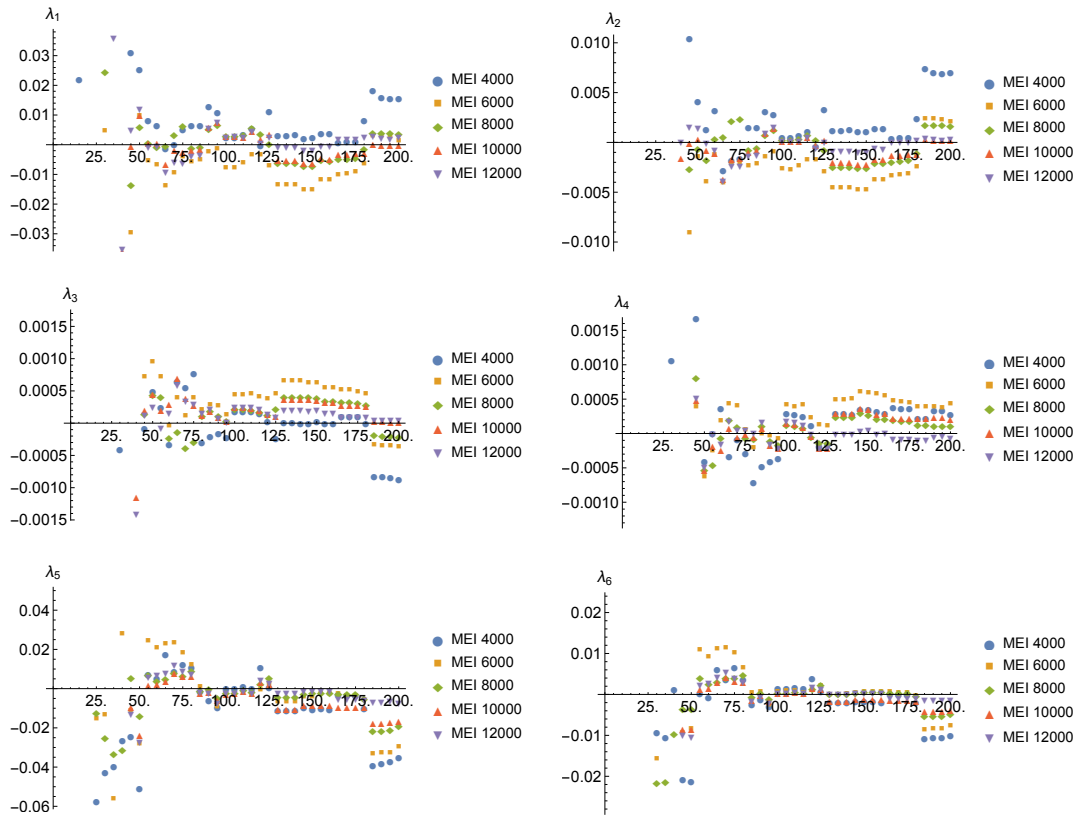
in which λ denotes the Källén function,

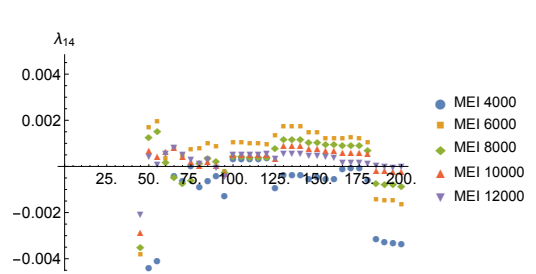
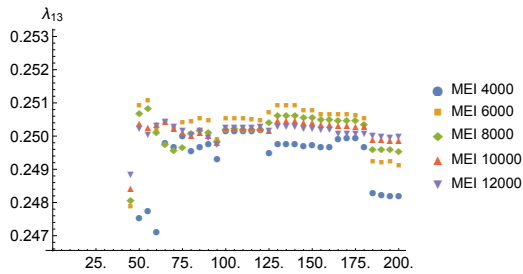
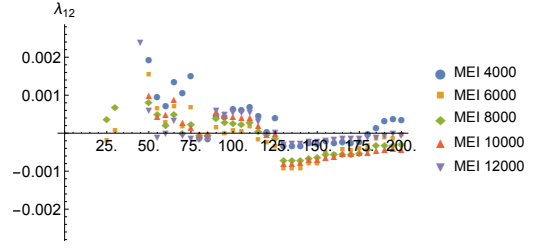
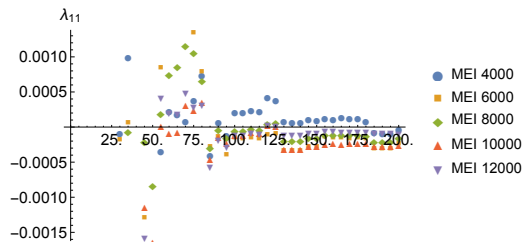
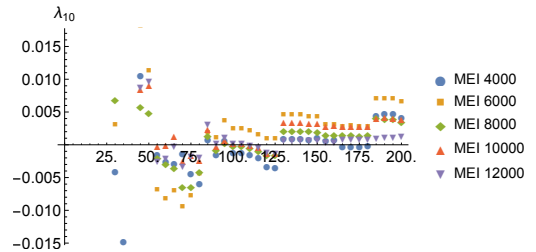
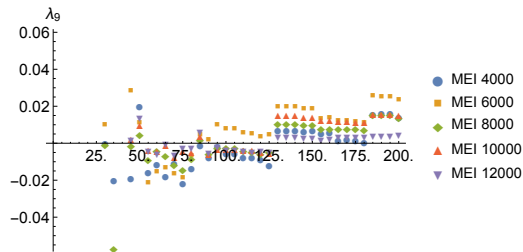
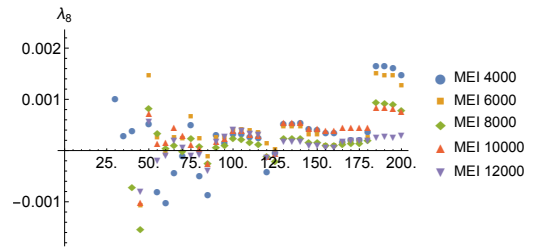
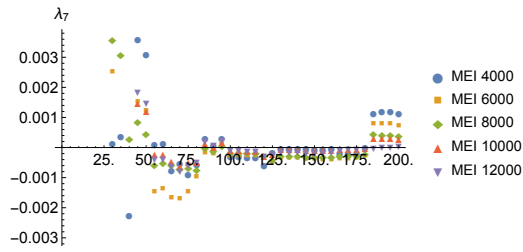
$$\lambda(a,b,c) = a^2 + b^2 + c^2 - 2ab - 2ac - 2bc. \tag{B.17}$$

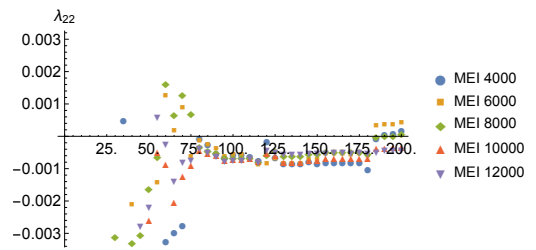
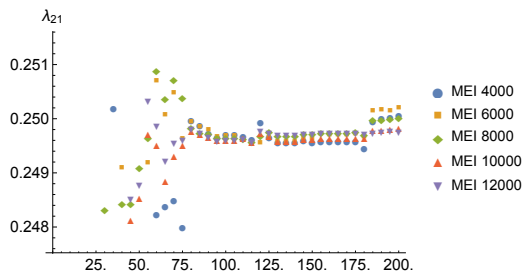
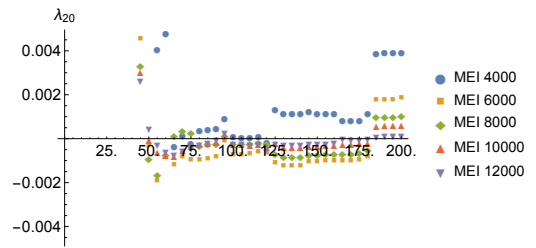
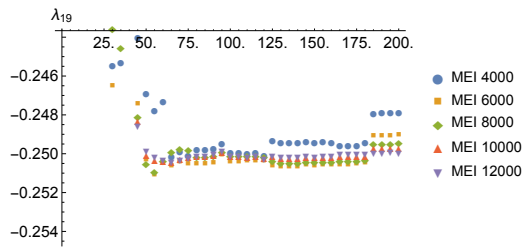
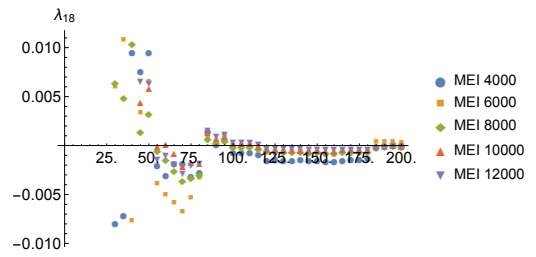
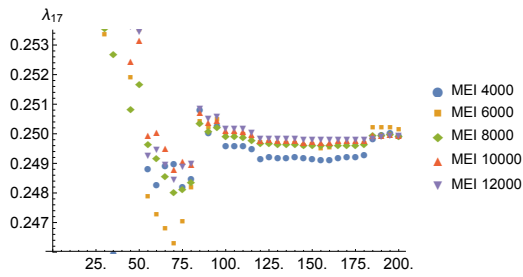
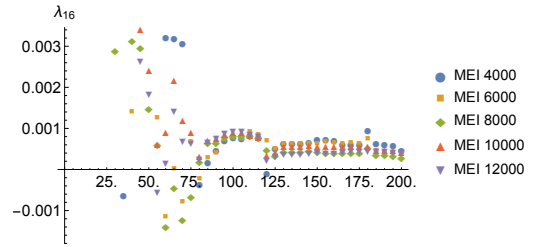
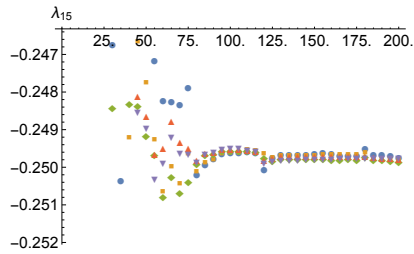
Appendix C

t_0 fitting details

Here we include the results of the `NMinimize` fit for the $t_0(\alpha_{23}, \alpha_{24}, \alpha_{34})$ ansatz, Eq. (4.44), for each parameter in turn. The size of the dataset used in fitting is given on the horizontal axis and the parameter's value on the vertical. The size of the dataset is varied in order to show convergence of the fit towards stable, rational values.







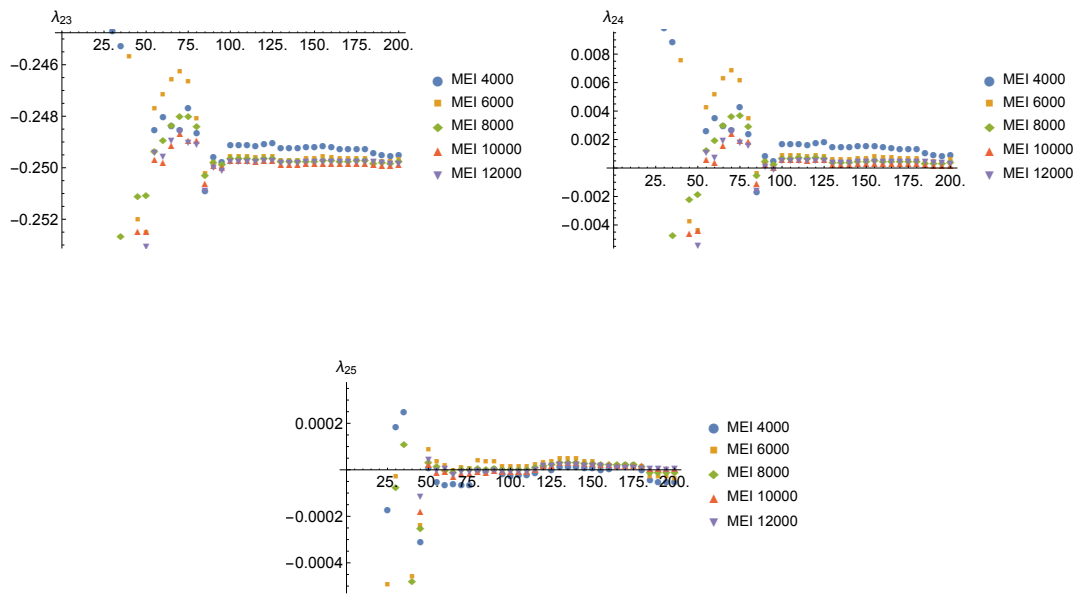


Figure C.1: Parameter fits for the t_0 ansatz. Horizontal axis indicates size of dataset in units of (number of points)/5. Vertical axis indicates fit value for corresponding parameter. The value of `MaxErrorIncreases` (MEI) used in integrating the data to fit is indicated.

Appendix D

t_1 fitting details

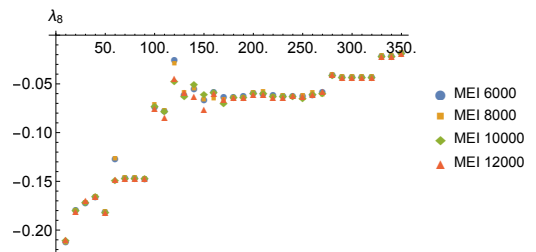
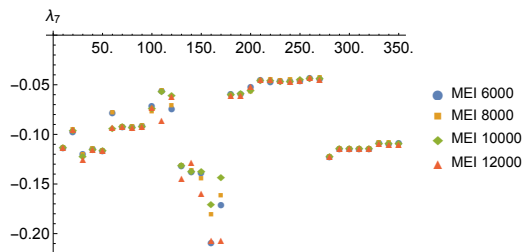
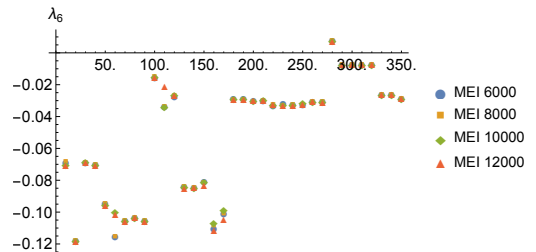
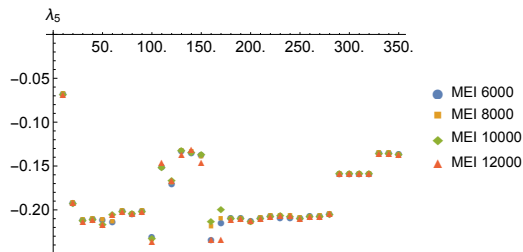
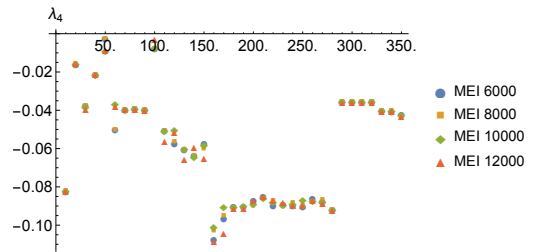
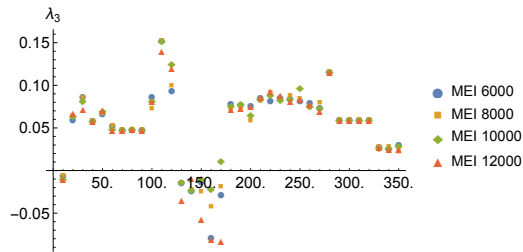
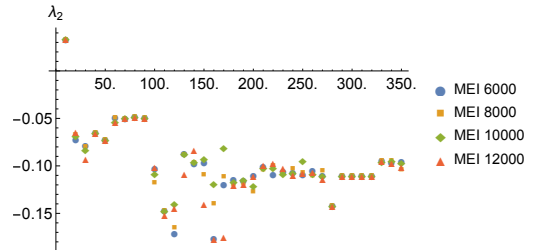
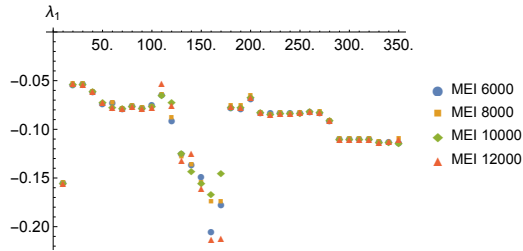
The plots below give on their vertical axis the least-squares fit values for their respective parameter λ_i from the $t_1(\alpha_{23}, \alpha_{24}, \alpha_{34})$ ansatz (constructed from Tabs. 4.4, 4.6, 4.5,

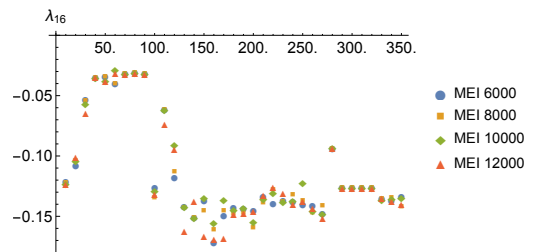
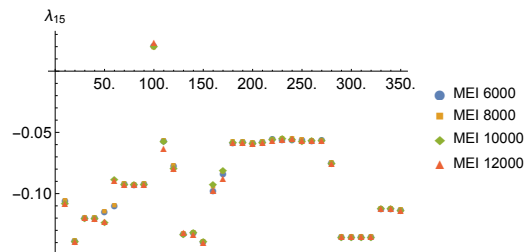
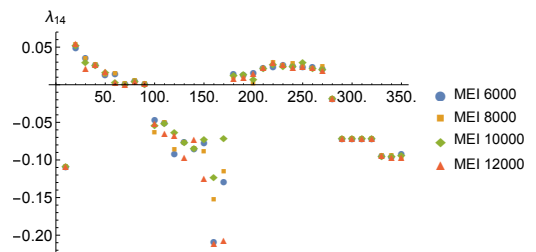
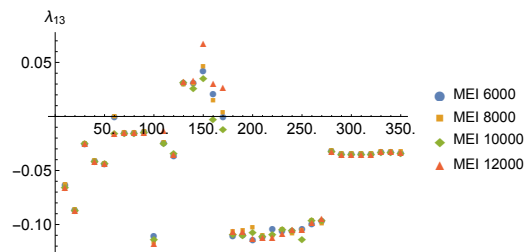
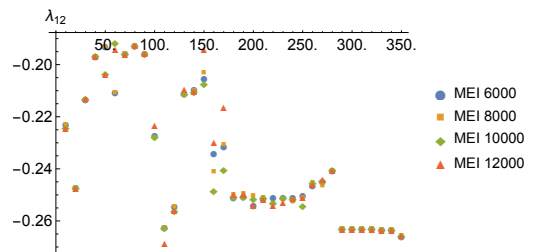
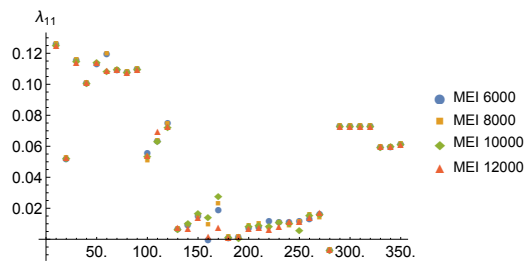
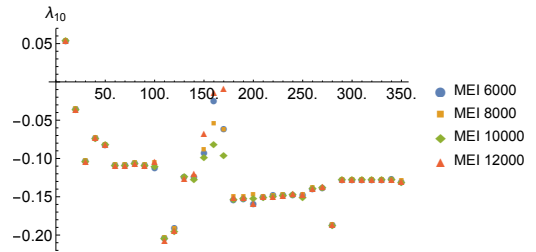
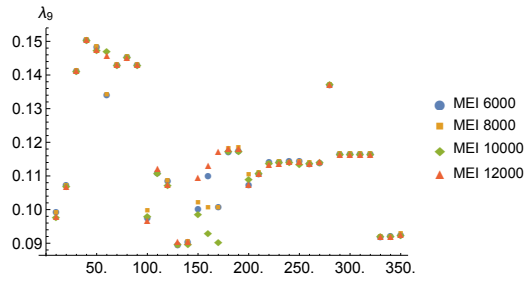
$$\begin{aligned}
 t_1 = & M_{000}^2(a_{23}) \left(M_{000}^2(a_{24}) - M_{000}^2(a_{34}) \right) \lambda_1 & (D.1) \\
 & + \left(M_{000}^2(a_{24}) - M_{000}^2(a_{34}) \right) \left(M_{000}^2(a_{24}) + M_{000}^2(a_{34}) \right) \lambda_2 \\
 & + \left(M_{000}(a_{24})^4 - M_{000}(a_{34})^4 \right) \lambda_3 \\
 & + \left(M_{000}(a_{24}) M_{020}(a_{24}) - M_{000}(a_{34}) M_{020}(a_{34}) \right) \lambda_4 \\
 & + \left(M_{100}^2(a_{24}) - M_{100}^2(a_{34}) \right) \lambda_5 \\
 & + \left(M_{111}(a_{24}) - M_{111}(a_{34}) \right) \lambda_6 \\
 & + \left(M_{000}(a_{24}) M_{200}(a_{24}) - M_{000}(a_{34}) M_{200}(a_{34}) \right) \lambda_7 \\
 & + M_{100}(a_{23}) r(a_{23}) \left(M_{000}^2(a_{24}) - M_{000}^2(a_{34}) \right) \lambda_8 \\
 & + M_{000}(a_{23}) r(a_{23}) \left(M_{011}(a_{24}) - M_{011}(a_{34}) \right) \lambda_9 \\
 & + M_{000}(a_{23}) r(a_{23}) \left(M_{000}(a_{24}) M_{100}(a_{24}) - M_{000}(a_{34}) M_{100}(a_{34}) \right) \lambda_{10} \\
 & + \left(M_{011}(a_{24}) + M_{011}(a_{34}) \right) \left(M_{000}(a_{24}) r(a_{24}) - M_{000}(a_{34}) r(a_{34}) \right) \lambda_{11} \\
 & + M_{011}(a_{23}) \left(M_{000}(a_{24}) r(a_{24}) - M_{000}(a_{34}) r(a_{34}) \right) \lambda_{12} \\
 & + M_{000}(a_{23}) M_{100}(a_{23}) \left(M_{000}(a_{24}) r(a_{24}) - M_{000}(a_{34}) r(a_{34}) \right) \lambda_{13} \\
 & + \left(M_{000}(a_{24}) M_{100}(a_{24}) + M_{000}(a_{34}) M_{100}(a_{34}) \right)
 \end{aligned}$$

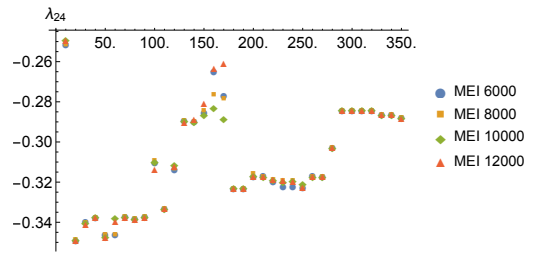
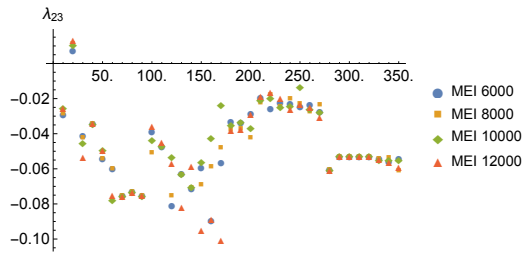
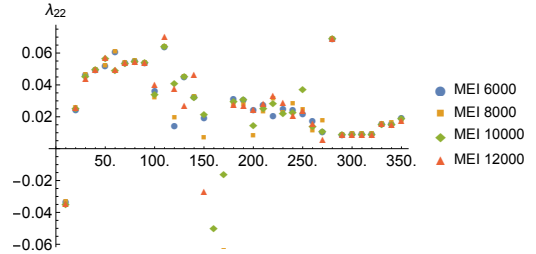
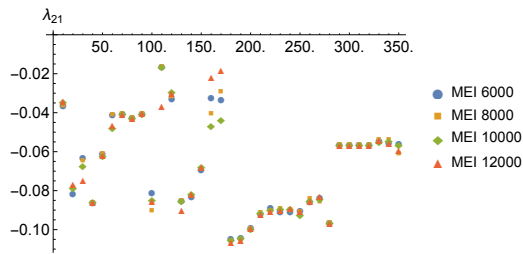
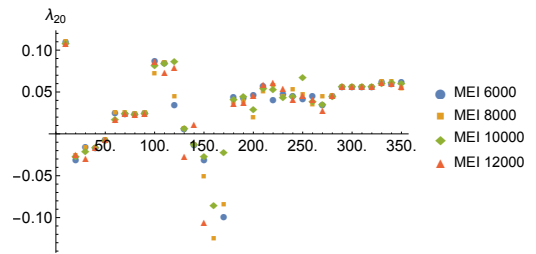
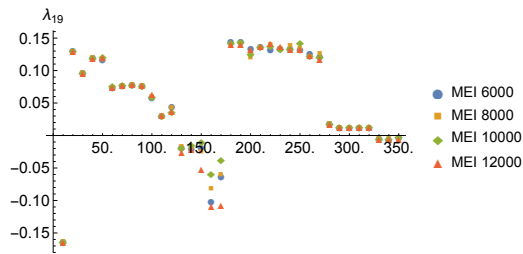
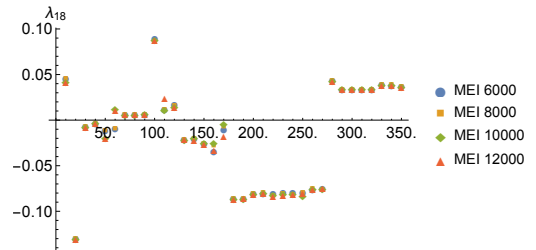
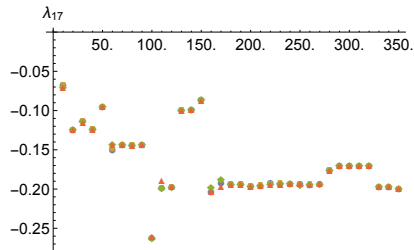
$$\begin{aligned}
& \times \left(M_{000}(a_{24}) r(a_{24}) - M_{000}(a_{34}) r(a_{34}) \right) \lambda_{14} \\
& + \left(M_{011}(a_{24}) - M_{011}(a_{34}) \right) \left(M_{000}(a_{24}) r(a_{24}) + M_{000}(a_{34}) r(a_{34}) \right) \lambda_{15} \\
& + \left(M_{000}(a_{24}) M_{100}(a_{24}) - M_{000}(a_{34}) M_{100}(a_{34}) \right) \\
& \quad \times \left(M_{000}(a_{24}) r(a_{24}) + M_{000}(a_{34}) r(a_{34}) \right) \lambda_{16} \\
& + \left(M_{000}(a_{24}) M_{011}(a_{34}) r(a_{24}) - M_{000}(a_{34}) M_{011}(a_{24}) r(a_{34}) \right) \lambda_{17} \\
& + \left(M_{000}(a_{24}) M_{011}(a_{24}) r(a_{24}) - M_{000}(a_{34}) M_{011}(a_{34}) r(a_{34}) \right) \lambda_{18} \\
& + M_{000}^2(a_{23}) \left(M_{100}(a_{24}) r(a_{24}) - M_{100}(a_{34}) r(a_{34}) \right) \lambda_{19} \\
& + \left(M_{000}^2(a_{24}) + M_{000}^2(a_{34}) \right) \left(M_{100}(a_{24}) r(a_{24}) - M_{100}(a_{34}) r(a_{34}) \right) \lambda_{20} \\
& + \left(M_{000}^2(a_{24}) - M_{000}^2(a_{34}) \right) \left(M_{100}(a_{24}) r(a_{24}) + M_{100}(a_{34}) r(a_{34}) \right) \lambda_{21} \\
& + \left(M_{000}^2(a_{34}) M_{100}(a_{24}) r(a_{24}) - M_{000}^2(a_{24}) M_{100}(a_{34}) r(a_{34}) \right) \lambda_{22} \\
& + \left(M_{000}^2(a_{24}) M_{100}(a_{24}) r(a_{24}) - M_{000}^2(a_{34}) M_{100}(a_{34}) r(a_{34}) \right) \lambda_{23} \\
& + \left(M_{102}(a_{24}) r(a_{24}) - M_{102}(a_{34}) r(a_{34}) \right) \lambda_{24} \\
& + \left(M_{120}(a_{24}) r(a_{24}) - M_{120}(a_{34}) r(a_{34}) \right) \lambda_{25} \\
& + \left(M_{300}(a_{24}) r(a_{24}) - M_{300}(a_{34}) r(a_{34}) \right) \lambda_{26} \\
& + \left(M_{000}(a_{24}) M_{000}(a_{34})^3 - M_{000}(a_{24})^3 M_{000}(a_{34}) \right) r(a_{24}) r(a_{34}) \lambda_{27} \\
& + \left(M_{000}(a_{24}) M_{020}(a_{34}) - M_{000}(a_{34}) M_{020}(a_{24}) \right) r(a_{24}) r(a_{34}) \lambda_{28} \\
& + \left(M_{000}(a_{24}) M_{200}(a_{34}) - M_{000}(a_{34}) M_{200}(a_{24}) \right) r(a_{24}) r(a_{34}) \lambda_{29} \\
& + M_{000}(a_{23})^3 r(a_{23}) \left(M_{000}(a_{24}) r(a_{24}) - M_{000}(a_{34}) r(a_{34}) \right) \lambda_{30} \\
& + M_{020}(a_{23}) r(a_{23}) \left(M_{000}(a_{24}) r(a_{24}) - M_{000}(a_{34}) r(a_{34}) \right) \lambda_{31} \\
& + M_{200}(a_{23}) r(a_{23}) \left(M_{000}(a_{24}) r(a_{24}) - M_{000}(a_{34}) r(a_{34}) \right) \lambda_{32} \\
& + M_{100}(a_{23}) r(a_{23}) \left(M_{100}(a_{24}) r(a_{24}) - M_{100}(a_{34}) r(a_{34}) \right) \lambda_{33} \\
& + M_{000}(a_{23}) r(a_{23}) \left(M_{000}^2(a_{24}) + M_{000}^2(a_{34}) \right) \\
& \quad \times \left(M_{000}(a_{24}) r(a_{24}) - M_{000}(a_{34}) r(a_{34}) \right) \lambda_{34} \\
& + M_{000}(a_{23}) r(a_{23}) \left(M_{000}^2(a_{24}) - M_{000}^2(a_{34}) \right)
\end{aligned}$$

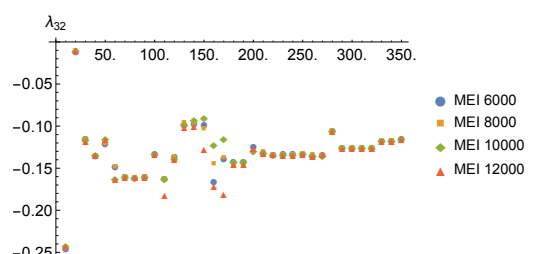
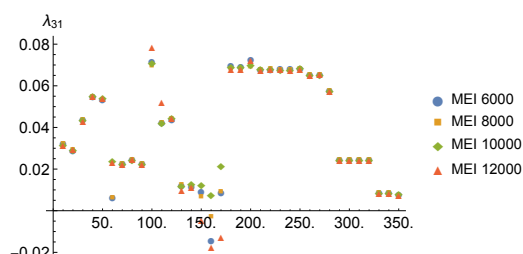
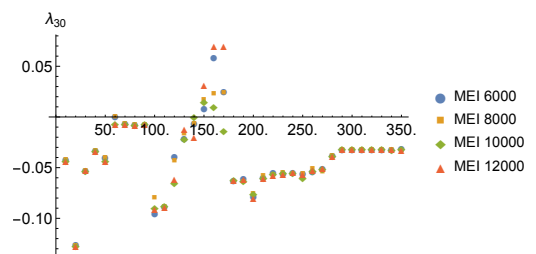
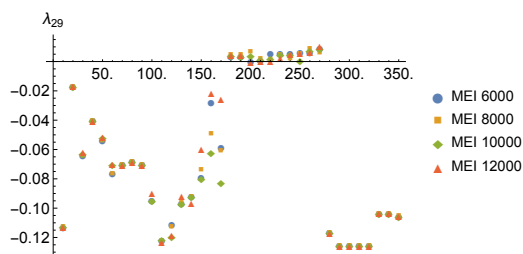
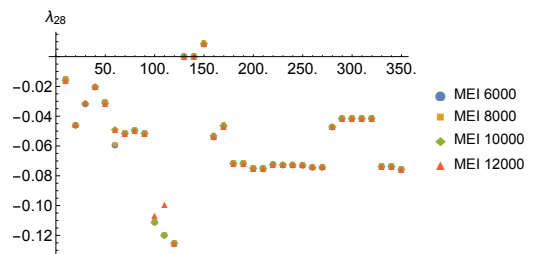
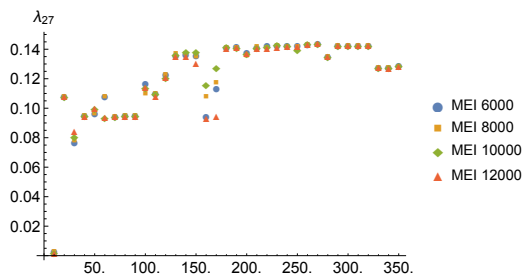
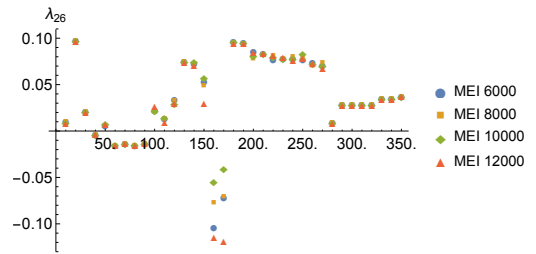
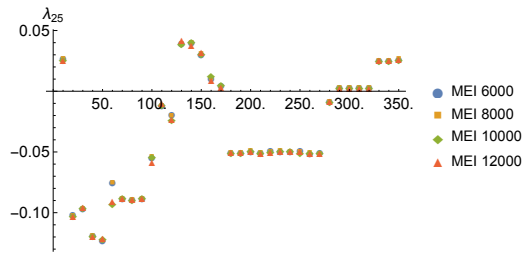
$$\begin{aligned}
& \times \left(M_{000}(a_{24}) r(a_{24}) + M_{000}(a_{34}) r(a_{34}) \right) \lambda_{35} \\
& + M_{000}(a_{23}) r(a_{23}) \\
& \quad \times \left(M_{000}(a_{24}) M_{000}^2(a_{34}) r(a_{24}) - M_{000}^2(a_{24}) M_{000}(a_{34}) r(a_{34}) \right) \lambda_{36} \\
& + M_{000}(a_{23}) r(a_{23}) \left(M_{000}(a_{24})^3 r(a_{24}) - M_{000}(a_{34})^3 r(a_{34}) \right) \lambda_{37} \\
& + M_{000}(a_{23}) r(a_{23}) \left(M_{020}(a_{24}) r(a_{24}) - M_{020}(a_{34}) r(a_{34}) \right) \lambda_{38} \\
& + M_{000}(a_{23}) r(a_{23}) \left(M_{200}(a_{24}) r(a_{24}) - M_{200}(a_{34}) r(a_{34}) \right) \lambda_{39} \\
& + M_{000}(a_{23}) r(a_{23}) \left(M_{000}(a_{34}) M_{100}(a_{24}) - M_{000}(a_{24}) M_{100}(a_{34}) \right) r(a_{24}) r(a_{34}) \lambda_{40}.
\end{aligned}$$

The size of the dataset used in the `NMinimize` least-squares fitting is given on the horizontal axis and is varied in order to see if convergence of the fit towards stable, rational values is achieved.









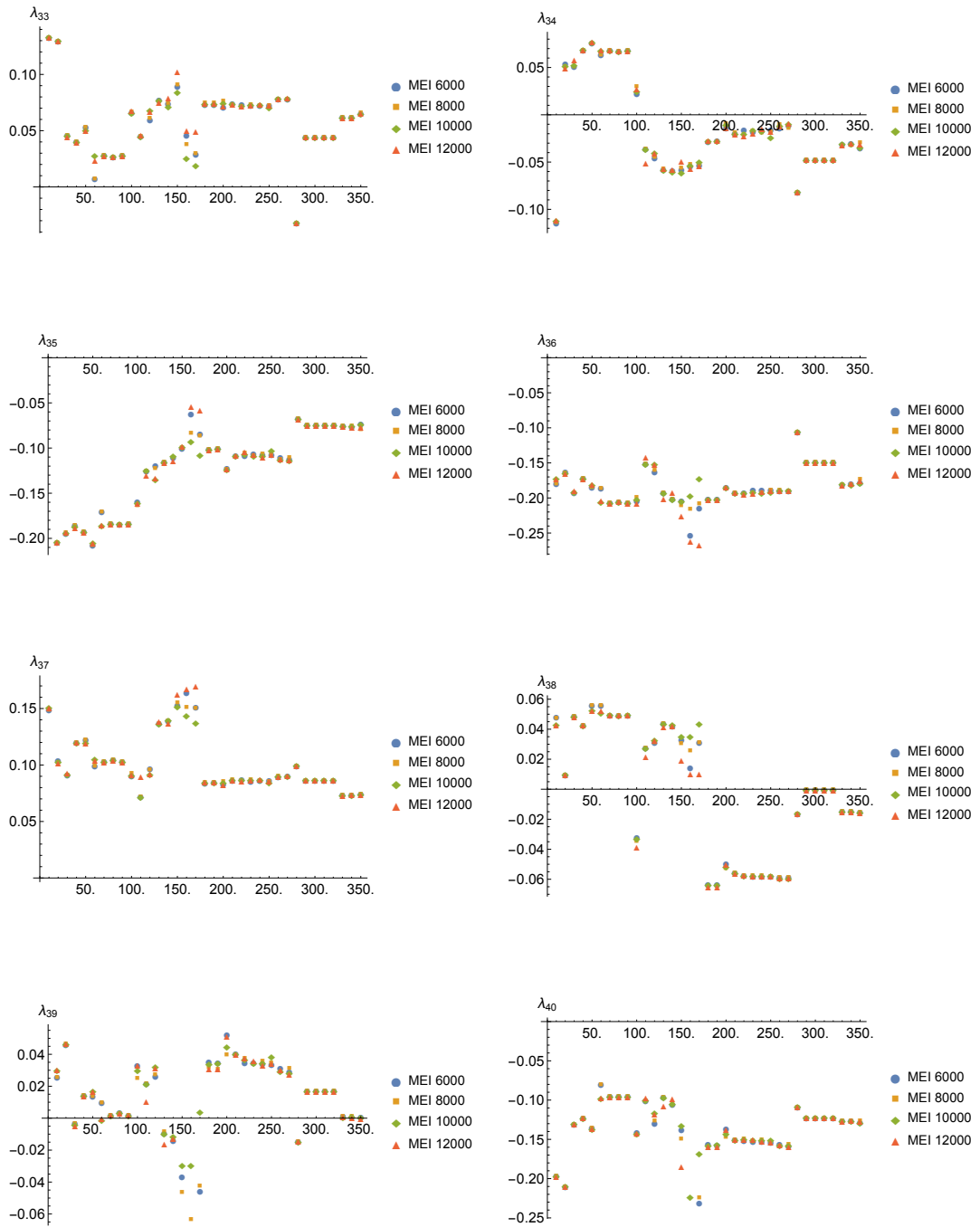


Figure D.1: Parameter fits for the t_0 ansatz. Horizontal axis indicates size of dataset in units of (number of points)/5. Vertical axis indicates fit value for corresponding parameter. The value of MaxErrorIncreases (MEI) used in integrating the data to fit is indicated.

Bibliography

- [1] G. Falcioni, E. Gardi, M. Harley, L. Magnea, and C. D. White, *Multiple Gluon Exchange Webs*, *JHEP* **10** (2014) 10, [1407.3477].
- [2] G. Falcioni, E. Gardi, M. Harley, L. Magnea, and C. D. White, *Webs containing a single three-gluon-vertex*, . to appear.
- [3] G. Korchemsky and A. Radyushkin, *Renormalization of the Wilson Loops Beyond the Leading Order*, *Nucl. Phys.* **B283** (1987) 342–364.
- [4] L. D. Landau, *On analytic properties of vertex parts in quantum field theory*, *Nucl. Phys.* **13** (1959) 181–192.
- [5] S. Coleman and R. E. Norton, *Singularities in the physical region*, *Nuovo Cim.* **38** (1965) 438–442.
- [6] G. F. Sterman, *Mass Divergences in Annihilation Processes. 1. Origin and Nature of Divergences in Cut Vacuum Polarization Diagrams*, *Phys. Rev.* **D17** (1978) 2773.
- [7] G. F. Sterman, *Mass Divergences in Annihilation Processes. 2. Cancellation of Divergences in Cut Vacuum Polarization Diagrams*, *Phys. Rev.* **D17** (1978) 2789.
- [8] G. F. Sterman, *Partons, factorization and resummation*, *TASI 95*, in *QCD and beyond. Proceedings, Theoretical Advanced Study Institute in Elementary Particle Physics, TASI-95, Boulder, USA, June 4-30, 1995*, 1995. [hep-ph/9606312](#).
- [9] T. Kinoshita, *Mass singularities of Feynman amplitudes*, *J. Math. Phys.* **3** (1962) 650–677.
- [10] T. D. Lee and M. Nauenberg, *Degenerate Systems and Mass Singularities*, *Phys. Rev.* **133** (1964) B1549–B1562.
- [11] G. F. Sterman and S. Weinberg, *Jets from Quantum Chromodynamics*, *Phys. Rev. Lett.* **39** (1977) 1436.
- [12] M. Ciafaloni, *The QCD Coherent State From Asymptotic Dynamics*, *Phys. Lett.* **B150** (1985) 379.

-
- [13] P. P. Kulish and L. D. Faddeev, *Asymptotic conditions and infrared divergences in quantum electrodynamics*, *Theor. Math. Phys.* **4** (1970) 745. [Teor. Mat. Fiz.4,153(1970)].
- [14] G. Giavarini and G. Marchesini, *IR Finite S Matrix in the QCD Coherent State Basis*, *Nucl. Phys.* **B296** (1988) 546.
- [15] F. Bloch and A. Nordsieck, *Note on the Radiation Field of the electron*, *Phys. Rev.* **52** (1937) 54–59.
- [16] S. Catani and M. H. Seymour, *A General algorithm for calculating jet cross-sections in NLO QCD*, *Nucl. Phys.* **B485** (1997) 291–419, [hep-ph/9605323]. [Erratum: Nucl. Phys.B510,503(1998)].
- [17] D. A. Kosower, *Antenna factorization of gauge theory amplitudes*, *Phys. Rev.* **D57** (1998) 5410–5416, [hep-ph/9710213].
- [18] D. A. Kosower, *Antenna factorization in strongly ordered limits*, *Phys. Rev.* **D71** (2005) 045016, [hep-ph/0311272].
- [19] A. Banfi, P. F. Monni, G. P. Salam, and G. Zanderighi, *Higgs and Z-boson production with a jet veto*, *Phys. Rev. Lett.* **109** (2012) 202001, [1206.4998].
- [20] A. von Manteuffel, R. M. Schabinger, and H. X. Zhu, *The Complete Two-Loop Integrated Jet Thrust Distribution In Soft-Collinear Effective Theory*, *JHEP* **03** (2014) 139, [1309.3560].
- [21] B. D. Pecjak, D. J. Scott, X. Wang, and L. L. Yang, *Resummed differential cross sections for top-quark pairs at the LHC*, 1601.07020.
- [22] A. Gehrmann-De Ridder, T. Gehrmann, E. W. N. Glover, and G. Heinrich, *NNLO corrections to event shapes in e^+e^- annihilation*, *JHEP* **12** (2007) 094, [0711.4711].
- [23] S. Weinzierl, *Event shapes and jet rates in electron-positron annihilation at NNLO*, *JHEP* **06** (2009) 041, [0904.1077].
- [24] R. Abbate, M. Fickinger, A. H. Hoang, V. Mateu, and I. W. Stewart, *Thrust at N³LL with Power Corrections and a Precision Global Fit for $\alpha_s(m_Z)$* , *Phys. Rev.* **D83** (2011) 074021, [1006.3080].
- [25] C. F. Berger, *Soft gluon exponentiation and resummation*, hep-ph/0305076.
- [26] T. Becher, A. Broggio, and A. Ferroglia, *Introduction to Soft-Collinear Effective Theory*, 1410.1892.
- [27] G. P. Korchemsky and A. V. Radyushkin, *Loop space formalism and renormalization group for the infrared asymptotics of QCD*, *Phys. Lett.* **B171** (1986) 459–467.

- [28] A. M. Polyakov, *Gauge Fields as Rings of Glue*, *Nucl. Phys.* **B164** (1980) 171–188.
- [29] I. Y. Arefeva, *Quantum contour field equations*, *Phys. Lett.* **B93** (1980) 347–353.
- [30] V. S. Dotsenko and S. N. Vergeles, *Renormalizability of Phase Factors in the Nonabelian Gauge Theory*, *Nucl. Phys.* **B169** (1980) 527.
- [31] R. A. Brandt, F. Neri, and M.-a. Sato, *Renormalization of Loop Functions for All Loops*, *Phys. Rev.* **D24** (1981) 879.
- [32] G. Korchemsky and A. Radyushkin, *Infrared asymptotics of perturbative QCD: Renormalization properties of the wilson loops in higher orders of perturbation theory*, *Sov. J. Nucl. Phys.* **44** (1986) 877.
- [33] G. P. Korchemsky and G. Marchesini, *Structure function for large x and renormalization of Wilson loop*, *Nucl. Phys.* **B406** (1993) 225–258, [[hep-ph/9210281](#)].
- [34] G. P. Korchemsky and G. Marchesini, *Resummation of large infrared corrections using Wilson loops*, *Phys. Lett.* **B313** (1993) 433–440.
- [35] I. Korchemskaya and G. Korchemsky, *High-energy scattering in QCD and cross singularities of Wilson loops*, *Nucl. Phys.* **B437** (1995) 127–162, [[hep-ph/9409446](#)].
- [36] I. Korchemskaya and G. Korchemsky, *On lightlike Wilson loops*, *Phys. Lett.* **B287** (1992) 169–175.
- [37] R. Akhouri, R. Saotome, and G. Sterman, *Collinear and Soft Divergences in Perturbative Quantum Gravity*, *Phys. Rev.* **D84** (2011) 104040, [[1109.0270](#)].
- [38] S. G. Naculich and H. J. Schnitzer, *Eikonal methods applied to gravitational scattering amplitudes*, *JHEP* **1105** (2011) 087, [[1101.1524](#)].
- [39] D. Miller and C. White, *The Gravitational cusp anomalous dimension from AdS space*, *Phys. Rev.* **D85** (2012) 104034, [[1201.2358](#)].
- [40] C. D. White, *Factorization Properties of Soft Graviton Amplitudes*, *JHEP* **1105** (2011) 060, [[1103.2981](#)].
- [41] S. Melville, S. Naculich, H. Schnitzer, and C. White, *Wilson line approach to gravity in the high energy limit*, [1306.6019](#).
- [42] C. Anastasiou, Z. Bern, L. J. Dixon, and D. A. Kosower, *Planar amplitudes in maximally supersymmetric Yang-Mills theory*, *Phys. Rev. Lett.* **91** (2003) 251602, [[hep-th/0309040](#)].
- [43] Z. Bern, L. J. Dixon, and V. A. Smirnov, *Iteration of planar amplitudes in maximally supersymmetric Yang-Mills theory at three loops and beyond*, *Phys. Rev.* **D72** (2005) 085001, [[hep-th/0505205](#)].

-
- [44] S. G. Naculich and H. J. Schnitzer, *IR divergences and Regge limits of subleading-color contributions to the four-gluon amplitude in $N=4$ SYM Theory*, *JHEP* **0910** (2009) 048, [0907.1895].
- [45] S. G. Naculich, H. Nastase, and H. J. Schnitzer, *Applications of Subleading Color Amplitudes in $N=4$ SYM Theory*, *Adv. High Energy Phys.* **2011** (2011) 190587, [1105.3718].
- [46] S. G. Naculich, H. Nastase, and H. J. Schnitzer, *All-loop infrared-divergent behavior of most-subleading-color gauge-theory amplitudes*, *JHEP* **1304** (2013) 114, [1301.2234].
- [47] L. F. Alday and J. M. Maldacena, *Gluon scattering amplitudes at strong coupling*, *JHEP* **0706** (2007) 064, [0705.0303].
- [48] B. Basso, G. P. Korchemsky, and J. Kotanski, *Cusp anomalous dimension in maximally supersymmetric Yang-Mills theory at strong coupling*, *Phys. Rev. Lett.* **100** (2008) 091601, [0708.3933].
- [49] D. Correa, J. Henn, J. Maldacena, and A. Sever, *The cusp anomalous dimension at three loops and beyond*, *JHEP* **1205** (2012) 098, [1203.1019].
- [50] J. M. Henn and T. Huber, *Systematics of the cusp anomalous dimension*, *JHEP* **1211** (2012) 058, [1207.2161].
- [51] D. Correa, J. Henn, J. Maldacena, and A. Sever, *An exact formula for the radiation of a moving quark in $N=4$ super Yang Mills*, *JHEP* **1206** (2012) 048, [1202.4455].
- [52] J. M. Henn and T. Huber, *The four-loop cusp anomalous dimension in $N=4$ super Yang-Mills and analytic integration techniques for Wilson line integrals*, 1304.6418.
- [53] O. Erdoğ an and G. Sterman, *Gauge Theory Webs and Surfaces*, *Phys. Rev.* **D91** (2015), no. 1 016003, [1112.4564].
- [54] I. Cherednikov, T. Mertens, and F. Van der Veken, *Evolution of cusped light-like Wilson loops and geometry of the loop space*, *Phys. Rev.* **D86** (2012) 085035, [1208.1631].
- [55] I. Cherednikov, T. Mertens, and F. Van der Veken, *Cusped light-like Wilson loops in gauge theories*, *Phys. Part. Nucl.* **44** (2013) 250–259, [1210.1767].
- [56] E. Gardi, E. Laenen, G. Stavenga, and C. D. White, *Webs in multiparton scattering using the replica trick*, *JHEP* **1011** (2010) 155, [1008.0098].
- [57] E. Gardi and C. D. White, *General properties of multiparton webs: Proofs from combinatorics*, *JHEP* **1103** (2011) 079, [1102.0756].

- [58] E. Gardi, J. M. Smillie, and C. D. White, *On the renormalization of multiparton webs*, *JHEP* **1109** (2011) 114, [1108.1357].
- [59] M. Dukes, E. Gardi, H. McAslan, D. J. Scott, and C. D. White, *Webs and Posets*, 1310.3127.
- [60] E. Gardi, *From Webs to Polylogarithms*, *JHEP* **1404** (2014) 044, [1310.5268].
- [61] E. Gardi, J. M. Smillie, and C. D. White, *The Non-Abelian Exponentiation theorem for multiple Wilson lines*, 1304.7040.
- [62] N. Kidonakis, *Two-loop soft anomalous dimensions and NNLL resummation for heavy quark production*, *Phys. Rev. Lett.* **102** (2009) 232003, [0903.2561].
- [63] A. Grozin, J. M. Henn, G. P. Korchemsky, and P. Marquard, *The n_f terms of the QCD cusp anomalous dimension*, 1406.7828.
- [64] A. Grozin, J. M. Henn, G. P. Korchemsky, and P. Marquard, *Three Loop Cusp Anomalous Dimension in QCD*, *Phys. Rev. Lett.* **114** (2015), no. 6 062006, [1409.0023].
- [65] S. M. Aybat, L. J. Dixon, and G. F. Sterman, *The two-loop anomalous dimension matrix for soft gluon exchange*, *Phys. Rev. Lett.* **97** (2006) 072001, [hep-ph/0606254].
- [66] S. M. Aybat, L. J. Dixon, and G. F. Sterman, *The two-loop soft anomalous dimension matrix and resummation at next-to-next-to leading pole*, *Phys. Rev.* **D74** (2006) 074004, [hep-ph/0607309].
- [67] A. Ferroglia, M. Neubert, B. D. Pecjak, and L. L. Yang, *Two-loop divergences of scattering amplitudes with massive partons*, *Phys. Rev. Lett.* **103** (2009) 201601, [0907.4791].
- [68] A. Ferroglia, M. Neubert, B. D. Pecjak, and L. L. Yang, *Two-loop divergences of massive scattering amplitudes in non-abelian gauge theories*, *JHEP* **11** (2009) 062, [0908.3676].
- [69] A. Mitov, G. F. Sterman, and I. Sung, *Computation of the Soft Anomalous Dimension Matrix in Coordinate Space*, *Phys. Rev.* **D82** (2010) 034020, [1005.4646].
- [70] Y.-T. Chien, M. D. Schwartz, D. Simmons-Duffin, and I. W. Stewart, *Jet Physics from Static Charges in AdS*, *Phys. Rev.* **D85** (2012) 045010, [1109.6010].
- [71] A. Mitov, G. Sterman, and I. Sung, *The Massive Soft Anomalous Dimension Matrix at Two Loops*, *Phys. Rev.* **D79** (2009) 094015, [0903.3241].
- [72] T. Becher and M. Neubert, *Infrared singularities of QCD amplitudes with massive partons*, *Phys. Rev.* **D79** (2009) 125004, [0904.1021].

-
- [73] M. Beneke, P. Falgari, and C. Schwinn, *Soft radiation in heavy-particle pair production: all-order colour structure and two-loop anomalous dimension*, *Nucl. Phys.* **B828** (2010) 69–101, [0907.1443].
- [74] M. Czakon, A. Mitov, and G. F. Sterman, *Threshold Resummation for Top-Pair Hadroproduction to Next-to-Next-to-Leading Log*, *Phys. Rev.* **D80** (2009) 074017, [0907.1790].
- [75] J.-y. Chiu, A. Fuhrer, R. Kelley, and A. V. Manohar, *Factorization Structure of Gauge Theory Amplitudes and Application to Hard Scattering Processes at the LHC*, *Phys. Rev.* **D80** (2009) 094013, [0909.0012].
- [76] A. Ferroglia, M. Neubert, B. D. Pecjak, and L. L. Yang, *Infrared Singularities and Soft Gluon Resummation with Massive Partons*, *Nucl. Phys. Proc. Suppl.* **205-206** (2010) 98–103, [1006.4680].
- [77] T. Becher and M. Neubert, *Infrared singularities of scattering amplitudes in perturbative QCD*, *Phys. Rev. Lett.* **102** (2009) 162001, [0901.0722].
- [78] T. Becher and M. Neubert, *On the Structure of Infrared Singularities of Gauge-Theory Amplitudes*, *JHEP* **06** (2009) 081, [0903.1126].
- [79] E. Gardi and L. Magnea, *Factorization constraints for soft anomalous dimensions in QCD scattering amplitudes*, *JHEP* **0903** (2009) 079, [0901.1091].
- [80] L. J. Dixon, L. Magnea, and G. F. Sterman, *Universal structure of subleading infrared poles in gauge theory amplitudes*, *JHEP* **08** (2008) 022, [0805.3515].
- [81] L. J. Dixon, *Matter Dependence of the Three-Loop Soft Anomalous Dimension Matrix*, *Phys. Rev.* **D79** (2009) 091501, [0901.3414].
- [82] L. J. Dixon, E. Gardi, and L. Magnea, *On soft singularities at three loops and beyond*, *JHEP* **02** (2010) 081, [0910.3653].
- [83] E. Gardi and L. Magnea, *Infrared singularities in QCD amplitudes*, *Nuovo Cim.* **032C** (2009) 137–157, [0908.3273].
- [84] T. Gehrmann, E. Glover, T. Huber, N. Iqbal, and C. Studerus, *Calculation of the quark and gluon form factors to three loops in QCD*, *JHEP* **1006** (2010) 094, [1004.3653].
- [85] V. Del Duca, C. Duhr, E. Gardi, L. Magnea, and C. D. White, *An infrared approach to Reggeization*, *Phys. Rev.* **D85** (2012) 071104, [1108.5947].
- [86] V. Del Duca, C. Duhr, E. Gardi, L. Magnea, and C. D. White, *The Infrared structure of gauge theory amplitudes in the high-energy limit*, *JHEP* **1112** (2011) 021, [1109.3581].

- [87] V. Ahrens, M. Neubert, and L. Vernazza, *Structure of Infrared Singularities of Gauge-Theory Amplitudes at Three and Four Loops*, *JHEP* **1209** (2012) 138, [1208.4847].
- [88] S. Caron-Huot, *When does the gluon reggeize?*, 1309.6521.
- [89] Ø. Almellid, C. Duhr, and E. Gardi, *Three-loop corrections to the soft anomalous dimension in multi-leg scattering*, 1507.00047.
- [90] G. F. Sterman, *Infrared divergences in perturbative QCD*, *AIP Conf. Proc.* **74** (1981) 22–40.
- [91] J. G. M. Gatheral, *Exponentiation of eikonal cross-sections in nonabelian gauge theories*, *Phys. Lett.* **B133** (1983) 90.
- [92] J. Frenkel and J. C. Taylor, *Nonabelian eikonal exponentiation*, *Nucl. Phys.* **B246** (1984) 231.
- [93] M. Dukes, E. Gardi, E. Steingrimsson, and C. D. White, *Web worlds, web-colouring matrices, and web-mixing matrices*, *J. Comb. Theory Ser. A* **120** (2013) 1012–1037, [1301.6576].
- [94] J. C. Collins, *Sudakov form-factors*, *Adv. Ser. Direct. High Energy Phys.* **5** (1989) 573–614, [hep-ph/0312336].
- [95] L. Magnea and G. F. Sterman, *Analytic continuation of the Sudakov form-factor in QCD*, *Phys. Rev.* **D42** (1990) 4222–4227.
- [96] G. P. Korchemsky, *Double Logarithmic Asymptotics in QCD*, *Phys. Lett.* **B217** (1989) 330–334.
- [97] A. Sen, *Asymptotic Behavior of the Sudakov Form-Factor in QCD*, *Phys. Rev.* **D24** (1981) 3281.
- [98] J. C. Collins, *Algorithm to Compute Corrections to the Sudakov Form-factor*, *Phys. Rev.* **D22** (1980) 1478.
- [99] A. H. Mueller, *On the Asymptotic Behavior of the Sudakov Form-factor*, *Phys. Rev.* **D20** (1979) 2037.
- [100] D. R. Yennie, S. C. Frautschi, and H. Suura, *The infrared divergence phenomena and high-energy processes*, *Ann. Phys.* **13** (1961) 379–452.
- [101] E. Laenen, G. Stavenga, and C. D. White, *Path integral approach to eikonal and next-to-eikonal exponentiation*, *JHEP* **03** (2009) 054, [0811.2067].
- [102] N. Kidonakis, G. Oderda, and G. F. Sterman, *Evolution of color exchange in QCD hard scattering*, *Nucl. Phys.* **B531** (1998) 365–402, [hep-ph/9803241].
- [103] N. Kidonakis and G. F. Sterman, *Resummation for QCD hard scattering*, *Nucl. Phys.* **B505** (1997) 321–348, [hep-ph/9705234].

- [104] M. Yu. Kalmykov, *Gauss hypergeometric function: Reduction, epsilon-expansion for integer/half-integer parameters and Feynman diagrams*, *JHEP* **04** (2006) 056, [[hep-th/0602028](#)].
- [105] A. B. Goncharov, *Multiple polylogarithms, cyclotomy and modular complexes*, *Math. Res. Lett.* **5** (1998) 497–516, [[1105.2076](#)].
- [106] A. B. Goncharov, *Multiple polylogarithms and mixed Tate motives*, [math/0103059](#).
- [107] A. B. Goncharov, *Galois symmetries of fundamental groupoids and noncommutative geometry*, *Duke Math. J.* **128** (2005) 209, [[math/0208144](#)].
- [108] F. Brown, *On the decomposition of motivic multiple zeta values*, [1102.1310](#).
- [109] C. Duhr, *Hopf algebras, coproducts and symbols: an application to Higgs boson amplitudes*, *JHEP* **1208** (2012) 043, [[1203.0454](#)].
- [110] C. Duhr, H. Gangl, and J. R. Rhodes, *From polygons and symbols to polylogarithmic functions*, *JHEP* **1210** (2012) 075, [[1110.0458](#)].
- [111] C. Duhr, *Mathematical aspects of scattering amplitudes*, in *Theoretical Advanced Study Institute in Elementary Particle Physics: Journeys Through the Precision Frontier: Amplitudes for Colliders (TASI 2014) Boulder, Colorado, June 2-27, 2014*, 2014. [1411.7538](#).
- [112] K.-T. Chen, *Iterated path integrals*, *Bull. Am. Math. Soc.* **83** (1977) 831–879.
- [113] A. B. Goncharov, M. Spradlin, C. Vergu, and A. Volovich, *Classical Polylogarithms for Amplitudes and Wilson Loops*, *Phys.Rev.Lett.* **105** (2010) 151605, [[1006.5703](#)].
- [114] S. Abreu, R. Britto, C. Duhr, and E. Gardi, *From multiple unitarity cuts to the coproduct of Feynman integrals*, *JHEP* **10** (2014) 125, [[1401.3546](#)].
- [115] S. Laporta and E. Remiddi, *Analytic treatment of the two loop equal mass sunrise graph*, *Nucl. Phys.* **B704** (2005) 349–386, [[hep-ph/0406160](#)].
- [116] S. Bloch and P. Vanhove, *The elliptic dilogarithm for the sunset graph*, [1309.5865](#).
- [117] F. C. S. Brown, *On the periods of some Feynman integrals*, [0910.0114](#).
- [118] E. Panzer, *Feynman integrals via hyperlogarithms*, *PoS LL2014* (2014) 049, [[1407.0074](#)].
- [119] E. Remiddi and J. Vermaseren, *Harmonic polylogarithms*, *Int.J.Mod.Phys.* **A15** (2000) 725–754, [[hep-ph/9905237](#)].
- [120] A. Bassetto, M. Ciafaloni, and G. Marchesini, *Jet Structure and Infrared Sensitive Quantities in Perturbative QCD*, *Phys. Rept.* **100** (1983) 201–272.

-
- [121] A. Goncharov, *A simple construction of Grassmannian polylogarithms*, 0908.2238.
- [122] A. Mitov, G. Sterman, and I. Sung, *Diagrammatic Exponentiation for Products of Wilson Lines*, *Phys. Rev.* **D82** (2010) 096010, [1008.0099].
- [123] A. Vladimirov, *Generating function for web diagrams*, 1406.6253.
- [124] E. E. Boos and A. I. Davydychev, *A Method of the Evaluation of the Vertex Type Feynman Integrals*, *Moscow Univ. Phys. Bull.* **42N3** (1987) 6–10. [Vestn. Mosk. Univ. Fiz. Astron.28N3,8(1987)].
- [125] F. Chavez and C. Duhr, *Three-mass triangle integrals and single-valued polylogarithms*, *JHEP* **11** (2012) 114, [1209.2722].
- [126] A. Bzowski, P. McFadden, and K. Skenderis, *Implications of conformal invariance in momentum space*, *JHEP* **03** (2014) 111, [1304.7760].
- [127] Wolfram Research, Inc., “*Mathematica 10.2.*”
<https://reference.wolfram.com/language/>, 2015.
- [128] Wolfram Research, Inc., “*NIntegrate Integration Strategies.*”
<https://reference.wolfram.com/language/tutorial/NIntegrateIntegrationStrategies.html>, 2015.
- [129] E. Panzer, *Algorithms for the symbolic integration of hyperlogarithms with applications to Feynman integrals*, *Comput. Phys. Commun.* **188** (2014) 148–166, [1403.3385].
- [130] K. G. Chetyrkin and F. V. Tkachov, *Integration by Parts: The Algorithm to Calculate beta Functions in 4 Loops*, *Nucl. Phys.* **B192** (1981) 159–204.
- [131] A. V. Kotikov, *Differential equations method: New technique for massive Feynman diagrams calculation*, *Phys. Lett.* **B254** (1991) 158–164.
- [132] A. V. Kotikov, *Differential equations method: The Calculation of vertex type Feynman diagrams*, *Phys. Lett.* **B259** (1991) 314–322.
- [133] A. V. Kotikov, *Differential equation method: The Calculation of N point Feynman diagrams*, *Phys. Lett.* **B267** (1991) 123–127.
- [134] A. V. Kotikov, *Differential equation method. The Calculation of n point diagrams*, in *3rd International Workshop on Software Engineering, Artificial Intelligence and Expert systems for High-energy and Nuclear Physics (AIHENP 93) Oberammergau, Germany, October 4-8, 1993*, 1993.
- [135] A. V. Kotikov, *Differential equations method: The Calculation of N ($N < 2$) points diagrams*, .

- [136] E. Remiddi, *Differential equations for Feynman graph amplitudes*, *Nuovo Cim.* **A110** (1997) 1435–1452, [hep-th/9711188].
- [137] J. M. Henn, *Multiloop integrals in dimensional regularization made simple*, *Phys. Rev. Lett.* **110** (2013) 251601, [1304.1806].